# INSTABILITIES IN MULTIPHASE AND ICING FLOWS

Evgeniy Shapiro

30th April 2004

Ph. D. Thesis

Department of Mathematics

University College London

Supervisors: Dr S.N. Timoshin, Prof F.T. Smith

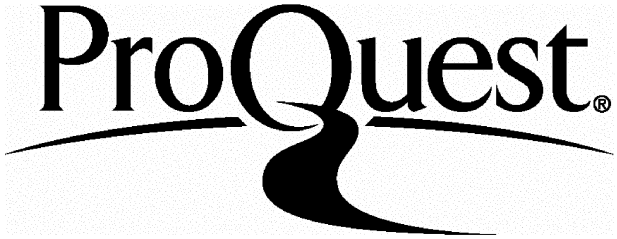

# Acknowledgments

*I would like to express my deep gratitude to my supervisors Dr Sergei Timoshin and Prof Frank Smith without whose guidance, patience and support this work would not have been be possible. I would also like to thank Dr Linzhong Li for valuable discussions and advice on the numerical methods.*

*To all postgraduates in the Department of Mathematics, thank you for creating the environment it is pleasure to work in. Thanks to the open-source community without whose tools the computations presented in this thesis would not be possible and to Richard Hoyle for the help in mastering them.*

*Thanks to my family, and especially to my ever-loving wife, thank you, for your support and for being able to bear with me on my "solver not working" days.*

*This work has been supported by Graduate Research Scholarship of the University College London and Overseas Research Scholarship of the Universities UK.*

# Abstract

The problem of the stability of water-coated ice layer is investigated for a free surface flow down an inclined plane for the cases of normal and thin (boundary-layer scale) water films. For the case of boundary-layer scale water film a Froude-based double-deck theory is developed which is then used to investigate linear two-dimensional (2D), three-dimensional (3D) and nonlinear 2D stability of the problem. The new mode of upstream-propagating instability arising because of the ice layer is found and its properties investigated. In the linear double-deck, analytic expressions for the dispersion relation and neutral curves are obtained for the case of $Pr = 1$. For the general case, linear stability problem is solved numerically using new $4^{th}$ order finite-difference scheme developed for Orr-Sommerfeld equations. Non-linear double-deck equations are solved with a new $2^{nd}$ order in space global-marching type scheme and the effects of nonlinearity are analysed. An explanation of the physical mechanism leading to the upstream propagation is derived.

The effect of the intersection and branch exchange between the interfacial mode and a shear mode is discovered in a 2-fluid plane Poiseuille flow and investigated in detail using linear stability theory and the numerical approach developed for the free-surface flows. The interaction between three instability modes present in the problem is analysed. It is shown that the question of mode identity becomes complicated because of the discovered intersection and the methods of establishing mode identity are discussed.

Finally, the longwave asymptotic analysis of the ice layer under a water/air plane Poiseuille flow is performed. The effect of ice on the modes present in the problem is discussed.

# Contents

# List of Figures

# List of Tables

# Nomenclature

| Subscript | Denotes |
|---|---|
| $a$ | Upper fluid - air |
| $l$ | Lower fluid (liquid phase) - water |
| $i$ | Solid phase of the lower fluid - ice |
| $w$ | Wall (lower ice boundary) |
| $al, la, ia$ ... | Dimensionless relation of the specified parameter in two layers, for example $\rho_{la} = \frac{\rho_l}{\rho_a}$ |
| $f$ | Freezing conditions |
| 0 | Initial solution |
| $b$ | Boundary layer |
| 1 | Lower viscous layer in double-deck |
| 2 | Upper inviscid layer in double-deck |

| Superscript | Denotes |
|---|---|
| $*$ | Dimensional values |
| $e$ | External boundary |
| $\infty$ | Incoming flow |

| Symbol | Denotes |
|---|---|
| $\vec{r} = (x, y, z)$ | Cartesian coordinates |
| $\vec{V} = (u, v, w)$ | Velocity vector and its components |
| $P$ | Pressure |
| $T$ | Temperature |
| $\vec{G}m$ | Mass forces |

| | |
|---|---|
| $\sigma$ | Incompressible stress tensor |
| $q$ | Heat flux |
| $E(x,y,z)=0$ | External air boundary |
| $F(x,y,z,t)=0$ | Air/Water interface |
| $H(x,y,z,t)=0$ | Water/Ice interface |
| $W(x,y,z)=0$ | Wall (lower ice boundary) |
| $\rho$ | Density |
| $\nu$ | Kinematic viscosity |
| $\mu$ | Dynamic viscosity |
| $Cp$ | Specific heat |
| $\lambda$ | Thermal conductivity |
| $\chi$ | Thermometric conductivity |
| $\gamma$ | Surface tension coefficient |
| $\kappa$ | Surface curvature |
| $H_{li}$ | Latent heat |
| $Re$ | Reynolds number |
| $Fr$ | Froude number |
| $Pr$ | Prandtl number |
| $Ek$ | Eckert number |
| $We$ | Weber number |
| $St$ | Stefan number |
| $\zeta$ | Surface tension parameter |

# 1 Introduction

The effect of ice formation under a wind or gravity driven water film is of great practical importance in many real-life problems. For example, this problem is encountered in aircraft icing and shallow drainage conduits used in diverse engineering structures subject to moisture collection. In the beginning of this thesis we would like to give a brief overview of the research done on this fascinating phenomenon up to date. This will allow us to understand the background of the problem formulated and investigated in this thesis.

The problem of ice formation in pipes has attracted much of researcher's attention because of the wide range of practical applications. Excellent summaries of the research done on solidification and melting problems can be found in Epstein and Cheung (1983), Epstein and Cheung (1984) and later in Yao and Prusa (1989).

For the forced convection problems there is a large number of experimental evidence of the solid-liquid interface instability. Gilpin (1979) performed a series of experiments in order to study ice growth in a pipe at or near transition Reynolds numbers. He found that for the entire range of the Reynolds numbers that was obtainable in the experiment (up to 14000), there existed a final steady-state ice profile with a cyclic variation in height along the length of the pipe. He named this periodic ice structure - 'ice-band' structure. In these experiments he observed the following icing behaviour: initially ice grows uniformly until some height is gained, afterwards a sharp expansion of the flow passage forms near the exit of the cooled section. Afterwards this expansion migrates upstream. As the first expansion migrates upstream, another ice growth may form near the pipe exit and propagate upstream in its turn. This process continues, leading to the development of an ice-band structure. Later Gilpin (1981) extended this study to the range of tran-

sitional and turbulent flows. In this second paper, Gilpin (1981) attributed the upstream propagation to the fact that turbulent heat transfer downstream of the separation point (separation occurred on the downstream inclined ice slope) melts away the ice on the downstream face of the ice-band. This explanation however does not seem to account for the initial stages of the ice-band formation when the perturbation of the uniform ice surface is sufficiently small, and no flow separation occurs.

Seki, Fukusako and Younan (1984) studied ice formation experimentally in a water flow between two cooled parallel plates. They found that in this configuration two distinct types of ice formation can be observed depending on the value of the $\frac{Re_H}{\Theta_c^{0.741}}$ parameter (where $Re_H$ is the Reynolds number based on channel height and $\Theta_c = \frac{T_f - Tw_c}{T_\infty - T_f}$ is the cooling temperature ratio). For the values of this ratio less then $10^4$, transition ice formation was observed where ice thickness varied because of the transition to turbulence of the laminar boundary layer formed on water-ice interface. For the ratio greater then $10^4$, smooth ice-surface formation has been observed. In the transition case, expansions in the melt passageway formed and migrated upstream as in Gilpin (1981) experiments.

Yao and Prusa (1989) in their review paper on solidification and melting noted that the phenomenon of solid-liquid interface instability, has been extensively observed experimentally but has been almost completely ignored in all modelling attempts.

One of the aspects of the solidification front instability was demonstrated analytically by Stephan (1969) in one of the early works on the solidification of a fluid flow along a plane wall. He deduced that for certain values of the ambient heat transfer and an imposed or known heat flux at the solid-liquid interface, there

can be two possible shapes of the fluid-solid interface, one of which is stable and another is unstable.

Lee (1993) in his PhD thesis performed analytical and full Navier-Stokes numerical analysis of the ice formation in a pipe flow. However the results did not show the ice-band structure as observed in the experiment. Instead a smooth solution was observed.

The problem of ice formation under a free-surface water film has been less investigated experimentally than icing in a pipe due to technical difficulties of developing icings on planar surfaces under controlled conditions. One experimental study can be found in Streitz, Ettema, Rothmayer and Tsao (1998) who performed a series of experiments to investigate initial ice formation on a cooled inclined plane coated with water film. The experiments were performed in a tilted wind-tunnel located in a refrigerated laboratory. The ice growth was investigated for different air velocities in the wind-tunnel. In all cases, the first ice observed comprised small spicules attached to the plane. The spicules evolved as dendrites oriented normal to the main flow, the dendrites continued to grow in the upstream direction until the ice roughness grew enough to break the water film and dam the flow forming mini-pools in front of it.

The topic of the icing of the leading edge of aircraft wings and related geometries has been subject of extensive research in both experimental and numerical works. Hirata, Gilpin, Cheng and Gates (1979) studied experimentally and analytically the formation of an ice layer on a constant temperature horizontal plate in a laminar parallel forced convection flow. The experimental observations demonstrated that in the laminar regime thermal instabilities can occur in the boundary layer which produce longitudinal grooves in the ice surface. Hirata, Gilpin and Cheng

(1979) also investigated turbulent regimes on the same experimental configuration and discovered that two distinct modes of transition to turbulence can occur: "smooth" transition, where ice thickness decreases smoothly in the turbulent region and the flow remains attached; and "step" transition, where the flow separation occurs and ice surface decreases rapidly. It was observed that "smooth" transition occurs generally on thin ice layer and "step" ice transition occurs on thick ice layers. Unfortunately the thermal instabilities observed on laminar regimes failed to attract further attention.

Vargas & Reshotko performed series of rigorous experimental studies of ice scallops formation on swept wings (Vargas and Reshotko (2000, 1999, 1998)). In these works glaze ice formation was observed under a wide range of conditions. Vargas and Reshotko (1999) indicated that it is necessary to consider boundary layer instabilities (namely cross-flow instability) as one of the physical mechanisms operating in the formation of ice scallops. This extensive study raised more questions concerning physical mechanisms responsible for ice growth.

It is necessary to note that the problem of ice growth is similar to the problems of alloy solidification and crystal growth. The hydrodynamic and morphological instabilities of the solidification interface in these problems has been a subject of extensive research. The suppressing of morphological instability and its interaction with the flow is a problem encountered in a number of practical applications, particularly in crystal growth and alloy solidification problems. Excellent reviews of the work done on this type of instability can be found in Glicksman, Coriell and McFadden (1986), Davis (1990) and more recently in Batchelor, Mofatt and Worster (2000). The coupling of a forced flow with morphological instabilities resulting in upstream propagations of solid/liquid interface disturbances is a well-

known effect in the models where the interface formation is determined by the concentration field near the interface. For example, Brattkus and Davis (1988) analysed the stability of a two-dimensional stagnation point (Hiemenz) flow over a solidifying interface with solidification process governed by concentration and showed that two-dimensional longwave disturbances are unstable for any degree of constitutional undercooling, and the disturbances of the interface propagate against the direction of the basic flow. Forth and Wheeler (1989) considered the effect of a model boundary layer flow on the hydrodynamic and morphological stability of a solidification of a binary alloy, with the interface growth governed by the alloy concentration gradient at the interface. Their asymptotic analysis has shown that the main effect of the flow on the solidification process is the production of traveling waves along the solidification interface, with a wave speed that can be either positive or negative. One of the possible physical explanations of the upstream propagation in these cases is the fact that the horizontal basic flow compresses the perturbed boundary layer at the upstream face of the surface perturbation, which facilitates the normal growth of the upstream face (Batchelor, Mofatt and Worster (2000)).

In the problems of ice growth under a water film, the solidification interface shape is driven by the temperature gradient, rather then concentration gradient and the analysis of ice growth under water films attracted much less attention then the solidification problems in casting and crystal growth. However for the aerodynamic icing problems this is a question of great importance, since the interaction between the ice surface can affect mean flow and add new mechanisms of instability and possibly influence the characteristics of transition to turbulence. The numerical simulation of flows past ice surface geometries on a wing done by Huebsch and Rothmayer (2000) has demonstrated that the influence of ice-induced roughness

can significantly change flow characteristics and lead to flow separation.

The question of the influence of an ice layer on the flow stability on a boundary layer scale has been tackled analytically by Rothmayer and Tsao (1998). They have developed a 2D viscous-inviscid interaction triple-deck theory in order to describe the interaction between the air boundary layer, water film and ice sheet. This triple-deck theory was further developed in Rothmayer and Tsao (2000-2). The important result of this study was the discovery of the new broad-band ice instability on regimes with simultaneous air and water cooling. Also unlike surface waves, the discovered instability propagated upstream, which was in good qualitative agreement with experimental results. However an attempt of quantitative comparison with experiments in Rothmayer and Tsao (2000-1) suggested that pure film model may fail to describe the creation of small-scale ice roughness. Furthermore the results of the research done in these works are a bit difficult to analyse since for the investigated regimes the water layer was supercooled in which case the steady-state solution as we will show later might not exist. Also in the case of an airfoil we are dealing with a complicated problem possessing instabilities even without ice layer, which makes the interpretation of the analytic results even more difficult.

The aim of this thesis is to consider gravity-driven water film flow down a cooled inclined plane and an air/water 2D Poiseuille flow between two planes with the water-coated wall maintained at a fixed sub-zero temperature, in order to understand how the interaction between the ice layer and the flow affects the stability characteristics of these problems. In both cases there exists a steady-state analytic solution for which it is possible to perform stability analysis.

For the free-surface flow problem we will first consider boundary-layer scale films

and develop a Froude-based double-deck theory in order to isolate icing instability. The new results obtained by this approach include an analytic dispersion relation for the case of $Pr = 1$ and detailed investigation of ice layer stability in a wide range of parameters. The effects of the non-linearity will be also considered.

Then, we will couple the analytic approach with the linear stability analysis and longwave asymptotics of the free-surface flow problem and demonstrate that the ice layer introduces a new instability mode in the free-surface gravity-driven flows. Apart from the detailed analysis of the ice instability mode behaviour, another important new result brought out by this approach is that the ice layer affects the behaviour of surface waves and stabilises them in the longwave limit.

Finally we will provide a simple physical explanation of the observed upstream propagation of ice surface perturbation and demonstrate that for the ice formation under free-surface flows, the upstream propagation is governed mainly by the interaction of the free surface shape and ice layer shape.

For the air/water/ice Poiseuille flow, we will perform longwave asymptotic analysis of the linear stability problem in order to investigate ice influence on the stability characteristics of the flow.

Also during the process of validation of the linear stability solver for air/water fluid channel flows, we discovered a new effect of mode coalescence in this well-investigated problem and one chapter of this thesis will be dedicated to the effect of mode-coalescence in the air/water Poiseuille channel flows. We will show that for these flows the interfacial mode can intersect and exchange branches with the Tollmien-Schlichting mode in water layer, producing a stable region inside the interfacial mode neutral curve. Previously, Blennerhassett (1980) in his well known work on the stability of the air/water channel flows mistook the neutral

curve corresponding to this stable region to the shear mode neutral curve. This new result together with detailed computations of stability characteristics for this problem clarifies the instability picture of two-fluid Poiseuille channel flows.

This thesis is subdivided into 6 parts. Part 1 presents the overview of the research done on the problem and explains the background of the problem. In Part 2 general problem formulation is given, boundary conditions are discussed and media properties that will be used throughout the whole thesis are determined. Also, in this part we will justify several assumptions made in the initial model and analyse $x$-independent flows in order to determine the conditions necessary for steady-state solutions to exist. Part 3 summarises the results for free-surface problems. Part 4 is dedicated to the investigation of the mode-coalescence effect in air/water Poiseuille channel flows. Part 5 presents the results for the ice formation in channel flows and, finally, conclusions are summarised in Part 6. Also there is an Appendix containing auxiliary derivations.

# 2 General problem formulation

In this chapter we will formulate the general problem for an air/water/ice flow and discuss boundary conditions and media properties. The problem is formulated at macroscopic scale. We consider the ice surface to be smooth and do not take the crystal nature of ice surface into account. This general problem formulation will be further used in order to derive equations and boundary conditions for problems in subsequent sections.

Let space coordinates be divided by the characteristic length $L^*$ and velocity by characteristic velocity $U^*$ appropriate for the problem in consideration, then the flow time scale is given by $\tau^* = \frac{L^*}{U^*}$. We will use the air flux in the incoming flow in order to normalise pressure for air/water/ice configurations as follows:

$$P = \frac{P^* - P_a^{*\infty}}{\rho_a^{*\infty} \cdot (u_a^{*\infty})^2}$$

Let us use the temperature difference $DT^*$, characteristic for a particular problem (for example, the difference between air temperature and water freezing temperature $T_a^{*e} - T_f^*$), in order to normalise temperature, also let us shift the temperature scale in order to make the dimensionless temperature corresponding to the freezing temperature 0. Then the dimensionless temperature will be given by:

$$T = \frac{T^* - T_f^*}{DT^*}$$

The following additional assumptions will be used in the general problem formulation:

- The temperature of the phase-change is constant (see Appendix A).
- All media properties are constant for all layers.
- Both upper and lower layer fluids are incompressible and Newtonian.
- The density of the solid phase is less than the density of the liquid phase ( $\frac{\rho_i}{\rho_l} < 1$ , see Appendix A).

The general scheme of a layered air/water/ice flow is given on the figure below:

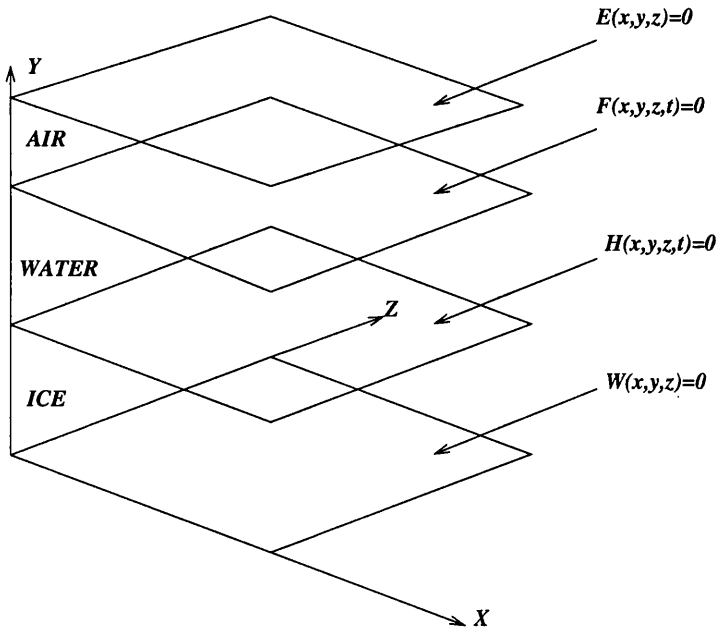


Figure 2.1: General flow scheme

## 2.1 Equations and boundary conditions

We will use the upper (air) layer media properties in order to build dimensionless values in the general case. Then, using the assumptions specified above, the governing equations in terms of the dimensionless variables in the upper (air) layer become:

$$\begin{cases} \frac{\partial \vec{V_a}}{\partial t} + \vec{V_a} \cdot \nabla \vec{V_a} = -\nabla P_a + \frac{1}{Re} \Delta \vec{V_a} + \frac{1}{Fr} \overrightarrow{Gm} \\ \nabla \cdot \vec{V_a} = 0 \\ \frac{\partial T_a}{\partial t} + \vec{V_a} \cdot \nabla T_a = \frac{1}{RePr} \Delta T_a \end{cases} \tag{2.1}$$

Here $Fr = \frac{gL^*}{U^{*2}}$ is the Froude number, $Re = \frac{U^* L^*}{\nu_a^*}$ is the Reynolds number, $Pr = \frac{\nu_a^*}{\chi_a^*}$ is the Prandtl number and $\overrightarrow{Gm}$ represents mass forces (gravity in our case). Viscous terms in the energy equations have been neglected, see Appendix B for justification. Also in all equations in this thesis we will denote the Laplacian operator by $\Delta$.

The governing equations in terms of the dimensionless variables in the middle (water) layer are given by:

$$\begin{cases} \frac{\partial \vec{V_l}}{\partial t} + \vec{V_l} \cdot \nabla \vec{V_l} = -\rho_{al} \nabla P_l + \frac{\nu_{la}}{Re} \Delta \vec{V_l} + \frac{1}{Fr} \overrightarrow{Gm} \\ \nabla \cdot \vec{V_l} = 0 \\ \frac{\partial T_l}{\partial t} + \vec{V}_l \cdot \nabla T_l = \frac{\chi_{la}}{RePr} \Delta T_l \end{cases} \tag{2.2}$$

Where according to our notation$\rho_{al} = \frac{\rho_a}{\rho_l}$ denotes the ratio of air density to water density, $\nu_{la} = \frac{\nu_l}{\nu_a}$ denotes the ratio of water kinematic viscosity to air kinematic viscosity and $\chi_{la} = \frac{\chi_l}{\chi_a}$ stands for the ratio of water thermometric conductivity to air thermometric conductivity.

The governing equation in terms of the dimensionless variables in the lower (ice) layer is given by:

$$\frac{\chi_{ia}}{RePr}\Delta T_i = \frac{\partial T_i}{\partial t} \tag{2.3}$$

Here $\chi_{ia} = \frac{\chi_i}{\chi_a}$ stands for the ratio of ice thermometric conductivity to water thermometric conductivity.

For the two-fluid flow and solid upper boundary (channel flow) we will consider no-slip and constant temperature conditions on the external boundary $E(x, y, z) = 0$:

$$\begin{cases} \vec{V_a} = 0 \\ T = T_a^e = const \end{cases} \tag{2.4}$$

At the air/water interface $F(x, y, z, t) = 0$, the following conditions will be used:

$$\begin{cases} \vec{V_a} \cdot \nabla F = -\frac{\partial F}{\partial t} \\ \vec{V_l} = \vec{V_a} \\ \left(-p_a\delta_{ij} + \frac{1}{Re}\left(\frac{\partial V_{ai}}{\partial x_j} + \frac{\partial V_{aj}}{\partial x_i}\right)\right) \cdot n_j - \frac{\kappa_{la}}{We} n_i = \\ \left(-p_l\delta_{ij} + \frac{\rho_{la}\nu_{la}}{Re}\left(\frac{\partial V_{li}}{\partial x_j} + \frac{\partial V_{lj}}{\partial x_i}\right)\right) \cdot n_j \\ T_l = T_a \\ \frac{\partial T_l}{\partial \vec{n}} = \lambda_{al}\frac{\partial T_a}{\partial \vec{n}} \end{cases} \tag{2.5}$$

$$i, j = 1, 2, 3$$

These conditions represent in turn the kinematic condition, the continuity of the velocity, stress, temperature and heat flux. Also here $\vec{n} = \frac{\nabla F}{|\nabla F|}$ is the unit normal

to the interface ($\frac{\partial}{\partial \vec{n}} = \vec{n} \cdot \nabla$), $\kappa_{la} = \nabla \cdot \frac{\nabla F}{|\nabla F|}$ is the curvature of the air/water interface and $We = \frac{\rho_a^* U^{*2} L^*}{\gamma^*}$ is the Weber number.

On the water/ice boundary $H(x, y, z, t) = 0$ the following conditions will be used:

$$\begin{cases} T_l = T_i = 0 \\ \lambda_{il} \frac{\partial T_i}{\partial \vec{n}} - \frac{\partial T_l}{\partial \vec{n}} = \frac{\chi_{al} Pr Re}{St} \frac{\vec{V_l} \cdot \nabla H}{|\nabla H|} \\ \vec{V_l} \cdot \nabla H = -\Theta_{il} \frac{\partial H}{\partial t} \end{cases} \tag{2.6}$$

where $\Theta_{il} = 1 - \frac{\rho_i}{\rho_l}$. The first condition specifies constant freezing temperature of the interface, the second one represents Stefan condition relating the difference of the heat flux on the ice boundary to the interface growth, and the last one represents the kinematic condition modified by the volume change effect. The Stefan number is defined using water specific heat $St = \frac{Cp_l DT}{H_{li}}$ , where $H_{li}$ is the latent heat of fusion. The derivation of the last two conditions and justification for the constant freezing temperature assumption can be found in Appendix A.

On the solid wall (lower ice) boundary $W(x, y, z) = 0$, the temperature is assumed to be a given function of coordinates:

$$T = T_w(x, z) \tag{2.7}$$

In most problems the lower wall temperature will be considered constant however for the nonlinear double-deck equations we will also consider varying wall temperature profiles.

## 2.2 Media properties

Ice properties depend on the type of ice and conditions under which it is formed. Since we consider an ice layer growing under a film of unfrozen water, it is reasonable to assume that we are dealing with glaze ice (see Poots (1996)). Glaze icing occurs both in channel flow and in inclined plane cases. In the case of ice accretion on structures under wetting rain conditions - rime ice can grow initially. However, as the initial rime layer grows in this case, transition from rime to glaze accretion occurs leading to the formation of glaze ice layer which then grows under a water film running on ice-covered surface (Poots (1996)). In the case of the aircraft wing icing, the surface water model of ice formation (see for example Rothmayer and Tsao (2000-2)) also assumes that the ice growth occurs under a water film formed by the supercooled droplets of water hitting the wing surface. And indeed Vargas and Reshotko (1998, 2000) observed glaze ice growth in their experiments with swept wings icing.

Therefore we will assume that we are dealing with glaze ice at 273K and choose water/air properties at this temperature. The following formulae for the thermal conductivity and the specific heat of ice were used in order to compute glaze ice properties at a given temperature (Alexiades and Solomon (1993)):

$$\lambda_i = 2.24 + 5.975 \cdot (273 - T)^{1.156} \cdot 10^{-3}$$

$$Cp_i = 1380 + 7.16 \cdot T$$

Latent heat for ice/water phase change was taken to be 333.4 $\frac{kJ}{kg}$. Surface tension coefficient was taken to be $S = 73.5 \cdot 10^{-3} \frac{N}{m}$ in order to make the results for

channel flows comparable with those of Blennerhassett (1980). The table below summarises the media properties used for air, water and ice. Ice properties have been taken from Poots (1996), Hobbs (1974) and Alexiades and Solomon (1993). Water and air properties have been taken from Cohen, Lide and Trigg (2003).

| **Property** | **Air** | **Water** | **Glaze Ice** |
|---|---|---|---|
| $\rho, \frac{kg}{m^3}$ | 1.293 | 999.8 | 920 |
| $\lambda, \frac{J}{m \cdot s \cdot K}$ | $2.42 \cdot 10^{-2}$ | 0.561 | 2.24 |
| $Cp, \frac{J}{kg \cdot K}$ | 1004 | 4218 | 2092.7 |
| $\chi, \frac{J}{kg \cdot K}$ | $1.92 \cdot 10^{-5}$ | $1.3303 \cdot 10^{-7}$ | $1.17 \cdot 10^{-6}$ |
| $\mu, \frac{kg}{m \cdot s}$ | $1.709 \cdot 10^{-5}$ | 0.001792 | - |
| $\nu, \frac{m^2}{s}$ | $1.32 \cdot 10^{-5}$ | $1.792 \cdot 10^{-6}$ | - |

Table 2.1: Media properties

## 2.3 Timescale analysis for water/ice flows

In this section we will attempt to derive an estimate for the ratio of the flow and ice growth timescales. The Stefan condition links the heat flux difference at the

water/ice boundary to the development of the ice surface shape. The starting point for us will be the assumption that the ice surface evolution occurs on a timescale different from that of the flow evolution timescale. Then we will analyse the Stefan condition in order to derive an estimate for the ratio of these timescales.

Let us denote the dimensional characteristic time for the ice growth in the problem by $\tau_i^*$. In general, this characteristic time can be different from the flow timescale $\tau_{flow}^* = \frac{L^*}{U^*}$. From the equations it can be seen that the Stefan condition is the only condition relating ice growth with the water flow. The Stefan condition can be written in the dimensional form as:

$$\lambda_i^* \frac{\partial T_i^*}{\partial \vec{n^*}} - \lambda_l^* \frac{\partial T_l^*}{\partial \vec{n^*}} = V_{ln}^* \rho_l^* H_{li} = -\Theta_{il} \rho_l^* H_{li} \frac{1}{\nabla H^*} \frac{\partial H^*}{\partial t^*}$$

Let us also assume that there are two different length scales in the problem $x^* \sim z^* \sim L^*$ and $y^* \sim H^*$ (with $y^*$ measuring normal distance from the solid wall) and the flow is close to a parallel one, i.e. $\frac{\partial}{\partial \vec{n^*}} \sim \frac{1}{H^*}$. Using the specified characteristic values, we obtain the dimensionless Stefan condition in the following form:

$$\lambda_{il} \frac{\partial T_i}{\partial \vec{n}} - \frac{\partial T_l}{\partial \vec{n}} = \frac{H^*}{\lambda_l^* DT^*} \Theta_{il} \rho_l^* H_{li} \frac{H^*}{\tau_i} \frac{1}{\nabla H} \frac{\partial H}{\partial t} = \Theta_{il} \frac{1}{StSh} X^2 PrRe \frac{1}{\nabla H} \frac{\partial H}{\partial t} \quad (2.8)$$

Here $Sh = \frac{\tau_i^*}{\tau_{flow}^*} = \frac{\tau_i^* U^*}{L^*}$ is the Strouhal number and $X = \frac{H^*}{L^*}$ is a stretching factor. Also in the Reynolds number and the Prandtl number in **(2.8)** are based on the liquid layer properties.

In order to preserve the interaction between the ice layer growth and the flow in our model, it is necessary to maintain the full form of the Stefan condition. Then the dimensionless combination on the right-hand side of **(2.8)** - $\Theta_{il} \frac{1}{StSh} X^2 PrRe$

should be of order $O(1)$, which yields the following estimate on the Strouhal number of the problem:

$$Sh \sim \Theta_{il} \frac{1}{St} X^2 Pr Re \tag{2.9}$$

The Stefan number for water/ice interface and $DT \sim O(1)$ is of order $10^{-2}$. Using the values of media properties given in the Table 2.1, we obtain that near $0^0C$ - $Pr = 13.47$ and $\Theta_{il} = 1 - \rho_{il} = 0.0798$. Then for the water/ice phase transition under specified conditions:

$$Sh \sim 10^2 \cdot X^2 Re$$

For the boundary layer scale icing $X^2 \sim \frac{1}{Re}$. For experimental channel flows (for example, Gilpin (1981, 1979)) and inclined planed flows (Streitz, Ettema, Rothmayer and Tsao (1998)) we have $X^2 Re \gg 1$, therefore for both configurations, the derived estimate yields:

$$\tau_i^* \gg \tau_{flow}^* \tag{2.10}$$

This result is fairly well known from the experiments and it shows that on the flow development time scale, the ice layer can be considered quasi-steady. Also this qualitative analysis shows that the dependence between the time for the ice structure to reach the final steady state should be inversely proportional to the Stefan number. This fact was observed in numerical computations of ice growth in a pipe flow by Lee (1993).

## 2.4 X-independent planar flows

In a certain case of icing flows in the $(x, y)$ plane, the velocity and temperature fields can become independent of the streamwise coordinate. These flow regimes can reflect an $x$-independent geometry, for example an infinite inclined plane or an infinite channel. If the flow evolves with time, in general, such flow is not unidirectional on account of the change of the water/air interface position. The aim of the study of such flows is two-fold. First, we will try to understand when a steady-state unidirectional flow solution can be found for given external parameters (such as air temperature and wall temperature). The second question is whether such steady state can be attained in a temporally evolving flow given an $x$-independent initial state which does not necessarily match the steady-state solution. As an example of a problem where the second issue is relevant, one may think of a gravity-driven water film in an inclined channel filled with air where the upper wall is moving with a constant velocity. The movement of the upper wall allows us to incorporate the interaction between the air and the water layers in a finite domain in the wall-normal direction. When the lower wall temperature is below $0^oC$, the layer of ice is formed on the lower wall. The scheme of this configuration is given below:

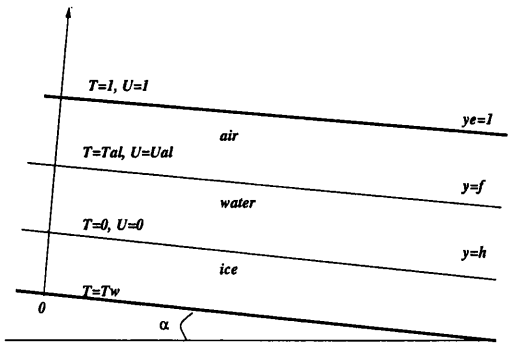


Figure 2.2: $x$-independent problem scheme

Here $T_{al}$ and $U_{al}$ denote the values of temperature and velocity at the air/water interface. In a steady-state, the configuration shown on the diagram above produces a plane Couette flow in the absence of gravity (zero angle of incline or very large Froude number) and a mixed Poiseuille-Couette flow when the effects of gravity are significant.

In the current section we will formulate the $x$-independent problem, then we will derive steady solutions and analyse conditions under which these exist, and finally we will solve the $x$-independent problem numerically in order to investigate the solution behaviour as it approaches the steady state.

### 2.4.1 Problem formulation

The $x$-independent problem we are considering is governed by the following set of equations for the velocity and temperature in air and water layers and temperature in the ice layer respectively (these equations follow directly from the equations **(2.1)-(2.3)** of the "2.1 Equations and boundary conditions" section):

$$\begin{cases} \frac{\partial u_a}{\partial t} + v_a \frac{\partial u_a}{\partial y} = \frac{1}{Re} \frac{\partial^2 u_a}{\partial y^2} \\ \frac{dv_a}{dt} = -\frac{\partial P_a}{\partial y} \qquad (air) \\ \frac{\partial T_a}{\partial t} + v_a \frac{\partial T_a}{\partial y} = \frac{1}{RePr} \frac{\partial^2 T_a}{\partial y^2} \end{cases} \tag{2.11}$$

$$\begin{cases} \frac{\partial u_l}{\partial t} + v_l \frac{\partial u_l}{\partial y} = \frac{\nu_{la}}{Re} \frac{\partial^2 u_l}{\partial y^2} + \frac{1}{Fr} \sin\alpha \\ \frac{dv_l}{dt} = -\frac{\partial P_l}{\partial y} \rho_{al} - \frac{1}{Fr} \cos\alpha \qquad (water) \\ \frac{\partial T_l}{\partial t} + v_l \frac{\partial T_l}{\partial y} = \frac{\chi_{la}}{RePr} \frac{\partial^2 T_l}{\partial y^2} \end{cases} \tag{2.12}$$

$$\begin{cases} \frac{\partial T_i}{\partial t} = \frac{\chi_{ia}}{RePr} \frac{\partial^2 T_i}{\partial y^2} \\ T(0) = T_w = const \end{cases} (ice) \tag{2.13}$$

Here $u_{a,l}$, $v_{a,l}$ and $T_{a,l,i}$ are functions of $y$ and $t$ only.

Let us choose the velocity at the upper air boundary $U_a^e$ as the characteristic velocity and normalise the temperature as described in the "2.1 Equations and boundary conditions" section. Also let us normalise the $y$ coordinate by the overall height of the channel. Then the boundary conditions are given by:

$$\begin{cases} u_a = 1 \\ T_a = 1 \end{cases} \quad (y = 1) \tag{2.14}$$

$$\begin{cases} u_a = u_l, \frac{\partial u_a}{\partial y} = \nu_{la}\rho_{la}\frac{\partial u_l}{\partial y} \\ v_a = v_l = \frac{df}{dt} \\ T_a = T_l, \frac{\partial T_a}{\partial y} = \lambda_{la}\frac{\partial T_l}{\partial y} \end{cases} \quad (y = f(t)) \tag{2.15}$$

$$\begin{cases} u_l = 0 \\ v_l = \Theta_{il}\frac{dh}{dt} \\ T_l = T_i = 0 \\ \lambda_{il}\frac{\partial T_i}{\partial y} - \frac{\partial T_l}{\partial y} = \frac{\chi_{al} Pr Re}{St} v \end{cases} \quad (y = h(t)) \tag{2.16}$$

Since the flow is $x$-independent, from the continuity equation it follows that vertical velocities in air and water layers $v_{a,l}$ are functions of time only. Also since from the boundary conditions at the air/water interface $v_a(t) = v_l(t)$ we will denote the vertical velocity in both air and water layers as $v(t)$. The air/water interface shape $f$ and the ice surface shape $h$ are the functions of time only, therefore from the kinematic boundary conditions at the air/water and water/ice interfaces it follows that:

$$v = \frac{df}{dt} = \Theta_{il}\frac{dh}{dt} \Rightarrow \frac{d(\Theta_{il}h - f)}{dt} = 0 \Rightarrow f(t) - \Theta_{il}h(t) = const \tag{2.17}$$

Let us denote the value of the constant $f(t) - \Theta_{il}h(t)$ by $\alpha_{fh}$. The equation **(2.17)** indicates that the shapes of the free surface and water/ice interface are not independent and $\alpha_{fh}$ is the invariant of the problem which is determined by the initial conditions. Since $f > h$, then if we assume that $\Theta_{il} = 1 - \frac{\rho_i}{\rho_l} < 1$, it follows from **(2.17)** that $\alpha_{fh} > 0$. The equation **(2.17)** represents the way the initial water film thickness is affected by ice growth. It can be rewritten as $\frac{d(f-h)}{dt} = -\frac{\rho_i}{\rho_l}\frac{dh}{dt}$, showing that the water film thickness derivative is related to the ice layer thickness derivative with a coefficient describing volume change effect. In the limiting case as $\rho_i \to 0$, the liquid film thickness is constant.

### 2.4.2 Steady solutions

**2.4.2.1 Air/Water/Ice** Let us consider a steady unidirectional system in order to determine the conditions for steady parallel solutions to exist. When the flow is steady - the temperature field is not linked with the velocity field through the Stefan condition. This means that the boundary-value problem for velocity fields can be solved independently of the boundary-value problem for the temperature profiles. From the kinematic conditions at the air/water and water/ice interfaces it follows that in the steady state $v = 0$. Then the profiles of the horizontal velocity in air and water can be determined from the following boundary-value problem:

$$\begin{cases} \frac{\partial^2 u_a}{\partial y^2} = 0, \ y \in [f, 1] \\ \frac{\partial^2 u_l}{\partial y^2} = -\frac{Re\nu_{al}}{Fr}\sin\alpha, \ y \in [h, f] \\ u_a(1) = 0 \\ u_a(f) = u_l(f), \frac{\partial u_a}{\partial y} = \mu_{la}\frac{\partial u_l}{\partial y} \\ u_l(h) = 0 \end{cases} \tag{2.18}$$

Let us use the symbol $d$ for $-\frac{Re\nu_{al}}{Fr}\sin\alpha$ in order to simplify the notation, then the solution to this problem in the air layer is given by the following linear function:

$$u_a = y\frac{\mu_{la}(2+d(f-h)^2)}{2(f-h+\mu_{la}(1-f))} + \frac{\mu_{la}f^2d+h(2+hd\mu_{la})-2f(1+\mu_{la}(hd-1))}{2(h-f+\mu_{la}(f-1))} \tag{2.19}$$

In the water layer, from **(2.18)** we obtain the following parabolic profile of the horizontal velocity $u_l$:

$$\begin{array}{l} u_l = d\frac{y^2}{2} + y\frac{2-d(-h^2+f^2(1-2\mu_{la})+2f\mu_{la})}{2(f-h+\mu_{la}(1-f))} + \\ +\frac{h(2+d(h\mu_{la}+f^2(2\mu_{la}-1)+f(h-2\mu_{la}-h\mu_{la})))}{2(h-f+\mu_{la}(f-1))} \end{array} \tag{2.20}$$

From the equations for the temperature in **(2.11)-(2.13)** it follows that in a steady state the temperature profiles are linear. If we denote the temperature at the air/water interface by $T_{al}$, the solutions for the temperature in air, water and ice are given by:

$$\begin{cases} T_a = \frac{y-f}{1-f}(1-T^{al}) + T^{al} \\ T_l = \frac{y-h}{f-h}T^{al} \\ T_i = \frac{h-y}{h}T_w \end{cases} \tag{2.21}$$

Here $T^{al}$, $f$ and $h$ are unknown and should be determined from the heat flux equivalence conditions at the air/water and water/ice interfaces:

$$\begin{cases} -\frac{T_w}{h}\lambda_{il} = \frac{T^{al}}{f-h} \\ T^{al}\frac{\lambda_{la}}{f-h} = \frac{1-T^{al}}{1-f} \end{cases}$$

It can be seen that for the steady-state problem as formulated we lack one condi-

tion in order to determine the solution. Let us give an interpretation that can help understand the lack of one boundary condition. Provided the media properties are known, the geometry of the flow ($f$ and $h$) uniquely determines velocity profiles. However the choice of the flow geometry should be such that the heat flux can be balanced at water/ice and air/water interfaces. The geometry for which the heat flux can be balanced at these interfaces is not unique and it can be selected by specifying one additional condition. For example, we can fix the ice height $h$ and determine the solution. However there is no steady solution for the supercooled water layer since if $T^a < 0$, then we have $T^{al} < 0$, then from the heat flux continuity condition on the ice surface we get $f < h$. In order for the water not to become supercooled, we need to require that the temperature in both air and water is above the freezing temperature (i.e. above 0 in our normalisation).

Now if we consider a steady state that is a result of the flow evolution problem **(2.11)-(2.16)**, then the natural choice of the additional condition that we need in order to determine the steady state is the invariant $\alpha_{fh}$. This constant links the steady state with the initial conditions of the flow evolution problem.

Given the additional condition in the form of $\alpha_{fh}$ invariant, we can determine the flow geometry in terms of $\alpha_{fh}$ and wall temperature $T_w$. Let us denote $-T_w$ as $\Omega_w$ in order to operate with positive quantities, then the coordinates of the ice surface and water surface are given by:

$$h(\alpha_{fh}, \Omega_w) = \frac{(\alpha_{fh}(1-\lambda_{la})+\lambda_{la})\Omega_w}{\lambda_{li}+\Omega_w(1+\Theta_{il}(\lambda_{la}-1))} \tag{2.22}$$

$$f(\alpha_{fh}, \Omega_w) = \frac{\alpha_{fh}\lambda_{li}+\alpha_{fh}\Omega_w+\Theta_{il}\lambda_{la}\Omega_w}{\lambda_{li}+\Omega_w(1+\Theta_{il}(\lambda_{la}-1))} \tag{2.23}$$

These expressions can be used in order to determine whether a steady state exists for given media properties, $\alpha_{fh}$ invariant and relative wall temperature $\Omega_w$. For the solution to exist we need $0 < h < f < 1$ to be true. This leads to the following conditions on the parameters of the problem:

1. Since $h > 0$, from **(2.22)** we obtain $\alpha_{fh} < \frac{\lambda_{la}}{\lambda_{la}-1}$. For the air and water properties specified in the Table 2 of this chapter $\frac{\lambda_{la}}{\lambda_{la}-1} = 1.04483$.

2. Since $h < f$, from **(2.17)** we obtain $h < \frac{\alpha_{fh}}{1-\Theta_{il}}$. Using **(2.22)** this condition can be rewritten as $\alpha_{fh} > \frac{(1-\Theta_{il})\Omega_w\lambda_{la}}{\lambda_{li}+\Omega_w\lambda_{la}}$.

3. From $f < 1$, using **(2.23)** we obtain $\alpha_{fh} < \frac{\lambda_{li}+(1-\Theta_{il})\Omega_w}{\lambda_{li}+\Omega_w}$.

Since for air/water/ice, for any $\Omega_w$ we have $\frac{\lambda_{la}}{\lambda_{la}-1} > \frac{\lambda_{li}+(1-\Theta_{il})\Omega_w}{\lambda_{li}+\Omega_w}$, the domain of solution existence is bounded by $h = f$ and $f = 1$ curves. An interesting feature is that as $\Omega_w \Rightarrow \infty$ both curves have the same limit $\alpha_{fh} = (1 - \Theta_{il})$ i.e. the domain of existence tends to zero as the lower wall temperature decreases for the fixed temperature of the upper wall:

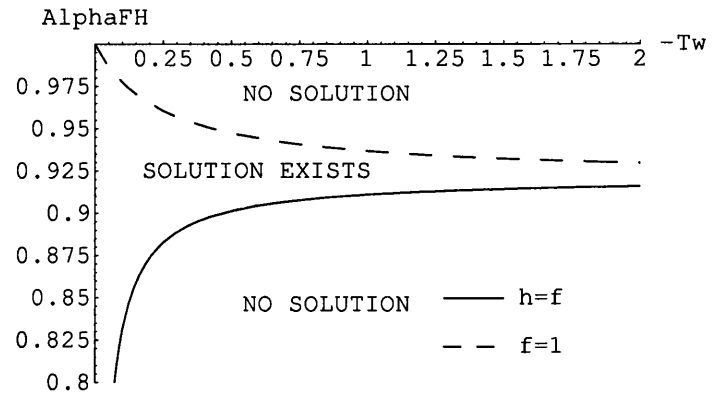


Figure 2.3: The domain of steady solution existence for air/water/ice flow

On the figure above, "no solution" describes the situation when all water is frozen. If we specify such $\alpha_{fh}$ and $T_w$ that they are out of the existence region specified on the diagram above, the water film thickness becomes zero in a finite time:

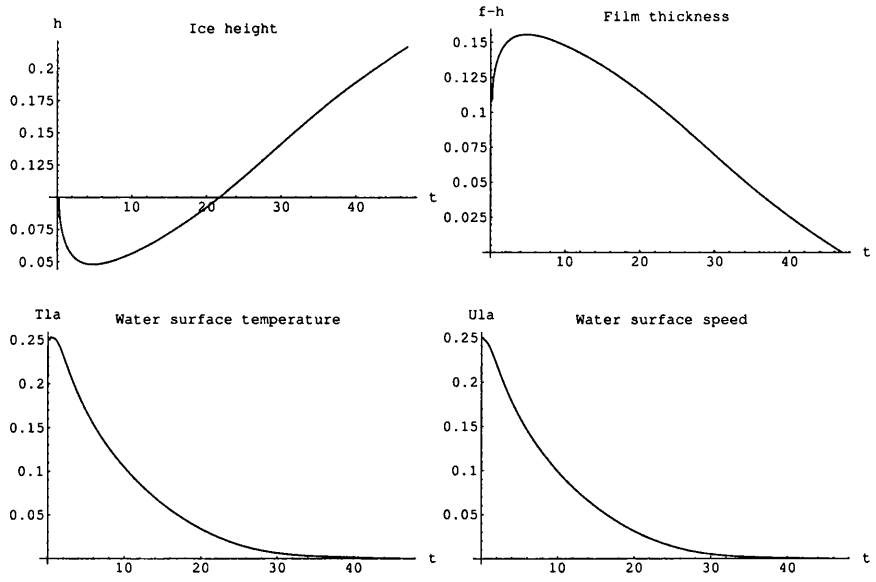


Figure 2.4: The evolution of water film under freezing conditions

The plots above show the behaviour of the problem parameters ($h$, $f-h$ , $T_{la}$ and $U_{la}$) as functions of time in such case ($\alpha_{fh} = 0.2$ and $T_w = -0.2$). Note that the film thickness does not approach zero asymptotically, but the interface temperature and velocity do.

The results presented in this section lead to the following question - what does it mean that the steady state solution does not exist for the flow evolution problem. Does this mean that the $x$-independent formulation is not a limiting case of a flow with constant water mass flux at $x = -\infty$? The answer to this question follows from the formulation of the problem **(2.11)-(2.16)**. This formulation does not contain any reference to the water mass-flux into the system and in fact it cannot

contain such a reference. As soon as we make an assumption that there are some conditions imposed on the left boundary - we introduce dependence on $x$ into the problem. When we specify that we are looking for the $x$-independent solution, we immediately obtain the $\alpha_{fh}$ invariant. This invariant means that the conservation of total mass is imposed on the system. The $\frac{d}{dt}(\rho_l(f-h)+\rho_i h) = 0$ relation that follows immediately from the equation **(2.17)** represents the conservation of mass. Therefore a problem with a constant water mass flux into the system does not have a solution in the $x$-independent domain in this configuration. Note that the analysis of the existence of steady solutions we have performed can still be applied in these cases, however for these problems another choice of the additional condition necessary to close the problem will be more relevant.

**2.4.2.2 Water/Ice** Let us neglect the air layer and consider the steady state solutions for water and ice only (as in the inclined plane gravity-driven film case). If we impose constant temperature condition at the free surface and use this temperature in normalisation ( $T = \frac{T^*-T_f^*}{T_a^*-T_f^*}$), then in the steady case, the solution for the temperature will be the following:

$$\begin{cases} T_l = \frac{y-h}{f-h} \\ T_i = \frac{h-y}{h} T_w \end{cases} \tag{2.24}$$

Applying heat flux continuity on water/ice boundaries and using mass flux condition as for air/water/ice case, we obtain:

$$\begin{cases} -\frac{T_w}{h}\lambda_{il} = \frac{1}{f-h} \\ f - \Theta_{il} h = \alpha_{fh} \end{cases} \tag{2.25}$$

In this case also if the air temperature is below freezing $T_a^* < T_f^*$ and the wall temperature is below freezing $T_w^* < T_f^*$, then the dimensionless wall temperature $T_w > 0$ and from the heat flux balance on the ice/water boundary we obtain that either $h < 0$ or $f < h$. And in terms of the invariant for the unsteady problem $\alpha_{fh}$, the ice surface coordinate $h$ is given by:

$$h(\alpha_{fh}, \Omega_{wa}\lambda_{li}) = \frac{\alpha_{fh}\Omega_w}{\lambda_{li} + \Omega_w(1 - \Theta_{il})} \tag{2.26}$$

In this case $h$ and $f - h$ are always greater then 0 and a steady solution with a linear temperature profile exists for any choice of the $\alpha_{fh}$ invariant (provided that wall temperature is negative and water surface temperature is positive). This is what we should expect as the water film cannot freeze completely since we specify that the free-surface temperature is positive. Also in this case the thickness of the film is not bounded by the upper wall.

### 2.4.3 Numerical solution for the unsteady problem

We assume that the $y$ component of the velocity is the function of time only, therefore it is possible to eliminate it from the equations using the boundary condition $v(t) = \Theta_{il}\frac{dh}{dt}$. We can also express $f$ in terms of $h$ using $f(t) - \Theta_{il}h(t) = \alpha_{fh}$. Then we obtain the following system of equations in air, water and ice respectively:

$$\begin{cases} \frac{\partial u_a}{\partial t} + \Theta_{il} \cdot \frac{dh}{dt} \cdot \frac{\partial u_a}{\partial y} = \frac{1}{Re}\frac{\partial^2 u_a}{\partial y^2} \\ \frac{\partial T_a}{\partial t} + v_a\frac{\partial T_a}{\partial y} = \frac{1}{RePr}\frac{\partial^2 T_a}{\partial y^2} \end{cases} \tag{2.27}$$

$$\begin{cases} \frac{\partial u_l}{\partial t} + \Theta_{il} \cdot \frac{dh}{dt} \cdot \frac{\partial u_l}{\partial y} = \frac{\nu_{la}}{Re} \frac{\partial^2 u_l}{\partial y^2} + \frac{1}{Fr} \sin \alpha \\ \frac{\partial T_l}{\partial t} + \Theta_{il} \cdot \frac{dh}{dt} \cdot \frac{\partial T_l}{\partial y} = \frac{\chi_{la}}{RePr} \frac{\partial^2 T_l}{\partial y^2} \end{cases} \tag{2.28}$$

$$\left\{ \frac{\partial T_i}{\partial t} = \frac{\chi_{ia}}{RePr} \frac{\partial^2 T_i}{\partial y^2} \right. \tag{2.29}$$

If we choose $U_a^e$ as the characteristic velocity and non-dimensionalise temperature as described in the general problem formulation ("2.1 Equations and boundary conditions" section), then the boundary conditions for this system are given by:

$$\begin{cases} u_a = 1 \\ T_a = 1 \end{cases} \quad (y = 1) \tag{2.30}$$

$$\begin{cases} u_a = u_l, \frac{\partial u_a}{\partial y} = \nu_{la} \rho_{la} \frac{\partial u_l}{\partial y} \\ T_a = T_l, \frac{\partial T_a}{\partial y} = \lambda_{la} \frac{\partial T_l}{\partial y} \end{cases} \quad (y = \alpha_{fh} + \Theta_{il} \cdot h(t)) \tag{2.31}$$

$$\begin{cases} u_l = 0 \\ T_l = T_i = 0 \\ \lambda_{il} \frac{\partial T_i}{\partial y} - \frac{\partial T_l}{\partial y} = \frac{\chi_{al} \cdot Pr \cdot Re}{St} \Theta_{il} \cdot \frac{dh}{dt} \end{cases} \quad (y = h(t)) \tag{2.32}$$

$$\{T = T_w = const \ (y = 0) \tag{2.33}$$

Here we have used the equation **(2.17)** in to obtain the expression for the air/water interface position in terms of the water/ice interface position.

In order to obtain the solution to the above system we will perform coordinate transformations in order to map the $y$ computational domain in each layer onto $[0, 1]$.

Then we will construct an iterative Newton method (see, for example, Isaacson and Keller (1966)) as follows:

- Consider $h$, $U_{la} = u_a(f)$ and $T_{la} = T_a(f)$ given, then we can obtain solution for each media and we will not need three of our boundary conditions (the Stefan condition, temperature flux balance and stress tensor continuity on air/water boundary).
- These three omitted boundary conditions are satisfied for the correct values of $(h, U_{la}, T_{la})$. Construct a vector function:

$$\vec{G}(h, U_{la}, T_{la}) = \begin{pmatrix} G_1(h, T_{la}) \\ G_2(h, T_{la}) \\ G_3(h, U_{la}) \end{pmatrix} = \begin{pmatrix} \lambda_{il}\frac{\partial T_i}{\partial y} - \frac{\partial T_i}{\partial y} - \frac{\chi_{al}\cdot Pr\cdot Re}{St}\Theta_{il}\cdot\frac{dh}{dt} \\ \frac{\partial T_a}{\partial y} - \lambda_{la}\frac{\partial T_l}{\partial y} \\ \frac{\partial u_a}{\partial y} - \nu_{la}\rho_{la}\frac{\partial u_l}{\partial y} \end{pmatrix} \tag{2.34}$$

- The correct values of $h$, $U_{la}$ and $T_{la}$are given by $\vec{G}(h, U_{la}, T_{la}) = 0$. In order to find them we will use Newton iterations on each time step.

**2.4.3.1 Air layer** Consider the following $(y,t) \Rightarrow (z,t)$ coordinate transformation in the air layer:

$$z = \frac{y - \Theta_{il}h - \alpha_{fh}}{1 - \Theta_{il}h - \alpha_{fh}} \tag{2.35}$$

This transformation maps the air layer $[f, 1]$ domain in $y$ onto $[0, 1]$ domain in $z$. The derivatives of this transformation are given by:

$$\begin{cases} \frac{\partial z}{\partial t} = -\frac{\Theta_{il}}{F_a}\frac{\partial h}{\partial t}(1 - z) \\ \frac{\partial z}{\partial y} = -\frac{1}{F_a} \end{cases} \tag{2.36}$$

Here $F_a = 1 - \Theta_{il} \cdot h - \alpha_{fh}$ is the thickness of the air layer. Then the equations and boundary conditions for the air layer in the new coordinate system become:

$$\begin{cases} \frac{\partial u_a}{\partial t} + \frac{\Theta_{il}}{F_a}\frac{dh}{dt} z \frac{\partial u_a}{\partial z} = \frac{1}{Re}\frac{1}{F_a^2}\frac{\partial^2 u_a}{\partial z^2} \\ \frac{\partial T_a}{\partial t} + \frac{\Theta_{il}}{F_a}\frac{dh}{dt} z \frac{\partial T_a}{\partial z} = \frac{1}{RePr}\frac{1}{F_a^2}\frac{\partial^2 T_a}{\partial z^2} \\ u_a(1,t) = 1 \; u_a(0,t) = U_{la} \\ T_a(1,t) = 1, \; T_a(0,t) = T_{la} \\ u_a(z,0) = u_{0a}(z), \; T_a(z,0) = T_{0a}(z) \end{cases} \tag{2.37}$$

The solution of the above problem can be obtained if we know the values of the temperature of the air/water interface $T_{la}$, velocity of the air/water interface $U_{la}$ and ice thickness $h$.

**2.4.3.2 Water layer** Similarly, consider the following $(y,t) \Rightarrow (z,t)$ coordinate transformation in the water layer:

$$z = \frac{y - h}{(\Theta_{il} - 1)h + \alpha_{fh}} \tag{2.38}$$

This transformation maps the water layer $[h, f]$ domain in $y$ onto $[0,1]$ domain in $z$. The derivatives of this transformation are given by:

$$\begin{cases} \frac{\partial z}{\partial t} = -\frac{1}{F_l}\frac{\partial h}{\partial t}(1 + z(\Theta_{il} - 1)) \\ \frac{\partial z}{\partial y} = \frac{1}{F_l} \end{cases} \tag{2.39}$$

Here $F_l = (\Theta_{il} - 1) \cdot h + \alpha_{fh}$ is the thickness of the water layer.

Then the equations and boundary conditions in the water layer in the new coordinate system are given by the system **(2.40)**.

$$\begin{cases} \frac{\partial u_l}{\partial t} + \frac{\Theta_{il}-1}{F_l}\frac{dh}{dt}(1-z)\frac{\partial u_l}{\partial z} = \frac{1}{Re}\frac{1}{F_l^2}\frac{\partial^2 u_l}{\partial z^2} + \frac{1}{Fr}\sin\alpha \\ \frac{\partial T_l}{\partial t} + \frac{\Theta_{il}-1}{F_l}\frac{dh}{dt}(1-z)\frac{\partial T_l}{\partial z} = \frac{\chi_{al}}{RePr}\frac{1}{F_l^2}\frac{\partial^2 T_l}{\partial z^2} \\ u_l(1) = U_{la},\ u_l(0) = 0 \\ T_l(1) = T_{la},\ T_l(0) = 0 \\ u_l(z,0) = u_{0l}(z),\ T_l(z,0) = T_{0l}(z) \end{cases} \tag{2.40}$$

**2.4.3.3 Ice** Finally, for the ice layer, we will use the following $(y,t) \Rightarrow (z,t)$ coordinate transformation:

$$z = \frac{y}{h} \tag{2.41}$$

The derivatives of this transformation are given by:

$$\begin{cases} \frac{\partial z}{\partial t} = -\frac{z}{F_i}\frac{\partial h}{\partial t} \\ \frac{\partial z}{\partial y} = \frac{1}{F_i} \end{cases} \tag{2.42}$$

Here $F_i = h$ is the ice layer thickness. Then the equations and boundary conditions in the new coordinate system become:

$$\begin{cases} \frac{\partial T_i}{\partial t} - \frac{z}{F_i}\frac{dh}{dt}\frac{\partial T_i}{\partial z} = \frac{\chi_{ia}}{RePr}\frac{1}{F_i^2}\frac{\partial^2 T_i}{\partial z^2} \\ T_i(1) = 0,\ T_i(0) = T_w \end{cases} \tag{2.43}$$

**2.4.3.4 Numerical scheme** We will use a finite difference second order implicit method in order to solve the equations in each layer.

Differential equations will be approximated on an equally-spaced grid using constant time step **(2.44)**.

$$\begin{cases} z^i_{a,l,i} = \Delta Z_{a,l,i} \cdot i \\ t^j = \Delta t \cdot j \\ i = [0, N_y^{a,l,i} - 1] \\ j = [0, N_t - 1] \end{cases} \tag{2.44}$$

The second order backward approximation will be used for time derivatives:

$$\frac{\partial u^{i,j}_{a,l}}{\partial t} = \frac{3u^{i,j}_{a,l} - 4u^{i,j-1}_{a,l} + u^{i,j-2}_{a,l}}{\Delta t} + O(\Delta t^2) \tag{2.45}$$

The central differences discretisation will be used for space derivatives:

$$\frac{\partial u^{i,j}_{a,l}}{\partial y} = \frac{u^{i+1,j}_{a,l} - u^{i-1,j}_{a,l}}{\Delta Z_{a,l}} + O(\Delta Z^2_{a,l}) \tag{2.46}$$

$$\frac{\partial^2 u^{i,j}_{a,l}}{\partial y^2} = \frac{u^{i+1,j}_{a,l} - 2u^{i,j}_{a,l} + u^{i-1,j}_{a,l}}{\Delta Z_{a,l}} + O(\Delta Z^2_{a,l}) \tag{2.47}$$

Then each differential equation can be transformed into a linear system of grid equations with tridiagonal matrix in the following form:

$$\begin{cases} a_{i-1,j} u^{i-1,j}_{a,l} + b_{i-1,j} u^{i,j}_{a,l} + c_{i-1,j} u^{i+1,j}_{a,l} = d_{i-1,j} \\ i = [1, N-1] \\ u^{0,j}_a = U_{la}, u^{0,j}_l = 0 \\ u^{N-1,j}_a = U^e_a, u^{N-1,j}_l = U_{la} \end{cases} \tag{2.48}$$

$$\begin{cases} a_{i-1,j}T_{a,l,i}^{i-1,j} + b_{i-1,j}T_{a,l,i}^{i,j} + c_{i-1,j}T_{a,l,i}^{i+1,j} = d_{i-1,j} \\ i = [1, N-1] \\ T_a^{0,j} = T_{la}, T_l^{0,j} = 0, T_i^{0,j} = T_w \\ T_a^{N-1,j} = T_a^e, T_l^{N-1,j} = T_{la}, T_i^{N-1,j} = 0 \end{cases} \tag{2.49}$$

The coefficients of the tridiagonal systems are given in the following tables:

| $T$ | | |
|---|---|---|
| | **Air** | **Water** |
| $a_{i,j}$ | $-\frac{\Theta_{il}}{2}\frac{dh}{dt}(i+1)F_a - \frac{1}{RePr}\frac{1}{\Delta Z_a^2}$ | $-\frac{\Theta_{il}-1}{2\Delta Z_l}\frac{dh}{dt}(1-(i+1)\Delta Z_l)F_l - \frac{1}{RePr}\frac{\chi_{la}}{\Delta Z_l^2}$ |
| $b_{i,j}$ | $\frac{3}{2}\frac{F_a^2}{\Delta t} + \frac{2}{RePr}\frac{1}{\Delta Z_a^2}$ | $\frac{3}{2}\frac{F_l^2}{\Delta t} + \frac{2\chi_{la}}{RePr}\frac{1}{\Delta Z_l^2}$ |
| $c_{i,j}$ | $\frac{\Theta_{il}}{2}\frac{dh}{dt}(i+1)F_a - \frac{1}{RePr}\frac{1}{\Delta Z_a^2}$ | $\frac{\Theta_{il}-1}{2\Delta Z_l}\frac{dh}{dt}(1-(i+1)\Delta Z_l)F_l - \frac{1}{RePr}\frac{\chi_{la}}{\Delta Z_l^2}$ |
| $d_{i,j}$ | $F_a^2\frac{4T_a^{i+1,j-1}-T_a^{i+1,j-2}}{2\Delta t}$ | $F_l^2\frac{4T_l^{i+1,j-1}-T_l^{i+1,j-2}}{2\Delta t}$ |

Table 2.2: Temperature coefficients for air and water matrices

| $T$ | |
|---|---|
| | **Ice** |
| $a_{i,j}$ | $-\frac{(i+1)h}{2}\frac{dh}{dt} - \frac{1}{Re}\frac{1}{\Delta Z_i^2}$ |
| $b_{i,j}$ | $\frac{3}{2}\frac{h^2}{\Delta t} + \frac{2\chi_{ia}}{RePr}\frac{1}{\Delta Z_i^2}$ |
| $c_{i,j}$ | $\frac{(i+1)h}{2}\frac{dh}{dt} - \frac{1}{Re}\frac{1}{\Delta Z_i^2}$ |
| $d_{i,j}$ | $h^2\frac{4T_i^{i+1,j-1}-T_i^{i+1,j-2}}{2\Delta t}$ |

Table 2.3: Temperature coefficients for the ice matrix

| $u$ | | |
|---|---|---|
| | **Air** | **Water** |
| $a_{i,j}$ | $-\frac{\Theta_{il}}{2}\frac{dh}{dt}(i+1)F_a - \frac{1}{Re}\frac{1}{\Delta Z_a^2}$ | $-\frac{\Theta_{il}-1}{2\Delta Y_l} - \frac{dh}{dt}(1-(i+1)\Delta Z_l)F_l - \frac{1}{Re}\frac{\nu_{la}}{\Delta Z_l^2}$ |
| $b_{i,j}$ | $\frac{3}{2}\frac{F_a^2}{\Delta t} + \frac{2}{Re}\frac{1}{\Delta Z_a^2}$ | $\frac{3}{2}\frac{F_l^2}{\Delta t} + \frac{2\nu_{la}}{Re}\frac{1}{\Delta Z_l^2}$ |
| $c_{i,j}$ | $\frac{\Theta_{il}}{2}\frac{dh}{dt}(i+1)F_a - \frac{1}{RePr}\frac{1}{\Delta Z_a^2}$ | $\frac{\Theta_{il}-1}{2\Delta Y_l}\frac{dh}{dt}(1-(i+1)\Delta Z_l)F_l - \frac{1}{Re}\frac{\nu_{la}}{\Delta Z_l^2}$ |
| $d_{i,j}$ | $F_a^2\frac{4u_a^{i+1,j-1}-u_a^{i+1,j-2}}{2\Delta t}$ | $-F_l^2\frac{\sin\alpha}{Fr} + F_l^2\frac{4u_l^{i+1,j-1}-u_l^{i+1,j-2}}{2\Delta t}$ |

Table 2.4: Horizontal velocity coefficients for air and water matrices

The resulting tridiagonal systems were solved with forward and backward substitution method (see, for example, Isaacson and Keller (1966)). Then Newton iterations are used to obtain the solution for $h$, $U_{la}$ and $T_{la}$ on each time step. Let $k$ denote the iteration number, then:

$$\begin{cases} G_{1,2}(h^k, T_{la}^k) + \frac{\partial G_{1,2}^k}{\partial h}(h^{k+1} - h^k) + \frac{\partial G_{1,2}^k}{\partial T_{la}}(T_{la}^{k+1} - T_{la}^k) = 0 \\ G_3(h^k, U_{la}^k) + \frac{\partial G_3^k}{\partial h}(h^{k+1} - h^k) + \frac{\partial G_3^k}{\partial U_{la}}(U_{la}^{k+1} - U_{la}^k) = 0 \end{cases} \tag{2.50}$$

From the above equations, we obtain the expressions for the increments $\Delta h^{k+1} = h^{k+1} - h^k$, $\Delta T_{la}^{k+1} = T_{la}^{k+1} - T_{la}^k$ and $\Delta U_{la}^{k+1} = U_{la}^{k+1} - U_{la}^k$ in the following form:

$$\Delta h^{k+1} = \frac{-G_1^k \frac{\partial G_2^k}{T_{la}} + G_2^k \frac{\partial G_1^k}{\partial T_{la}}}{\frac{\partial G_1^k}{\partial h}\frac{\partial G_2^k}{\partial T_{la}} - \frac{\partial G_2^k}{\partial h}\frac{\partial G_1^k}{\partial T_{la}}} \tag{2.51}$$

$$\Delta T_{la}^{k+1} = \frac{-G_2^k \frac{\partial G_1^k}{\partial h} + G_1^k \frac{\partial G_2^k}{\partial h}}{\frac{\partial G_1^k}{\partial h}\frac{\partial G_2^k}{\partial T_{la}} - \frac{\partial G_2^k}{\partial h}\frac{\partial G_1^k}{\partial T_{la}}} \tag{2.52}$$

$$\Delta U_{la}^{k+1} = -\frac{G_3^k + \frac{\partial G_3^k}{\partial h} \cdot \Delta h^{k+1}}{\frac{\partial G_3^k}{\partial U_{la}}} \tag{2.53}$$

In order for the system **(2.51)-(2.53)** to have a unique solution the following conditions are to be satisfied:

$$\begin{cases} \frac{\partial G_1^k}{\partial h}\frac{\partial G_2^k}{\partial T_{la}} - \frac{\partial G_2^k}{\partial h}\frac{\partial G_1^k}{\partial T_{la}} \neq 0 \\ \frac{\partial G_3^k}{\partial U_{la}} \neq 0 \end{cases} \tag{2.54}$$

Thus at each time step we take the values of $h$, $U_{la}$ and $T_{la}$ from the previous time step as an initial guess and iterate the $\vec{G}$-system until the solution for $h$, $U_{la}$ and $T_{la}$ converges. The following criterion was used in order to determine

convergence: $max_{i=1,2,3}|G_i| < \epsilon$. Time and space convergence for the proposed numerical scheme has been tested in a wide range of parameters.

It is easy to see that the Stefan number appears only in the coefficient before the ice surface derivative that vanishes as we approach the steady state and therefore it determines the relationship between ice and flow time scales. Thus, if we seek to obtain a steady solution we can adjust the value of Stefan number in the numerical procedure in order to increase the speed of convergence to a steady state.

**2.4.3.5 Results** In this section we present some results for the angle of incline $\alpha = 0.01$ and the following flow configuration:

| | **Initial guess** | **Steady State** |
|---|---|---|
| $\alpha_{fh}$ | 0.9 | |
| $T_w$ | −0.01 | |
| $h$ | 0.1 | 0.115615 |
| $f$ | 0.907908 | 0.909143 |

Table 2.5: Configurations for $x$-independent unsteady computations

In order to introduce a strong perturbation into the system we have set the initial guess for the temperature and velocity fields to be:

$$\begin{cases} T_a(y) = 1 \\ U_a(y) = 1 \\ T_l(y) = \frac{1}{4} \\ U_l(y) = \frac{1}{4} \\ T_i(y) = T_w \end{cases} \tag{2.55}$$

Grid containing 500 discretisation joints in each layer and $\Delta t = 0.01$ was used in all computations presented here.

Our computations show that the steady state is approached asymptotically (the plots are shown for $Re = 10$, $St = 1$):

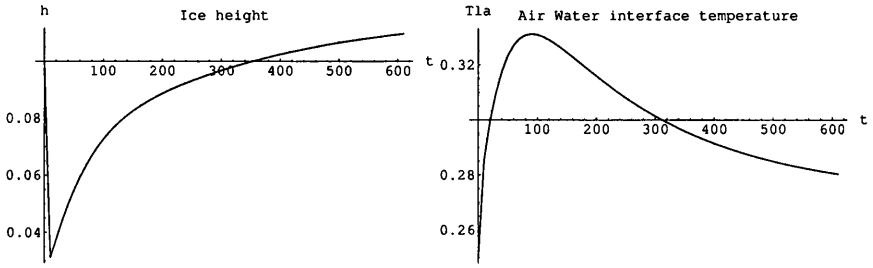


Figure 2.5: Ice height and air/water interface temperature evolution

The time necessary to reach the final steady-state solution depends linearly on the Reynolds number and $Log(t_{95})$ depends linearly on $Log(St)$ for small Stefan numbers, where $t_{95}$ is defined as the time necessary in order to reach the state when the ice height differs from the steady-state ice height by 5% (a similar result was obtained from the numerical modelling of full Navier-Stokes equations by Lee (1993)). The plots below show examples of $t_{95}(Re)$ and $t_{95}(St)$ :

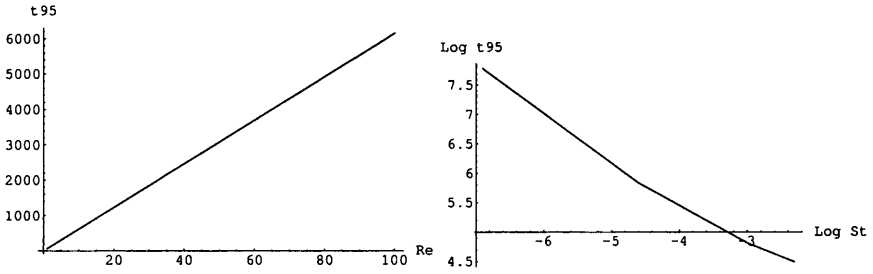


Figure 2.6: The dependence of $t_{95}$ on Reynolds and Stefan numbers

An interesting result is that the linear dependency between $Log(t_{95})$ and $Log(St)$ holds for small Stefan numbers only. For ice/water flows, typically the Stefan number is of order $10^{-2} \div 10^{-1}$. However if we consider flows with large Stefan

numbers then $t_{95}$ becomes practically independent of the Stefan number, as shown on the Fig. 2.7.

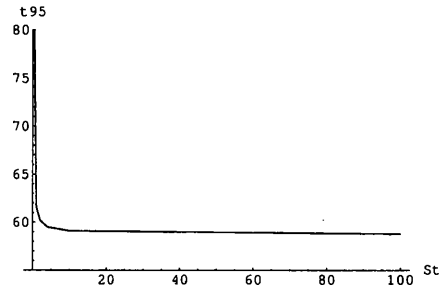


Figure 2.7: The behaviour of $t_{95}$ at large Stefan numbers ($Re = 1$)

When $T_w$ and $\alpha_{fh}$ are chosen in the domain where the solution does not exist, the initially set water film freezes completely at a finite time.

## 2.5 Conclusions

In this chapter we have summarised the general equations that will serve as a basis for particular problems discussed in further sections and indicated media properties values that will be used throughout this thesis.

We have also performed timescale analysis to estimate the characteristic time-scale of the ice-growth and derived an estimation formula for the Strouhal number of the problem. This estimation has demonstrated that the ice-growth characteristic times are much greater then the characteristic time of the flow, which means that the ice layer can be considered quasi-steady with respect to the fluid flow. Also if the time derivatives are retained in the equations for the fluid flow, we can expect characteristic wave speed of any ice-related modes in the linear stability problem to be significantly smaller than the characteristic wave speeds of flow-related modes.

However we should bear in mind that in principle long enough waves in the fluid flow can evolve sufficiently slowly for the flow timescale to become comparable to the ice timescale.

Apart from that we have considered possible $x$-independent solutions and derived existence criteria for steady solutions. Also we have performed computations for $x$-independent unsteady flow to investigate the way the flow approaches steady state. We should note that it is possible to consider the behaviour of the solution as it approaches steady state separately by deriving a solution linearised around the steady state solution, however the numeric solution is preferable in our case since it allows us to analyse the time necessary to reach the steady state as well. An interesting result of the analysis of the steady-state solutions is that for an infinite plane air/water/ice configuration, the steady-state solution does not exist for arbitrary values of boundary and initial conditions. Instead there is a well-defined domain of solution existence determined by the initial condition characteristic value $\alpha_{fh}$ and normalised wall temperature $T_w$.

The results of numerical computations for the $x$-independent problem demonstrate that the steady state is approached asymptotically and $Log(t_{95})$ depends linearly on $Log(St)$ for small Stefan numbers which is in agreement with the results obtained from a much more complicated full Navier-Stokes modelling by Lee (1993).

# 3 Ice layer stability in free-surface flows

In this chapter we consider the problems of ice layer instability and ice layer growth under a gravity-driven water film. Since one of the most interesting questions is that of instability of similar configurations with and without ice layer, it is necessary to give a brief summary of the research done in the field of the liquid layer stability before. However, since the stability of the free-surface flows has been a subject of numerous research, we will list only the works most relevant to the problem in consideration.

In one of the pioneering theoretical works on the subject Benjamin (1957) considered linear stability of the gravity-driven liquid film flow down an inclined plane. He used power series expansion in $y$ and obtained neutral stability curves for interfacial waves in analytic form for small values of $\alpha Re$, where $\alpha$ is the wavenumber. This work demonstrated that the flow is unstable for any Reynolds number if the angle of incline is $90^o$ and the flow can be stable for sufficiently small $Re$ when the angle of incline is less then $90^o$. In the same work, Benjamin (1957) also performed linear stability analysis of the problem in the longwave limit and obtained the dispersion relation in analytic form for this case. The analytic results for the vertical falling film were in good agreement with experiments by Binnie (1957).

Yih (1963) performed linear stability analysis of interfacial and shear waves for the problem for the cases of small Reynolds number, long waves and short waves. The results of this work demonstrated that surface waves govern stability characteristics of the problem at small Reynolds numbers.

Later De Bruin (1974) solved Orr-Sommerfeld problem numerically for a flow down an inclined plane in the case of small angle of incline. In this work it was shown that although the stability characteristics are governed by interfacial waves

for $3' < \theta < 1^o$ (where $\theta$ is the angle of incline), for very small angles ($\theta < 1'$) the dominant instability of the flow is due to a shear mode.

Chin, Abernathy and Bertschy (1986) analysed the influence of the angle of incline and surface tension on shear and surface instabilities in the problem for half-parabolic base flow velocity profiles modified by a $5th$ degree polynomial addition in order to simulate the developing flow in a water channel (Bertschy et al (1983)). In the range of parameters of this work ($\theta > 1^o$, $1000 < Re < 5000$, $0 < \gamma < 5000$, where $\theta$ is the angle of incline and $\gamma$ is the surface tension number) an increase of the angle of incline moderately destabilised the surface mode and slightly stabilised the shear mode. The increase of surface tension stabilised the surface mode and slightly destabilised the shear mode. An interesting result of this work consisted of the observation that the form-factor governing the initial velocity profile has almost no effect on surface waves and enormous effect on the Tollmien-Schlichting instabilities.

Floryan, Davis and Kelly (1987) performed a detailed numerical study of the linear stability of the problem for a wide range of Reynolds numbers and angles of incline with particular attention paid to the effect of surface tension on shear and interfacial instabilities. The results obtained indicate that the critical Reynolds number for the shear mode varies non-monotonically with the angle of incline and surface tension parameter. This work will be often referred to in the linear stability analysis in this chapter since it contained detailed tables of mode values and critical parameters, thus providing an excellent opportunity for the verification of our numerical code.

In all these works air was essentially neglected and the zero shear stress condition was imposed on the air/water boundary. We will adhere to this formulation.

In this chapter we will first consider the case of a thin ($O(Re^{-\frac{1}{2}})$) water film and develop a Froude-based double-deck theory for this problem. Next we will consider the Orr-Sommerfeld stability formulation for the $O(1)$ scale film and finally consider a longwave limiting case.

Also we should note that the question of comparison of the stability characteristics for water films with and without ice layer is relevant to the second section of this chapter, as the Froude-based double-deck analysis represents a completely new approach to the problem.

## 3.1 Froude-based double-deck analysis

In this section we consider a thin water film with height of order $Re^{-\frac{1}{2}}$ where Reynolds number is based on the characteristic length in the $x$ direction. Zero friction is assumed on the upper boundary of the liquid layer. From below, the water layer is bounded by an ice sheet. In order to reduce the number of free parameters in the problem, we assume that the Reynolds number is sufficiently high so that the flow is governed by the boundary-layer equations. The flow scheme for this configuration is shown on the figure below:

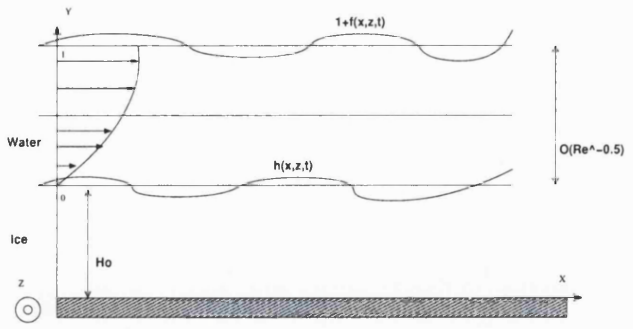


Figure 3.1: Flow scheme for a water film in the boundary-layer regime

We consider the flow to be three-dimensional in the general problem formulation, derivation of the double-deck and linear solutions, however we compute nonlinear double-deck equations in two-dimensional case only. The air/water and water/ice boundaries be given by $1 + f(x, z, t)$ and $h(x, z, t)$ accordingly.

For this problem it is more convenient to normalise pressure as follows - $P_b = \frac{P - P_a^*}{\rho^* g^* h^*}$ and use the height of the unperturbed film $h^*$ as a characteristic length in the $y$ direction. Also we use integral mean by profile in the unperturbed flow as the characteristic velocity $U^*$ and define the Froude number as $Fr = \frac{U^{*2}}{g^* h^*}$.

We assume that $\frac{h^*}{L^*} \sim Re^{-\frac{1}{2}} \ll 1$. In order to isolate the icing instability, we consider the problem at the ice growth timescale. In this case, since the Strouhal number $St = \frac{\tau_i^*}{\tau_{flow}^*}$ of the problem is large (see the section "2.3 Timescale analysis for water/ice flows" of the previous chapter), we can neglect the time derivatives in the boundary layer equations. Since the only time derivative left in the problem is in the Stefan condition, we can re-scale time by the Stefan number ($t \Rightarrow St \cdot t$) and the Stefan condition can be rewritten as:

$$\lambda_{il} \frac{\partial T_i}{\partial y} - \frac{\partial T_l}{\partial y} = Pr \cdot \Theta_{il} h_t = a h_t \tag{3.1}$$

Here $a = Pr \cdot \Theta_{il} \sim 1$ for water/ice. Note that this formulation is not valid when $\frac{\rho_i}{\rho_l} \to 1$ (when solid and liquid phases have the same densities, the problem becomes essentially steady).

Then in the conventional boundary layer scaling, the equations in water and ice layers are given by **(3.2)** and **(3.3)** respectively.

$$\begin{cases} uu_x + vu_y + wu_z = -\frac{P_x}{Fr} + \frac{\sqrt{Re}\sin\phi}{Fr} + u_{yy} \\ uw_x + vw_y + ww_z = -\frac{P_z}{Fr} + w_{yy} \\ P_y = -\cos\phi \\ u_x + v_y + w_z = 0 \\ uT_x + vT_y + wT_z = \frac{1}{Pr}T_{yy} \end{cases} \tag{3.2}$$

$$\frac{\chi_{ia}}{Pr}T_{yy} = 0 \tag{3.3}$$

Here $\phi$ is the angle of incline. We will consider the half-Poiseuille initial solution in water, then for our choice of characteristic values, the dimensionless initial solution is given by:

$$\begin{cases} u_0 = 3\left(y - \frac{y^2}{2}\right) \\ v_0 = 0 \\ P_0 = (1-y)\cos\phi \\ T_0 = y \end{cases} \tag{3.4}$$

As the solution far upstream is gravity-driven, viscous dissipation balances gravity parallel to the slope (as in Bowles (1995)) yielding:

$$\frac{\sqrt{Re}\sin\phi}{Fr} = 3 \tag{3.5}$$

Now let us consider the case when $Fr \gg 1$. Then in order to maintain the pressure gradients in the equations **(3.2)**, it is necessary to introduce a two-layer system with the lower "viscous" layer maintaining the full system of equations and the upper inviscid layer where equations become simplified (in the similar way as the

conventional triple-deck is derived, see, for example, Sychev, Ruban, Sychev and Korolev (1998)).

### 3.1.1 Viscous layer: problem formulation

In the lower viscous layer (1) $u \sim y$ then, we can see that in order to maintain all terms in the continuity equation, we need $v \sim \frac{y^2}{x}$ and $w \sim \frac{yz}{x}$. In order to maintain the full form of the horizontal momentum equation, we need $\frac{P_x}{Fr} \sim u_{yy} \to \frac{P}{xFr} \sim \frac{1}{y}$ and $\frac{P}{xFr} \sim vu_y \to \frac{P}{xFr} \sim \frac{y^2}{x}$. Combining these, we obtain $P \sim Fry^2 \sim \frac{xFr}{y}$, therefore $y^3 \sim x$. Then as the variation of pressure is of the same order as the variation of height: $P \sim y \sim Fry^2$ which leads to $y \sim Fr^{-1}$ and $x \sim Fr^{-3}$.

Similarly from the $z$ component of the momentum equation: $uw_x \sim \frac{P_z}{Fr} \to w \sim \frac{Px}{zyFr} \sim \frac{yz}{x} \to z^2 \sim \frac{x^2}{yFr} \to z \sim x \sim Fr^{-3}$ and $w \sim \frac{x}{Frz} \sim Fr^{-1}$.

Now as the initial temperature profile is linear, $T \sim y$ and the heat flux is of order 1, also $h \sim y \sim Fr^{-1}$. Then in order to maintain the time derivative $h_t$ in the viscous sublayer we need to consider the problem at the timescale $t_1 \sim Fr^{-1}$.

Therefore, in order to maintain the whole system of equations in the viscous sublayer and time derivative in the Stefan equation, the scaling in the lower viscous layer has to be in the form:

$$x_b = Fr^{-3}x_1,\ y_b = Fr^{-1}y_1,\ z_b = Fr^{-3}z_1,\ t_b = Fr^{-1}t_1$$

$$u_b = Fr^{-1}u_1,\ v_b = Frv_1,\ w_b = Fr^{-1}w_1$$

$$P_b = Fr^{-1}P_1,\ T_b = Fr^{-1}T_1$$

Let the ice surface coordinate in the viscous sublayer scaling be given by $h = H_1 \cdot Fr^{-1}$, where $H_1 \sim 1$. At the ice surface, the normal vector is given by

$\vec{n} = (-H_{1x}, 1, -H_{1z})$ and we can choose the linearly independent tangent vectors to be given by $\vec{\tau_1} = (1, H_{1x}, 0)$ and $\vec{\tau_2} = (0, H_{1z}, 1)$ respectively.

Let us omit subscript 1 for the perturbations, then the leading-order equations and the Stefan condition in the viscous layer become:

$$\begin{cases} uu_x + vu_y + wu_z = -P_x + u_{yy} \sim Fr \\ uw_x + vw_y + ww_z = -P_z + w_{yy} \sim Fr \\ P_y = \cos\phi \sim Fr^{-1} \\ u_x + v_y + w_z = 0 \sim Fr^2 \\ uT_x + vT_y + wT_z = \frac{1}{Pr} T_{yy} \sim Fr \end{cases} \tag{3.6}$$

The constant temperature condition on the ice surface yields $T_l(H) = T_i(H) = 0$. The boundary-value problem for the ice layer temperature is given by:

$$\begin{cases} \frac{\partial^2 T_i}{\partial y^2} = 0 \\ T_i(-H_0) = T_w \\ T_i(H) = 0 \end{cases} \tag{3.7}$$

This problem can be solved analytically and the solution is given by:

$$T_i = T_w \frac{H - y}{H + H_0} \tag{3.8}$$

Note that the nonlinearity of the above expression in $H$ holds only if $H \sim H_0$. If $H \ll H_0$ then the above expression can be linearised (see the "3.1.4 Linear stability of the viscous layer" section). Then, Stefan condition becomes:

$$\frac{\partial T_l}{\partial y} = \lambda_{il} \frac{\partial T_i}{\partial y} - aH_t = -\lambda_{il} T_w \frac{1}{H + H_0} - aH_t \tag{3.9}$$

The double-deck scaled velocity conditions on the ice surface are given by:

1. $V_n = 0 \Rightarrow v - uH_x - wH_z = 0$
2. $V_{\tau_1} = 0 \Rightarrow u = 0$
3. $V_{\tau_2} = 0 \Rightarrow w = 0$

In order to formulate the boundary-value problem we need perturbations to decay as $x \to -\infty$. Conditions as $y \to \infty$ will be determined from the solution in the upper inviscid layer.

### 3.1.2 Inviscid layer: problem formulation and solution

In the inviscid layer (2) $x_2 \sim x_1 \sim Fr^{-3}$ and $u \sim 1$. Then, assuming that the streamlines inclination is the same in both layers:

$$\frac{1}{v_2} \sim \frac{\sqrt{u_1^2 + w_1^2}}{v_1} \sim Fr^{-2} \to v_2 \sim Fr^2$$

Therefore, if $u = u_0(y) + u_2(x, y, z, t)$, from the continuity equation we obtain: $u_2 \sim \frac{vx}{y} \sim Fr^{-1}$. Also the pressure perturbation is the same in both layers, i.e. $P_2 \sim P_1 \sim Fr^{-1}$. In order for the $z$ component of the Navier-Stokes equation not to become singular we need $\frac{P_z}{Fr} \sim u_0 w_x \to w \sim \frac{Fr^{-1}x}{zFr}$ and therefore (as from the viscous layer it follows that $z \sim x$) we obtain $w \sim Fr^{-2}$. Finally, the appropriate expansion in the upper layer becomes:

$$x_b = Fr^{-3}x_2,\ y_b = y_2,\ z_b = Fr^{-3}z_2$$

$$u_b = u_0(y) + Fr^{-1}u_2,\ v_b = v_2 Fr^2,\ w_b = w_2 Fr^{-2}$$

$$P_b = P_0(y) + Fr^{-1}P_2,\ T_b = T_0(y) + Fr^{-1}T_2$$

The expansion for the free surface shape is given by $f = 1 + Fr^{-1}F_2$. On the free surface the normal vector is given by $\overrightarrow{n} = (-F_{2x}, 1, -F_{2z})$ and the two linearly independent tangent vectors can be taken as $\overrightarrow{\tau_1} = (1, F_{2x}, 0)$ and $\overrightarrow{\tau_2} = (0, F_{2z}, 1)$ .

Let us omit subscript 2 for the perturbations, then the equations for the first order perturbations are of the form:

$$\begin{cases} u_0 u_x + v u_{0y} = 0 \\ u_0 w_x = -P_z \\ P_y = 0 \\ u_x + v_y = 0 \\ u_0 T_x + v T_{0y} = 0 \end{cases} \tag{3.10}$$

From the system of equations **(3.10)** it immediately follows that $P = P(x, z, t)$. Then from the linearised kinematic condition at the free surface, we obtain the following expression:

$$v = u_0 F \tag{3.11}$$

At the free surface the temperature is constant and the perturbation of the temperature is zero. The boundary condition for the perturbation of temperature on the unperturbed free surface ($y = 1$) can be obtained by writing Taylor expansion of the temperature profile near $y = 1$:

$$T_0(1 + Fr^{-1} \cdot F_2) + Fr^{-1}T_2(Fr^{-1} \cdot F_2) =$$
$$T_0(1) + Fr^{-1}(F_2 \tfrac{\partial T_0}{\partial y}(1) + T_2(1)) + O(Fr^{-2})$$

The base temperature profile satisfies the boundary condition at the unperturbed free surface, therefore $T_2(x,1) = -F_2(x)\frac{\partial T_0}{\partial y}(1)$.

The stress tensor continuity condition at the free surface can be written (before the expansion in $Fr^{-1}$) in the matrix form as:

$$-\frac{f_{zz}+f_{xx}}{We}\begin{pmatrix} -f_x \\ 1 \\ -f_z \end{pmatrix} = \begin{pmatrix} -\frac{P}{Fr}+2\frac{u_x}{Re} & \frac{u_y+v_x}{Re} & \frac{u_z+w_x}{Re} \\ \frac{u_y+v_x}{Re} & -\frac{P}{Fr}+2\frac{v_y}{Re} & \frac{v_z+w_y}{Re} \\ \frac{u_z+w_x}{Re} & \frac{v_z+w_y}{Re} & -\frac{P}{Fr}+2\frac{w_z}{Re} \end{pmatrix}\begin{pmatrix} -f_x \\ 1 \\ -f_z \end{pmatrix} \tag{3.12}$$

The above condition leads to $u_{2y} = 0$ , $w_{2y} = 0$ and also yields the pressure-displacement law in the following form:

$$P_2 = F_2\cos\phi - \frac{F_{2xx}+F_{2zz}}{We}\frac{\sin\phi}{3} \tag{3.13}$$

Then the expression for the perturbation of the $z$ component of the velocity is given by:

$$\begin{gathered} w_2 = -\frac{1}{u_0}\int(F_{2z}\cos\phi + \frac{\sin\phi}{3We}(F_{2xxz}+F_{2zzz}))dx = \\ -\frac{1}{3(y-\frac{y^2}{2})}\int(F_{2z}\cos\phi + \frac{\sin\phi}{3We}(F_{2xxz}+F_{2zzz}))dx = \\ -\frac{K(F)}{3(y-\frac{y^2}{2})} \end{gathered} \tag{3.14}$$

Here $K(F) = K(z,x,t)$ denotes the integral.

From the form of the governing equations and boundary conditions, it can be

deduced that the solution in the upper layer can be expressed in the following form:

$$\begin{cases} v_2 = u_0(y)A_x(x,z,t) \\ u_2 = -u_{0y}(y)A(x,z,t) + C_1(y,z,t) \\ T_2 = -T_{0y}(y)A(x,z,t) + C_2(y,z,t) \end{cases} \tag{3.15}$$

With arbitrary functions $A$, $C_1$ and $C_2$. Assuming an unperturbed solution in the incoming flow we obtain:

$$\begin{cases} A_x \to 0, A \to 0 \\ C_1 = 0 \qquad x \to -\infty \\ C_2 = 0 \end{cases} \tag{3.16}$$

Then, from the boundary conditions for the temperature and velocity at free surface, it follows that $A_x = F_{2x} \to A = F_2$. Finally, the solution in the upper layer takes the following form:

$$\begin{cases} v_2 = 3(y_2 - \frac{y_2^2}{2})F_{2x} \\ u_2 = -3(1-y_2)F_2 \\ T_2 = -F_2 \\ w_2 = -\frac{K(z_2,x_2,t)}{3(y_2-\frac{y_2^2}{2})} \end{cases} \tag{3.17}$$

The system **(3.17)** expresses the solution in the upper inviscid layer found in terms of the perturbation of the free surface $F_2$. Now we must consider the lower viscous layer in order to find the perturbation of the free surface $F_2$ using the inviscid solution **(3.17)** to derive boundary conditions on the outer edge of the viscous layer.

In order to obtain the boundary conditions at the outer edge of the viscous layer, we write the complete solution in the inviscid layer in terms of the viscous sublayer variable ($y_2 = y_1 Fr^{-1}$):

$$\begin{cases} v = Fr^2 v_2 = 3Fr^2(y_1 Fr^{-1} - \frac{y_1^2 Fr^{-2}}{2})F_{2x} = 3y_1 Fr F_{2x} + O(1) \\ u = u_0 + Fr^{-1}u_2 = 3(y_1 Fr^{-1} - \frac{y_1^2 Fr^{-2}}{2}) - 3Fr^{-1}(1 - y_1 Fr^{-1})F_2 = \\ (3y_1 - 3F_2)Fr^{-1} + O(Fr^{-2}) \\ T = T_0 + Fr^{-1}T_2 = (y_1 - F_2)Fr^{-1} + O(Fr^{-2}) \\ w = -\frac{K(x,z,t)}{3y_1}Fr^{-1} + O(Fr^{-2}) \end{cases} \tag{3.18}$$

Then the upper boundary conditions for the viscous layer leading terms in Froude number as $y_1 \to \infty$ will be given by:

$$\begin{cases} v_1 = 3y_1 F_{2x} \\ u_1 = 3y_1 - 3F_2 \\ T_1 = y_1 - F_2 \\ w_1 = -\frac{K}{3y_1} \end{cases} \tag{3.19}$$

### 3.1.3 Double-deck validity domain

It is possible to estimate the domain of the validity for the derived double-deck theory. The underlying asymptotic procedure requires, first of all that $Re \gg 1$ and $Fr \gg 1$. Also, for a gravity-driven flow, $Fr = \frac{\sqrt{Re}\sin\phi}{3}$. In the boundary layer equations for the vertical velocity, the $\frac{1}{\sqrt{Re}}uv_x$ term was neglected as it was small comparing to $P_y\sqrt{Re}$. When we introduce the double-deck scaling, the multiplier of the $uv_x$ in the inviscid layer is much greater than 1 and the multiplier of $P_y$ is

much less then 1. However the convection term should still be much smaller than the pressure gradient term. This requirement leads to the following restriction $\frac{1}{\sqrt{Re}}Fr^4 \ll \sqrt{Re}Fr^{-1}$. Therefore, in order for the double-deck expansion to be valid, it is necessary that the following conditions are satisfied (expressed in terms of $Re$ and $\phi$) :

$$\begin{cases} Re \gg 1 \\ \sin\phi \gg Re^{-\frac{1}{2}} \\ \sin^5\phi \ll Re^{-\frac{3}{2}} \end{cases} \tag{3.20}$$

The first inequality has to be satisfied in order for boundary layer approximation to be valid. The second inequality represents $Fr \gg 1$ condition, necessary for double-deck expansion. The third inequality has to be satisfied in order for the double-deck expansion to be applicable within the scope of boundary-layer equations.

In order to satisfy the last two inequalities, the angle of incline should be bounded by $Re^{-\frac{1}{2}} \ll \sin\phi \ll Re^{-\frac{3}{10}}$. In order to build curves limiting the validity domain let us consider that $a \gg b$ when $\frac{a}{b} \sim O(5)$. The domain of validity for this estimate is shown on the following plot:

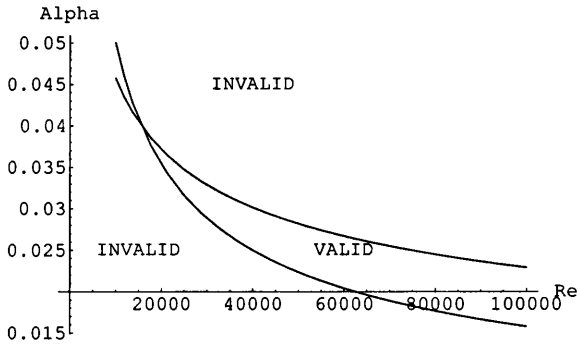


Figure 3.2: Double-deck validity domain in $(Re, \phi)$ plane

Double-deck validity domain is the high-Reynolds number wedge between the dashed and the solid lines. Later, this estimate will be used in the ice mode computations in the full free-surface flow stability analysis (see the "3.2 Linear stability analysis of O(1) height film" section).

### 3.1.4 Linear stability of the viscous layer

Let us consider the behaviour of the viscous layer solution for a small perturbation of the ice surface ($\varepsilon \sim H_1 \sim F_2 \ll H_0$). We can write the perturbed solution to the first order in $\varepsilon$ in the following form:

$$\begin{cases} H_1 = \varepsilon H_{11} \\ F_2 = \varepsilon F_{11} \\ v_1 = \varepsilon v_{11} \\ w_1 = \varepsilon w_{11} \\ P_1 = P_0 + \varepsilon P_{11} = (1 - y_1)\cos\phi + \varepsilon P_{11} \\ u_1 = u_0 + \varepsilon u_{11} = 3y_1 + \varepsilon u_{11} \\ T_1 = T_0 + \varepsilon T_{11} = y_1 + \varepsilon T_{11} \end{cases} \tag{3.21}$$

The freezing temperature is constant, therefore, the perturbation of temperature is zero on the ice surface. The boundary condition for the perturbation of temperature on the unperturbed ice surface ($y = 0$) can be obtained by writing Taylor expansion of the temperature profile near $y = 0$:

$$T(\varepsilon H_{11}) = (T_0 + \varepsilon T_{11})(H_{11}\varepsilon) =$$
$$T_0(0) + \varepsilon T_{11}(0) + \varepsilon \frac{dT_0}{dy}(0) H_{11} = 0$$

The base temperature profile satisfies the boundary condition at the unperturbed

ice surface, therefore $T_{11}(0) = -H_{11}$. Also, since the initial temperature profiles are linear, we have:

$$\begin{cases} \frac{\partial T_{1l}}{\partial y}(\varepsilon H_{11}) = \frac{\partial (T_{0l}+\varepsilon T_{11l})}{\partial y}(\varepsilon H_{11}) = \frac{\partial T_{0l}}{\partial y}(0) + \varepsilon \frac{\partial T_{11l}}{\partial y}(0) + O(\varepsilon^2) \\ \frac{\partial T_{1i}}{\partial y}(\varepsilon H_{11}) = \frac{\partial T_{0i}}{\partial y}(0) + \varepsilon \frac{\partial T_{11i}}{\partial y}(0) + O(\varepsilon^2) \end{cases}$$

In the ice layer $T_{1iyy} = 0$ and the derivative of the ice temperature is given by $\frac{\partial T_{1i}}{\partial y} = -\frac{T_w}{\varepsilon H_{11}+H_0}$. Since the perturbation of the surface is small, the derivative of the perturbed ice temperature profile is given by $\frac{\partial T_{1i}}{\partial y} = -\frac{T_w}{H_{11}+H_0} = -\frac{T_w}{H_0}(1 - \varepsilon \frac{H_{11}}{H_0}) + O(\epsilon^2)$ and the first order perturbation of the ice temperature derivative is given by $\frac{\partial T_{11i}}{\partial y} = \delta\left(\frac{\partial T_{1i}}{\partial y}\right) \simeq \frac{T_w H_{11}}{H_0^2}$. In the base state solution the heat flux on the ice/water boundary from the ice side is equal to the heat flux on the ice/water boundary from the water side. Also from the heat flux balance for the base state ice temperature solution $-\lambda_{il}\frac{T_w}{H_0} = 1$. Using these expressions the Stefan condition can be written as an equation relating the ice surface growth to the derivative of the liquid temperature on the ice/water boundary:

$$\frac{\partial T_{11l}}{\partial y} = -a\frac{\partial H_{11}}{\partial t} - \frac{H_{11}}{H_0}$$

Then the system of equations for the perturbations will be in the following form (omitting subscripts 11):

$$\begin{cases} 3yu_x + 3v = -P_x + u_{yy} \\ 3yw_x = -P_z + w_{yy} \\ u_x + v_y + w_z = 0 \\ 3yT_x + v = \frac{1}{Pr}T_{yy} \end{cases} \tag{3.22}$$

The boundary conditions for the perturbations at the ice surface and on the outer edge of the viscous sublayer are given by **(3.23)** and **(3.24)** respectively.

$$\begin{cases} v = 3yF_x \\ u = -3F \\ T = -F \\ w = -\frac{K}{3y} \end{cases} \quad y \to \infty \tag{3.23}$$

$$\begin{cases} v = 0 \\ u = -3H \\ w = 0 \\ T = -H \\ T_y = -aH_t - \frac{H}{H_0} \end{cases} \quad y = 0 \tag{3.24}$$

Taking Fourier transform in $x$ and $z$ (so that $l(x,y,z,t) = \int\int L(\alpha,\beta,y,t)e^{i\alpha x + i\beta z}d\alpha d\beta$) we obtain the following system for the transforms (from now on in this section, we will operate with transforms only, therefore we will use the same notation for transforms as for original functions in order to simplify the notation):

$$\begin{cases} 3i\alpha yu + 3v = -i\alpha P + u_{yy} \\ 3i\alpha yw = -i\beta P + w_{yy} \\ i\alpha u + v_y + i\beta w = 0 \\ 3i\alpha yT + v = \frac{1}{Pr}T_{yy} \end{cases} \tag{3.25}$$

The pressure displacement law for Fourier transform $P$ can be written as:

$$P = \Phi F \tag{3.26}$$

Here the function $\Phi$ is the function of wavenumbers $\alpha$ and $\beta$:

$$\Phi = \cos\phi + \frac{\alpha^2 + \beta^2}{We}\frac{\sin\phi}{3} \tag{3.27}$$

Then in the leading order the boundary conditions at the ice surface become:

$$\begin{cases} u = -3H \\ v = 0 \\ w = 0 \qquad y = 0 \\ T = -H \\ T_y = -aH_t - \frac{H}{H_0} \end{cases} \tag{3.28}$$

In numerical computations we apply boundary conditions at some large $y = y_e$. In this case, better precision can be obtained if we derive one more term in $v$ expansion and use it as a correction to the boundary condition for $v$. In order to do this, we write the condition for $v$ as $y \to \infty$ in the form $v = 3i\alpha yF + X$, where $X$ is some unknown function. Then, we take the limit of the equation for $u$ in **(3.25)** as $y \to \infty$ which leads to the following equation:

$$-9i\alpha yF + 9i\alpha yF + 3X = -i\alpha P + 0 \tag{3.29}$$

Then, the second term for $v$ does not depend on $y$ and is the boundary condition for $v$ as $y \to \infty$ is given by:

$$v = 3i\alpha yF - \frac{i\alpha}{3}F\Phi \tag{3.30}$$

Also, from the solution for $w$ given by **(3.14)** it follows that in terms of Fourier transforms, the boundary condition for $w$ as $y \to \infty$ is given by:

$$w = -\frac{\beta}{3\alpha} F\Phi \frac{1}{y} \tag{3.31}$$

Finally, with the correction for $v$ taken into account the boundary conditions on the outer edge of the viscous layer can be written as:

$$\begin{cases} u = -3F \\ v = 3i\alpha y F - \frac{i\alpha}{3} F\Phi \\ w = -\frac{\beta}{3\alpha} F\Phi \frac{1}{y} \\ T = -F \end{cases} \quad y \to \infty \tag{3.32}$$

**3.1.4.1 Analytic solution, $Pr = 1$.** When the base-flow velocity profile is linear the Orr-Sommerfeld equations contain solutions in terms of the Airy functions (for example, see Hooper and Boyd (1983)). In our case, the equations for $u$ and $T$ are similar if $Pr = 1$ and the solution can be obtained analytically in terms of the Airy functions for the system with temperature as well.

The equation for $w$ can be rewritten in the form of the Scorer equation. By setting $M(z) = w(y)$, $z = (3i\alpha)^{1/3} y$ and $\eta(\alpha, \beta) = \frac{i\beta}{(3i\alpha)^{\frac{2}{3}}} P = \frac{i\beta}{(3i\alpha)^{\frac{2}{3}}} F\Phi$ we obtain:

$$M_{zz} - zM = \eta(\alpha, \beta) \tag{3.33}$$

Then the general solution for the equation above can be found in the form:

$$M(z) = C_1 \cdot M_1(z) + C_2 \cdot M_2(z) - \pi\eta(\alpha, \beta) M_3(z) \tag{3.34}$$

Here $M_1$ and $M_2$ are two linearly independent solutions of the Airy equation and $M_3$ is any particular solution of the Scorer equation:

$$W_{zz} - zW = \frac{1}{\pi} \tag{3.35}$$

Taking $Ai(z)$, $Bi(z)$ and $Gi(z)$ as a group of solutions for the Scorer equation (see, for example, Abramowitz and Stegun (1972)) and noticing that $Bi$ is not limited at $\infty$, we obtain the solution to **(3.33)** in the following form:

$$M(z) = C_1 \cdot Ai(z) - \pi\eta(\alpha,\beta)Gi(z) \tag{3.36}$$

Also, from the boundary condition for the transversal velocity $w$ on the ice surface, it follows that $M(0) = 0$, therefore $C_1 = \pi\eta(\alpha,\beta)\frac{Gi(0)}{Ai(0)} = \pi\eta(\alpha,\beta)\frac{1}{\sqrt{3}}$, and the expression for $M(z)$ can be written in the form:

$$M(z) = \left(\frac{Ai(z)}{\sqrt{3}} - Gi(z)\right)\pi\eta(\alpha,\beta) \tag{3.37}$$

which leads to the following solution for $w$:

$$w(y) = (\frac{Ai((3i\alpha)^{\frac{1}{3}}y)}{\sqrt{3}} - Gi((3i\alpha)^{\frac{1}{3}}y))\pi\frac{i\beta}{(3i\alpha)^{\frac{2}{3}}}F\Phi \tag{3.38}$$

If we multiply the partial derivative by $y$ of the first equation in **(3.25)** by $i\alpha$, add it to the partial derivative by $y$ of the second equation in **(3.25)** multiplied by $i\beta$ $(i\alpha\frac{\partial(1)}{\partial y} + i\beta\frac{\partial(2)}{\partial y})$ and use the expression for $v_y$ from the continuity equation $(v_y = -i\alpha u - i\beta w)$, we obtain the following equation for $v$:

$$v_{yyyy} = 3i\alpha y v_{yy} \tag{3.39}$$

**(3.39)** can be rewritten as an Airy equation:

$$E_{zz} = zE \tag{3.40}$$

by setting $z = (3i\alpha)^{1/3}y$ and $E(z) = v_{yy}(y)$. The solution for **(3.40)** is given by

$$E = v_{yy} = -i\alpha u_y - i\beta w_y = W(\alpha,\beta)Ai(z) = W(\alpha,\beta)Ai(y(3i\alpha)^{\frac{1}{3}}) \tag{3.41}$$

Using **(3.41)** and **(3.38)**, we obtain the following expression for the first derivative of the horizontal velocity:

$$u_y = -\frac{v_{yy}+i\beta w_y}{i\alpha} = -\frac{WAi((3i\alpha)^{\frac{1}{3}}y)+i\beta\left(\frac{Ai_z((3i\alpha)^{\frac{1}{3}}y)}{\sqrt{3}}-Gi_z((3i\alpha)^{\frac{1}{3}}y)\right)\frac{i\beta\pi F\Phi}{(3i\alpha)^{\frac{1}{3}}}}{i\alpha} \tag{3.42}$$

If we substitute the solution for $v$ directly into the equation for temperature in **(3.25)**, we obtain a Scorer-type equation with non-constant right-hand side. However if $Pr = 1$ then the first and the last equations of **(3.25)** are similar. Let us multiply the equation for temperature by 3 and subtract the equation for the horizontal velocity component from it, then we obtain the following equation for the combination of functions $(3T - u)$:

$$3i\alpha y(3T-u) - i\alpha P = (3T-u)_{yy} \tag{3.43}$$

The above equation can be rewritten as the Scorer equation by setting $S(z) = (3T - u)$ and $z = (3i\alpha)^{1/3}y$:

$$S_{zz} - zS = -\frac{(i\alpha)^{\frac{1}{3}}}{3^{\frac{2}{3}}}F\Phi = -\sigma(\alpha,\beta) \tag{3.44}$$

Following the same procedure as for the $w$ velocity component, we obtain the solution of **(3.44)** in the form:

$$S(z) = 3T - u = (-\frac{Ai(z)}{\sqrt{3}} + Gi(z))\pi\sigma = \pi(\frac{Ai(z)}{\sqrt{3}} - Gi(z))\frac{(i\alpha)^{\frac{1}{3}}}{3^{\frac{2}{3}}}F\Phi \qquad (3.45)$$

These results give us solutions for $u$, $v$, $w$ and $T$ in terms of $H$, $F$ and $W$. Now let us use the boundary conditions in order to determine the relations between $H$, $F$ and $W$ in order to reduce the Stefan condition to a differential equation containing $H$ alone.

From the equations for $u$ and $w$ in the system **(3.25)** taken at 0 we obtain the following expressions for the second derivatives of $u$ and $v$:

$$u_{yy}(0) = i\alpha F\Phi \qquad (3.46)$$

$$w_{yy}(0) = i\beta F\Phi \qquad (3.47)$$

Substituting **(3.46)** and **(3.47)** into the expression for the third derivative of $v$ solution derived from **(3.41)**, we obtain the following formula:

$$v_{yyy}(0) = (3i\alpha)^{\frac{1}{3}}Ai_z(0)W = -i\alpha u_{yy} - i\beta w_{yy} = F\Phi(\alpha^2 + \beta^2) \qquad (3.48)$$

This gives us the relation between $F$ and $W$:

$$W = X_0 F \qquad (3.49)$$

where:

$$X_0 = (\alpha^2 + \beta^2)\frac{\Phi}{Ai_z(0)(3i\alpha)^{\frac{1}{3}}} \tag{3.50}$$

Now let us take the integral from 0 to $\infty$ in $y$ of $v_{yy}$ given by **(3.41)**, and apply the boundary conditions **(3.28)** and **(3.32)**:

$$\begin{aligned}\int_0^\infty v_{yy}dy &= v_y(\infty) - v_y(0) = -i\alpha u(\infty) + i\alpha u(0) = \\ &3i\alpha(F - H) = (3\alpha)^{-\frac{1}{3}}W\int_0^\infty Ai(ti^{\frac{1}{3}})dt = (3\alpha)^{-\frac{1}{3}}W\frac{1}{3}i^{-\frac{1}{3}}\end{aligned}$$

From the above expression follows the second equation for $F$, $H$ and $W$:

$$3i\alpha(F - H) = W(3i\alpha)^{-\frac{1}{3}}\frac{1}{3} \tag{3.51}$$

Expressing $W$ in terms of $F$ from **(3.49)**, we can obtain the relation between $F$ and $H$ from **(3.51)**. It is convenient to write this relation in the following form:

$$F = \mathrm{X}_1 H \tag{3.52}$$

where:

$$X_1 = \left(1 - \frac{\Phi(\alpha^2 + \beta^2)}{3Ai_z(0)(3i\alpha)^{\frac{5}{3}}}\right)^{-1} \tag{3.53}$$

Finally, the solution for $S = 3T - u$ given by **(3.45)** yields the following expression for the temperature:

$$3T = u + \pi(\frac{Ai(z)}{\sqrt{3}} - Gi(z))\frac{(i\alpha)^{\frac{1}{3}}}{3^{\frac{2}{3}}}F\Phi \tag{3.54}$$

Using **(3.54)** and taking into account that $\left(-\frac{Ai_z(0)}{\sqrt{3}} + Gi_z(0)\right) = -\frac{2}{\sqrt{3}}Ai_z(0)$, the Stefan condition given in **(3.28)** can be rewritten as:

$$\begin{aligned} S_z(0) &= \pi\frac{(i\alpha)^{\frac{1}{3}}}{3^{\frac{2}{3}}}F\Phi(Gi_z(0) - \frac{Ai_z(0)}{\sqrt{3}}) = (3i\alpha)^{-\frac{1}{3}}(3T_y - u_y) = \\ & (3i\alpha)^{-\frac{1}{3}}(-3(aH_t + \frac{H}{H_0}) - u_y(0)) \end{aligned}$$

From the equation **(3.42)**, we can express $u_y(0)$ in terms of the ice surface perturbation transform $H$, using the expressions **(3.49)** and **(3.52)**:

$$\begin{aligned} u_y(0) = & -\frac{WAi(0) - (\frac{Ai_z(0)}{\sqrt{3}} - Gi_z(0))\frac{\pi\beta^2}{(3i\alpha)^{\frac{1}{3}}}F\Phi}{i\alpha} = \\ & -\frac{X_0X_1Ai(0) - (\frac{Ai_z(0)}{\sqrt{3}} - Gi_z(0))\frac{\pi\beta^2}{(3i\alpha)^{\frac{1}{3}}}X_1\Phi}{i\alpha}H = \\ & -\frac{X_0X_1Ai(0) - 2Ai_z(0)\frac{\pi\beta^2}{\sqrt{3}(3i\alpha)^{\frac{1}{3}}}X_1\Phi}{i\alpha}H \end{aligned}$$

Then the Stefan condition gives us the following ordinary differential equation defining the evolution of disturbances to the ice surface:

$$H_t = G(\phi, \alpha, \beta, H_0, a)H \tag{3.55}$$

Here the complex growth rate $G$ is given by:

$$G = \frac{X_1}{3ai\alpha}\left(\pi\frac{2(3i\alpha)^{\frac{5}{3}}}{3^{\frac{5}{2}}}\Phi Ai_z(0) - \frac{3i\alpha}{H_0X_1} + X_0Ai(0) - \frac{2Ai_z(0)\pi\beta^2}{\sqrt{3}(3i\alpha)^{\frac{1}{3}}}\Phi\right) \tag{3.56}$$

with $\Phi$, $X_0$ and $X_1$ defined by the equations **(3.27)**, **(3.50)** and **(3.53)** respectively.

The imaginary part of the corresponding complex phase speed is given by $c_i = Re(G)$ and the real phase speed of the wave traveling in the direction $(\alpha, \beta, 0)$ by $c_r = -\frac{Im(G)}{\sqrt{\alpha^2+\beta^2}}$. The formula for the growth rate of 2D disturbances can be obtained by taking the limit of **(3.56)** as $\beta \to 0$.

From the formula for the complex growth rate it can be seen immediately that Prandtl number and solid/liquid density ratio do not influence the neutral curves of the linear problem (provided our initial assumption $\frac{\rho_i}{\rho_l} < 1$ holds).

If the flow can become unstable for certain values of $(\alpha, \beta, \phi, We)$, then the neutral stability domain is given by $c_i = Re(G) = 0$. For given media parameters and angle of incline $\phi$, the neutral curve represents a surface in $(\alpha, \beta, H_0)$. From **(3.56)** it follows that this neutral surface is given by the following expression:

$$H_0(\alpha, \beta, We, \phi) = 2\frac{1 - \sqrt{3}A_2 + A_2^2}{-1 + \sqrt{3}A_2}\frac{1}{-A_1 + A_3 + A_4} \tag{3.57}$$

with the coefficient functions $A_{1-4}$ defined as follows:

$$A_1(\alpha, \beta, We, \phi) = \pi\frac{2(3\alpha)^{\frac{2}{3}}}{3^{\frac{3}{2}}}Ai_z(0) = 2\pi Ai_z 3^{-\frac{5}{6}}\alpha^{\frac{2}{3}} \tag{3.58}$$

$$A_2(\alpha,\beta,We,\phi) = -(3\alpha)^{-\frac{5}{3}}\frac{\alpha^2+\beta^2}{Ai_z(0)}\left(\cos\phi + \frac{\alpha^2+\beta^2}{We}\frac{\sin\phi}{3}\right) \tag{3.59}$$

$$A_3(\alpha,\beta,We,\phi) = \frac{Ai(0)}{Ai_z(0)}\frac{\alpha^2+\beta^2}{3^{\frac{1}{3}}\alpha^{\frac{4}{3}}}\left(\cos\phi + \frac{\alpha^2+\beta^2}{We}\frac{\sin\phi}{3}\right) \tag{3.60}$$

$$A_4(\alpha,\beta,We,\phi) = -2Ai_z(0)\frac{\pi\beta^2}{3^{\frac{5}{6}}\alpha^{\frac{4}{3}}}\left(\cos\phi + \frac{\alpha^2+\beta^2}{We}\frac{\sin\phi}{3}\right) \tag{3.61}$$

The 2D expressions for the neutral curve can be obtained from **(3.57)** by letting $\beta \to 0$ in the above expressions.

**3.1.4.1.1 2D Instability** In 2D case, for given media parameters and angle of incline $\phi$, **(3.57)** yields neutral curves in $(\alpha, H_0)$ plane (where $H_0$ - is the initial ice thickness). A typical neutral curve in 2D case in the $(\alpha, H_0)$ plane is shown below, the analysis of the sign of $c_i$ indicates that the flow is unstable for the combinations of $\alpha$ and $H_0$ within the curve and stable for the combinations of $\alpha$ and $H_0$ outside the curve:

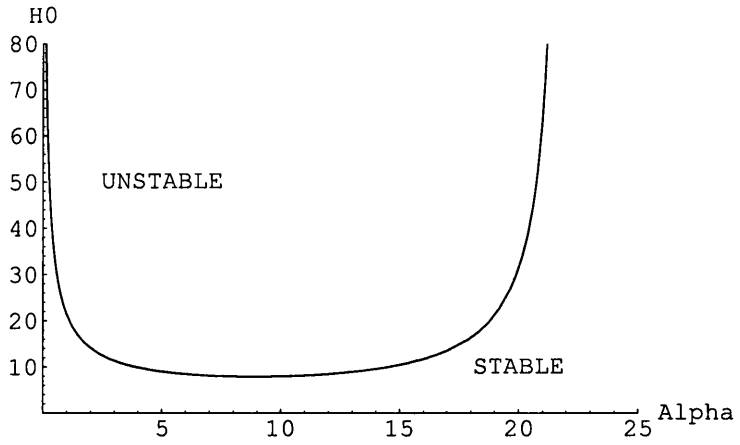


Figure 3.3: Typical analytic 2D neutral curve for the case of $Pr = 1$

For $H_0 \to \infty$, there are two vertical asymptotes, one corresponds to $\alpha = 0$ and the other one gives the maximum unstable wave number. In case of $We \gg 1$ or $\phi \ll 1$ the maximum unstable wave number is given by:

$$\alpha = \left(3^{\frac{13}{6}} Ai_z(0)\right)^3 \tag{3.62}$$

For the non-zero surface tension case the limiting wave number has to be determined numerically. The asymptote for the lower branch in Fig. 3.3 ($\alpha \to 0$) is given by:

$$H_0 \sim 5.198\alpha^{-\frac{2}{3}} \tag{3.63}$$

The increase of the surface tension effectively dampens short waves, the increase in the angle of incline increases short wave instability (for negligible surface tension). The figure 3.4 shows 2D neutral curves in $(\alpha, H_0)$ plane for different values of the Weber number and angle of incline $\phi$:

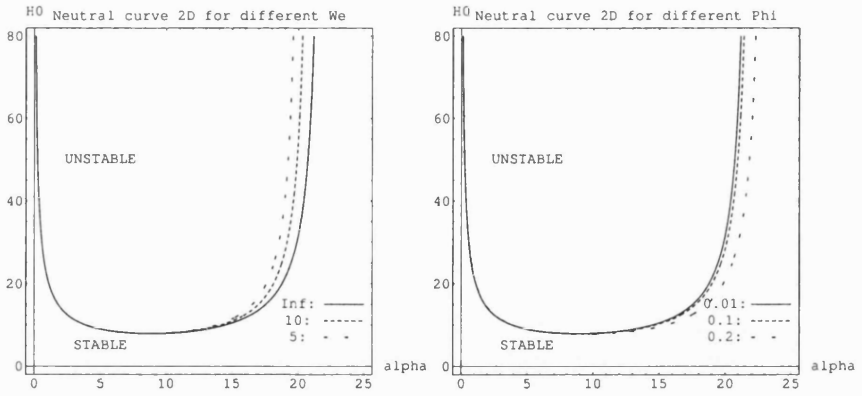


(a) Phi=0.001 (b) We=10000

Figure 3.4: 2D neutral curves dependence on $We$ and $\phi$

As can be seen from the expression **(3.56)** for $G$, the value of $H_0$ has no influence on the phase speed. The plots below show the imaginary and real parts of the complex phase speed $c$ as functions of the wave number $\alpha$ for different values of the initial ice thickness $H_0$ in 2D case:

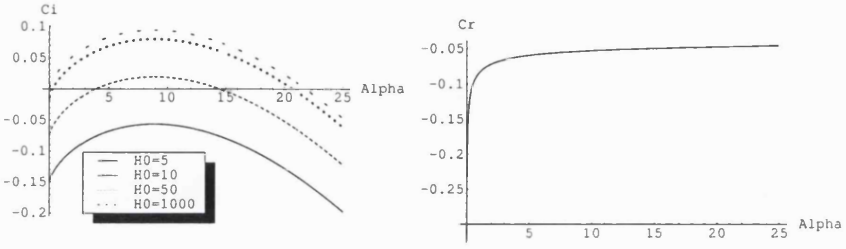


(a) Re(c) (b) Im(c)

Figure 3.5: 2D case, $c_i(\alpha)$ and $c_r(\alpha)$ for $\phi = 0.001$ and $We = 1000$

Note that the sign of $c_r$ is negative. It is possible to show that unstable disturbances propagate upstream either using the spatio-temporal analysis of eigenvalues described by Briggs (1964) or by considering the evolution of a spatially localised initial condition. In the next section the latter method is employed in order to analyse the disturbances propagation. The upstream propagation is an important feature of the icing instability, it was observed in all unstable cases in this thesis.

**3.1.4.1.2 2D Initial-value problem** Using the solution obtained for $Pr = 1$, we can consider evolution of small disturbances of the ice surface. In this section we will look at the evolution of a small disturbance in the Gaussian form ($H_{init} = e^{-x^2}$). In order to do this we utilise the analytic solution and obtain the original function by inverting the Fourier transform and computing the resulting integral numerically.

The computations for the chosen form of the initial disturbance demonstrate that the disturbance introduced into the flow under unstable conditions grows and propagates upstream, and the disturbance introduced under stable conditions decays, but still propagates upstream. Fig. 3.6 illustrates the behaviour of decaying and growing solutions for the initial perturbation given by $H_{init} = e^{-x^2}$.

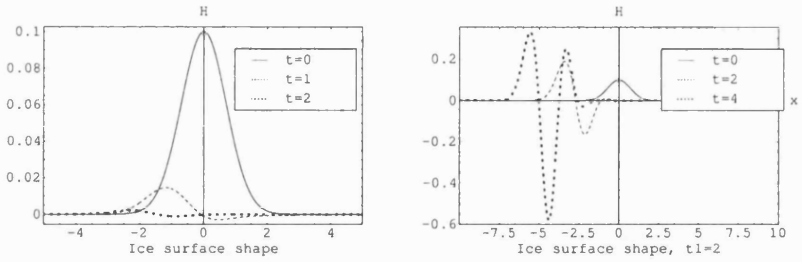


(a) Stable case, H0=5 (b) Unstable case, H0=30

Figure 3.6: $H(t)$, 2D case for $\phi = 0.001$ and $We = 1000$

The figure above illustrates two important effects that have been observed in all our computations:

1. The phase speed for the unstable disturbances is always negative (which is what can be observed in experiments Gilpin (1981, 1979); Seki, Fukusako and Younan (1984); Streitz, Ettema, Rothmayer and Tsao (1998))

2. Increasing the unperturbed height of the ice layer increases the icing instability which is also in the agreement with the experimental results (Gilpin (1981, 1979))

Provided that the qualitative description holds for the channel case as well, the scenario of the ice-band formation as observed, for example, by Gilpin (1981,

1979) can be understood then as an upstream propagating icing instability. The downstream exit of the pipe introduces disturbances into the flow. When the absolute value of the wall temperature is sufficiently small ($H_0$ is small), the disturbances propagate upstream and decay. When $H_0$ is supercritical, the disturbances grow and propagate upstream, and their growth is limited by nonlinearity (see the section "3.1.5 Numerical solution for 2D nonlinear viscous layer"). This process repeats forming the ice-band structure.

**3.1.4.1.3 3D Instability** In the 3D case the neutral curve is actually a surface in $(\alpha, \beta, H_0)$ space. However since this 3D representation is difficult to analyse, we have chosen to look at the level curves of this surface for fixed values of $H_0$ instead. The plot below shows such neutral curves in $(\alpha, \beta)$ plane for different values of the initial ice thickness $H_0$:

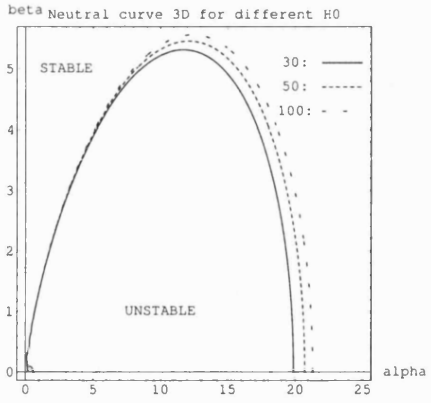


Figure 3.7: 3D neutral curves

The instability domain is bounded by the curves shown on the plot above. The increase of the initial ice thickness $H_0$ destabilises the flow, however there is a limiting curve which is approached rapidly (there is no visible difference in the curves for $H_0 = 100$ and $H_0 = 1000$).

An interesting feature of the problem is that there is a small range of $H_0$ for which the flow is essentially unstable to 3D disturbances and stable to 2D disturbances (Fig. 3.8).

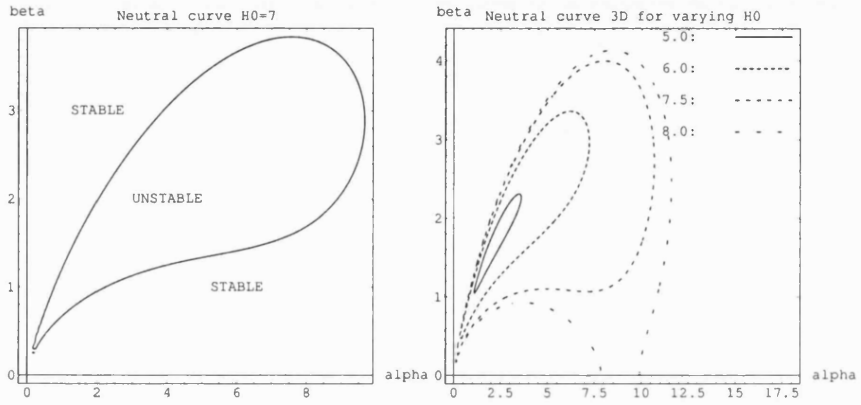


Figure 3.8: Purely 3D Instability

This result is consistent since the Squire theorem (Squire (1933)) is not relevant to the double-deck equations because of the absence of the Reynolds number in the equations.

**3.1.4.1.4 3D Initial-value problem** In 3D case we can use the solution obtained for the ice surface shape in order to analyse the propagation of an introduced 3D disturbance of the ice surface. In this section we will look at the development of a Gaussian perturbation in the form of $e^{-(x^2+z^2)}$. Our computations show that for a 3D disturbance, initially the ice height rapidly decreases and a wake is generated (Fig. 3.9-3.10). However later, when, the front becomes close to a 2D one, the perturbation starts to propagate upstream and grow. An example of 3D disturbance development is shown on Fig. 3.11-3.12 for $H_0 = 50$.

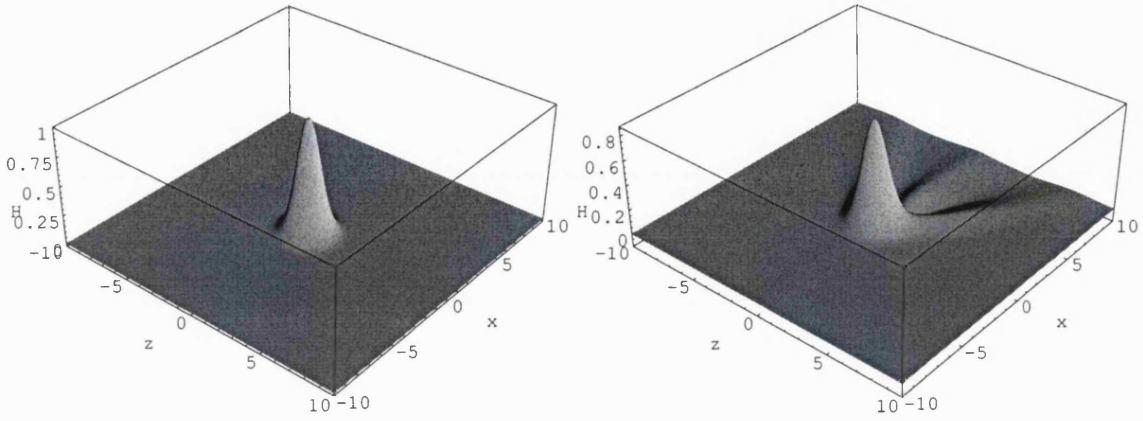


(a) t=0 (b) t=1

Figure 3.9: 3D Ice surface, $We = 1000$, $\phi = 0.001$, $t = 0, 0.1$

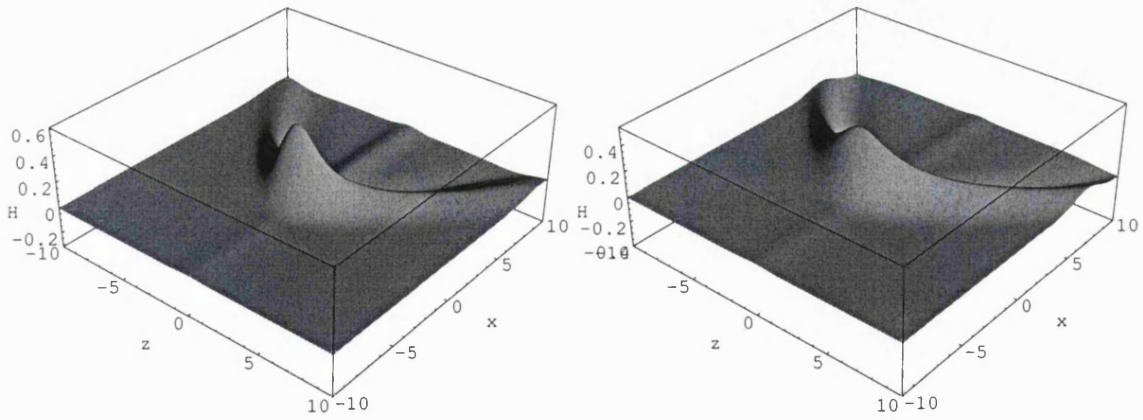


(a) t=4 (b) t=8

Figure 3.10: 3D Ice surface, $We = 1000$, $\phi = 0.001$, $t = 4, 8$

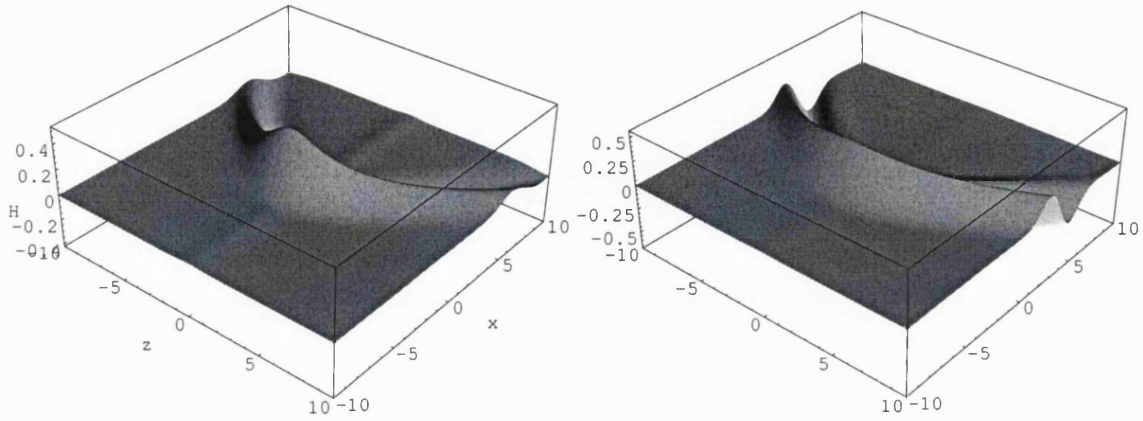


(a) t=10 (b) t=20

Figure 3.11: 3D Ice surface, $We = 1000$, $\phi = 0.001$, $t = 10, 20$

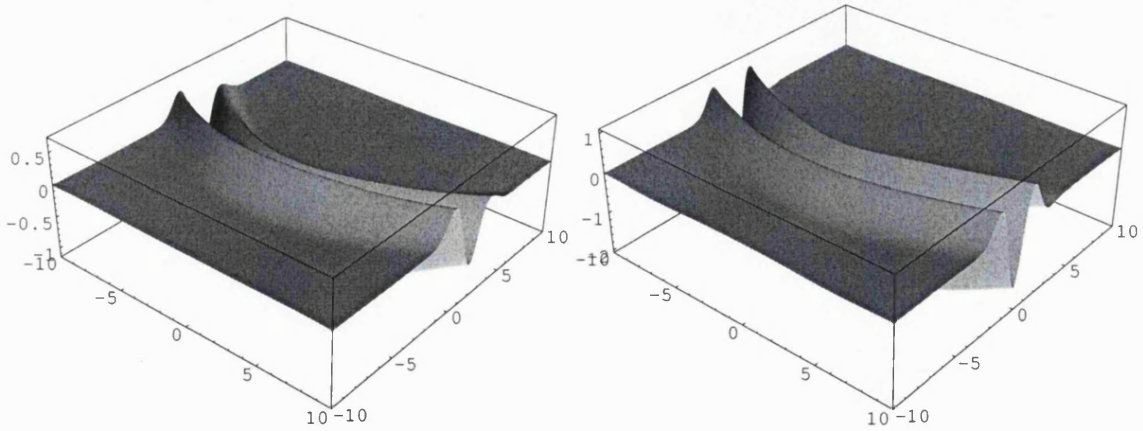


(a) t=30 (b) t=40

Figure 3.12: 3D Ice surface, $We = 1000$, $\phi = 0.001$, $t = 30, 40$

**3.1.4.2 Numerical solution** In the general case $Pr \neq 1$ and, therefore, equations for temperature and horizontal velocity cannot be combined, but the solutions for velocity components $u$, $v$ and $w$ (which can be obtained from the

equations **(3.42)**, **(3.41)** and **(3.38)**) will still be valid. In this case, it is possible to use the solution for velocity field in terms of Airy functions and solve the equation for temperature numerically. However this methods leads to a Scorer-type equation for the temperature with non-constant right-hand side, where the source term contains a double integral of the Airy $Ai$ function $Ai(z)$. In order to write this equation with the zero condition at $\infty$, we will introduce a new function $R$ related to the temperature by $T = F(R-1)$. Then, in terms of the function $R$, the equation takes the following form:

$$\begin{cases} \frac{1}{Pr} R_{yy} - 3i\alpha y R = \lambda(y, \alpha, \beta, \phi) \\ R(\infty) = 0,\ R(0) = 1 - \frac{1}{X_1} \end{cases} \tag{3.64}$$

Here $X_1$ is the same for $Pr = 1$ (equation **(3.53)**). The solution of this system can then be used in order to solve the ice surface evolution equation:

$$H_t = \frac{1}{a}\left(-\frac{1}{H_0} - R_y(0)X_1\right) H \tag{3.65}$$

However the source term $\lambda$ is given by $\lambda = 3i\alpha\left(\frac{1}{X_1} - 1\right) y + X_0 \int_0^y \int_0^\tau Ai(q(3i\alpha)^{\frac{1}{3}}) dq d\tau$ and in order to solve **(3.64)**, we the need to integrate Airy $Ai$ function twice and this could be done making use of an external library providing special functions support. On the other hand, if we build a numerical solver for the Airy-type equations, then it is extremely easy to solve the whole problem numerically without reducing it to **(3.64)**, as the same generic numerical scheme can be applied for the whole governing system of equations expressed in matrix form. This approach seems to be easier and more efficient than solving **(3.64)** directly.

The system of linear stability equations for the double-deck can be converted into

a system of $2^{nd}$ order ODEs by introducing the following system of functions:

$$\begin{cases} V = \frac{v}{F} - 3i\alpha y \\ V_{II} = \frac{1}{F}\frac{d^2v}{dy^2} \\ \tau = \frac{T}{F} + 1 \end{cases} \tag{3.66}$$

From **(3.25)** and **(3.39)**, we obtain the following system of equations for $V$, $V_{II}$ and $\tau$:

$$\left\{ \begin{array}{c} \frac{d^2V_{II}}{dy^2} = 3i\alpha y V_{II} \\ \frac{d^2V}{dy^2} = V_{II} \\ \frac{d^2\tau}{dy^2} = 3i\alpha y\tau + V \end{array} \right| \tag{3.67}$$

with the following boundary conditions at 0 and $\infty$:

$$\left\{ \begin{array}{c} \frac{dV_{II}}{dy}(0) = (\alpha^2+\beta^2)\left(\cos\phi + \frac{\alpha^2+\beta^2}{We}\frac{\sin\phi}{3}\right) \\ V(0) = 0 \\ \tau(0) = 1 - \frac{1}{X_1} \\ V_{II}(\infty) = 0 \\ V(\infty) = -\frac{i\alpha}{3}\left(\cos\phi + \frac{\alpha^2+\beta^2}{We}\frac{\sin\phi}{3}\right) \\ \tau(\infty) = 0 \end{array} \right| \tag{3.68}$$

The numerical solution of this system yields $\frac{d\tau}{dy}(0)$ necessary in order to solve the evolution equation for $H$:

$$H_t = -\frac{H}{a}\left(X_1\frac{d\tau}{dy}(0) + \frac{1}{H_0}\right) = GH \tag{3.69}$$

Then we can take the inverse Fourier transform of $H(\alpha,\beta,t)$ and obtain the real

ice surface perturbation function $H(x,z,t)$. Also since $G$ does not depend on $t$, the system should be solved only once on the desired grid in $(\alpha,\beta)$ space, then the resulting $G$ matrix can be used to determine $H(x,z,t)$ for any $t$.

The $2^{nd}$ order system **(3.67)-(3.68)** was approximated with $2^{nd}$ order accuracy using central differences, the resulting 3-diagonal linear systems of grid equations were solved using forwards-backwards substitution (for example, see Isaacson and Keller (1966)). The original $H(x,z,t)$ function was obtained from the Fourier image with direct numerical integration using trapezoidal rule.

**3.1.4.2.1 Grids used** The numerically determined approximation order in $y$ was of $\sim 1.992$ on a grid of 1000 in $y$ and better for finer grids. The upper boundary conditions have to be set at some finite $y = y^e$, the numerically determined convergence in $y^e$ was $\sim M\frac{1}{y^e}$, where $M = const < 10^{-3}$ for $y^e > 10$. In all cases presented below in this section, the equally-spaced grid of 2000 points in $y$ was used with $y^e = 20$.

For the 2D case the following grids were used:

$$\{\alpha \in [-25,25],\ \alpha_n = \tfrac{n}{60},\ n = -1500..1500\}$$
$$\{x \in [-40,40],\ x_n = \tfrac{n}{50},\ n = -2000..2000\}$$

For the 3D case the following grids were used:

$$\{\alpha,\beta \in [-20,20],\ \alpha_n,\beta_n = \tfrac{n}{10},\ n = -200..200\}$$
$$\{x,z \in [-10,10],\ x_n,z_n = \tfrac{n}{20},\ n = -200..200\}$$

**3.1.4.2.2 Influence of the Prandtl number** With numerical solution at hand, the obvious question to ask is how relevant is the analytic solution for

$Pr = 1$. I.e. how different is the solution for a real Prandtl number for water ($\sim 13.47$ at $0^oC$) from the solution for $Pr = 1$?

In order to analyse the influence of the Prandtl number on the linear solutions, we note that the Prandtl number appears in the equations only in two places, namely, in the equation for temperature $3i\alpha yT + v = \frac{1}{Pr}T_{yy}$ and in the Stefan condition: $T_y = -Pr\Theta_{il}H_t - \frac{H}{H_0}$.

Let us consider the following three cases:

1. $Pr_1 = 13.47$, water at $0^o$ , computed numerically at time $t = t_1$.
2. $Pr_2 = 1.0$, analytic solution at $t = t_1$.
3. $Pr_2 = 1.0$, analytic solution at $t = t_2 = t_1\frac{Pr_2}{Pr_1}$.

The comparison between these three cases for an example of 2D case where $H_0 = 100$, $\phi = 0.001$ and $We = 1000.0$ is given on Fig. 3.13 (computations for other values of problem parameters yielded similar results, therefore we use only one point in parametric space as an illustration).

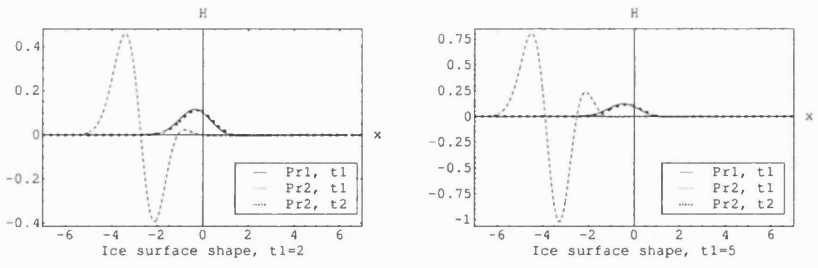


Figure 3.13: The dependency of the linear problem solution on the Prandtl number

It can be clearly seen that the analytic solution for $Pr = 1$ with rescaled time differs negligibly from the numeric solution for $Pr = 13.47$. This demonstrates

that the major influence of the $Pr$ number is in the growth rate coefficient and the analytic solution can be used when $Pr \neq 1$, provided we re-scale the time accordingly. The 3D problem exhibited similar behaviour. This result essentially means that in the linear problem, the thermal boundary layer thickness affects the speed of disturbances propagation but has no significant impact on the shape of disturbances.

### 3.1.5 Numerical solution for 2D nonlinear viscous layer

Let us now consider 2D nonlinear viscous layer. Here, as in the linear case, we can obtain the exact solution for the temperature distribution in the ice layer. Using this solution in order to eliminate the ice temperature from the boundary conditions at the ice surface, we obtain the boundary-value problem for the nonlinear viscous double-deck layer in form given by **(3.70)**.

$$\begin{cases} uu_x + vu_y = -P_x + u_{yy} \\ u_x + v_y = 0 \\ uT_x + vT_y = \frac{1}{Pr} T_{yy} \\ P = F\cos\phi - \frac{F_{xx}}{We}\frac{\sin\phi}{3} \\ u(H) = 0,\ u(\infty) = 3y - 3F \\ T(H) = 0,\ T(\infty) = y - F \\ v(H) + u(H)\frac{\partial H}{\partial x} = 0, \\ v(\infty) = 3yF_x \\ \frac{\partial T}{\partial y}(H) = -\lambda_{il}\frac{T_w}{H+H_0} - a\frac{\partial H}{\partial t} \end{cases} \tag{3.70}$$

The problem we are trying to solve is similar to the problems arising in the triple-deck theory. Therefore it seems reasonable to employ numerical approaches that

have been successfully applied in the triple-deck theory for steady and unsteady separation problems.

We will derive a global-marching type scheme for this problem, similar to the schemes used by Ruban (1990, 1976) and Cassel, Ruban and Walker (1995), using the conservative form of the equations. In order to do this we introduce derivatives in pseudo-time $\tau$ in order to construct the iterative process and rewrite our equations in the conservative form (see for example Chung (2002)) in Cartesian coordinates:

$$\frac{\partial \vec{Q_c}}{\partial \tau} + \frac{\partial \vec{E_c}}{\partial x} + \frac{\partial \vec{G_c}}{\partial y} = 0 \tag{3.71}$$

$$\vec{Q_c} = \left\| \begin{array}{c} Q_{c1} \\ Q_{c2} \end{array} \right\| \tag{3.72}$$

$$\vec{E_c} = \left\| \begin{array}{c} u^2 + P \\ uT \end{array} \right\| \tag{3.73}$$

$$\vec{G_c} = \left\| \begin{array}{c} uv - u_y \\ vT - \frac{1}{Pr} T_y \end{array} \right\| \tag{3.74}$$

Here $\vec{Q_c}$ is the iterational function that can be varied in order to obtain better convergence. These equations together with the continuity equation form our system.

Then we will map our $(-\infty .. + \infty, 0 .. + \infty)$ computational domain in $(x, y)$ to a rectangle $(-1 .. +1, 0 .. +1)$ using the arctangent transform similar to the transform

used by Cassel, Ruban and Walker (1995), but with a time-dependent lower boundary included into the transform:

$$\begin{cases} \xi = \frac{2}{\pi} \arctan\left(\frac{x-x_0}{A}\right) \\ \eta = \frac{2}{\pi} \arctan\left(\frac{y-H(x,t)}{B}\right) \end{cases} \tag{3.75}$$

$$\begin{cases} x = x_0 + A \tan\left(\frac{\pi}{2}\xi\right) \\ y = H(x,t) + B \tan\left(\frac{\pi}{2}\eta\right) \end{cases} \tag{3.76}$$

The partial derivatives that we need in order to derive the expression for the Jacobian and transformed equations are given by:

$$\begin{cases} \frac{\partial \xi}{\partial x} = \frac{2}{A\pi} \cos^2\left(\frac{\pi}{2}\xi\right) \\ \frac{\partial \xi}{\partial y} = 0 \end{cases} \tag{3.77}$$

$$\begin{cases} \frac{\partial \eta}{\partial x} = -\frac{2}{B\pi} H_\xi \frac{\partial \xi}{\partial x} \cos^2\left(\frac{\pi}{2}\eta\right) = -\frac{1}{AB}\left(\frac{2}{\pi}\right)^2 H_\xi \cos^2\left(\frac{\pi}{2}\eta\right) \cos^2\left(\frac{\pi}{2}\xi\right) = -H_\xi \frac{\partial \eta}{\partial y}\frac{\partial \xi}{\partial x} \\ \frac{\partial \eta}{\partial y} = \frac{2}{B\pi} \cos^2\left(\frac{\pi}{2}\eta\right) \end{cases} \tag{3.78}$$

The transformation depends on $H$ and, therefore is time dependent, however the Jacobian of the transformation $J$ does not depend on time:

$$J(\xi,\eta) = \frac{\partial(x,y)}{\partial(\xi,\eta)} = AB\left(\frac{\pi}{2}\right)^2 \frac{1}{\cos^2\left(\frac{\pi}{2}\xi\right)\cos^2\left(\frac{\pi}{2}\eta\right)} \tag{3.79}$$

Also we will need the following derivative for the pressure-displacement law:

$$\frac{\partial^2 \xi}{\partial x \partial \xi} = -\frac{4}{A\pi}\frac{\pi}{2} \cos\left(\frac{\pi}{2}\xi\right) \sin\left(\frac{\pi}{2}\xi\right) = -\frac{1}{A}\sin(\pi\xi) \tag{3.80}$$

Apart from transferring boundary conditions to fixed surfaces, this transformation provides us with an adaptive mesh in $\eta$ direction. The mesh is condensed towards the ice boundary in $\eta$ direction and towards a fixed point fixed point in $\xi$ direction. The $A$ and $B$ parameters of the transformation effectively govern the density of the nodes distribution in physical space:

$$\Delta x_i = x_{i+1} - x_i = A\left(\tan\left(\frac{\pi}{2}\xi_{i+1}\right) - \tan\left(\frac{\pi}{2}\xi_i\right)\right) \tag{3.81}$$

$$\Delta y_i = y_{i+1} - y_i = B\left(\tan\left(\frac{\pi}{2}\eta_{i+1}\right) - \tan\left(\frac{\pi}{2}\eta_i\right)\right) \tag{3.82}$$

The grid compression in $x$ direction is extremely important since the disturbance propagates upstream and the grid is fixed in $x$ direction. Let index $i$ run from $-\frac{N}{2}$ to $\frac{N}{2}$ including 0 (say $N$ is even), then:

$$\Delta\xi_i = \xi_{i+1} - \xi_i = const = \Delta\xi = \frac{2}{N}$$

$$\xi_i = i\Delta\xi$$

$$\Delta x_i = x_{i+1} - x_i = A\left(\tan\left(\tfrac{\pi}{2}\xi_{i+1}\right) - \tan\left(\tfrac{\pi}{2}\xi_i\right)\right) = A\frac{\sin\left(\frac{\pi}{2}\xi_{i+1}\right)\cos\left(\frac{\pi}{2}\xi_i\right) - \cos\left(\frac{\pi}{2}\xi_{i+1}\right)\sin\left(\frac{\pi}{2}\xi_i\right)}{\cos\left(\frac{\pi}{2}\xi_{i+1}\right)\cos\left(\frac{\pi}{2}\xi_i\right)} = 2A\frac{\sin\left(\frac{\pi}{2}\Delta\xi\right)}{\cos\left(\frac{\pi}{2}\Delta\xi\right) + \cos\left(\frac{\pi}{2}(\xi_{i+1}+\xi_i)\right)} = 2A\frac{\tan\left(\frac{\pi}{2}\Delta\xi\right)}{1 + \frac{\cos\left(\frac{\pi}{2}(2i+1)\Delta\xi\right)}{\cos\left(\frac{\pi}{2}\Delta\xi\right)}}$$

It follows from the last formula that the smallest step in the physical space at $x_0$ is $A\tan\left(\frac{\pi}{2}\Delta\xi\right)$. The most important question about the transformed grid is whether

it will be able to resolve the perturbations as they propagate upstream, since the physical domain grid step increases upstream and downstream. Therefore it is necessary to choose the condensation parameter $A$ in such a way that $\Delta x_i$ will be sufficiently small at a given point $x_P$ with the total number of nodes fixed (the total number of nodes will depend on the computational resources). The previous equation yields for $i \gg 1$:

$$\begin{aligned}\Delta x_i &= 2A\frac{\sin\left(\frac{\pi}{2}\Delta\xi\right)}{\cos\left(\frac{\pi}{2}\Delta\xi\right)+\cos\left(2\arctan\frac{x_P-x_0}{A}\right)} = \\ &2A\frac{\sin\left(\frac{\pi}{2}\Delta\xi\right)}{\cos\left(\frac{\pi}{2}\Delta\xi\right)+2\cos^2\left(\arctan\frac{x_P-x_0}{A}\right)-1} = \\ &2A\frac{\sin\left(\frac{\pi}{2}\Delta\xi\right)}{\cos\left(\frac{\pi}{2}\Delta\xi\right)+\frac{2}{1+\left(\frac{x_P-x_0}{A}\right)^2}-1}\end{aligned}$$

If we fix the number of nodes (and therefore $\frac{\pi}{2}\Delta\xi$) and the value of $\Delta x_i$, then the above expression leads to a cubic equation for $A$ which can be solved in order to obtain the suitable value of the condensation parameters.

The definition of a time-dependent mesh in $\xi$ direction that will follow the disturbance propagation seems problematic since, although we can predict the disturbance propagation speed from linear estimates, it is not clear how the disturbance propagation speed will be modified by the nonlinearity. Therefore we fix $x_0$ bearing in mind that the resolution can drop as the perturbation propagates upstream and choosing the grid dimension in the $\xi$ direction accordingly.

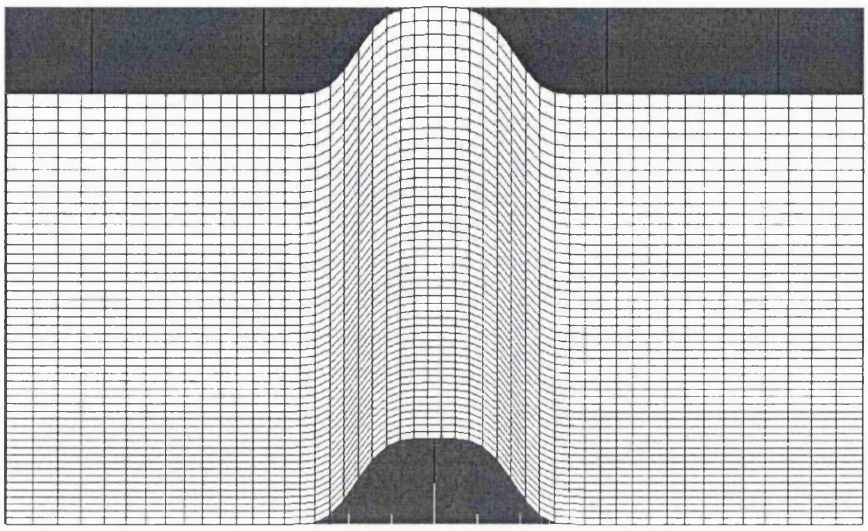

Figure 3.14: An example of grid for nonlinear computations

An example of the grid constructed with the transformation described is given on the figure above. This example corresponds to a coarse grid with compression parameters $A = 5$ and $B = 5$, number of nodes $N_x = N_y = 50$ and the physical domain covered ($x \in [-5, 5], y \in [0, 5]$).

Since the system is written in the conservative form, the transformation of the system of equations from $(x, y, t)$ space to $(\xi, \eta, t)$ is obtained immediately (see, for example, Chung (2002)). The general transformation for the Cartesian vector variables $\vec{Q_c}$, $\vec{E_c}$ and $\vec{G_c}$ is given by the following expressions:

$$\begin{cases} \vec{Q_c} = J\vec{Q} \\ \vec{E_c} = J\left(\vec{E}\frac{\partial \xi}{\partial x} + \vec{G}\frac{\partial \xi}{\partial y}\right) \\ \vec{G_c} = J\left(\vec{E}\frac{\partial \eta}{\partial x} + \vec{G}\frac{\partial \eta}{\partial y}\right) \end{cases} \tag{3.83}$$

And the transformed system of equations in $(\xi, \eta)$ retains conservative form **(3.84)**.

$$\frac{\partial \vec{Q}}{\partial \tau} + \frac{\partial \vec{E}}{\partial \xi} + \frac{\partial \vec{G}}{\partial \eta} = 0 \tag{3.84}$$

In our transformation $\xi$ does not depend on $y$, therefore $\xi$- flux is given by:

$$\vec{E} = J(\xi, \eta)\frac{\partial \xi}{\partial x}\left\| \begin{array}{c} u^2 + P \\ uT \end{array} \right\| \tag{3.85}$$

However $\eta$ depends on both $x$ and $y$, therefore we maintain the full form of $\eta$-flux:

$$\vec{G} = J(\xi, \eta)\left(\frac{\partial \eta}{\partial x}\left\| \begin{array}{c} u^2 + P \\ uT \end{array} \right\| + \frac{\partial \eta}{\partial y}\left\| \begin{array}{c} uv - \frac{\partial \eta}{\partial y}u_\eta \\ Tv - \frac{1}{Pr}\frac{\partial \eta}{\partial y}T_\eta \end{array} \right\|\right) \tag{3.86}$$

The continuity equation in $(\xi, \eta)$ variables becomes:

$$\frac{\partial \xi}{\partial x}\frac{\partial u}{\partial \xi} + \frac{\partial \eta}{\partial x}\frac{\partial u}{\partial \eta} + \frac{\partial \eta}{\partial y}\frac{\partial v}{\partial \eta} = 0 \tag{3.87}$$

The pressure-displacement law can be expressed in the new variables as:

$$P = F\cos\phi - \frac{\sin\phi}{3We}\frac{\partial \xi}{\partial x}\left(\frac{\partial^2 F}{\partial \xi^2}\frac{\partial \xi}{\partial x} + \frac{\partial F}{\partial \xi}\frac{\partial^2 \xi}{\partial x \partial \xi}\right) \tag{3.88}$$

For the computational purposes, we cannot set the upper boundary at $\eta = 1$ as we have $y(\xi, \eta)$ in the boundary conditions on the outer edge of the viscous sublayer. Therefore we will choose some cut-off $\eta = \eta_e$ and evaluate boundary conditions at this point. Note, that unlike in linear problem computations, we have a compressed grid, therefore we can set $\eta_e$ to be sufficiently large so that we do not need the second order correction in the boundary condition for $v$ at $\eta_e$.

For the boundary conditions at the ice surface and the outer edge of the viscous sublayer we then have:

$$\begin{cases} u = 0 \\ v = 0 \\ T = 0 \\ aH_t = -\frac{\partial T}{\partial \eta}\frac{\partial \eta}{\partial y} - \lambda_{il}\frac{T_w}{H+H_0} \end{cases} \qquad \eta = 0 \tag{3.89}$$

$$\begin{cases} v = 3yF_x \\ u = 3y(\xi,\eta) - 3F \\ T = y(\xi,\eta) - F \end{cases} \qquad \eta \to 1$$

Respectively on the left boundary we assume the incoming flow:

$$\begin{cases} u = 3y(\xi,\eta) \\ v = 0 \\ T = -y(\xi,\eta) \end{cases} \qquad \xi \to -1$$

On the right boundary two types of condition can be used:

1. The "strong" condition - incoming flow assumed on the right boundary.
2. The "weak" condition - conditions on the right boundary are obtained by linear extrapolation from the computational domain, which is equivalent to setting $2^{nd}$ derivatives to zero on the right boundary.

For the computational purposes, we will set the domain in $\xi$ to be $[-\xi_e, \xi_e]$ where $\xi_e$ is a sufficiently large number.

The solution algorithm used in this work implies solving the system of the unsteady boundary-layer equations in order to obtain a steady solution for the fixed lower boundary $H$ and then using the Stefan condition in order to update the ice shape $H$ and proceed to the next time step in the following schematic sequence:

1. We consider the ice surface shape $H$ to be fixed at some time step.

2. For this fixed ice surface shape, we perform $u - v - F$ iterations while the appropriate derivative in pseudo-time (used to construct the iterational process) is greater then the computational precision according to the following procedure:

   (a) First, we solve the first equation of the system **(3.84)** for $u$ at each $\xi$ using $v$ , $F$ , $P$ and nonlinear terms from the previous iteration in pseudo-time. This step is repeated several ($\sim 3$) times, each time we update terms nonlinear in $u$ using the solution obtained for $u$ in order to stabilise $\xi$-flux , we will refer to this process as "$\xi$- flux levelling". $\xi$- flux levelling is necessary for unsteady computations. However, even if we are looking for a steady state solution, this procedure increases convergence speed and stability of the algorithm.

   (b) Then we compute $v$ by integrating the continuity equation in $\eta$ from the lower boundary for every $\xi$.

   (c) Finally, we update $F$ for every $\xi$ using the boundary condition for $v$ at the outer edge of the viscous layer $\eta = \eta_e$ .

3. We perform $T$ iterations for fixed ice and free surface shapes and known velocity field. In this iterative process the second equation of the system

**(3.84)** is solved for $T$ at each $\xi$ while the appropriate derivative in pseudo-time (used to construct the iterational process) is greater then the computational precision. The energy equation is linear in $T$ and the iterative process essentially corresponds to obtaining the steady-state solution for the temperature distribution for a "frozen" velocity field and fixed boundaries.

4. As the result of the steps 1-3, we obtain the solution for the temperature field corresponding to the fixed ice shape at a given time step. Then we use the Stefan condition in order to find the ice surface shape at the next time step.

The description above can be translated in the form of the following diagram:

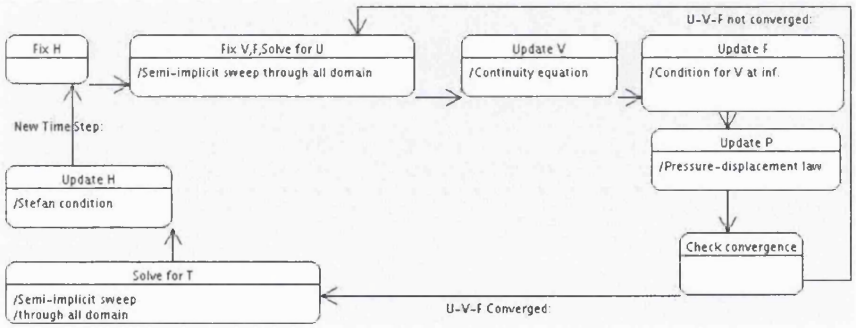


Figure 3.15: Numerical algorithm for nonlinear double-deck

To obtain a steady solution we used $2^{nd}$ order in space and $1^{st}$ order in time finite-difference scheme. Without $\xi$-flux levelling, the scheme is written as:

$$\frac{Q_{i,j}^{k} - Q_{i,j}^{l-1}}{\Delta\tau} + \frac{E_{i+1,j}^{k-1,l-1} - E_{i-1,j}^{k-1,l-1}}{2\Delta\xi} + \frac{G_{i,j+1/2}^{k,l-1} - G_{i,j-1/2}^{k,l-1}}{\Delta\eta} = 0 \qquad (3.90)$$

Here $i \in [0, N_\xi - 1]$ , $j \in [0, N_\eta - 1]$, $k$ denotes flux iterations and $l$ denotes pseudo-time iterations.

$\xi$- flux levelling adds another level of iterations when sweeps through the domain in the $\xi$ direction are made until a steady value of $\xi$-flux $E$ is obtained. I.e. when the solution for $u$ is obtained on level $k$, it is used to update $\xi-$flux, and the equations are solved for $u$ once again. This process is repeated until a norm of the $\xi$-flux change between these iterations becomes less than some given small $\epsilon$. The absolute value norm $max_{i,j} \left|u_{i,j}^{k} - u_{i,j}^{k-1}\right|$ was used to determine the $\xi$-flux iterations convergence. Although $\xi$- flux levelling is not necessary for steady-state computations, it proved to increase the speed of convergence to a steady state and the overall stability of the algorithm.

The $\eta$-flux $G$ was computed at midpoints in order to keep the linear system of the grid equations 3-diagonal. The corresponding values in midpoints were approximated by: $f_{j+\frac{1}{2}} = \frac{1}{2}(f_j + f_{j+1})$.

**3.1.5.1 Solving for $u$** Two values of $Q_{1i,j}^{l}$ were used in computations, $u_{i,j}^{l}$ and $u_{i,j}^{l}u_{i,j}^{l-1}$. The latter is equivalent to the solution with a local non-uniform time step defined by $\Delta\tau_{i,j}^{l} = \frac{\Delta\tau}{u_{i,j}^{l-1}}$. The local time step approach proved to increase the speed of convergence towards a steady state solution, therefore here we give formulas corresponding to the local time step approach.

The expressions for iterational variable $Q$, $\xi$- flux $E$ and $\eta$-flux $G$ are given by:

$$Q_{1i,j}^{k} = J_{i,j}u_{i,j}^{k}u_{i,j}^{l-1}$$

$$Q_{1i,j}^{l-1} = J_{i,j}u_{i,j}^{l-1}u_{i,j}^{l-1}$$

$$E_{1i+1,j}^{k-1,l-1} = J_{i+1,j}\left(\frac{\partial\xi}{\partial x}\right)_{i+1}\left(\left(u_{i+1,j}^{k-1}\right)^2 + P_{i+1}^{l-1}\right)$$

$$E^{k-1,l-1}_{1i-1,j} = J_{i-1,j}\left(\frac{\partial\xi}{\partial x}\right)_{i-1}\left(\left(u^{k-1}_{i-1,j}\right)^2 + P^{l-1}_{i-1}\right)$$

$$\begin{aligned} G^{k,l-1}_{1i,j+\frac{1}{2}} &= J_{i,j+\frac{1}{2}}\Bigg(\left(\frac{\partial\eta}{\partial x}\right)^{l-1}_{i,j+\frac{1}{2}}\left(\left(u^{k-1}_{i,j+\frac{1}{2}}\right)^2 + P^{l-1}_{i}\right) + \\ &\left(\frac{\partial\eta}{\partial y}\right)_{j+\frac{1}{2}}\left[u^{k}_{i,j+\frac{1}{2}}v^{l-1}_{i,j+\frac{1}{2}} - \left(\frac{\partial\eta}{\partial y}\right)_{j+\frac{1}{2}}\frac{u^{k}_{i,j+1}-u^{k}_{i,j}}{\Delta\eta}\right]\Bigg) \end{aligned}$$

$$\begin{aligned} G^{k,l-1}_{1i,j-\frac{1}{2}} &= J_{i,j-\frac{1}{2}}\Bigg(\left(\frac{\partial\eta}{\partial x}\right)^{l-1}_{i,j-\frac{1}{2}}\left(\left(u^{k-1}_{i,j-\frac{1}{2}}\right)^2 + P^{l-1}_{i}\right) + \\ &\left(\frac{\partial\eta}{\partial y}\right)_{j-\frac{1}{2}}\left[u^{k}_{i,j-\frac{1}{2}}v^{l-1}_{i,j-\frac{1}{2}} - \left(\frac{\partial\eta}{\partial y}\right)_{j-\frac{1}{2}}\frac{u^{k}_{i,j}-u^{k}_{i,j-1}}{\Delta\eta}\right]\Bigg) \end{aligned}$$

Substituting these expressions into **(3.90)** we obtain a linear system of equations for $u^k_{i,j}$ at each point in $\xi$. The matrix of the system is 3-diagonal and the system can be written in the following form:

$$A_{i,j-1}u^k_{i,j-1} + B_{i,j-1}u^k_{i,j} + C_{i,j-1}u^k_{i,j+1} = D_{i,j-1} \tag{3.91}$$

The coefficients of the 3-diagonal system are given by:

$$A_{i,j-1} = -J_{i,j-\frac{1}{2}}\left(\frac{\partial\eta}{\partial y}\right)_{j-\frac{1}{2}}\left(\frac{1}{2}v^{l-1}_{i,j-\frac{1}{2}} + \frac{1}{\Delta\eta}\left(\frac{\partial\eta}{\partial y}\right)_{j-\frac{1}{2}}\right)$$

$$\begin{aligned} B_{i,j-1} &= J_{i,j}u^{l-1}_{i,j}\frac{\Delta\eta}{\Delta\tau} + J_{i,j+\frac{1}{2}}\left(\frac{\partial\eta}{\partial y}\right)_{j+\frac{1}{2}}\left(\frac{1}{2}v^{l-1}_{i,j+\frac{1}{2}} + \frac{1}{\Delta\eta}\left(\frac{\partial\eta}{\partial y}\right)_{j+\frac{1}{2}}\right) - \\ &-J_{i,j-\frac{1}{2}}\left(\frac{\partial\eta}{\partial y}\right)_{j-\frac{1}{2}}\left(\frac{1}{2}v^{l-1}_{i,j-\frac{1}{2}} - \frac{1}{\Delta\eta}\left(\frac{\partial\eta}{\partial y}\right)_{j-\frac{1}{2}}\right) \end{aligned}$$

$$C_{i,j-1} = J_{i,j+\frac{1}{2}} \left(\frac{\partial \eta}{\partial y}\right)_{j+\frac{1}{2}} \left(\frac{1}{2} v^{l-1}_{i,j+\frac{1}{2}} - \frac{1}{\Delta \eta} \left(\frac{\partial \eta}{\partial y}\right)_{j+\frac{1}{2}}\right)$$

$$D_{i,j-1} = J_{i,j} \frac{\Delta \eta}{\Delta \tau} \left(u^{l-1}_{i,j}\right)^2 -$$
$$\frac{\Delta \eta}{2\Delta \xi} \left(J^{l-1}_{i+1,j} \left(\frac{\partial \xi}{\partial x}\right)^{l-1}_{i+1} \left(\left(u^{k-1}_{i+1,j}\right)^2 + P^{l-1}_{i+1}\right) - J^{l-1}_{i-1,j} \left(\frac{\partial \xi}{\partial x}\right)^{l-1}_{i-1} \left(\left(u^{k-1}_{i-1,j}\right)^2 + P^{l-1}_{i-1}\right)\right) -$$
$$- \left(J_{i,j+\frac{1}{2}} \left(\frac{\partial \eta}{\partial x}\right)_{i,j+\frac{1}{2}} \left(\left(u^{k-1}_{i,j+\frac{1}{2}}\right)^2 + P^{l-1}_{i}\right) - J_{i,j-\frac{1}{2}} \left(\frac{\partial \eta}{\partial x}\right)_{i,j-\frac{1}{2}} \left(\left(u^{k-1}_{i,j-\frac{1}{2}}\right)^2 + P^{l-1}_{i}\right)\right)$$

The resulting 3-diagonal system is solved for $u^k_{i,j}$ with forwards-backwards substitution (see, for example, Isaacson and Keller (1966)).

**3.1.5.2 Updating $v$** Once we have a settled field for the horizontal component of the velocity $u$ on a pseudo-time step, we can update the vertical component of the velocity $v$. Integrating the continuity equation from 0 to $\eta$ we obtain:

$$v(\xi, \eta) = -\int_0^\eta \left(\frac{\partial \xi}{\partial x}\frac{\partial u}{\partial \xi} + \frac{\partial \eta}{\partial x}\frac{\partial u}{\partial \eta}\right) \frac{1}{\frac{\partial \eta}{\partial y}} d\eta \tag{3.92}$$

This expression can be further simplified using the properties of our coordinate transformation. From **(3.78)** it follows that:

$$\begin{aligned} \frac{\partial \eta}{\partial x} / \frac{\partial \eta}{\partial y} = -\frac{\frac{1}{AB}\left(\frac{2}{\pi}\right)^2 \frac{\partial H}{\partial \xi} \cos^2\left(\frac{\pi}{2}\eta\right) \cos^2\left(\frac{\pi}{2}\xi\right)}{\frac{2}{B\pi} \cos^2\left(\frac{\pi}{2}\eta\right)} = \\ \frac{2}{\pi A} \frac{\partial H}{\partial \xi} \cos^2\left(\frac{\pi}{2}\xi\right) = -H_\xi \frac{\partial \xi}{\partial x} = f(\xi) \end{aligned} \tag{3.93}$$

Since $\frac{\partial \eta}{\partial x} / \frac{\partial \eta}{\partial y}$ does not depend on $\eta$, the second term in the integral **(3.92)** can be integrated analytically:

$$v(\xi, \eta) = -\frac{\partial \xi}{\partial x} \left(-u(\xi, \eta) H_\xi + \int_0^\eta \left(\frac{\partial u}{\partial \xi} / \frac{\partial \eta}{\partial y}\right) d\eta\right) \tag{3.94}$$

Then as $\frac{\partial u}{\partial \xi}(\xi, 0) = 0$, the discrete form of the above equation can be written as:

$$v_{i,j} = \left(\frac{\partial \xi}{\partial x}\right)_i \left(u_{i,j}\frac{H_{i+1} - H_{i-1}}{2\Delta\xi} - (\frac{1}{2}f_{i,j} + \sum_{n=1}^{j-1} f_{i,n})\Delta\eta\right) \tag{3.95}$$

Here $f_{i,n} = \frac{1}{\left(\frac{\partial \eta}{\partial y}\right)_n}\frac{u_{i+1,n} - u_{i-1,n}}{2\Delta\xi}$ in the computational domain.

**3.1.5.3 Updating $F$** After we have computed the vertical velocity field $v$, we can update the free surface shape $F$ from the condition for $v$ at the upper boundary evaluated at $\eta = \eta_e$. Written in terms of derivative in $\xi$, this condition becomes:

$$v(\xi, \eta_e) = 3y(\xi, \eta_e)\frac{\partial F}{\partial \xi}\frac{\partial \xi}{\partial x} = \frac{6}{A\pi}\cos^2\left(\frac{\pi}{2}\xi\right) y(\xi, \eta_e)\frac{\partial F}{\partial \xi} \tag{3.96}$$

We will use $2^{nd}$ order backwards finite-difference approximation for $\frac{\partial F}{\partial \xi}$, which gives the following formula for the discrete values of $F_i$:

$$F_i = \frac{1}{3}\left(4F_{i-1} - F_{i-2} + \frac{2\Delta\xi}{3y_{i,N_\eta-1}}\frac{v_{i,N_\eta-1}}{\left(\frac{\partial \xi}{\partial x}\right)_i}\right) \tag{3.97}$$

In order to calculate the shape of the free surface $F$ at the first step ($i = 1$) we will need one fictitious point on the upstream boundary, therefore we will assume that the flow is unperturbed at $i = -1$.

**3.1.5.4 Updating $P$** If the shape of the free surface $F$ is known, the pressure $P$ can be obtained from the pressure-displacement law:

$$P = F\cos\phi + \frac{\sin\phi}{3We}\frac{\partial \xi}{\partial x}\left(\frac{\partial^2 F}{\partial \xi^2}\frac{\partial \xi}{\partial x} + \frac{\partial F}{\partial \xi}\frac{\partial^2 \xi}{\partial \xi \partial x}\right) \tag{3.98}$$

We will use central differences approximation for the first and second derivatives of $F$, which leads to the following formula for the discrete values $P_i$:

$$P_i = F_i \cos\phi + \frac{\sin\phi}{3We}\left(\frac{\partial\xi}{\partial x}\right)_i \left(\frac{F_{i+1} - 2F_i + F_{i+1}}{\Delta\xi^2}\left(\frac{\partial\xi}{\partial x}\right)_i + \frac{F_{i+1} - F_{i+1}}{2\Delta\xi}\left(\frac{\partial^2\xi}{\partial\xi\partial x}\right)_i\right) \tag{3.99}$$

Then the equation for $u$ is solved again and the cycle is repeated until the following convergence condition is satisfied:

$$max_{i,j}\left(\frac{\left|\left(u^l_{i,j} - u^{l-1}_{i,j}\right)u^{l-1}_{i,j}\right|}{\Delta\tau}\right) < \epsilon \ll 1 \tag{3.100}$$

**3.1.5.5 Solving for T** The $\xi$-flux for temperature $J(\xi,\eta)\frac{\partial\xi}{\partial x}uT$ is linear in $T$, therefore no flux levelling iterations are required. The difference equations for $T$ are similar to the difference equations for $u$ and the resulting 3-diagonal system for $T$ is:

$$A_{i,j-1}T^l_{i,j-1} + B_{i,j-1}T^l_{i,j} + C_{i,j-1}T^l_{i,j+1} = D_{i,j-1} \tag{3.101}$$

$$\begin{aligned} A_{i,j-1} \;=\; & -\frac{J_{i,j-1/2}}{2}\Bigg(\left(\frac{\partial\eta}{\partial x}\right)_{i,j-1/2}\left(u_{i,j-1/2}\right) + \\ & \left(\frac{\partial\eta}{\partial y}\right)_{j-1/2}\left(v_{i,j-1/2} + \left(\frac{\partial\eta}{\partial y}\right)_{j-1/2}\frac{2}{Pr\Delta\eta}\right)\Bigg) \end{aligned}$$

$$\begin{aligned} & B_{i,j-1} = J_{i,j}T^{l-1}_{i,j}\frac{\Delta\eta}{\Delta\tau} + \\ & J_{i,j+1/2}\left(\left(\tfrac{\partial\eta}{\partial x}\right)_{i,j+1/2}\left(u_{i,j+1/2}\right)\tfrac{1}{2} + \left(\tfrac{\partial\eta}{\partial y}\right)_{i,j+1/2}\left(v_{i,j+1/2}\tfrac{1}{2} + \tfrac{1}{Pr}\left(\tfrac{\partial\eta}{\partial y}\right)_{i,j+1/2}\tfrac{1}{\Delta\eta}\right)\right) - \\ & -J_{i,j-1/2}\left(\left(\tfrac{\partial\eta}{\partial x}\right)_{i,j-1/2}\left(u_{i,j-1/2}\right)\tfrac{1}{2} + \left(\tfrac{\partial\eta}{\partial y}\right)_{i,j-1/2}\left(v_{i,j-1/2}\tfrac{1}{2} - \tfrac{1}{Pr}\left(\tfrac{\partial\eta}{\partial y}\right)_{i,j-1/2}\tfrac{1}{\Delta\eta}\right)\right) \end{aligned}$$

$$C_{i,j-1} = \frac{J_{i,j+1/2}}{2}\left(\left(\frac{\partial\eta}{\partial x}\right)_{i,j+1/2}\left(u_{i,j+1/2}\right) + \left(\frac{\partial\eta}{\partial y}\right)_{i,j+1/2}\left(v_{i,j+1/2} - \left(\frac{\partial\eta}{\partial y}\right)_{i,j+1/2}\frac{2}{Pr\Delta\eta}\right)\right)$$

$$D_{i,j-1} = J_{i,j}\left(T_{i,j}^{l-1}\right)^2\frac{\Delta\eta}{\Delta\tau} + \left(J_{i-1,j}^{l-1}\left(\frac{\partial\xi}{\partial x}\right)_{i-1}^{l-1}u_{i-1,j}T_{i-1,j}^{l-1} - J_{i+1,j}^{l-1}\left(\frac{\partial\xi}{\partial x}\right)_{i+1}^{l-1}u_{i+1,j}T_{i+1,j}^{l-1}\right)\frac{\Delta\eta}{2\Delta\xi}$$

The equations for $T_{i,j}^{l}$ are iterated until the following convergence condition is satisfied:

$$max_{i,j}\left(\frac{\left|\left(T_{i,j}^{l} - T_{i,j}^{l-1}\right)T_{i,j}^{l-1}\right|}{\Delta\tau}\right) < \epsilon \ll 1 \tag{3.102}$$

**3.1.5.6 Updating $H$** When the temperature field is known at an $n^{th}$ level in real time for the fixed ice surface shape $H_i^n$, we use the Stefan condition in order to obtain the ice surface shape at the next time step $H_i^{n+1}$. For a non-constant wall temperature case, it is convenient to express wall temperature in the following form:

$$T_w(x,t) = T_{w0} + T_{w1}(x,t) \tag{3.103}$$

Here $T_{w0}$ is a constant corresponding to the constant ice height $H_0$. This representation is more convenient, since then we can start computations with a uniform incoming flow solution corresponding to $T_w = T_{w0}$ and then "grow" ice by either adding $T_{w1}(x,t)$ smoothly increasing from 0 or by stating that at $t = 0$ the wall temperature undergoes a jump of $T_{w1}(x)$. Then the Stefan condition can be

written in the following form:

$$H_t = -\frac{1}{a}\left(\frac{\partial T}{\partial \eta}\frac{\partial \eta}{\partial y} + \lambda_{il}\frac{T_{w0} + T_{w1}(x,t)}{H_0 + H}\right) \tag{3.104}$$

We use first order approximation for the time derivative, which leads to the following formula for the discrete values $H_i^{n+1}$:

$$H_i^{n+1} = H_i^n + \frac{\Delta t}{a}\left(-\left(\frac{\partial T}{\partial \eta}\frac{\partial \eta}{\partial y}\right)_{j=0} + \lambda_{il}\frac{T_{w0} + T_{w1}}{H_0 + H}\right)_i^n \tag{3.105}$$

$\eta$ derivatives at $j = 0$ were calculated with second order accuracy using 3 points.

**3.1.5.7 Computational parameters and implementation details** Since the boundary condition for the vertical velocity at $\infty$ includes $y$, we have to choose (as in Cassel, Ruban and Walker (1995)) the cut-off value of $y_{max}$ for the upper end of the computational domain. Our computations demonstrated that there is no noticeable change in solutions for $y_{max} > 10$. For the major part of the computations the following grid parameters were used:

$$\begin{cases} y_{max} = 20 \\ N_\xi = N_\eta = 200 \\ \Delta t = 0.1 \end{cases} \tag{3.106}$$

The condensation parameters $A$ and $B$ in **(3.75)** are set to 5 for the computations when perturbations are largely confined to $[-10, 10]$ interval in the streamwise direction and to 2 when perturbations extend to the interval of order $[-20, 20]$ in the streamwise direction. The code was implemented in C++ and all computations have been performed on a Toshiba Satellite 1410 laptop (1.8GHz/512Mb RAM).

The numerical approach we have developed includes solution of a steady or unsteady (depending on the choice of $Q$) double-deck problem with the fixed lower boundary as a subproblem. We have used this fact in order to test the capability of the developed scheme and algorithm to resolve small-scale separations. In order to do this, we have computed a case corresponding to a "step" geometry of the lower surface, which for the double-deck pressure-displacement law should produce a separated flow for sufficiently steep rise of the step. An example of streamlines for the problem with an unsteady vortex structure is given below:

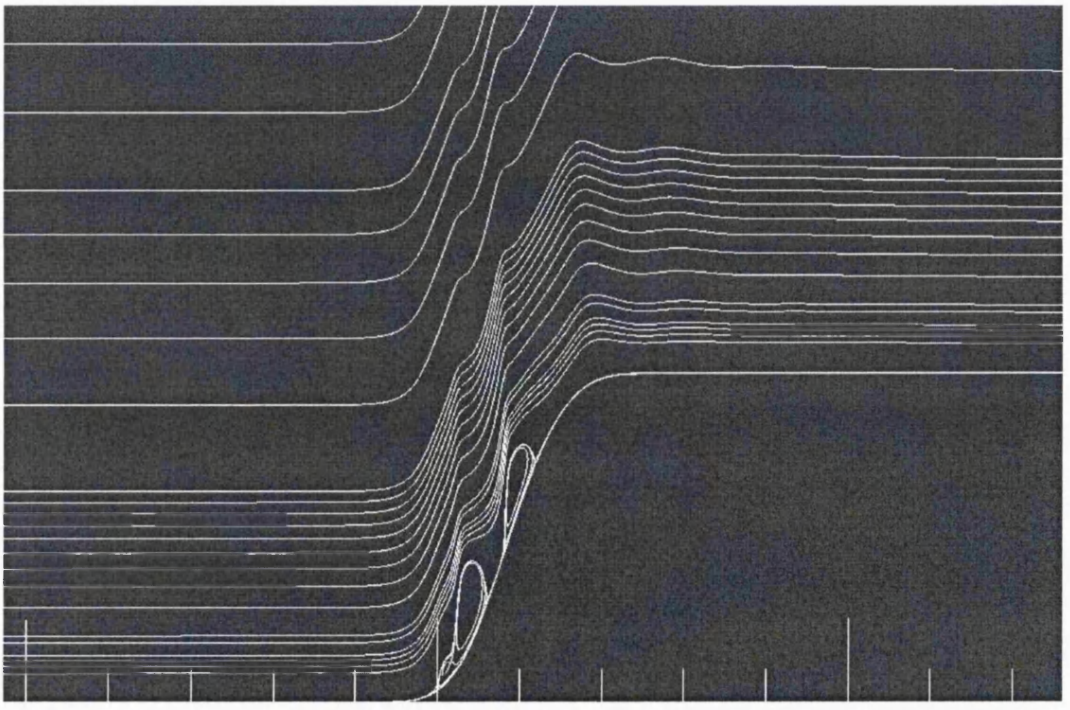

Figure 3.16: An example of separated flow

The above example is an essentially unsteady solution however it demonstrates that our code can resolve flows with regions of separation (simple marching methods based schemes would diverge in these cases).

#### 3.1.5.8 Results

**3.1.5.8.1 Constant wall temperature** In the computations presented in this section we have used water and ice media properties. The angle of incline was set to 0.001 and the Weber number to 1000. In order to compare nonlinear results with linear results for the same configuration, we note that if media properties and the Weber number are fixed, then the only free parameter left in the linear problem is the initial ice height $H_0$.

First let us consider the strongly linearly unstable case, the analytic results indicate that the growth rate increases with the initial ice height and $c_i(\alpha)$ tends to a limiting curve as $H_0 \to \infty$. Therefore in order to investigate the nonlinearity effect in a highly linearly unstable case we will set $H_0 = 1000$. The initial perturbation was taken to be $H_a e^{-x^2}$ with the amplitude $H_a = 0.1$.

The profiles of the free surface $f$ and ice surface $h$ obtained from the linear problem are plotted below at different time steps:

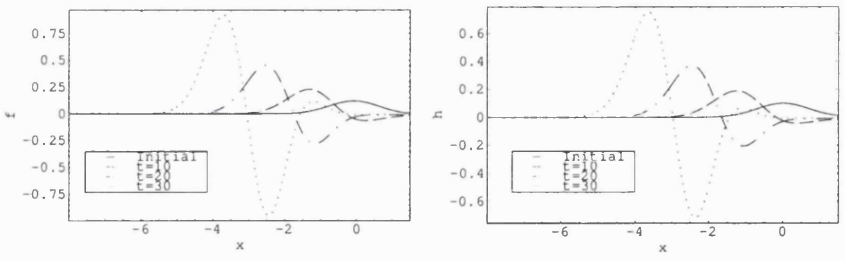


(a) Free surface shape (b) Ice surface shape

Figure 3.17: The evolution of free surface and ice surface shapes in linear solution for $H_0 = 1000$

The nonlinear solution has the same phase speed at small times, however the growth rate is smaller than that of the linear solution. The comparison between linear and nonlinear results for the free surface shape at relatively small values of time is shown on Fig. 3.18-3.19.

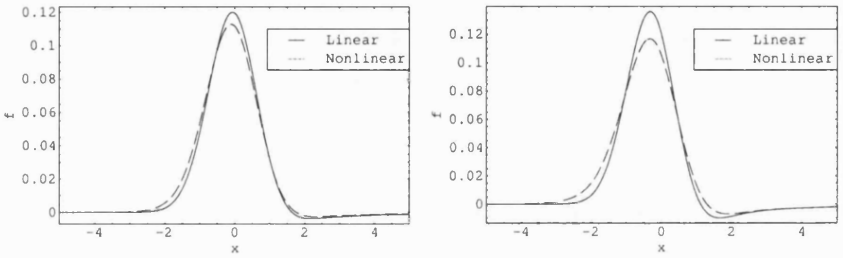


(a) t=0 (b) t=2

Figure 3.18: Linear and nonlinear free surface shape, small $t$ =0,2, $H_0 = 1000$

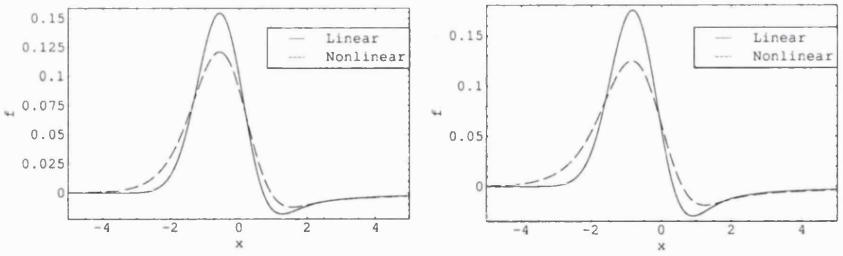


(a) t=4 (b) t=6

Figure 3.19: Linear and nonlinear free surface shape, small $t = 4, 6$ , $H_0 = 1000$

At large timescale it is noticeable that the nonlinear solution does not have the strong dispersion characteristics of the linear one, and the propagation speed of the first peak is higher in nonlinear case. Fig. 3.20-3.21 demonstrates linear and nonlinear results for the free surface shape at relatively large values of time.

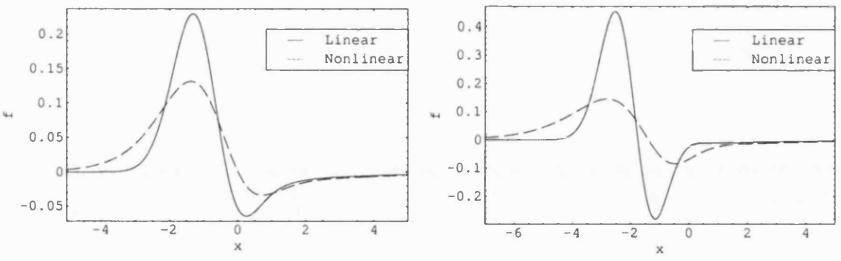


(a) t=10 (b) t=20

Figure 3.20: Linear and nonlinear free surface shape, large $t = 10, 20$, $H_0 = 1000$

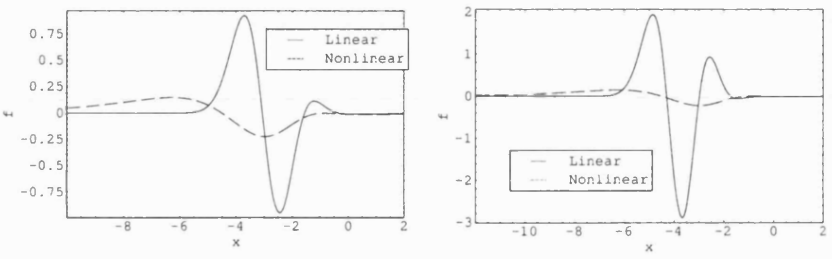


(a) t=30 (b) t=40

Figure 3.21: Linear and nonlinear free surface shape, large $t = 30, 40$, $H_0 = 1000$

Fig. 3.22 shows evolution of the ice surface in linear and nonlinear problem on the same scale in $x$ direction, the comparison between linear and nonlinear solution demonstrates extra stabilisation introduced by nonlinearity and higher upstream propagations speeds of the nonlinear solution.

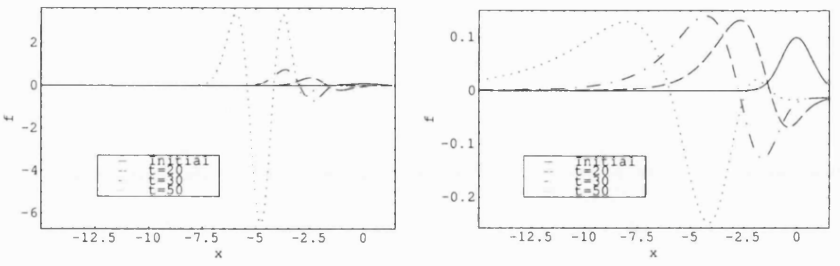


(a) Linear (b) Nonlinear

Figure 3.22: Linear and nonlinear ice surface shape development, $H_0 = 1000$

At 60 time units, the linear solution represents a developing wave packet, while in the nonlinear solution only one secondary peak is observed. Also, as can be seen from the results plotted below, the upstream influence is much stronger in the non-linear case:

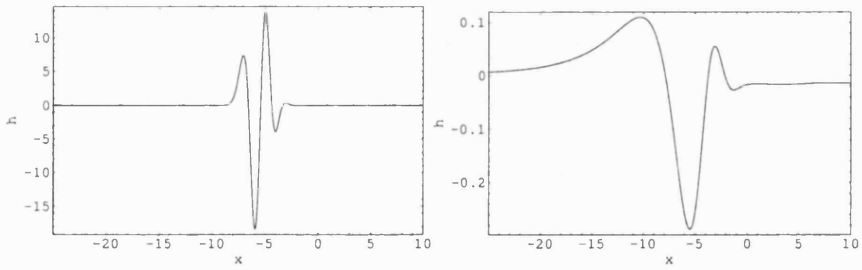


(a) Linear (b) Nonlinear

Figure 3.23: Linear and nonlinear ice surface shape, $t = 60$, $H_0 = 1000$

Due to the slow evolution of the nonlinear solution and its rapid upstream propagation, it was not possible to follow the solution development on very large timescale, since the numerical grids that could be used proved insufficient in order to resolve the solution far upstream. However a certain tendency of the limiting behaviour

can be seen if we consider a suitable norm of the solution and plot it as a function of time. In order to do this, we have chosen to use the norm in the form:

$$||H|| = max_{i=1,Nx} H_i - min_{i=1,Nx} H_i$$

This choice was motivated by the fact that the absolute value norm will not account for the development of negative peaks in the solution. The comparison between the norm of linear and nonlinear solution is shown below for the ice surface shape. The norm of the linear solution grows exponentially as it should, however the norm of the nonlinear solution norm exhibits linear growth initially and then tends to stabilise:

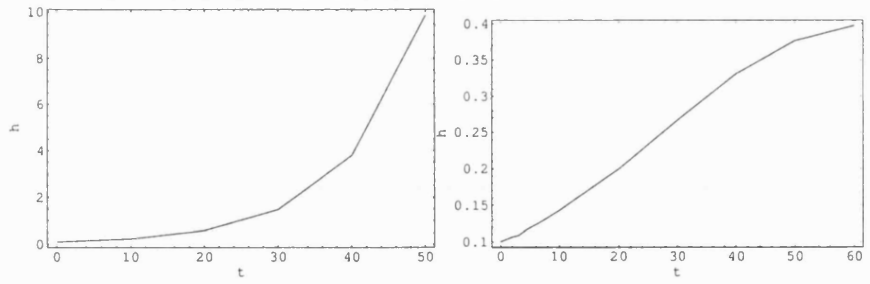


(a) Linear (b) Nonlinear

Figure 3.24: The evolution of the ice surface shape norm, $H_0 = 1000$

**3.1.5.8.2 Variable wall temperature** In this section we will consider configurations where the wall temperature is not constant but varies with the $x$ coordinate instead.

With variable wall temperature we can create configurations where the wall temperature is not constant in a limited domain only. The solutions of such problems can help us understand the upstream influence of a localised temperature jump.

In addition, and perhaps of more importance, is the question of a wall-temperature driven growth of ice structures which create regions of localised icing instability in the flow. The results of linear stability analysis indicate that the stability of the flow is associated with the initial value of the ice layer thickness $H_0$ and we can destabilise the flow by increasing $H_0$. Let us say that some value of the wall temperature $T_{w0}$ corresponds to a linearly stable initial ice thickness $H_0$ if the flow with constant wall temperature equal to $T_{w0}$ is linearly stable. Respectively, let us say that some value of the wall temperature $T_{w1}$ corresponds to a linearly unstable initial ice thickness $H_0$ if the flow with constant wall temperature equal to $T_{w1}$ is linearly unstable. Then, using variable wall temperature we can create configurations where the initial ice thickness in part of the flow corresponds to the linearly unstable case and another part of the flow corresponds to linearly stable case. Of particular interest are the cases where the temperature profile upstream corresponds to a linearly stable value of the initial ice thickness and temperature profile downstream corresponds to a linearly unstable value of the initial ice thickness. If icing instability arises in such configuration, then an interesting question is what will happen to the perturbations as they propagate upstream and enter a linearly stable domain. Also in the nonlinear icing problem, the variable wall temperature can be considered as a forcing term, and it is known that, for example, in stratified fluid flows (Smyth (1988)) the interaction of the forcing and dissipation can lead to the formation of a steady state in a problem that otherwise is essentially unsteady.

Since the stability of the linear solution depends primarily on the initial ice thickness $H_0$ it is possible to devise $x$-dependent wall temperature profile in such a form that $H_0$ will be at the linearly stable zone in the upstream part of the computational domain and in linearly unstable zone in the downstream part of the

computational domain (a "step" profile). Alternatively a localised region of the computational domain can be in linearly unstable zone and the rest of the domain in linearly stable zone (a "bump" profile). For both "step" and "bump" configurations we will consider two cases with the same value of the temperature jump on the wall, but one of them with temperature jump corresponding to ice thicknesses completely in the linearly stable zone and another with lower temperature corresponding to the unstable initial ice thickness and the higher temperature corresponding to the linearly stable ice thickness. Comparing the results for these configurations we will be able to understand the effect of the ice instability on the upstream propagation.

For this problem, we have set the Weber number and the angle of incline to be equal to 4000 and 0.0001 correspondingly. The linear neutral curve in $(H_0, \alpha)$ plane for these parameters is given below (the flow is unstable for the values of $H_0$ and $\alpha$ inside the curve and stable for the values of $H_0$ and $\alpha$ outside the curve):

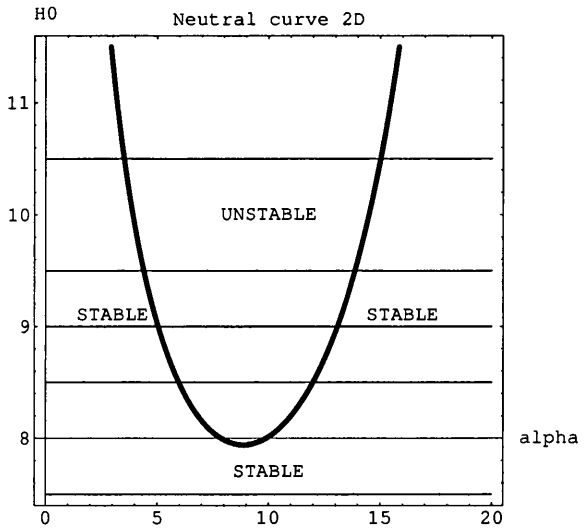


Figure 3.25: Linear neutral curve for $We = 4000$ and $\phi = 0.0001$

In order to study the flow with a gradual drop in the wall temperature, we have chosen to use the following "step" wall temperature profile:

$$T_w(x) = \begin{cases} T_{w0} + (T_{w1} - T_{w0})\, e^{-\left(\frac{x-2.7}{2}\right)^n} & x \leq 2.7 \\ T_{w1} & x > 2.7 \end{cases} \tag{3.107}$$

The choice of the power $n$ allows us to control the smoothness of the step. We used $n = 2$ for a "smooth" step and $n = 4$ a "steep" step.

For the second case, namely with a localised wall temperature variation, we have chosen to use the temperature profile corresponding to a localised Gaussian bump in the following form:

$$T_w(x) = T_{w0} + T_{w1} e^{-\left(\frac{x}{2}\right)^8} \tag{3.108}$$

In both cases two different configurations are considered:

1. A flow where both $T_{w0}$ and $T_{w1}$ correspond to the values of initial ice thickness $H_0$ for which the flow is linearly stable.

2. A flow where $T_{w0}$ corresponds to a value of the initial ice thickness $H_0$ for which the flow is linearly stable and $T_{w1}$ corresponds to a value of the initial ice thickness $H_0$ for which the flow is linearly unstable.

| | **Stable case** | **Unstable case** |
|---|---|---|
| $Tw_0$ | −1.637 | −1.888 |
| $H_0$ | 6.5 | 7.5 |
| $Tw_1$ | −1.888 | −2.14 |
| $H_1$ | 7.5 | 8.5 |

Table 3.1: Variable wall temperature parameters

Table 3.1 shows the values of wall temperature used in our computations for stable and unstable cases and corresponding initial ice heights. The temperature differences have been chosen to be sufficiently small in order for the flow on the upstream side of the bump and step to occur without separations. The figure below shows the corresponding wall temperature profiles for unstable configurations:

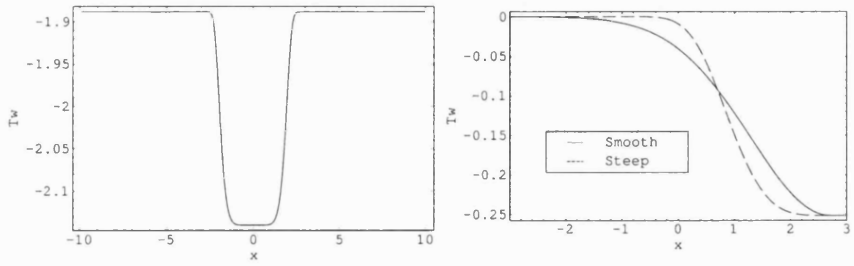


(a) Bump (b) Step

Figure 3.26: Variable wall temperature profiles

Here plots for the "step" show the difference from the upstream temperature $T_{w0}$. In nonlinear computations we consider that the temperature profiles in the form **(3.107)** or **(3.108)** respectively are switched on in the beginning of computation at $t = 0$. Also, since nonlinear computations are quite time-consuming, we have used an initial guess for the ice shape proportional to the shape of the temperature profile for the both configurations in the following form:

$$H_0^{step}(x) = \begin{cases} H_0(T_{w0}) + (H_0(T_{w1}) - H_0(T_{w0}))\, e^{-\left(\frac{x-2.7}{2}\right)^n} & x \leq 2.7 \\ H_0(T_{w1}) & x > 2.7 \end{cases} \tag{3.109}$$

$$H_0^{bump}(x) = H_0(T_{w0}) + H_0(T_{w1}) e^{-\left(\frac{x}{2}\right)^8} \tag{3.110}$$

where $H_0(T_w) = -\lambda_{il} T_w$ is the initial ice thickness of a flat ice layer with constant wall temperature $T_w$.

**3.1.5.8.3 "Step" configuration** An example of the adaptive grid for the "step" configuration is shown below (snapshot taken at $t = 10$):

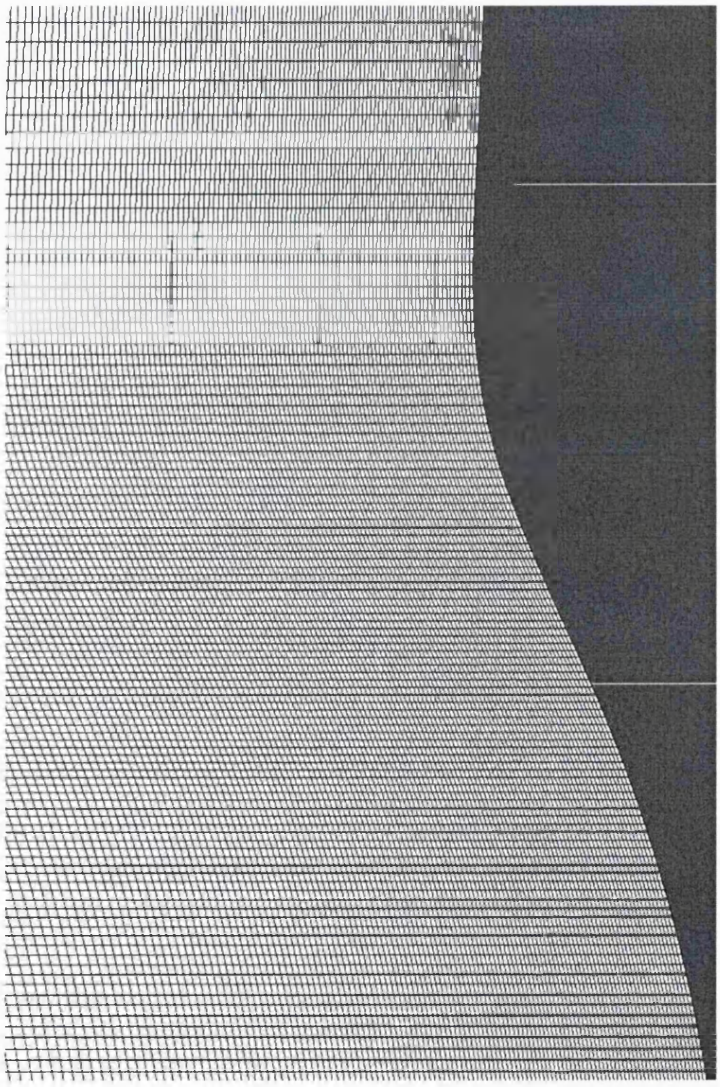

Figure 3.27: An example of grid for the "step" temperature profile

Our computations for both stable and unstable temperature profile configurations quickly converged to a steady solution.

The time necessary for solution to saturate to a steady one did not exceed 10 units. The plots below show the evolution of the smooth step ice shape in stable and unstable case:

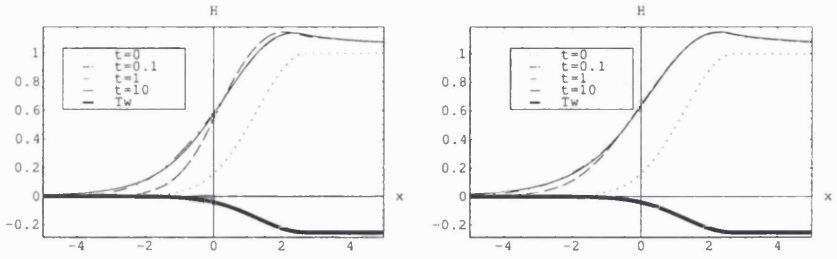


(a) Stable (b) Unstable

Figure 3.28: The evolution of the ice surface for smooth "step" wall temperature profile

Note that in the flow region illustrated on this figure (and all other figures in this section) the ice surface deviation from the initial upstream level is shown instead of full ice surface shape. This allows us to compare the results for stable and unstable flows on one diagram (since the deviation from the upstream temperature level is of the same order in both cases) also this enables us to compare ice and free surface shapes on one plot.

In the "step" configuration, the ice surface formed a bump at the upper part of the step. The mechanism of the bump formation is likely to be due to the interaction between the ice surface shape and free surface shape via heat flux. The elevation of the free surface upstream of the ice bump causes heat flux to the ice surface to fall which leads to the growth of the ice layer. This process

continues until the upstream face of the ice surface is smooth enough so that the thickness of the water film increases smoothly upstream. A simple illustration of this mechanism can be found in the "3.3 A mechanism for upstream propagation of liquid/solid interface perturbations in free-surface flows" section of this chapter. The figure below shows free surface and ice surface shapes for the "step" flow with the temperature downstream corresponding to linearly unstable ice height at two moments of time. The first diagram shows the configuration at $t = 0$ (the initial guess for ice surface and corresponding computed free surface shape) and the second diagram shows the configuration at $t = 10$, where the solution has already converged to a steady one:

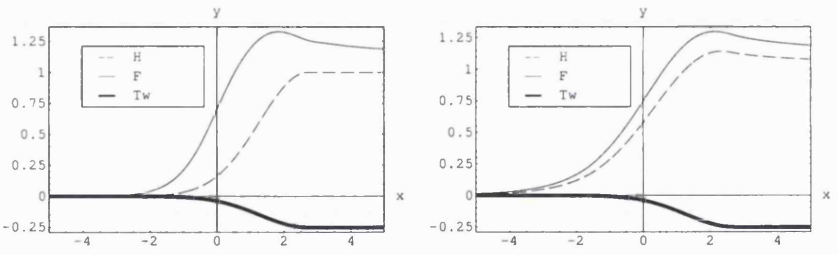


(a) t=0 (b) t=10

Figure 3.29: The comparison between the free surface shape and the ice shape at different time steps for the " step" wall temperature profile

Now let us compare the results computed for the "step" configuration with step height belonging to the domain where the flow is linearly stable against the results computed for the case where step height belongs to the domain where the flow is linearly unstable. Our computations indicate that in the steady state, there is no significant difference between these two configurations, the "unstable" configuration demonstrates a slight increase of the bump on the upper part of the step

and slightly stronger upstream propagation. The figure below shows the steady results for the ice surface shape for smooth and steep steps, each diagram contains both the ice surface shape corresponding to the "unstable" flow and the ice surface shape corresponding to the "stable" flow:

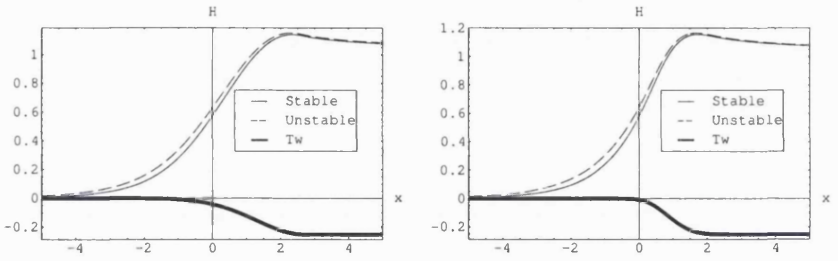


(a) Smooth step (b) Steep step

Figure 3.30: The comparison between the "stable" and "unstable " flow ice shape for the " step" wall temperature profile

The steep "step" temperature profile resulted in a slightly bigger bump on the upper part of the step, although the upstream influence did not depend much on the steepness of the temperature profile:

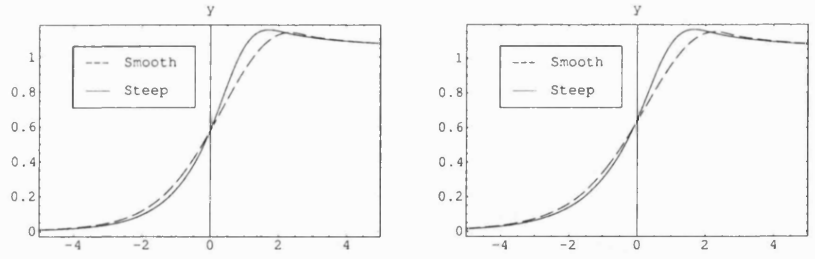


(a) Stable case (b) Unstable case

Figure 3.31: The comparison between the ice shapes corresponding to steep and smooth "step" wall temperature profiles

**3.1.5.8.4 "Bump" configuration** An example of the adaptive grid for the "bump" configuration is given below at $t = 10$:

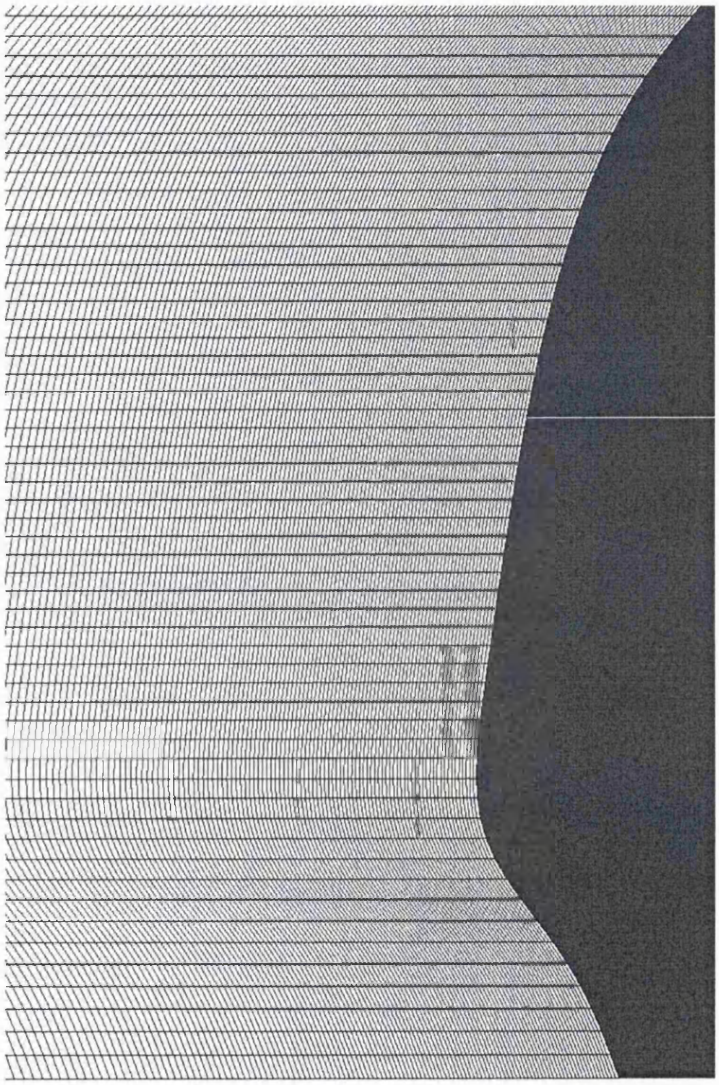

Figure 3.32: An example of grid example for the "bump" wall temperature profile

As with the step configuration, the solution for the bump profile quickly converges to a steady one. The tendency of the upper part of the ice bump to move upstream is however more distinct:

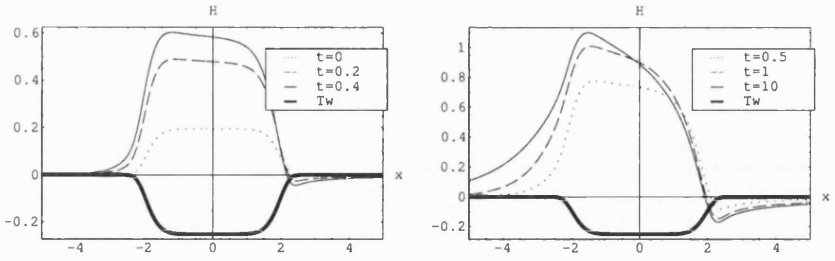


(a) Stable case (b) Unstable case

Figure 3.33: The evolution of the ice surface for the "bump" wall temperature profile

The mechanism of the upstream propagation is the same in this case as well, with the ice growth governed by the development of the free surface:

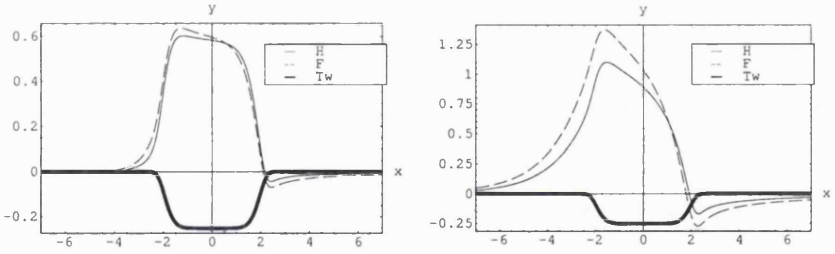


(a) t=0.4 (b) t=10

Figure 3.34: The comparison between the free surface shape and the ice shape at different time steps for the "bump" wall temperature profile

Also as in the step configuration, moving temperature perturbation into the linearly unstable zone slightly increased the upstream propagation effect (Fig. 3.35).

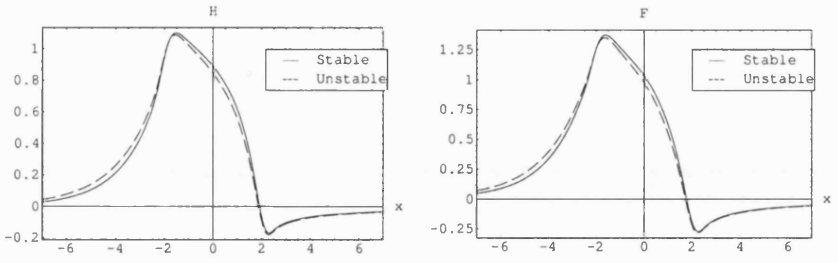


(a) Ice surface (b) Free surface shape

Figure 3.35: The comparison between the "stable" and "unstable " flow ice shape for the "bump" wall temperature profile

The results of the nonlinear computations for the flow evolution problem with an $x$-dependent temperature profile provide a valuable insight into the upstream propagation mechanism. Based on the evolution of the flow observed we provided a simple explanation of the upstream propagation, which is given in the section "3.3 A mechanism for upstream propagation of liquid/solid interface perturbations in free-surface flows" later in this chapter.

Also, contrary to our expectations, we have obtained steady solutions in case where a linearly unstable region is present in the flow. This result can be caused by the effect of forcing-dissipation interaction similar to that observed in Smyth (1988) for resonant flow of a stratified fluid over topography, however it is difficult to relate our problem to the problem investigated in Smyth (1988) explicitly. One more possible explanation can be given based on the timescale of flow development. In our computations, the time necessary for the solution to converge to a steady one did not exceed 10 time units. From the results presented in the section "3.1.5.8.1 Constant wall temperature" of this chapter (for example, see Fig. 3.24), it can be seen that this timescale is insufficient in order for the disturbances to develop

in the nonlinear problem. Note that the the results presented in the "3.1.5.8.1 Constant wall temperature" section of this chapter reflect a strongly unstable case with $H_0 = 1000$. In our case $H_0 \leq 8.5$ and the growth rate of the disturbances will be even lower. In order to increase the growth rate of disturbances, larger temperature jumps should be used, however higher temperature differences mean higher "step" (or "bump") which causes the separation region to develop on the upstream face of a "step" (or "bump"), and it becomes difficult to obtain a steady solution for a fixed ice surface shape.

## 3.2 Linear stability analysis of O(1) height film

In the section "3.1 Froude-based double-deck analysis" we have described the icing instability using an asymptotic flow scheme valid for large values of Reynolds and Froude numbers. Now let us consider linear stability problem for a gravity-driven flow down an inclined plane at finite values of Reynolds and Froude numbers. In this section we will use the same characteristic values as in Floryan, Davis and Kelly (1987) in order to simplify the comparison. Lengths are scaled on the height of unperturbed film $h^*$, velocity on $U^* = \frac{g^* h^{*2}}{2\nu_l^*} \sin\phi$ and pressure on $\frac{\mu_l^*}{h^*} U^*$. Then the Reynolds number is given by $Re = \frac{h^{*3} g^* \sin\phi}{2\nu_l^{*2}}$. Also we will use the same coordinate system as used by Floryan, Davis and Kelly (1987) with $y = 0$ at the free surface and the $y$-axis pointing down. Then the base flow is given by:

$$\begin{cases} u_0(y) = 1 - y^2 \\ v_0(y) = 0 \\ p_0(y) = 2y \cot\phi \\ T_{0l}(y) = 1 - y, \; T_{0i}(y) = T_w \frac{y-1}{H_0 - 1} \end{cases} \tag{3.111}$$

Here $y = H_0$ gives the coordinate of the cold wall and $y = 1$ gives the coordinate of the unperturbed free surface.

As the Squire theorem holds for this case, we can safely limit our analysis to 2D disturbances.

To investigate the linear stability of the steady flow with a half-Poiseuille velocity profile we will linearise the equations for small perturbations, and apply afterwards the normal modes method:

$$\begin{cases} u(x,y,t) = u_0(y) + \varepsilon u_1(y) e^{i\alpha(x-ct)} \\ |\varepsilon| \ll 1 \end{cases} \tag{3.112}$$

This leads to the Orr-Sommerfeld problem formulated in terms of the disturbances of the vertical velocity and temperature in the water layer:

$$\begin{cases} \frac{d^4 v_l}{dy^4} + \left(-2\alpha^2 + i\alpha Re(c - u_{0l})\right) \frac{d^2 v_l}{dy^2} + \\ \left(\alpha^4 + i\alpha^3 Re(u_{0l} - c) + i\alpha Re \frac{d^2 u_{0l}}{dy^2}\right) v_l = 0 \\ \frac{d^2 T_l}{dy^2} + \left(-\alpha^2 + i\alpha RePr(c - u_{0l})\right) T_l - RePr \frac{dT_{0l}}{dy} v_l = 0 \end{cases} \tag{3.113}$$

For the ice layer, the normal modes method yields the following equation for the perturbation of temperature:

$$\left\{ \frac{d^2 T_i}{dy^2} + \left(-\alpha^2 + i\alpha RePr\chi_{li}\right) T_i = 0 \right. \tag{3.114}$$

The kinematic condition, written at the unperturbed free surface $f_0 = 0$, leads to the following expression for the perturbation of the free surface $f$:

$$f = -\frac{i v_l}{\alpha(u_{0l} - c)} \tag{3.115}$$

The balance of stress tensor and surface tension at the unperturbed free surface $f_0 = 0$ yields the following boundary conditions :

$$\begin{cases} \frac{d^2v_l}{dy^2} + \left(\alpha^2 - \frac{d^2u_{0l}}{dy^2}\frac{1}{(u_{0l}-c)}\right) v_l = 0 \\ \frac{d^3v_l}{dy^3} + (-3\alpha^2 + i\alpha Re(c-u_{0l}))\frac{dv_l}{dy} + \\ i\alpha\frac{v_l}{(u_{0l}-c)}\left(\alpha^2 Re^{-\frac{2}{3}}\left(\frac{3}{2}\sin\phi\right)^{-\frac{1}{3}}\zeta + 2\cot\phi\right) = 0 \end{cases} \tag{3.116}$$

Here $\zeta = \left(\frac{3\rho^l S^3}{g\mu^4}\right)^{\frac{1}{3}}$ is the surface tension parameter which depends only on media properties (see, for example Floryan, Davis and Kelly (1987)). We have used the kinematic condition at the free surface in order to eliminate $f$ from the stress tensor condition in order to obtain the form of the stress tensor condition given above. Finally, we will impose the constant temperature condition at the free surface, which at $y = 0$ gives:

$$T_l - \frac{iv_l}{\alpha(u_{0l}-c)}\frac{dT_{0l}}{dy} = 0 \tag{3.117}$$

At the ice surface the kinematic conditions yields the following expression for the perturbation of the ice surface $h$:

$$h = \frac{iv_l}{\Theta_{il}\alpha c} \tag{3.118}$$

This can be used to eliminate the perturbation of the ice surface $h$ from the velocity and temperature conditions on the ice surface. Then, velocity and temperature conditions at the unperturbed ice surface $y = H_0$ can be written in the form given by **(3.119)** and **(3.120)** respectively.

$$\frac{dv_l}{dy} + \frac{v_l}{\Theta_{il}c}\frac{du_{0l}}{dy} = 0 \tag{3.119}$$

$$T_i + \frac{iv_l}{\Theta_{il}\alpha c}\frac{dT_{0i}}{dy} = T_l + \frac{iv_l}{\Theta_{il}\alpha c}\frac{dT_{0l}}{dy} = 0 \tag{3.120}$$

The full form of the Stefan condition written at the unperturbed ice surface $y = 1$ is given by:

$$\frac{dT_l}{dy} - \lambda_{il}\frac{dT_i}{dy} + \frac{iv_l}{\Theta_{il}kc}\left(\frac{d^2T_{0l}}{dy^2} - \lambda_{il}\frac{d^2T_{0i}}{dy^2}\right) = -\frac{PrRe}{St}v_l \tag{3.121}$$

However since the base temperature profiles in water and ice layers are linear, the Stefan condition is reduced to:

$$\frac{dT_l}{dy} - \lambda_{il}\frac{dT_i}{dy} = -\frac{Pr \cdot Re}{St}v_l \tag{3.122}$$

Also we consider the wall temperature to be constant, therefore $T_i(H_0) = 0$.

### 3.2.1 Solution in ice

The boundary-value formulation for the Fourier image of the ice temperature perturbation can be written as:

$$\begin{cases} \frac{d^2T_i}{dy^2} + \omega_i^2 T_i = 0 \\ \omega_i^2 = -\alpha^2 + i\alpha cRePr\chi_{li} \\ T_i(H_0) = 0 \\ T_i(1) = -\frac{iv_l}{\Theta_{il}\alpha c}\frac{dT_{0i}}{dy} \end{cases} \tag{3.123}$$

This problem can be solved analytically and the solution is given by:

$$T_i(y) = -\frac{iv_l}{\Theta_{il}\alpha c}\frac{dT_{0i}}{dy}\frac{\sinh(i\omega_i(H_0-y))}{\sinh(i\omega_i(H_0-1))} \tag{3.124}$$

Therefore, the derivative of the ice temperature at the ice/water boundary is given by:

$$\lambda_{il}\frac{dT_i}{dy}(1) = -\lambda_{il}\frac{v_l\omega_i}{\Theta_{il}kc}\frac{dT_{0i}}{dy}\frac{\cosh(i\omega_i(H_0-1))}{\sinh(i\omega_i(H_0-1))} \tag{3.125}$$

Also from the heat balance at the ice surface for the initial solution it follows that $H_0 = 1 - \lambda_{il}T_w$, which leads to the following expression for the weighted heat flux in the unperturbed ice layer:

$$\lambda_{il}\frac{dT_{0i}}{dy} = \lambda_{il}T_w\frac{1}{H_0-1} = -1 \tag{3.126}$$

Using **(3.125)** and **(3.126)** we can eliminate the ice temperature from the Stefan condition to obtain the following equation linking the derivative of the water temperature on the ice/water boundary to the $y$- component of the water velocity on the ice/water boundary:

$$\frac{dT_l}{dy} = \left(\frac{\omega_i}{\Theta_{il}kc}\coth\left(i\omega_i(H_0-1)\right) - \frac{PrRe}{St}\right)v_l$$

### 3.2.2 Numerical approach

**3.2.2.1 Numerical scheme** In order to find the eigenmodes of the stability problem **(3.113)** we use finite-differences to construct a compact $4^{th}$order scheme and then employ the algorithm based on Gaussian elimination (see, for example Thomas (1953); Blennerhassett (1980)) in order to find the values of the complex

phase speed $c$ corresponding to non-zero solutions. In order to do this we rewrite the equations in the following form:

$$\begin{cases} \frac{d^4 v_l}{dy^4} + c_l^{2v}(y)\frac{d^2 v_l}{dy^2} + c_l^{1v}(y)v_l = 0 \\ \frac{d^2 T_l}{dy^2} + c_l^{2T}(y)T_l + c_l^{1T}(y)v_l = 0 \end{cases} \tag{3.127}$$

Here the coefficient functions $c_l^{(1,2)(v,T)}$ are given by:

$$c_l^{1v} = \alpha^4 + i\alpha^3 Re(u_{0l} - c) + i\alpha Re\frac{d^2 u_{0l}}{dy^2} \tag{3.128}$$

$$c_l^{2v} = -2\alpha^2 - i\alpha Re(u_{0l} - c) \tag{3.129}$$

$$c_l^{1T} = -RePr\frac{dT_{0l}}{dy} \tag{3.130}$$

$$c_l^{2T} = -\alpha^2 - i\alpha RePr(u_{0l} - c) \tag{3.131}$$

Then we build a compact approximation for the system **(3.127)** in terms of $v$, $v^{II} = \frac{d^2 v}{dy^2}$, $v^{IV} = \frac{d^4 v}{dy^4}$, $T$ and $T^{II} = \frac{d^2 T}{dy^2}$ on a uniform grid with a step $\Delta y$, using the approach similar to that reported in Li (1998). In order to derive a $4th$ order numerical scheme for this problem we will construct 3 finite-difference equations accurate to the $4^{th}$ order in $\Delta y$, and then couple them with the original equations **(3.127)** by using the representation of the $4^{th}$ order derivative in $y$ taken from **(3.127)**.

Consider the following finite difference equations:

$$\begin{cases} \frac{v^{IV}_{n-1}+10v^{IV}_n+v^{IV}_{n+1}}{12} = \frac{v^{II}_{n-1}-2v^{II}_n+v^{II}_{n+1}}{\Delta y^2} \\ \frac{v^{II}_{n-1}+10v^{II}_n+v^{II}_{n+1}}{12} = \frac{v_{n-1}-2v_n+v_{n+1}}{\Delta y^2} \\ \frac{T^{II}_{n-1}+10T^{II}_n+T^{II}_{n+1}}{12} = \frac{T_{n-1}-2T_n+T_{n+1}}{\Delta y^2} \end{cases} \tag{3.132}$$

All these equations are true to the fourth order in $\Delta y$ (see Appendix C). Now, let us express $v^{IV}$ and $T^{II}$ in terms of $v$, $v^{II}$ and $T$ using the original system **(3.127)** and substitute the resulting expressions into **(3.132)**. Then we obtain the following system of difference equations:

$$\left\{\begin{array}{c} \frac{v^{II}_{n-1}+10v^{II}_n+v^{II}_{n+1}}{12} = \frac{v_{n-1}-2v_n+v_{n+1}}{\Delta y^2} \\ \frac{-c^{2v}_{n-1}v^{II}_{n-1}-c^{1v}_{n-1}v_{n-1}-10\left(c^{2v}_n v^{II}_n-c^{1v}_n v_{n+1}\right)-c^{2v}_{n+1}v^{II}_{n+1}-c^{1v}_{n+1}v_{n+1}}{12} = \frac{v^{II}_{n-1}-2v^{II}_n+v^{II}_{n+1}}{\Delta y^2} \\ \frac{-c^{2T}_{n-1}T_{n-1}-c^{1T}_{n-1}v_{n-1}+10\left(c^{2T}_n T_n+c^{1T}_n v_n\right)-c^{2T}_{n+1}T_{n+1}-c^{1T}_{n+1}v_{n+1}}{12} = \frac{T_{n-1}-2T_n+T_{n+1}}{\Delta y^2} \end{array}\right. \tag{3.133}$$

Thus, for the unknown functions vector:

$$X = \begin{pmatrix} v \\ v^{II} \\ T \end{pmatrix}$$

we obtain the block-tridiagonal system of algebraic equations which approximates the original system of ordinary differential equations **(3.127)** with the $4^{th}$ order accuracy in space:

$$A_{n-1}X^{n-1} + B_{n-1}X^n + C_{n-1}X^{n+1} = D_{n-1} \tag{3.134}$$

Here $A$, $B$, $C$ and $D$ are 3x3 matrices:

$$A = \begin{pmatrix} 1 & -\frac{1}{12}\Delta y^2 & 0 \\ \frac{1}{12}\Delta y^2 c^{1v}_{n-1} & \left(1+\frac{1}{12}\Delta y^2 c^{2v}_{n-1}\right) & 0 \\ \frac{1}{12}\Delta y^2 c^{1T}_{n-1} & 0 & \left(1+\frac{1}{12}\Delta y^2 c^{2T}_{n-1}\right) \end{pmatrix} \tag{3.135}$$

$$B = \begin{pmatrix} -2 & -\frac{10}{12}\Delta y^2 & 0 \\ \frac{10}{12}\Delta y^2 c_n^{1v} & \left(-2+\frac{10}{12}\Delta y^2 c_n^{2v}\right) & 0 \\ \frac{10}{12}\Delta y^2 c_n^{1T} & 0 & \left(-2+\frac{10}{12}\Delta y^2 c_{n-1}^{2T}\right) \end{pmatrix} \tag{3.136}$$

$$C = \begin{pmatrix} 1 & -\frac{1}{12}\Delta y^2 & 0 \\ \frac{1}{12}\Delta y^2 c_{n+1}^{1v} & \left(1+\frac{1}{12}\Delta y^2 c_{n+1}^{2v}\right) & 0 \\ \frac{1}{12}\Delta y^2 c_{n+1}^{1T} & 0 & \left(1+\frac{1}{12}\Delta y^2 c_{n+1}^{2T}\right) \end{pmatrix} \tag{3.137}$$

$$n = 1...N-2$$

Next, we need a $4^{th}$ order approximation of the boundary conditions in order to maintain the same order of accuracy in both equations and boundary conditions approximation. Apart from our variables $(v, v^{II}, T)$, the boundary conditions include their first derivatives $(\frac{dv}{dy}, \frac{dv^{II}}{dy}, \frac{dT}{dy})$. These first derivatives are approximated with the $4^{th}$ order of accuracy using 5 grid points:

$$\left.\frac{df}{dy}\right|_y = \frac{1}{\Delta y}\left(\pm\frac{25}{12}f_y \mp 4f_{y\mp\Delta y} \pm 3f_{n\mp 2\Delta y} \mp \frac{4}{3}f_{n\mp 3\Delta y} \pm \frac{1}{4}f_{n\mp 4\Delta y}\right) + O(\Delta y^4) \tag{3.138}$$

At the free surface this gives the following difference equations for the temperature and the tangential component of stress:

$$\begin{cases} v_{N-1}^{II} + \left(\alpha^2 - \frac{d^2u_{0l}}{dy^2}\frac{1}{(u_{0l}-c)}\right)v_{N-1} = 0 \\ T_{N-1} - \frac{i}{\alpha(u_{0l}-c)}\frac{dT_{0l}}{dy}v_{N-1} = 0 \end{cases} \tag{3.139}$$

Similarly, for the normal stress we obtain:

$$\begin{gathered}\frac{dv_l^{II}}{dy}+(-3\alpha^2+i\alpha Re(c-u_{0l}))\frac{dv_l}{dy}+\frac{i\alpha}{Re(u_{0l}-c)}\left(\alpha^2Re^{-\frac{2}{3}}\left(\frac{3}{2}\sin\phi\right)^{-\frac{1}{3}}\zeta+2\cot\phi\right)v_l\\=-\tfrac{25}{12}v_{N_l-1}^{II}+4v_{N_l-2}^{II}-3v_{N_l-3}^{II}+\tfrac{4}{3}v_{N_l-4}^{II}-\tfrac{1}{4}v_{N_l-5}^{II}+\\(-3\alpha^2+i\alpha Re(c-u_{0l}))\left(-\tfrac{25}{12}v_{N_l-1}+4v_{N_l-2}-3v_{N_l-3}+\tfrac{4}{3}v_{N_l-4}-\tfrac{1}{4}v_{N_l-5}\right)+\\\frac{i\alpha\Delta y}{Re(u_{0l}-c)}\left(\alpha^2Re^{-\frac{2}{3}}\left(\frac{3}{2}\sin\phi\right)^{-\frac{1}{3}}\zeta+2\cot\phi\right)v_{N_l-1}=0\end{gathered}\tag{3.140}$$

At the ice surface the approximated boundary conditions can be written as:

$$\frac{dv_l}{dy}+\frac{v_l}{\Theta_{il}c}\frac{du_{0l}}{dy}=\left(\frac{25}{12}+\frac{\Delta y}{\Theta_{il}c}\frac{du_{0l}}{dy}\right)v_0-4v_1+3v_2-\frac{4}{3}v_3+\frac{1}{4}v_4=0\tag{3.141}$$

$$T_l+\frac{iv_l}{\Theta_{il}\alpha c}\frac{dT_{0l}}{dy}=T_0+\frac{i}{\Theta_{il}\alpha c}\frac{dT_{0l}}{dy}v_0\tag{3.142}$$

$$\begin{gathered}\frac{dT_l}{dy}+\left(\lambda_{il}\frac{\omega_i}{\Theta_{il}\alpha c}\frac{dT_{0i}}{dy}\frac{\cosh(i\omega_i(H_0-1))}{\sinh(i\omega_i(H_0-1))}+\frac{PrRe}{St}\right)v_l=\\\tfrac{25}{12}T_0-4T_1+3T_2-\tfrac{4}{3}T_3+\tfrac{1}{4}T_4+\\+\left(\lambda_{il}\frac{\omega_i}{\Theta_{il}\alpha c}\frac{dT_{0i}}{dy}\frac{\cosh(i\omega_i(H_0-1))}{\sinh(i\omega_i(H_0-1))}+\frac{PrRe}{St}\right)v_0\end{gathered}\tag{3.143}$$

So altogether the matrix $A$ of the linear system of algebraic equations determining the discrete values $(v_i, v_i^{II}, T_i)$ is bounded by 10 diagonals. This essentially means that we need to store only 10 central diagonals for Gaussian elimination.

**3.2.2.2 Finding a mode** We are interested only in complex frequency values for which the problem **(3.127)** has non-zero solutions. Since the linear system

of algebraic equations for discrete values $(v_i, v_i^{II}, T_i)$ has a zero solution, we are looking for the value of the complex phase speed $c$ such that:

$$Rank[A(c, Re, \alpha)] < 3N - 1 \tag{3.144}$$

In order to find this value, we apply the algorithm first used by Thomas (1953) to determine normal modes of the Poiseuille flow in a channel. We perform Gaussian elimination with column pivoting to bring linear system matrix $A$ to the upper-triangular form. Then we can regard the last element at $(3N-1, 3N-1)$ (all indexes start with 0) as a function $W(c)$ of the complex phase speed. The matrix $A$ will become singular when $W(c) = 0$. Therefore, in order to find the values of the complex phase speed that correspond to non-zero solutions, we need to find the roots of $W(c) = 0$. This can be done with any iterational method suitable for the functions of complex variable. We have chosen to use the Newton method (see, for example, Isaacson and Keller (1966)) :

$$c_{k+1} = c_k - \frac{W(c_k)}{\frac{\partial W(c_k)}{\partial c}} \tag{3.145}$$

where the derivative is approximated numerically with the first order of accuracy:

$$\frac{\partial W(c_k)}{\partial c} = \frac{W(c_k + \delta c) - W(c_k)}{\delta c} \tag{3.146}$$

and $\delta c$ is a small real constant.

In order for the iterative process to converge we need a sufficiently good guess for the starting point $c_0$. For the ice-induced instability, such guess can be obtained either from the asymptotic solution for large Reynolds and Froude numbers de-

rived in the section "3.1 Froude based double-deck analysis" or from the longwave asymptotic analysis which we perform in the "3.2.3 Longwave asymptotics for the linear stability problem". For the eigenmodes corresponding to shear and interfacial instabilities we can use well-known solutions of the stability problem for the flow on an inclined plane without an ice layer (see, for example, Floryan, Davis and Kelly (1987)) as an initial guess.

If we have computed a mode at some point of the problem parametric space $(\alpha^0, Re^0, H_0^0, St^0, \phi^0)$ and we need to know the value of this mode at some other point $(\alpha^1, Re^1, H_0^1, St^1, \phi^1)$ - we build a line in parametric space linking these points and obtain the mode at the final point by marching along this line with a small step using the results from the previous step as a guess value on the next step. Further we will refer to this process as mode tracing.

**3.2.2.3 Building a neutral curve** In order to find a point on a neutral curve for a fixed Reynolds number $Re_0$ we will use the following iterational procedure:

1. Trace the mode in consideration $c(Re, \alpha)$ from some point in the $(Re, \alpha)$ plane where the value of $c$ is known, say $Re_{init}, \alpha_{init}$ to $Re_0$ along the straight line $\alpha = \alpha_{init}$ by walking along this line with small increments using the value of $c$ from the previous step as the initial guess. This will produce an initial guess which is necessary to start refining the root of the equation for the neutral point $c_i(\alpha, Re_0) = 0$.

2. Apply Newton method to the equation $c_i(\alpha, Re_0) = 0$ in order to refine $\alpha$ and find the root of $c_i(Re_0, \alpha) = 0$.

3. Continue the neutral curve by going with a given step in $Re$, performing step 2 for each new $Re$, using the previous $(\alpha, c)$ as a guess value. The step in

$Re$ is generally variable, particularly for the shear mode neutral curve where we can suppose that the curve will be more smooth at high $Re$. For shear mode, variable steps were used, with the step length increasing towards high Reynolds numbers as some power of $Re$.

4. The process ends when there's no convergence in $\alpha$ for $c_i(Re_0, \alpha) = 0$. Then we can suppose that we approached the point where $\frac{d\alpha}{dRe} \to \infty$, i. e. the critical point, and we need to use the algorithm to obtain $Re_{crit}$ described in the next section "3.2.2.4 Finding critical Reynolds number".

Note that the same algorithm can be applied in order to build neutral curve by going with a given step in $\alpha$ and solving $c_i(\alpha_0, Re) = 0$ for $Re$ instead. The derivatives $\frac{\partial c_i}{\partial \alpha}$ and $\frac{\partial c_i}{\partial Re}$ necessary for the Newton method are computed numerically.

**3.2.2.4 Finding a critical Reynolds number** We can assume that the critical point $P_{crit}$ is given by $B(\alpha) = \frac{dRe}{d\alpha}(\alpha) = 0$. Also we assume that in the vicinity of $P_{crit}$ the function $B$ is a smooth analytic function. Then we can use Newton iterations to find the zero of $B$. The second derivative $\frac{d^2Re}{d\alpha^2}$ necessary for the iterative process is computed numerically.

**3.2.2.5 Numerical scheme tests** When $St^{-1} = 0$, the temperature disturbance field is independent of the velocity field and the stability problem is equivalent to the problem without ice. This fact was used to test the results against those in De Bruin (1974) and Floryan, Davis and Kelly (1987). In order to compare solutions with and without ice layer influence we will use the following two solvers:

1. The Orr-Sommerfeld problem solver with the temperature equations and proper boundary conditions at the water/ice interface.

2. The Orr-Sommerfeld problem solver with the temperature equations and boundary conditions at the water/ice interface replaced with the conditions corresponding to a solid impermeable boundary. We will refer to this as a "fake ice" case.

The second case essentially disables the interaction between the momentum and temperature equations and makes the problem equivalent to the problem without ice.

In the next table we have summarised the results of comparison between the values of the complex frequency for the so-called hard (shear) mode without ice (taken from De Bruin (1974)) and the results we have computed for this mode in the same configuration with ice and with "fake ice":

| DeBruin | Fake Ice | Ice |
|---|---|---|
| $c = 0.2044$ | $c = 0.2044434$ | $c = 0.2044430$ |

Table 3.2: Comparison of our results for the complex phase speed $c$ for shear mode with De Bruin (1974) results ($Re = 24065$, $\alpha = 1.0354$, $\phi = 1^o$)

The results of the comparison of the soft (interfacial) mode from De Bruin (1974) with our computations are summarised in the following table:

| DeBruin | Fake Ice | Ice |
|---|---|---|
| $c = 1.8141$ | $c = 1.8141517$ | $c = 1.8141562$ |

Table 3.3: Comparison of our results for the complex phase speed $c$ for surface mode with De Bruin (1974) results ($Re = 100$, $\alpha = 0.3579$, $\phi = 1^o$)

In De Bruin (1974), the stability problem formulation did not include the effect of surface tension. In order to examine the code performance with surface tension present, we will compare the results with those of Floryan, Davis and Kelly (1987) for the surface tension number value corresponding to a water layer. In the next table the results of comparison for the complex phase speed $c$ are summarised for the surface mode:

| $Re$ | Floryan, Davis & Kelly | Fake Ice | Ice |
|---|---|---|---|
| 1000 | $1.09780 + 0.0260614i$ | $1.09978 + 0.0260602i$ | $1.09978 + 0.0260602i$ |
| 5000 | $1.03441 + 0.0141295i$ | $1.03442 + 0.0141294i$ | $1.03442 + 0.0141294i$ |
| 10000 | $1.02241 + 0.0105362i$ | $1.02241 + 0.0105361i$ | $1.02241 + 0.0105361i$ |
| 25000 | $1.01295 + 0.00703645i$ | $1.01295 + 0.00703643i$ | $1.01295 + 0.00703643i$ |

Table 3.4: Comparison of our results for the complex phase speed $c$ for surface mode with Floryan, Davis and Kelly (1987) results ($Re = 100$, $\alpha = 0.270$, $\phi = 1^o$, $\zeta = 4899.38$)

Clearly, the results obtained with our code based on our numerical scheme demonstrate good comparison with those reported by De Bruin (1974) and Floryan, Davis and Kelly (1987). Therefore, we can conclude that the numerical scheme and the code are working properly.

**3.2.2.6 Implementation details** The code was implemented in C++ and all computations were performed on a Toshiba Satellite 1410 laptop (1.8GHz/512Mb RAM).

For the major part of the computations grids of 500 points in $y$ were used for traces and neutral curves computations. For the critical parameters, eigenvectors and single mode value computations, we have used grids of 800 points in $y$.

The problem in consideration involves operations on complex numbers with extremely large ratio of real to imaginary part. In such cases complex arithmetics

implementation can lead to significant precision losses, especially on division operations (see, for example, Press, Teuklowski, Vetterling and Flannery (1992)). In order to make sure that this does not occur, a class for complex numbers representation has been implemented in C++ and used in computations.

### 3.2.3 Longwave asymptotics for the linear stability problem

Yih (1963) considered longwave asymptotics for a gravity-driven flow down an inclined plane. In this section we will discuss the similar case in the presence of an ice layer. The longwave asymptotic solution derived here will be used in the full numerical solution of the Orr-Sommerfeld problem in order to provide an initial guess on the complex phase speed for ice and interfacial modes in the longwave limit. In addition, the longwave solution is interesting in itself as it provides an additional insight into the physics of the icing instability compared with the more familiar surface mode of instability.

To simplify the comparison with Yih (1963) we will write the equations in terms of the streamfunction $\psi$. Let $\alpha \to 0$ and $\psi = O(1)$ in the Orr-Sommerfeld equations. Consider the following expansion:

$$\begin{cases} \psi_l^\Sigma \sim \psi_l + \alpha\psi_l^1 + ... \\ T_l^\Sigma \sim T_l + \alpha T_l^1 + ... \\ c^\Sigma \sim c + \alpha c^1 + ... \end{cases} \tag{3.147}$$

Then, as $\psi = i\frac{v}{\alpha}$, the equations and boundary conditions in terms of the disturbances of streamfunction and temperature become (in $O(1)$ order):

$$\begin{cases} \frac{d^4\psi_l}{dy^4} = 0 \\ \frac{d^2T_l}{dy^2} = 0 \\ \frac{d^2T_i}{dy^2} = 0 \end{cases} \tag{3.148}$$

$$\begin{cases} \frac{d^3\psi_l}{dy^3} = 0 \\ T_l - \frac{dT_{0l}}{dy}\frac{1}{u_{0l}-c}\psi_l = 0 \quad (y=0) \\ \frac{d^2\psi_l}{dy^2} - \frac{d^2u_{l0}}{dy^2}\frac{1}{u_{0l}-c}\psi_l = 0 \end{cases} \tag{3.149}$$

$$\begin{cases} \frac{d\psi_l}{dy} + \frac{du_{0l}}{dy}\frac{1}{\Theta_{il}c}\psi_l = 0 \\ T_l + \frac{dT_{0l}}{dy}\frac{1}{\Theta_{il}c}\psi_l = T_i + \frac{dT_{0i}}{dy}\frac{1}{\Theta_{il}c}\psi_l = 0 \quad (y=1) \\ \frac{dT_l}{dy} - \lambda_{il}\frac{dT_i}{dy} = i\alpha\frac{PrRe}{St}\psi = ia\psi \end{cases} \tag{3.150}$$

$$\begin{cases} T_i = 0 \quad (y = H_0) \end{cases} \tag{3.151}$$

In order for the derived longwave asymptotics to be valid, we need $\alpha \ll 1$ and $\alpha Re \ll 1$. Also in order to keep the influence of ice in the problem formulated above, we need $\frac{\alpha RePr}{St} \sim 1$.

In order to estimate the domain where these assumptions are valid, let us consider water/ice media properties. For water and ice $St \sim 10^{-2} \ll 1$ and $Pr = 13.47$at $0^oC$, then $a \sim 10^3 \alpha Re$. Therefore $a \sim 1$ assumption holds for $\alpha Re \sim 10^{-3}$.

The solution of the above system **(3.148)-(3.151)** should be in the form given by **(3.152).**

$$\begin{cases} \psi = C_2 y^2 + C_1 y + C_0 \\ T_l = C_4 y + C_3 \end{cases} \tag{3.152}$$

From the heat flux balance at ice surface in the base-flow solution $\frac{dT_{0i}}{dy} = \frac{T_w}{H_0 - 1} = -\lambda_{li}$, therefore $T_i = \psi(1)\frac{H_0 - y}{H_0 - 1}\frac{\lambda_{li}}{\Theta_{il}c}$ . Substituting **(3.152)** into the boundary conditions **(3.149)-(3.151)** we obtain the following system for the constants $C_{1-4}$:

$$\begin{pmatrix} 0 & 1 & 0 & 0 & -\frac{dT_{0l}}{dy}(0)\frac{1}{u_{0l}-c} \\ 0 & 0 & 2 & 0 & -\frac{d^2u_{0l}}{dy^2}(0)\frac{1}{u_0(0)-c} \\ 0 & 0 & 2+\frac{du_{0l}}{dy}(1)\frac{1}{\Theta_{il}c} & 1+\frac{du_{0l}}{dy}(1)\frac{1}{\Theta_{il}c} & \frac{du_{0l}}{dy}(1)\frac{1}{\Theta_{il}c} \\ 1 & 1 & \frac{dT_{0l}}{dy}(1)\frac{1}{\Theta_{il}c} & \frac{dT_{0l}}{dy}(1)\frac{1}{\Theta_{il}c} & \frac{dT_{0l}}{dy}(1)\frac{1}{\Theta_{il}c} \\ 1 & 0 & \frac{1}{H_0-1}\frac{1}{\Theta_{il}c} - ia & \frac{1}{H_0-1}\frac{1}{\Theta_{il}c} - ia & \frac{1}{H_0-1}\frac{1}{\Theta_{il}c} - ia \end{pmatrix} \begin{pmatrix} C_4 \\ C_3 \\ C_2 \\ C_1 \\ C_0 \end{pmatrix} = 0 \tag{3.153}$$

In order for the system **(3.153)** to have non-zero solutions, the determinant of the matrix on the left has to be zero. This condition leads to the following quadratic equation for the complex phase speed $c$:

$$iac^2(H_0 - 1)\Theta_{il}c^2 - c(2ia\Theta_{il}(H_0 - 1) + H_0 - \Theta_{il}(H_0 - 1)) + 2 = 0 \tag{3.154}$$

The solution of this equation yields two distinct modes:

$$c_{+,-} = \frac{(2ia\Theta_{il}(H_0-1)+H_0-\Theta_{il}(H_0-1))\pm \sqrt{(2ia\Theta_{il}(H_0-1)+H_0-\Theta_{il}(H_0-1))^2-8ia(H_0-1)\Theta_{il}}}{4ia(H_0-1)\Theta_{il}} \tag{3.155}$$

When $H_0 \to 1$, i.e. when the ice sheet vanishes, $c = 2$ as in Yih (1963) (with a

rescaling applied as different normalisation of the base-flow solution is taken here).

When $H_0 \to \infty$, there are two distinct roots:

$$\begin{cases} c_+ = 0 \\ c_- = 2 - i\frac{1-\Theta_{il}}{a\Theta_{il}} \end{cases} \tag{3.156}$$

In this limit, the next order of approximation is necessary in order to analyse the sign of $c_+$ and $c_-$ is stable as $\Theta_{il} < 1$. The second root turns to Yih's solution when $\Theta_{il} = 1$ i.e. when the ice density is negligible. In the limit of a large $a$ (small Stefan number), there are two neutrally-stable modes in the first order of approximation:

$$\begin{cases} c_+ = 0 \\ c_- = 2 \end{cases} \tag{3.157}$$

The behaviour of the roots is illustrated in Fig. 3.36 - 3.39 for different values of $H_0$ and $a$ where it is seen that both roots occur to be stable.

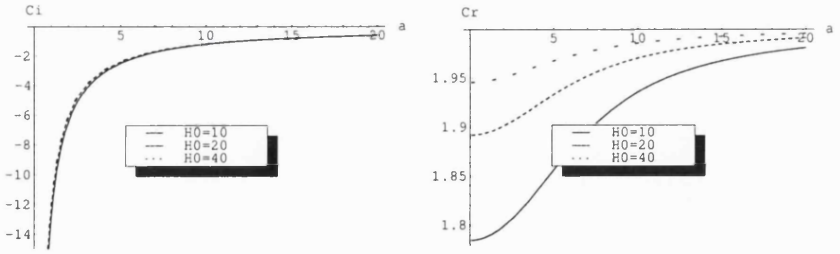


(a) Ci for mode C+ (b) Cr for mode C+

Figure 3.36: The dependence of the longwave mode $c_+$ on $a$ for different $H_0$

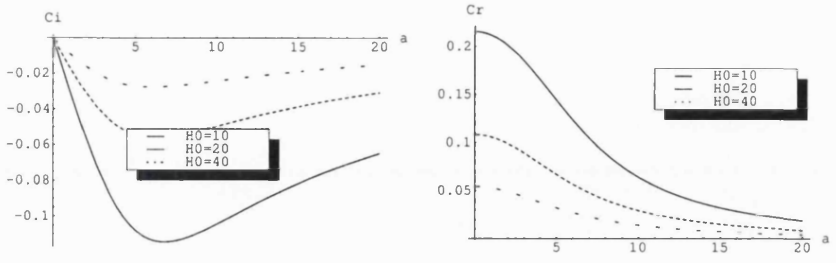


(a) Ci for mode C- (b) Cr for mode C-

Figure 3.37: The dependence of the longwave mode $c_-$ on $a$ for different $H_0$

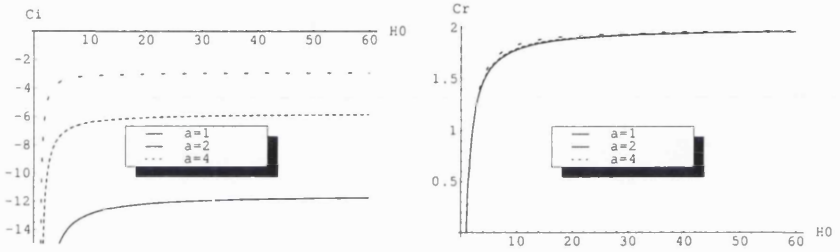


(a) Ci for mode C+ (b) Cr for mode C+

Figure 3.38: The dependence of the longwave mode $c_+$ on $H_0$ for different $a$

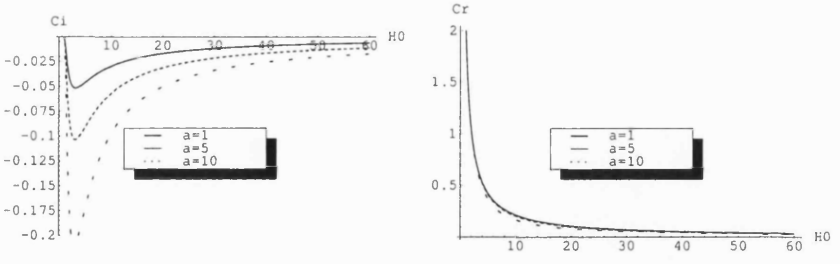


(a) Ci for mode C- (b) Cr for mode C-

Figure 3.39: The dependence of the longwave mode $c_-$ on $H_0$ for different $a$

Instead of one neutrally-stable interfacial mode as obtained by Yih (1963), the longwave stability formulation including ice/water interaction provides two stable modes. Later we will compare these modes with shear, interfacial and ice modes in the full Orr-Sommerfeld formulation and show that one of these modes is a surface mode modified by the presence of an ice layer and another mode corresponds to the icing instability.

### 3.2.4 Detecting the ice mode in Orr-Sommerfeld computations

In order for the Newton iterations procedure to converge it is necessary to have a sufficiently good initial estimate for the complex phase speed $c$. In order to obtain such an estimate we will take a point in the parameter space of the problem where the double-deck solution of "3.1 Froude-based double-deck analysis" section is likely to be valid, then take a double-deck result for $c$, rescale it to the Orr-Sommerfeld problem scale and use it as an initial guess. To simplify the procedure, we will use the case without surface tension to obtain the initial guess.

Let us use a subscript "$bl$" for boundary-layer variables, subscript "$vs$" for the double-deck viscous sublayer variables and subscript "$os$" for the Orr-Sommerfeld problem variables. Then in the boundary layer:

$$x_{bl} = \frac{x^*}{L^*},\ y_{bl} = \frac{y^*}{h^*},\ t_{bl} = \frac{t^*}{L^*}U^*_{bl}$$

$$\alpha_{bl} = \alpha^* L^*,\ c_{bl} = \frac{c^*}{U^*_{bl}}$$

$$\frac{L^*}{h^*} = \sqrt{Re_{bl}}\ ,\ Re_{bl} = \frac{U^*_{bl}L^*}{\nu_l},\ Fr_{bl} = \frac{U^{*2}_{bl}}{gh^*}$$

In the viscous sublayer the scaling is given by:

$$x_{vs} = x_{bl} Fr_{bl}^3,\ y_{vs} = y_{bl} Fr_{bl},\ t_{vs} = t_{bl} Fr_{bl}$$

$$\alpha_{vs} = \alpha_{bl} Fr_{bl}^{-3},\ c_{vs} = c_{bl} Fr_{bl}^2$$

For the Orr-Sommerfeld problem we have:

$$x_{os} = \frac{x^*}{h^*},\ y_{os} = \frac{y^*}{h^*},\ t_{os} = \frac{t^*}{h^*} U_{os}^*$$

$$\alpha_{os} = \alpha^* h^*,\ c_{os} = \frac{c^*}{U_{os}^*}$$

Then:

$$\frac{L^{*2}}{h^{*2}} = Re_{bl} = \frac{U_{bl}^* L^*}{\nu_l^*} = \frac{L^*}{h^*} \frac{U_{bl}^*}{U_{os}^*} \frac{U_{os}^* h^*}{\nu_l^*} = \frac{L^*}{h^*} \frac{U_{bl}^*}{U_{os}^*} Re_{os} \rightarrow \frac{L^*}{h^*} = \frac{U_{bl}^*}{U_{os}^*} Re_{os} \rightarrow Re_{bl} = \left(\frac{U_{os}^*}{U_{bl}^*}\right)^2 Re_{os}^2$$

$$Fr_{bl} = \frac{U_{bl}^{*2}}{gh^*} = \frac{U_{bl}^{*2}}{U_{os}^{*2}} \frac{U_{os}^{*2}}{gh^*} = \frac{U_{bl}^{*2}}{U_{os}^{*2}} Fr_{os} = \left(\frac{U_{bl}^*}{U_{oz}^*}\right)^2 Re_{os} \frac{\sin\phi}{2}$$

Since for the Orr-Sommerfeld problem, $Fr_{os} = \frac{Re_{os} \sin\phi}{2}$. Then the conversions from the double-deck viscous layer variables to the Orr-Sommerfeld problem variables are given by:

$$x_{os} = x_{bl} \frac{L^*}{h^*} = x_{vs} Fr_{bl}^{-3} \frac{L^*}{h^*} = x_{vs} Fr_{bl}^{-3} \sqrt{Re_{bl}} = x_{vs} \left(\frac{U_{bl}^{*2}}{U_{os}^{*2}} Re_{os} \frac{\sin\phi}{2}\right)^{-3} \left(\frac{U_{os}^*}{U_{bl}^*}\right) Re_{os} = x_{vs} \left(\frac{U_{os}^*}{U_{bl}^*}\right)^5 \frac{8}{Re_{os}^2 \sin^3\phi}$$

$$y_{os} = y_{bl} = y_{vs} Fr_{bl}^{-1} = y_{vs} \left(\frac{U_{bl}^{*2}}{U_{os}^{*2}} Re_{os} \frac{\sin\phi}{2}\right)^{-1} = y_{vs} \left(\frac{U_{os}^*}{U_{bl}^*}\right)^2 \frac{2}{Re_{os} \sin\phi}$$

$$c_{os} = c_{bl} \frac{U_{bl}^*}{U_{os}^*} = c_{vs} Fr_{bl}^{-2} \frac{U_{bl}^*}{U_{os}^*} = c_{vs} \left(\frac{U_{os}^*}{U_{bl}^*}\right)^3 \frac{4}{Re_{os}^2 \sin^2\phi}$$

$$\alpha_{os} = \alpha_{bl} \frac{h^*}{L^*} = \alpha_{vs} Fr_{bl}^3 \frac{h^*}{L^*} = \alpha_{vs} Fr_{bl}^3 \frac{1}{\sqrt{Re_{bl}}} = \alpha_{vs} \left(\frac{U_{bl}^{*2}}{U_{oz}^{*2}} Re_{os} \frac{\sin\phi}{2}\right)^3 \left(\frac{U_{bl}^*}{U_{os}^*}\right) \frac{1}{Re_{os}} = \alpha_{vs} \left(\frac{U_{bl}^*}{U_{os}^*}\right)^7 \frac{Re_{os}^2 \sin^3\phi}{8}$$

The characteristic velocities ratio is $\frac{U_{bl}^*}{U_{oz}^*} = \frac{2}{3} = \widetilde{u}$ takes into account the fact that the choice of the characteristic velocity is different for the double-deck asymptotics. Let us pick the following test case in Orr-Sommerfeld variables:

$$Re_{os} = 10000,\ \alpha_{os} = 0.06,\ H_{0os} = 10,\ St_{os} = 0.0625,\ \phi_{os} = 0.002$$

The viscous-layer scaled parameters for this case will be:

$$H_{0vs} = H_{0os}\widetilde{u}^2\frac{Re_{os}\sin\phi_{os}}{2} = 44.44,\ \alpha_{vs} = \widetilde{u}^{-7}\frac{8}{Re_{os}^2\sin^3\phi}\alpha_{os} = 10.25$$

Our analytic solution for the double-deck approximation with $Pr = 1$ yields the following value of $c$ for these parameters (rescaled to $Pr = 13.47$ and $St = 0.0625$ according to the procedure described in the "3.1.4.2.2 Influence of the Prandtl number" section):

$$c_{vs} = -0.004046 + 0.0005768i$$

Using this guess value in the numerical solution of the Orr-Sommerfeld problem, we obtain the following value of $c_{os}$:

$$c_{os} = -0.0001785 + 0.00001892i$$

In order to check whether this is the ice mode, we will trace the shear and interfacial modes (guess values for shear and interfacial modes were obtained in the "3.2.2.5 Numerical scheme tests" section) to the same point of the problem parameter space and compare the resulting values of complex phase speed $c$ with the newly found mode. The results of this comparison are summarised in the Table 3.5 demonstrate that the new mode is different from the well-known shear and surface modes.

| Shear mode | Surface mode | Ice mode |
|---|---|---|
| $0.0882816 - 0.09789i$ | $1.18037 + 0.00734659i$ | $-0.0001785 + 0.00001892i$ |

Table 3.5: Mode comparison at $Re = 10000$, $\alpha = 0.06$, $H_0 = 10$, $St = 0.0625$ and $\phi = 0.002$

The $v$ eigenfunction profile for shear and surface modes is essentially the same as can be seen in De Bruin (1974) and Chin, Abernathy and Bertschy (1986). The $v$ eigenfunction profile for ice mode resembles surface mode in its real part but is completely different in the imaginary part as shown in Fig. 3.40:

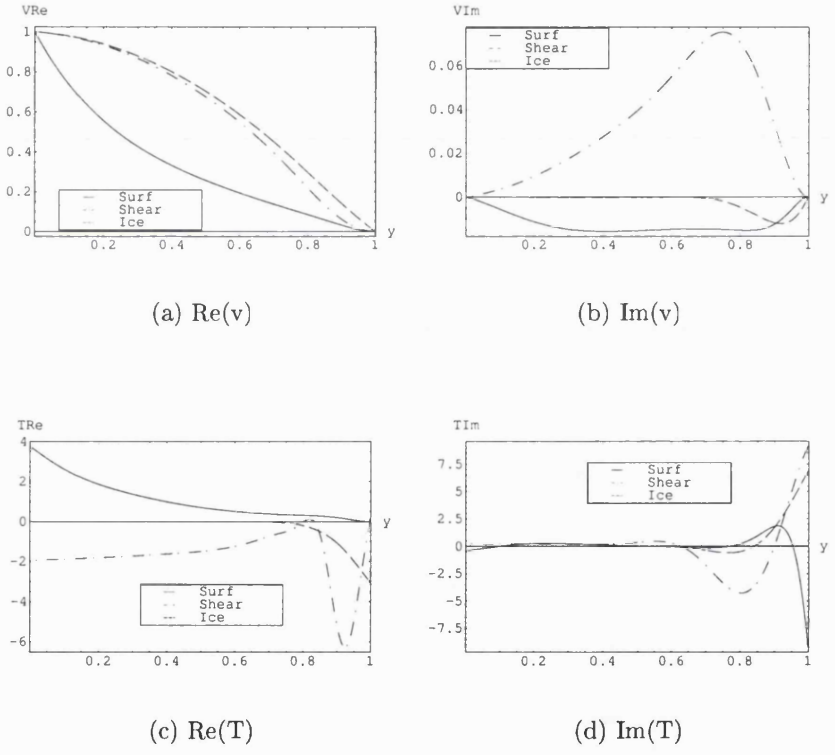


(a) Re(v) (b) Im(v)

(c) Re(T) (d) Im(T)

Figure 3.40: Surface, shear and icing instability eigenfunctions

Therefore the new unstable mode discovered in the Orr-Sommerfeld formulation is clearly not a shear or surface mode. The plots below show $c_i(\alpha)$ and $c_r(\alpha)$ for

all three modes at the test point in the parameter space ($Re = 10000$):

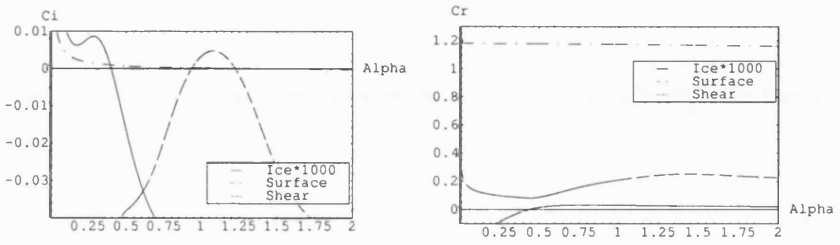


(a) Ci (b) Cr

Figure 3.41: Comparison between interfacial, shear and ice modes

The absolute values of $c_{i,r}$ for the ice mode are much smaller then those of shear and surface modes. This is consistent with the timescale analysis and experimental results as characteristic time of the ice layer growth observed in the experiments is much larger then the characteristic time of the flow development. Also the test plots above show that the phase speed of the ice mode is negative and the perturbations propagate upstream.

Another argument for the fact that the new mode is connected with the ice layer is that this mode is not observed in the "fake ice" case, when solid wall boundary conditions are specified on the ice surface (as described in the "3.2.2.5 Numerical scheme tests" section).

### 3.2.5 Ice instability

The typical neutral curves for all modes in a flow with an ice layer are given below for the following configuration:

$$H_0 = 10,\ St = 0.0625,\ \phi = 0.002,\ \zeta = 0$$

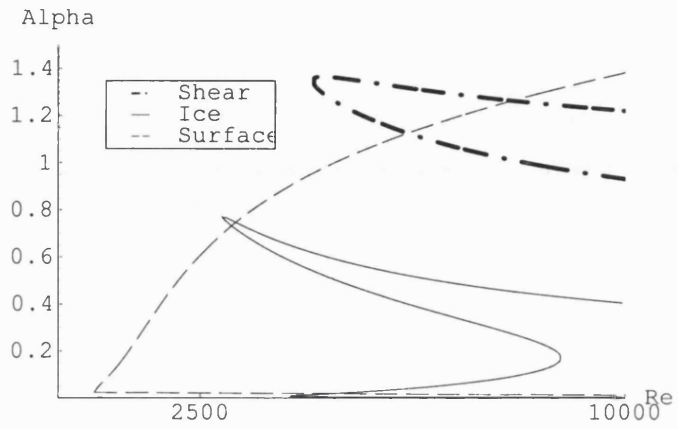


(a) Ci

Figure 3.42: Surface, shear and ice mode neutral curves

The surface mode becomes unstable first. However the ice mode becomes unstable at lower Reynolds numbers than the shear mode. The ice mode neutral curve consists of two characteristic branches. Later in this section we will demonstrate that this topology of the ice mode neutral curve stays the same in the wide range of problem parameters. The phase speed of the ice mode is always negative inside the ice mode neutral curve.

From the Fig. 3.42, it can be seen that the neutral curve corresponding to the surface mode is modified by the ice presence. The surface mode is stabilised by the ice layer in the longwave limit and its neutral curve does not include $Re$ axis any more. This effect will be considered later in the "3.2.7 Ice influence on the surface mode" section.

In order to study the influence of the flow parameters on the neutral curve of the ice mode, we will fix the media properties, then the stability characteristics depend on $(H_0, St, \phi)$ only (we consider the surface tension effect separately).

**3.2.5.1 The influence of surface tension** In order to investigate the effect of surface tension, we compare the neutral curves and critical conditions for the ice mode with and without surface tension. Since we have fixed media properties the comparison reduces to two cases, namely $\zeta = 0$ and $\zeta = 4899.38$ (see, for example Floryan, Davis and Kelly (1987)). In the equations the influence of the surface tension is confined to the $i\alpha\frac{v_l}{(u_{0l}-c)}\alpha^2 Re^{-\frac{2}{3}}\left(\frac{3}{2}\sin\phi\right)^{-\frac{1}{3}}\zeta$ term in the normal stress tensor condition **(3.116)** on the free surface. From the form of this term it follows that in order for it to be significant for a fixed value of $\phi$, it is necessary to have a sufficiently small Reynolds number and sufficiently large wavenumber. Therefore the impact of surface tension is visible only on the upper branch of the ice mode neutral curve near the critical point, as shown on the following figure:

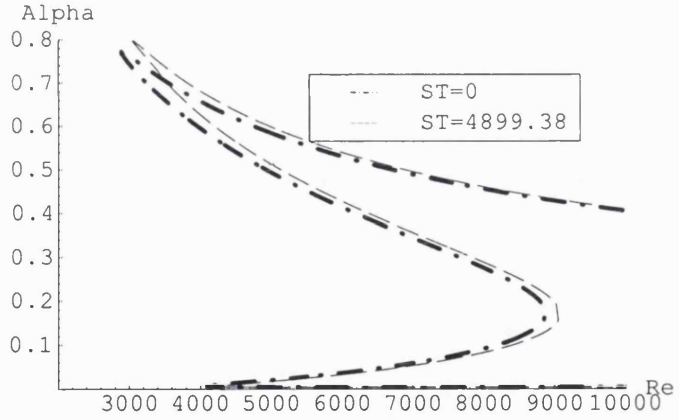


Figure 3.43: The influence of surface tension on the ice mode neutral curve

The computations here were performed for $H_0 = 10$, $St = 0.0625$ and $\phi = 0.002$. The computed critical parameters for the case with and without surface tension are given in the Table 3.6. The critical point for the lower branch is $Re_c = 4094.2$, $\alpha_c = 0.00696$, $c_{rc} = -0.001034$ and it is not affected by surface tension within the precision of computations. This result can be expected since the effect of surface

tension on waves of that length should be negligible.

| | $\zeta = 0$ | $\zeta = 4899.38$ |
|---|---|---|
| $Re_c$ | 2884.7 | 3041.4 |
| $\alpha_c$ | 0.772 | 0.796 |
| $c_{rc}$ | −0.0000793 | −0.0000753 |

Table 3.6: The influence of surface tension on the critical parameters for the upper branch of the ice mode

**3.2.5.2 The influence of the Stefan number** Let us consider the effect of the Stefan number on the ice mode for constant water/ice properties and constant values of $(H_0, \phi, \zeta) = (10, 0.002, 4899.38)$. Since $St = \frac{Cp_l DT}{H_{li}}$, we find that $St \simeq 0.01265DT$. Therefore, for the fixed media properties, the Stefan number is determined by the characteristic temperature difference $DT = T_a^{*e} - T_f^*$ only. We will consider the values of the characteristic temperature difference $DT$ in the range of $[1, 10]$, which corresponds to $St \in [0.01265, 0.1265]$.

The dependence of the ice mode complex phase speed on the Stefan number is not monotonic. In particular, $c_i(St)$ has a maximum for fixed $Re$ or $\alpha$ and the position of this maximum varies with $Re$ and $\alpha$, as shown on Fig. 3.44 and 3.45:

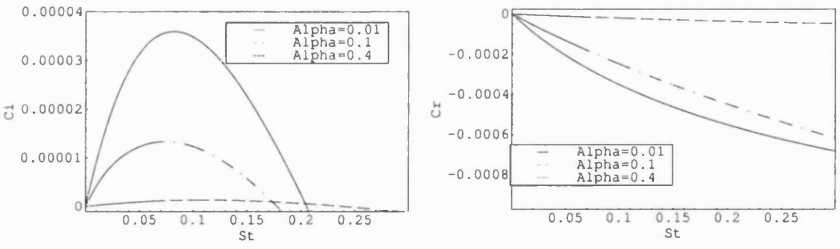


(a) Ci (b) Cr

Figure 3.44: $c(St)$ for $Re = 10000$ and varying $\alpha$

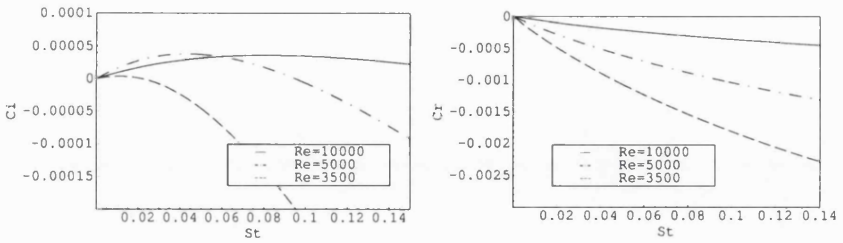


(a) Ci (b) Cr

Figure 3.45: $c(St)$ for $\alpha = 0.01$ and varying $Re$

The variation of the Stefan number significantly alters the longwave branch of the neutral curve. The diagram below shows neutral curves for the ice mode for different values of the Stefan number:

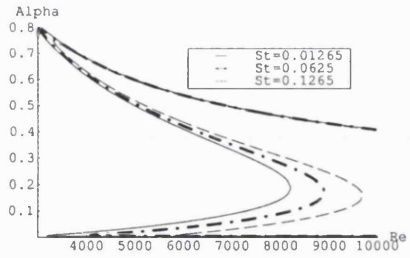


Figure 3.46: The influence of the Stefan number on the ice mode neutral curve

The decrease of Stefan number causes critical Reynolds to decrease monotonically on the upper branch:

| | $St = 0.01265$ | $St = 0.0625$ | $St = 0.1265$ |
|---|---|---|---|
| $Re_c$ | 2925.7 | 3041.4 | 3315.8 |
| $\alpha_c$ | 0.819 | 0.796 | 0.749 |
| $c_{rc}$ | −0.0000167 | −0.0000753 | −0.000132 |

Table 3.7: The influence of the Stefan number on the critical parameters of the ice mode (upper branch)

The same effect takes place on the lower branch, however for long waves the destabilising effect of the Stefan number decrease is more significant:

| | $St = 0.01265$ | $St = 0.0625$ | $St = 0.1265$ |
|---|---|---|---|
| $Re_c$ | 3196.7 | 4094.2 | 5930.7 |
| $\alpha_c$ | 0.00619 | 0.00696 | 0.00968 |
| $c_{rc}$ | −0.000390 | −0.00103 | −0.00934 |

Table 3.8: The influence of the Stefan number on the critical parameters of the ice mode (lower branch)

**3.2.5.3 The influence of the initial ice height** Initial ice height is related to the wall temperature by $H_0 - 1 = -\lambda_{il} T_w = -\lambda_{il} \frac{T_w^* - T_f^*}{T_a^{*e} - T_f^*} \simeq 4.0 \frac{T_f^* - T_w^*}{T_a^{*e} - T_f^*}$. We will compare the stability characteristics for different values of $H_0$ and fixed Stefan number $St = 0.0625$ (which corresponds to $T_a^{*e} - T_f^* \simeq 5$). Then $H_0 \simeq 1 + \frac{4}{5}\left(T_f^* - T_w^*\right)$ therefore for reasonable wall temperatures ($> -30^o C$), the values of $H_0$ are in the range $H_0 \in (1.0, 25]$.

The decrease of the initial ice thickness $H_0$ causes the lower branch of the neutral curve to disappear gradually:

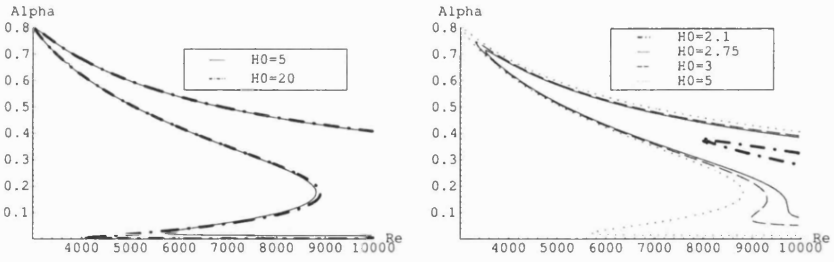


(a) Large H0 (b) Small H0

Figure 3.47: The influence of the initial ice height $H_0$ on the ice mode neutral curve

As $H_0$ increases, the critical Reynolds numbers for both upper and lower branches tend to asymptotes as shown on Fig. 3.48. For $\phi = 0.002$, the critical Reynolds number for the upper branch is always lower then the critical Reynolds number for the lower branch:

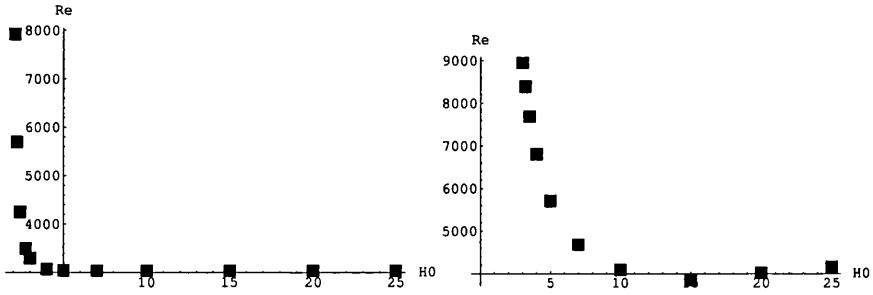


(a) Critical Reynolds (Upper Branch)

(b) Critical Reynolds (Lower Branch)

Figure 3.48: The influence of the initial ice height $H_0$ on the ice mode critical Reynolds number

However, the critical Reynolds number for the ice mode is still greater than that of the surface mode in all computed cases.

The variation of the critical wavenumber and phase speed also decreases with the increase of the the initial ice height, as shown on Fig. 3.49 and 3.50. The critical wavenumber for the upper branch increases and the critical wavenumber of the lower branch decreases as the initial ice height increases. The critical phase speed increases for both branches as the initial ice height increases.

Generally as in the double-deck theory, the increase of the initial ice height has destabilising effect on the ice mode.

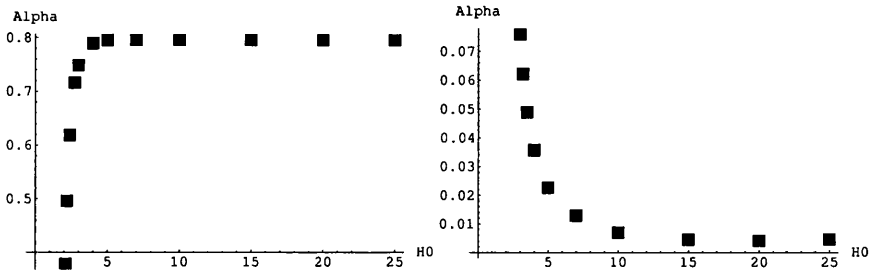


(a) Critical Wavenumber (Upper Branch)

(b) Critical Wavenumber (Lower Branch)

Figure 3.49: The influence of the initial ice height $H_0$ on the ice mode critical wave number

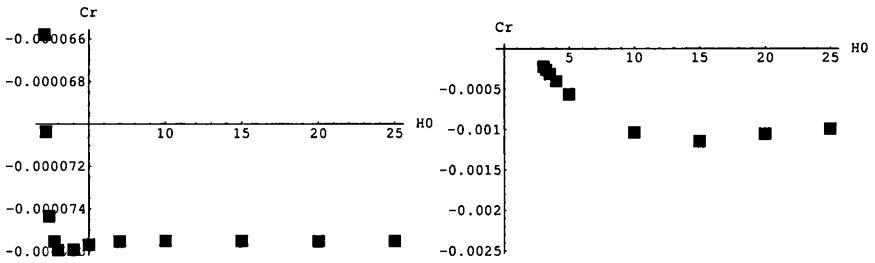


(a) Critical Phase Speed (Upper Branch)

(b) Critical Phase Speed (Lower Branch)

Figure 3.50: The influence of the initial ice height $H_0$ on the ice mode critical phase speed

**3.2.5.4 The influence of the angle of incline** Since the parametric space of the problem is too large to consider all possible parameter combinations, we fix the media properties (which sets surface tension number to $\zeta = 4899.38$) and Stefan number ($St = 0.0625$) and consider the influence of angle of incline variation for several different values of $H_0 \in [3, 20]$. The choice of the initial ice thickness is motivated by the results obtained in the previous section which demonstrate that

the ice mode is more unstable at large values of $H_0$ and critical parameters tend to have asymptotes as $H_0$ grows.

The first noticeable feature of the ice mode is that $c_i$ is non-monotonic in the angle of incline but rather develops a maximum for fixed $(Re, \alpha)$. Also $c(\phi)$ varies extremely slowly with $H_0$ and tends to a limit as $H_0$ grows. Below are several examples of typical $c(\phi)$ curves:

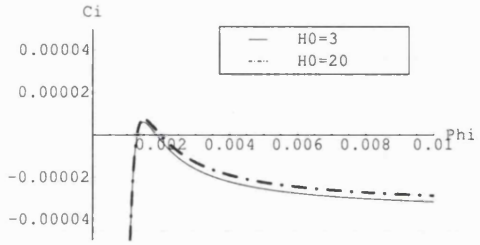


(a) alpha=0.41

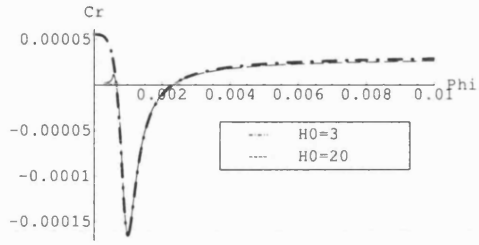


(b) alpha=0.41

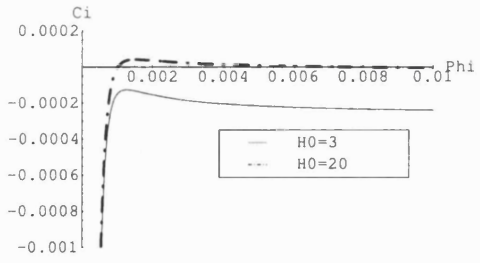


(c) alpha=0.01

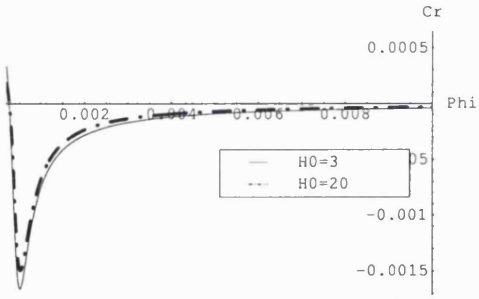


(d) alpha=0.01

Figure 3.51: The influence of the angle of incline on the ice instability mode complex phase speed, $Re = 10000$

For the fixed height of the initial ice layer, the neutral curves exhibit strong dependency on the angle of incline with critical Reynolds number decreasing as the

angle of incline increases. Also, as $\phi$ decreases, the Reynolds number corresponding to the turning point of the neutral curve (where upper and lower branches join) increases rapidly:

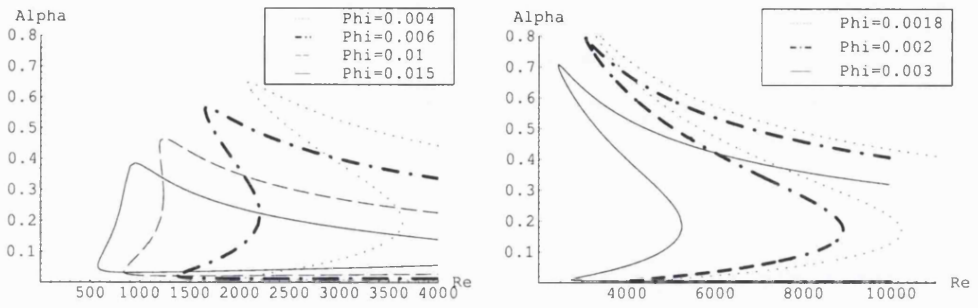


(a) Large angles

(b) Small angles

Figure 3.52: The influence of the angle of incline on the ice instability mode neutral curves, $H_0 = 10$

It is more interesting however, that as we increase the angle of incline $\phi$, the critical Reynolds number of the lower branch becomes less then the critical Reynolds number of the upper branch at some point. This means that although the critical Reynolds number is a continuous function of $\phi$, both $\alpha_{cr}$ and $c_{cr}$ as functions of the angle of incline$\phi$ are not continuous.

Fig. 3.53 demonstrates the dependence of critical Reynolds number, wave number and phase speed on the angle of incline. Critical Reynolds number shown on this figure was defined as $min(Re_{cr}^{upper}, Re_{cr}^{lower})$.

We should note, that although the critical Reynolds number of the ice mode decreases significantly as the angle of incline increases, it always larger than the critical Reynolds number of the surface mode.

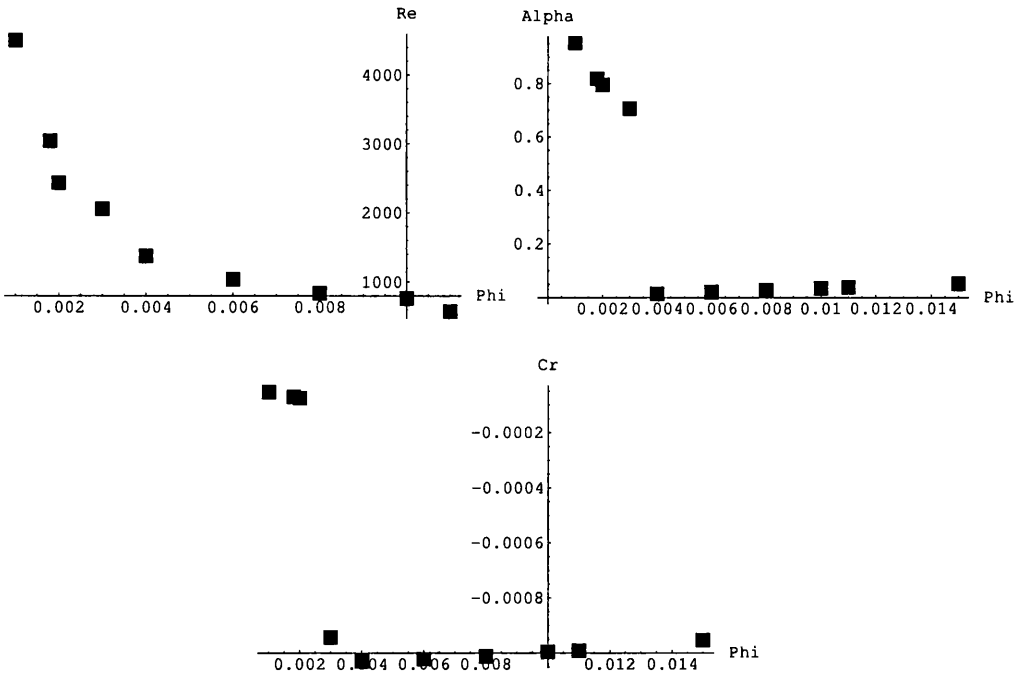


Figure 3.53: The dependence of the ice mode critical parameters on the angle of incline ($H_0 = 10$)

### 3.2.6 Comparison with longwave asymptotics

In order to understand the nature of the modes obtained in the longwave limit, we will analyse the behaviour of ice, surface and shear modes numerically for long waves and compare the results with the analytic results of the longwave asymptotics derived in the "3.2.6 Longwave asymptotics for the linear stability problem" section.

In the longwave limit it is possible to obtain the function $c_{i,r}(\alpha)$ plots by plotting the dependency on $a = \alpha\frac{RePr}{St}$ for fixed $Re$, $Pr$ and $St$ numbers. In order to make the comparison easier, we will fix the angle of incline ($\phi = 0.002$), Stefan number ($St = 0.0625$) and media properties ($Pr = 13.47$) and compare the modes with and without surface tension for different $Re$ and $H_0$.

The graphs below in Fig. 3.54 show the comparison between the ice mode for the Orr-Sommerfeld solution (dot-dashed line) and the $c_-$ mode of the longwave asymptotics (solid line) for Reynolds number $Re = 10000$ and initial ice height value of $H_0 = 10$ without surface tension:

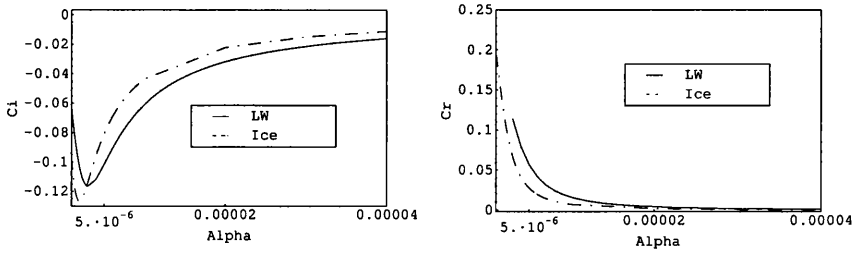


(a) Ci (b) Cr

Figure 3.54: The comparison between longwave asymptotics mode $c_-$ and the ice mode in the longwave limit

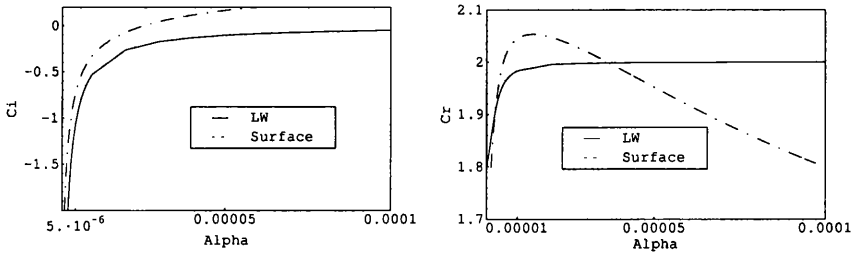


(a) Ci (b) Cr

Figure 3.55: The comparison between the longwave asymptotics mode $c_+$ and the surface mode in the longwave limit

There is a reasonable agreement between $c_-$ and ice mode. As $\alpha \to 0$ both modes tend to the limiting value given for the chosen $H_0$ by the longwave asymptotic solution, namely $c = 0.2155$.

The other mode of the longwave asymptotics $c_+$ behaves as a surface mode in the limiting cases when $\Theta_{il} \to 1$ and $H_0 \to \infty$. Fig. 3.55 shows the comparison between the surface mode and the $c_+$ mode of the longwave asymptotics.

Both the longwave asymptotic solution and the surface mode exhibit the same behaviour for small $\alpha$. As $\alpha \to 0$ the phase speed for both solutions tends to the limiting value given for the chosen value of $H_0$ by longwave asymptotic solution:

$$c = 1.785 - i\frac{H_0 - \Theta_{il}(H_0 - 1)}{a(H_0 - 1)}$$

The longwave behaviour of the shear mode is distinctly different from that of the other modes:

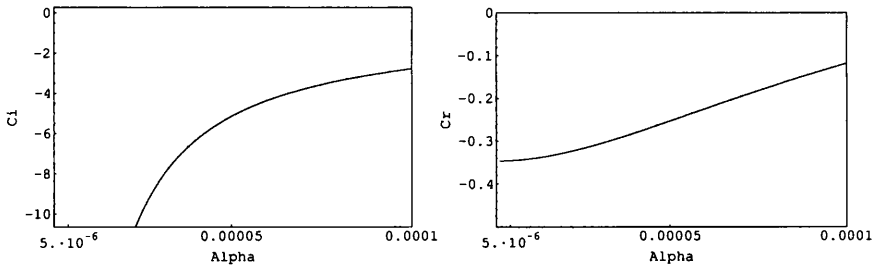


(a) Ci (b) Cr

Figure 3.56: The longwave behaviour of the shear mode

The results presented in this section allow us to identify the longwave asymptotic modes $c_-$ and $c_+$ as the ice mode and the surface mode (modified by the ice layer) respectively.

### 3.2.7 Ice influence on the surface mode

The initial observations made in the section "3.2.6 Comparison with longwave asymptotics" demonstrate that the interaction between the ice layer and the flow stabilises interfacial mode in the longwave limit. In order to verify this statement we will compare the longwave behaviour of the interfacial mode computed with and without ("fake ice") thermodynamic interaction. The plots below show $c_i(\alpha)$ for these two cases with fixed $St = 0.0625$, $H_0 = 10$, and $\phi = 0.002$ and different Reynolds numbers:

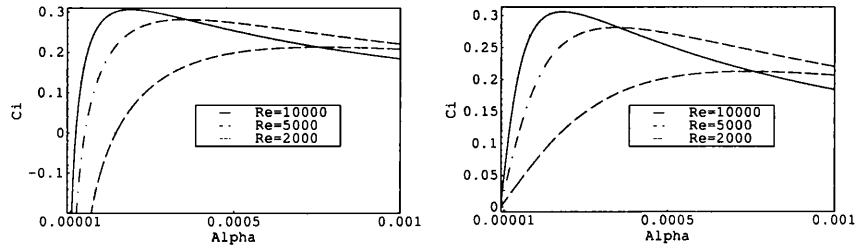


(a) With ice (b) With solid boundary

Figure 3.57: The effect of longwave stabilisation of the surface mode for different $Re$

As can be seen from Fig. 3.57-3.58, the surface mode is unstable in the longwave limit without an ice layer and stable in the longwave limit when an ice layer is present. From the results of computations it follows that the variation of the initial ice height has no significant influence on the longwave stabilisation effect.

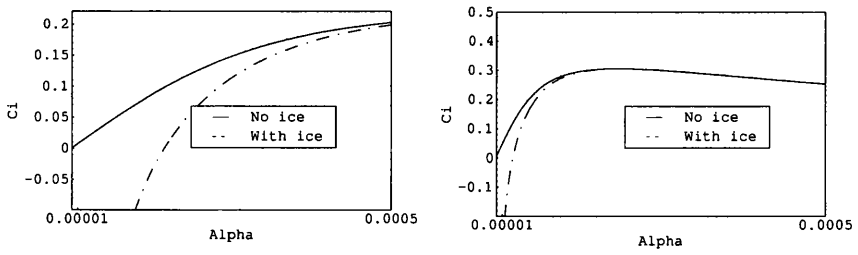


(a) Re=2000 (b) Re=10000

Figure 3.58: The comparison between the longwave behaviour of surface mode with and without ice

Increasing the Stefan number leads to the increase of the longwave stable region for the surface mode. Below is an example of the influence of the Stefan number, shown as $c_i(\alpha)$ plots for $H_0 = 10$, $Re = 2000$, $\phi = 0.002$ and $\zeta = 0$:

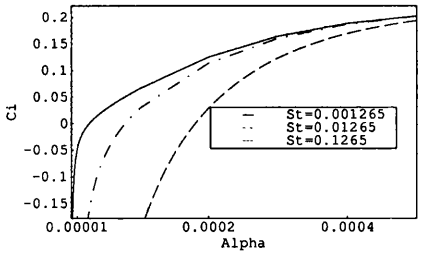


Figure 3.59: The influence of the Stefan number on the longwave stabilisation of the interfacial mode

When there is no ice layer, the surface mode neutral curve intersects with $Re$ axis (see, for example Floryan, Davis and Kelly (1987)). However when an ice layer is present, the neutral curve of the surface mode no longer intersects with $Re$ axis, but has a distinct critical point instead. The plots below show neutral curves for the surface mode near the critical point with and without ice for $H_0 = 10$ and different angles of incline and Stefan numbers. The set of the angles of incline has

been chosen to be the same as in the computations performed by Floryan, Davis and Kelly (1987) to allow the comparison between our and their results for the "fake ice" case:

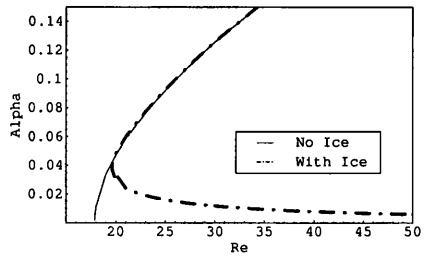


(a) Phi=4 deg

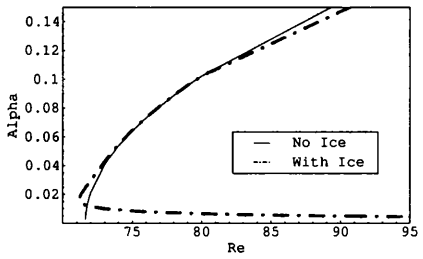


(b) Phi=1 deg

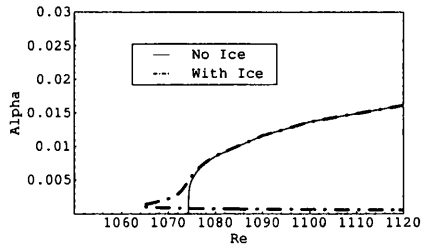


(c) Phi=4 min

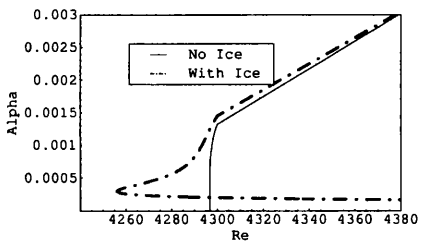


(d) Phi=1 min

Figure 3.60: The influence of an ice layer on the surface mode neutral curves, $St = 0.0625$

The ice layer increases the critical Reynolds number of the surface mode for large angles of incline and decreases it for small angles of incline. Fig. 3.61 illustrates the influence of the angle of incline on the critical Reynolds number of the surface mode with and without ice (here $\phi$ is given in degrees as in Floryan, Davis and Kelly (1987) ).

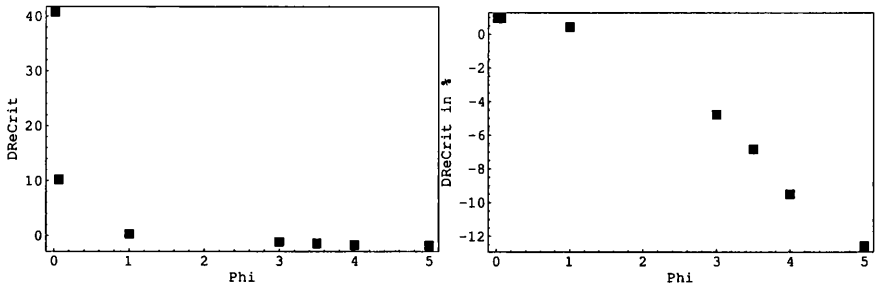


(a) Difference in Re (b) Difference in Re

Figure 3.61: The influence of the angle of incline on the surface mode critical Reynolds number, $St = 0.0625$

The two plots above show the values of $Re_c^{noice} - Re_c^{ice}$ and $\frac{Re_c^{noice} - Re_c^{ice}}{Re_c^{noice}} \cdot 100$ respectively. For small angles of incline ($\phi < 2^o$), the difference $Re_c^{noice} > Re_c^{ice}$ and presence of ice destabilises the surface mode. For larger angles of incline ($\phi > 2^o$) $Re_c^{noice} < Re_c^{ice}$ and the ice layer stabilises the surface mode. The difference between the critical Reynolds number for the cases with and without ice falls steadily as the angle of incline increases, however the difference in % of the critical Reynolds number without ice increases steadily. The maximum drop of 12.59% in the critical Reynolds number was computed at $\phi = 5^o$ .

Figure 3.62 shows the dependence of the critical phase speed $c_r$ and critical wavenumber $\alpha$ on the angle of incline. It can be seen that the increase in the angle of incline leads to an increase in both critical wave speed and critical wavenumber for the surface mode.

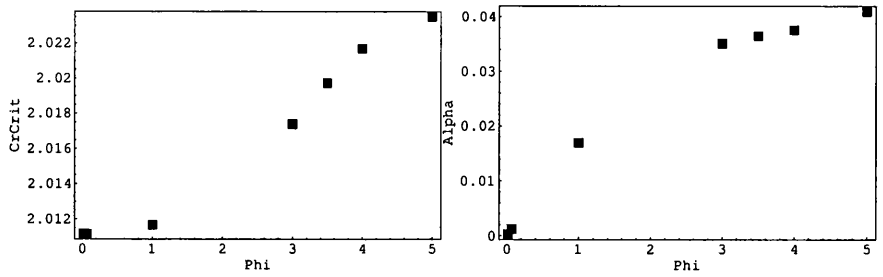


(a) Cr (b) Alpha

Figure 3.62: The influence of the angle of incline on the critical wave speed and wave number of the surface mode, $St = 0.0625$

The increase of the Stefan number destabilises the flow for small angles of incline ($\phi \lesssim 2$) and stabilises the flow for large angles of incline ($\phi \gtrsim 2$):

| $St\backslash\phi$ | $1'$ | $1^o$ | $2^o$ | $3^o$ | $5^o$ |
|---|---|---|---|---|---|
| 0.01265 | 4284.6 | 71.6 | 36.22 | 24.7 | 15.7 |
| 0.0625 | 4256.1 | 71.2 | 36.25 | 25.0 | 16.5 |
| 0.1265 | 4242.6 | 71.0 | 36.32 | 25.2 | 17.0 |

Table 3.9: The influence of the Stefan number on the surface mode critical Reynolds number

The critical wavenumber steadily grows as the Stefan number increases:

| $St\backslash\phi$ | $1'$ | $1^o$ | $2^o$ | $3^o$ | $5^o$ |
|---|---|---|---|---|---|
| 0.01265 | 0.00026642 | 0.014262 | 0.022308 | 0.027186 | 0.031044 |
| 0.0625 | 0.00029866 | 0.016952 | 0.028524 | 0.035106 | 0.040934 |
| 0.1265 | 0.00033697 | 0.019297 | 0.030972 | 0.038326 | 0.045936 |

Table 3.10: The influence of the Stefan number on the surface mode critical wave number

The critical wavespeed also grows as we increase the Stefan number, however the variation is extremely small:

| $St\backslash\phi$ | $1'$ | $1^o$ | $2^o$ | $3^o$ | $5^o$ |
|---|---|---|---|---|---|
| 0.01265 | 2.00323 | 2.00352 | 2.00464 | 2.00571 | 2.00797 |
| 0.0625 | 2.01117 | 2.01116 | 2.01408 | 2.01739 | 2.02352 |
| 0.1265 | 2.01522 | 2.01565 | 2.02056 | 2.02473 | 2.03107 |

Table 3.11: The influence of the Stefan number on the surface mode critical wave speed

The results discussed in this section demonstrate that the ice layer stabilises the surface mode in the longwave limit and affects the critical Reynolds number of the surface mode. The influence of the ice layer on the critical Reynolds number of the surface mode depends on the angle of incline. For small angles of incline the ice layer decreases the critical Reynolds number of the surface mode and for sufficiently large values of the angle of incline the ice layer increases the critical Reynolds number of the surface mode.

## 3.3 A mechanism for upstream propagation of liquid/solid interface perturbations in free-surface flows

In this section we attempt to derive a physical explanation of the observed upstream propagation of the icing instability based on the interaction between the free surface shape and the shape of the ice layer alone.

Since the argument we pursue does not depend on the fact that the interface growth is determined by the temperature field, it seems reasonable to consider a slightly more general case. Consider a 2D problem of liquid film flow over a solid phase under the following assumptions:

1. The timescale of the solidification process is much larger than that of the liquid flow.

2. The solidification process is governed by the balance of the normal flux of some scalar $G_{i,l}$ (in our case $G$ represents temperature) on the solid/liquid interface with weights $\lambda_{i,l}$ respectively and this scalar is continuous at the interface

3. The initial distribution of this scalar is linear and both the solid phase surface and the free surface are flat initially.

4. The scalar value $G$ governing the solidification process is constant at the lower boundary of the solid phase, solid/liquid interface and free surface.

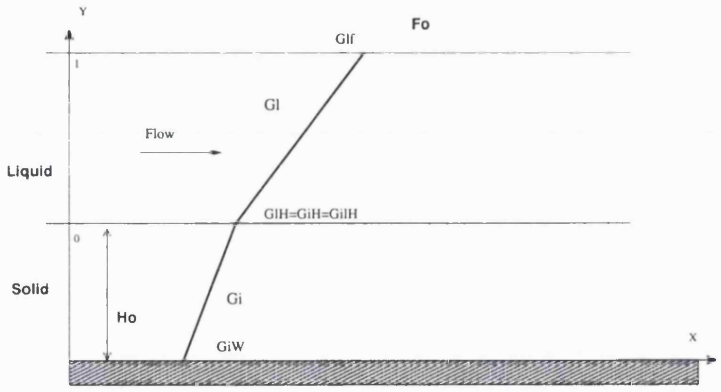


Figure 3.63: Liquid/solid interface instability mechanism, initial state

At the equilibrium state, the flux balance at the liquid/solid interface can be written as:

$$\lambda_i \frac{\partial G_i}{\partial n} = \lambda_l \frac{\partial G_l}{\partial n} \tag{3.158}$$

Under our assumptions, the expression above is equivalent to:

$$\lambda_i \frac{\partial G_i}{\partial y} = \lambda_l \frac{\partial G_l}{\partial y} \tag{3.159}$$

Since the unperturbed profile is linear, the $y$ derivatives expressed in terms of the boundary values and initial thicknesses $H_0$ and $F_0$ are given by:

$$\frac{\partial G_i}{\partial y} = \frac{G_{ilh} - G_w}{H_0} \tag{3.160}$$

$$\frac{\partial G_l}{\partial y} = \frac{G_{lf} - G_{ilh}}{F_0} \tag{3.161}$$

Now, suppose the ice surface is given a localised small perturbation $h(x)$, small enough for the $G_{i,l}$ profiles to remain linear at leading order. The assumption of the linearity of the $G_{i,l}$ distribution can be relevant, for example, to longwave disturbances. Since we assume that the timescale of the solid surface growth is much larger than the timescale of the flow, the problem is quasi-steady and the film flow can be determined for a fixed form of the solid surface $h(x)$ and the solution of this problem will give us the perturbation of the free surface $f(x)$ as shown on the following diagram:

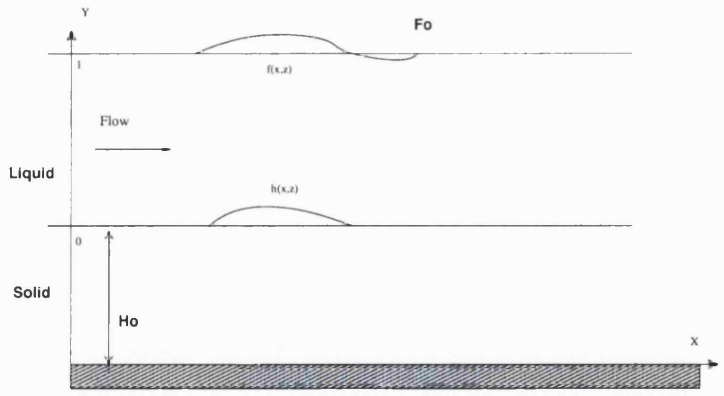


Figure 3.64: Liquid/solid interface instability mechanism, perturbed state

The problem of a liquid film flow over an obstacle is well investigated and it

is known that the free-surface is perturbed upstream of the obstacle (see, for example, Bowles (1995)). Same result can be illustrated with the results of our computations, the figure below shows an example of free surface shape computed for the Gaussian ice bump in linear and nonlinear Froude based double-deck:

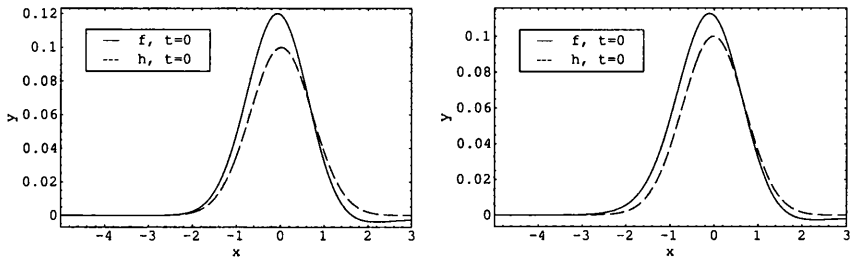


(a) Linear (b) Nonlinear

Figure 3.65: The shape of the free surface over an ice bump

Let us consider a point $x_0$ in $x$ located in front of the liquid/solid interface perturbation. If the solid/liquid perturbation is small, and the profiles of the scalar functions $G_{i,l}$ can still be considered linear, then the flux imbalance condition for the growth of the ice surface disturbance can be written at this point as:

$$\lambda_i \frac{G_{ilh} - G_w}{H_0} > \lambda_l \frac{G_{lf} - G_{ilh}}{F_0 + f(x_0)} \tag{3.162}$$

The flux from the liquid side decreased as the thickness of the liquid layer increased. For ice-growth problem this means that the heat flux from the liquid side has decreased and therefore the ice surface will grow in order to level the heat-flux balance. Therefore the small perturbation of the ice surface will propagate upstream.

## 3.4 Conclusions

In this chapter we have developed a Froude number based double-deck theory for the boundary-layer scaled free-surface flows and considered linear and nonlinear stability of the half-Poiseuille flow down an inclined plane covered with an ice layer. We have discovered a new mode of upstream propagating instability arising because of the presence of an ice layer and investigated its properties.

In the linear approximation for the viscous sublayer of the double-deck theory, we have obtained an analytic solution in terms of Airy functions in the 3D and 2D case for $Pr = 1$. Then, we demonstrated that this analytic solution is applicable in the case where $Pr = 13.47$ (water near freezing temperature), provided the time is rescaled accordingly, which means that in the linear problem, the thermal boundary layer thickness affects the speed of disturbances propagation but has no significant impact on the shape of disturbances. In the general case where $Pr \neq 1$, the problem was solved numerically in 3D and 2D case using a new compact $4^{th}$order finite-differences scheme developed for Orr-Sommerfeld-type equations. In the 3D case we discovered that the flow can become unstable to 3D perturbations before it becomes unstable to 2D perturbations for certain values of the initial ice thickness.

For the nonlinear double-deck equations, we developed a global-marching type scheme, and used it to solve the 2D nonlinear problem numerically. The nonlinear solution demonstrated the tendency of nonlinearity to weaken the dispersive properties of the solution and increase dissipation and upstream propagation speed. We have also analysed numerically the configurations with a sudden wall temperature jump and provided an explanation of the physical mechanism of the upstream propagation observed for the ice surface disturbances in free surface flows.

Also we considered the linear stability problem for a half-Poiseuille flow down an inclined plane covered with an ice layer when the film thickness is $O(1)$. We derived longwave asymptotics for the resulting Orr-Sommerfeld problem and demonstrated that instead of one mode given by longwave asymptotic solution for this problem without ice layer (Yih (1963)), two modes are obtained when an ice layer is present. For these two modes we obtained analytical expressions and used them in order to analyse the behaviour of the longwave modes in a wide range of problem parameters.

Then, we solved the full Orr-Sommerfeld problem numerically and discovered the ice mode using the double-deck solution as an initial guess. Also we investigated the behaviour of the ice mode in the Orr-Sommerfeld problem in a wide range of problem parameters. Using the numerical solver developed for the Orr-Sommerfeld problem, we matched the modes obtained from the longwave asymptotic analysis with the modes obtained from the numerical solution of the linear stability problem and identified the longwave modes $c_+$ and $c_-$ as ice and surface modes of the Orr-Sommerfeld problem respectively.

Another important finding was the effect of longwave stabilisation of the surface mode caused by the ice layer. We investigated this effect and computed critical parameters for the surface mode in a wide range of problem parameters. We demonstrated that the presence of an ice layer can either increase or decrease the critical Reynolds number of the surface mode depending on the value of the angle of incline.

The mode of the icing instability we have discovered in the scope of the Froude-based double-deck theory and in the linear stability analysis of $O(1)$ thick film is present in the flow without supercooling and cannot be explained by the freezing

temperature modification via Gibbs-Thomson effect (see Appendix A). We demonstrated that the mode of instability we have observed does not have the same nature as the flow-induced morphological instability of the solidification front, which can also propagate upstream under certain conditions (see, for example Forth and Wheeler (1989); Brattkus and Davis (1988); Batchelor, Mofatt and Worster (2000)), but is due to the interaction between the free surface and the ice surface shape instead. Also we provided a simple explanation of the upstream propagation of the ice mode.

The results obtained in this chapter provide qualitative explanation for the icing behaviour observed in the experiments on an inclined plane done by Streitz, Ettema, Rothmayer and Tsao (1998).

# 4 Mode-coalescence in the air/water channel flows

The present chapter is dedicated to the phenomenon of mode coalescence between the interfacial and shear mode in plane Poiseuille air/water channel flow.

Initially, we studied the plane Poiseuille flow of air above water in order to be able to compare the results for this flow with and without ice. Since the problem without ice layer seemed to be very well investigated, we tried to compare our results against those of Blennerhassett (1980) in order to verify our computations. However, when we were computing neutral curve for the shear mode to verify the solver against the results presented in Blennerhassett (1980), it occurred that the shear mode neutral curve which appears on Fig. 2 in this work in fact encloses stable region instead of unstable. This deviation from the results of Blennerhassett (1980) caused us to investigate the linear stability of plane Poiseuille flow of air above water in more detail. The results of this investigation are summarised in the current chapter.

The linear stability problem for a two-fluid Poiseuille flow in a planar channel was approached by many authors from different angles. A longwave asymptotic analysis performed by Yih (1967) illustrates the origin of interfacial instability in the flow. In general, interfacial modes can coexist with the more common for a channel flow instability of a Tollmien-Schlichting variety. This was studied computationally by Blennerhassett (1980), in his work the focus was on linear and nonlinear waves in a two-layer flow of air over water with equal layer depths. Yantsios and Higgins (1988, 1989) performed accurate computations for linear instabilities in a Poiseuille flow with two superimposed fluids. Their work was centred on the behaviour of the interfacial wave mode and its dependence on the relative depths and kinematic viscosities of fluid layers. Hooper (1989) studied

instabilities in a Poiseuille-Couette channel flow of two viscous fluids. An extensive review of the stability problem for two-fluid plane channel flows can be found in the book by Joseph and Renardy (1993).

We will follow the formulation of this problem given by Blennerhassett (1980). We consider a 2D two layer air-water configuration, with the majority of the results obtained for the case of equal layer depths. The fact that it is sufficient to consider only two-dimensional perturbations in determining the marginal stability boundary in linear stability analysis that has been first demonstrated by Squire (1933) for one fluid, has been successfully extended to two-fluid configurations by Yih (1955) and later by Hesla, Pranckh and Preziosi (1986), therefore we will limit our analysis to 2D problem.

It is interesting to note that generally, it can occur that we have a stabilising mechanism in the problem that is confined to the direction of the flow and a destabilising mechanism that acts both in the direction of the flow and in the perpendicular direction as well. For example, Renardy (1985) demonstrated that a 2D flow of a heavy fluid above light fluid can, in certain cases, be stabilised by viscous stratification and surface tension, but the gravitational instability is clearly not compensated in the direction perpendicular to the basic flow. Therefore, the applicability and relevance of Squire theorem should be considered separately for each particular problem. However in our case the density of the upper fluid (air) is much less then the density of the lower layer (water) and we can safely confine our analysis to 2D cases.

In our analysis, we will focus on two issues. First, in a search for novel instability modes, we extend the results of Blennerhassett to higher Reynolds numbers. The second, and perhaps more interesting, issue stems from the following remarkable

property. Blennerhassett (1980) neutral curves in Fig. 2 of his paper, reproduced on the figure below from our computations, show clearly a broadband interfacial instability in the flow starting from the Reynolds number of order 2000:

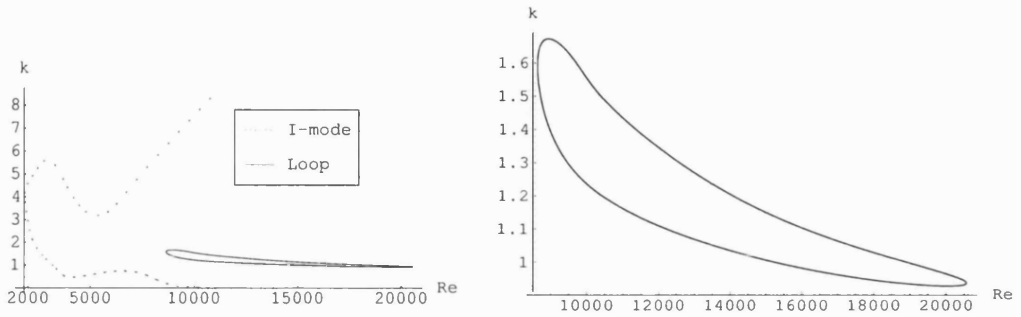


(a) Interfacial waves neutral curve and loop

(b) Loop

Figure 4.1: The neutral stability curve for interfacial waves and the stable region loop

In addition, a narrow band of waves marked by a neutral curve in the Reynolds number range of order 10000 seems to indicate the appearance of a second instability mode. Blennerhassett attributed this second instability to a Tollmien-Schlichting mechanism. However, we found that the narrow neutral curve was in fact a loop closed down at Reynolds numbers of order 20000. Of more significance for our study is the fact (entirely omitted in Blennerhassett's computations) that neutral-wave solutions for the points on the loop can be connected through a wavenumber continuation with the solutions on the broadband interfacial neutral curve. This observation (illustrated in more detail later) raises the question of physical identity for various instability modes in the flow. We will show that the neutral curves on the figure above (and further neutral curves discovered at higher Reynolds numbers) are a product of a complicated interaction and inter-

section of several key modes associated with three more or less distinct instability mechanisms:

- Tollmien-Schlichting instability in the air layer,
- Tollmien-Schlichting instability in the water layer and
- Interfacial instability

In particular, Tollmien-Schlichting instabilities are found to arise as two initially distinct modes at Reynolds numbers of order 15000 which is beyond the Reynolds number range covered in Blennerhassett.

It is not uncommon for a neutral curve of a layered flow to have several branches. Yantsios and Higgins (1988, 1989) were probably the first to note that the interfacial waves can be stabilised in a certain range of wavenumbers. Later the same effect was noted by Kuru, Sangalli, Uphold and McCready (1993), Miesen and Boersma (1995) and Sangalli, McCready and Chang (1997). It appears that under certain conditions the curve of the growth rate as a function of the wavenumber, $c_i(k)$, for the interfacial mode can develop a local minimum that produces a stable region with $c_i(k) < 0$. The formation of this stable region can be also seen in the study of interfacial waves behaviour in oil-water channel flows performed by McCready, Uphold and Gifford (1997). Another reason for the appearance of complicated neutral curve diagrams in two-fluid flows is the effect of mode crossing between interfacial and Tollmien-Schlichting waves considered for a boundary layer with high Reynolds numbers in Ozgen, Degrez and Sarma (1998) and Timoshin and Hooper (2000). In our study we find both the interfacial mode splitting and interfacial/Tollmien-Schlichting wave interaction present in certain

ranges of the wavenumber. In what follows we refer to the modes of interfacial instability, Tollmien-Schlichting instability due to air flow and Tollmien-Schlichting instability in water (liquid) as the I-mode, TSA-mode and TSL-mode, respectively.

## 4.1 Problem formulation

In order to enable comparison with the results of Blennerhassett (1980), we will use the same problem formulation and media parameters as in his work. Assuming a flow in a horizontal channel, we use the upper (air) layer density and viscosity as reference quantities. The velocity is nondimensionalised on the integral mean value $U$ of the undisturbed velocity across both layers. The coordinates are nondimensionalised on the air layer thickness $L$, with the origin at the undisturbed interface. For the majority of this study the base water layer is assumed to have the same thickness as the layer of undisturbed air. The media properties are given in the table below. The surface tension coefficient $S$ was taken to be $0.0735\, N/m$. The flow is entirely laminar and 2-dimensional.

| Media | Density, $\rho$ $(kg/m^3)$ | Dynamic viscosity $\mu$,$(kg/(m \cdot s))$ |
|---|---|---|
| Air | 1.225 | 0.0000177625 |
| Water | 999.1 | 0.0011369758 |

Table 4.1: Media properties for the study of mode coalescence

The horizontal velocity component in the base flow in the air layer ("$a$" subscript) and in the water layer ("$l$" subscript) can be taken in the form:

$$\begin{aligned} u_{0a} &= (1 + b_a y + a_a y^2)\,\tfrac{1}{d}, \qquad 0 \le y \le 1 \\ u_{0l} &= (1 + b_l y + a_l y^2)\,\tfrac{1}{d}, \qquad -1 \le y \le 0 \end{aligned} \tag{4.1}$$

with the constant parameters defined as:

$$
\begin{aligned}
b_a &= \tfrac{\mu_{la}-1}{2}, a_a = -\tfrac{\mu_{la}+1}{2}, \\
b_l &= \tfrac{\mu_{la}-1}{2\mu_{la}}, a_l = -\tfrac{\mu_{la}+1}{2\mu_{la}}, \\
d &= \tfrac{1}{2}\left(2 + \tfrac{b_a-b_l}{2} + \tfrac{a_l+a_a}{3}\right).
\end{aligned}
$$

The linear stability problem reduces then to a pair of Orr-Sommerfeld equations written in terms of the perturbation in the vertical velocity in each layer, $v(y)\exp(ik(x-ct))$ with the wavenumber $k$ and complex phase speed $c$:

$$
\begin{cases}
\frac{d^4v_a}{dy^4} + (-2k^2 + ikRe(c-u_{0a}))\frac{d^2v_a}{dy^2} + \\
\left(k^4 + ik^3Re(u_{0a}-c) + ikRe\frac{d^2u_{0a}}{dy^2}\right)v_a = 0 \\
\frac{d^4v_l}{dy^4} + (-2k^2 + ikRe\nu_{al}(c-u_{0l}))\frac{d^2v_l}{dy^2} + \\
\left(k^4 + ik^3Re\nu_{al}(u_{0l}-c) + ikRe\nu_{al}\frac{d^2u_{0l}}{dy^2}\right)v_l = 0
\end{cases}
\tag{4.2}
$$

The required boundary conditions follow from the velocity and stress continuity at the interface:

$$
\begin{aligned}
\tfrac{d^2v_a}{dy^2} + k^2v_a &= \mu_{la}\left(\tfrac{d^2v_l}{dy^2} + k^2v_l\right), \\
\tfrac{d^3v_a}{dy^3} - \mu_{la}\tfrac{d^3v_l}{dy^3} - 3k^2\tfrac{dv_a}{dy} + 3\mu_{la}k^2\tfrac{dv_l}{dy} + ikRe(c-u_{0a})\tfrac{dv_a}{dy} - & \\
-ikRe\rho_{la}(c-u_{0a})\tfrac{dv_l}{dy} + ikRev_a\tfrac{du_{0a}}{dy} - ikRe\rho_{la}v_l\tfrac{du_{0l}}{dy} &= \\
\tfrac{ikv_aRe}{(u_{0a}-c)}\left(\tfrac{1}{We}k^2\rho_{la} + Fr(\rho_{la}-1)\right), & \\
v_a &= v_l, \\
\tfrac{dv_a}{dy} - \tfrac{v_l}{u_{0a}-c}\tfrac{du_{0a}}{dy} &= \tfrac{dv_l}{dy} - \tfrac{v_l}{u_{0a}-c}\tfrac{du_{0l}}{dy},
\end{aligned}
\tag{4.3}
$$

and the no-slip conditions on the channel walls at $y = \pm 1$:

$$\begin{aligned} v_a(1) &= \tfrac{dv_a}{dy}(1) = 0 \\ v_l(-1) &= \tfrac{dv_l}{dy}(-1) = 0 \end{aligned} \tag{4.4}$$

Then, following Blennerhassett (1980), we note that $Fr$, $Re$ and $We$ numbers are not independent for fixed fluids as $F = FrRe^2 = g^*L^{*3}/\nu_a^{*2}$ and $T = Re^2/We = \gamma^*L^*/(\rho_l^*\nu_a^{*2})$ depend on $L^*$ only. Hence we introduce a dimensionless parameter, $k_s = \sqrt{\frac{(1-\rho_{al})F}{T}} = \sqrt{\frac{(\rho_l^*-\rho_a^*)g^*}{\gamma^*}}L^*$, representing the non-dimensional wavenumber of the inviscid surface wave with the minimum phase speed (see Blennerhassett (1980)). All the computations presented in this chapter have been performed for $k_s = 29.18$ to allow comparisons with the results on Fig. 2 in the paper by Blennerhassett (1980).

## 4.2 Numerical approach

### 4.2.1 Numerical scheme

For this problem we will use the same numerical approach as was used for free-surface flow in Chapter 3 of this thesis. We developed a compact finite-difference scheme of the $4^{th}$ order of accuracy derived on the principles described by Hirsh (1975) and Li (1998). The Orr-Sommerfeld equations are written in the form:

$$\frac{d^4v_{a,l}}{dy^4} + c_{a,l}^2(y)\frac{d^2v_{a,l}}{dy^2} + c_{a,l}^1(y)v_{a,l} = 0, \tag{4.5}$$

$$c^1_{a,l} = \begin{cases} k^4 + ik^3 Re(u_{0a} - c) + ikRe\frac{d^2u_{0a}}{dy^2} \\ k^4 + ik^3 Re\nu_{al}(u_{0l} - c) + ikRe\nu_{al}\frac{d^2u_{0l}}{dy^2} \end{cases} \tag{4.6}$$

$$c^2_{a,l} = \begin{cases} -2k^2 - ikRe(u_{0a} - c) \\ -2k^2 - ikRe\nu_{al}(u_{0l} - c) \end{cases} \tag{4.7}$$

Let $v^{II} = d^2v/dy^2$ and $v^{IV} = d^4v/dy^4$ then the following relations are true to $O(\Delta y^4)$ (see Appendix C) on a uniform grid:

$$\begin{cases} \frac{v^{IV}_{n-1}+10v^{IV}_n+v^{IV}_{n+1}}{12} = \frac{v^{II}_{n-1}-2v^{II}_n+v^{II}_{n+1}}{\Delta y^2} \\ \frac{v^{II}_{n-1}+10v^{II}_n+v^{II}_{n+1}}{12} = \frac{v_{n-1}-2v_n+v_{n+1}}{\Delta y^2} \end{cases} \tag{4.8}$$

Substituting the expression for $v^{IV}$ from the Orr-Sommerfeld equations into these difference equalities and approximating boundary conditions with the same order of accuracy we obtain for the unknown vector function $X = (v, v^{II}, T)$ a system of linear equations whose matrix differs from a tridiagonal one only in lines containing boundary conditions:

$$A_{n-1}X^{n-1} + B_{n-1}X^n + C_{n-1}X^{n+1} = D_{n-1} \tag{4.9}$$

$$A = \begin{pmatrix} 1 & -\frac{1}{12}\Delta y^2 & 0 \\ \frac{1}{12}\Delta y^2 c_{n-1}^{1v} & \left(1+\frac{1}{12}\Delta y^2 c_{n-1}^{2v}\right) & 0 \\ \frac{1}{12}\Delta y^2 c_{n-1}^{1T} & 0 & \left(1+\frac{1}{12}\Delta y^2 c_{n-1}^{2T}\right) \end{pmatrix} \tag{4.10}$$

$$B = \begin{pmatrix} -2 & -\frac{10}{12}\Delta y^2 & 0 \\ \frac{10}{12}\Delta y^2 c_{n}^{1v} & \left(-2+\frac{10}{12}\Delta y^2 c_{n}^{2v}\right) & 0 \\ \frac{10}{12}\Delta y^2 c_{n}^{1T} & 0 & \left(-2+\frac{10}{12}\Delta y^2 c_{n-1}^{2T}\right) \end{pmatrix} \tag{4.11}$$

$$C = \begin{pmatrix} 1 & -\frac{1}{12}\Delta y^2 & 0 \\ \frac{1}{12}\Delta y^2 c_{n+1}^{1v} & \left(1+\frac{1}{12}\Delta y^2 c_{n+1}^{2v}\right) & 0 \\ \frac{1}{12}\Delta y^2 c_{n+1}^{1T} & 0 & \left(1+\frac{1}{12}\Delta y^2 c_{n+1}^{2T}\right) \end{pmatrix} \tag{4.12}$$

$$n = 1...N_l - 2, N_l + 1, ...N_a + N_l - 1$$

The grid contains $N_a + N_l$ points where the air/water interface corresponds to points $N_l - 1$ and $N_l$ (all indices start from 0). On the upper wall $n = N_a + N_l - 1$ and the perturbations must be zero. Let $N_a + N_l - 1 = N$, then the conditions on the upper channel wall are given by:

$$\begin{cases} v_N = 0 \\ \frac{25}{12}v_N - 4v_{N-1} + 3v_{N-2} - \frac{4}{3}v_{N-3} + \frac{1}{4}v_{N-4} = 0 \end{cases} \tag{4.13}$$

On the air/water boundary the conditions should be distributed between 2 grid points. We will write the normal velocity match and tangential stress match at $N_l - 1$ **(4.14)**.

$$\begin{cases} v_{N_l} - v_{N_l-1} = 0 \\ v^{II}_{N_l} - \mu_{la} v^{II}_{N_l-1} + k^2(1-\mu_{la}) v_{N_l-1} = 0 \end{cases} \tag{4.14}$$

The tangential velocity match and normal stress match written at $N_l$ yield the following difference equations:

$$\begin{aligned} &\frac{25}{12}v_{N_l-1} - 4v_{N_l-2} + 3v_{N_l-3} - \frac{4}{3}v_{N_l-4} + \frac{1}{4}v_{N_l-5} + \\ &\frac{25}{12}v_{N_l} - 4v_{N_l+1} + 3v_{N_l+2} - \frac{4}{3}v_{N_l+3} + \frac{1}{4}v_{N_l+4} + \frac{1}{u_{0a}-c}\left(\frac{du_{0l}}{dy} - \frac{du_{0l}}{dy}\right)v_{N_l} = \\ &\frac{1}{u_{0a}-c}\left(\frac{50}{12} + \frac{du_{0l}}{dy} - \frac{du_{0l}}{dy}\right)v_{N_l} - 4v_{N_l-2} + 3v_{N_l-3} - \frac{4}{3}v_{N_l-4} + \frac{1}{4}v_{N_l-5} - \\ &-4v_{N_l+1} + 3v_{N_l+2} - \frac{4}{3}v_{N_l+3} + \frac{1}{4}v_{N_l+4} = 0 \end{aligned}$$

$$\begin{aligned} &\frac{25}{12}v^{II}_{N_l} - 4v^{II}_{N_l+1} + 3v^{II}_{N_l+2} - \frac{4}{3}v^{II}_{N_l+3} + \frac{1}{4}v^{II}_{N_l+4} + \\ &+\mu_{la}\left(\frac{25}{12}v^{II}_{N_l-1} - 4v^{II}_{N_l-2} + 3v^{II}_{N_l-3} - \frac{4}{3}v^{II}_{N_l-4} + \frac{1}{4}v^{II}_{N_l-5}\right) + \\ &+(-3\mu_{la}k^2 + +ikRe\rho_{la}(c-u_{0l}))\left(\frac{25}{12}v_{N_l-1} - 4v_{N_l-2} + 3v_{N_l-3} - \frac{4}{3}v_{N_l-4} + \frac{1}{4}v_{N_l-5}\right) + \\ &+(3k^2 - ikRe(c-u_{0a}))\left(\frac{25}{12}v_{N_l} - 4v_{N_l+1} + 3v_{N_l+2} - \frac{4}{3}v_{N_l+3} + \frac{1}{4}v_{N_l+4}\right) - \\ &-\left(ikRe\frac{du_{0a}}{dy} - ikRe\rho_{la}\frac{du_{0l}}{dy} - \frac{ikRe}{(u_{0a}-c)}\left(R_We k^2 + R_{Fr}\right)\right)v_{N_l} = 0 \end{aligned}$$

Also the perturbations must be zero on the lower channel wall ($n = 0$):

$$\begin{cases} \frac{25}{12}v_0 - 4v_1 + 3v_2 - \frac{4}{3}v_3 + \frac{1}{4}v_4 = 0 \\ v_0 = 0 \end{cases} \tag{4.15}$$

Therefore the resulting linear system is $AX = 0$, where $A$ a $3(N_a + N_l - 1) \times 3(N_a + N_l - 1)$ matrix which is tridiagonal except for the lines corresponding to boundary conditions. Then we can generalise the Thomas (1953) method which was also applied for the linear stability problem of two fluids in a plane channel by Blennerhassett (1980) by using Gaussian elimination in order to bring the matrix $A$ to the following form:

$$A = \begin{pmatrix} a_{0,0} & a_{0,1} & . & . & 0 & 0 & . & . & . & 0 \\ & a_{1,1} & . & . & . & . & . & . & . & . \\ & & . & . & . & . & . & . & . & . \\ & & & a_{i-1,i-1} & 0 & 0 & . & . & . & . \\ 0 & . & . & 0 & a_{ii} & 0 & . & . & . & 0 \\ . & & & & 0 & a_{i+1,i+1} & a_{i+1,i+2} & . & . & . \\ . & & & & 0 & a_{i+2,i+1} & . & . & . & . \\ . & & & & . & . & . & . & . & . \\ . & & & & . & . & . & . & . & . \\ 0 & . & . & . & 0 & . & . & . & . & a_{n-1,n-1} \end{pmatrix} \tag{4.16}$$

Then the only non-zero element in the $i_{th}$ row and $i_{th}$ column is $a_{i,i}$. In order for the matrix determinant to be zero in this case, this element has to be zero. Therefore, $a_{i,i}$ can be regarded as a function of the complex phase speed $c$ - $a_{i,i} = B(c)$ and its roots can be determined with an iterative method. The value of $i$ then can be adjusted to improve convergence of the iterative procedure. For two-fluid flows the optimal choice for $i$ was a point on the air/water boundary. Apart from the construction of the function $B(c)$, the solution method is exactly the same as the

one used for the free surface problem in Chapter 3.

The code was implemented in C++ and all computations were performed on a Pentium-III/800MHz/256Mb RAM. Complex arithmetics was implemented in C++ in order to assure the accuracy of the results.

For the major part of the computations grids of 500 points in $y$ were used for traces and neutral curves computations. For the critical parameters, eigenvectors and single mode value computations grids of 800 points in $y$ were used.

### 4.2.2 Solver tests

**4.2.2.1 One fluid Poiseuille flow** A plane Poiseuille flow of one fluid in a channel represents a sub-problem of our problem. The solution for one-fluid flow can be obtained by formally setting all media properties ratios ($\rho_{al}$, $\mu_{al}$, etc) in the problem to 1. Thus we can test our solver against the results of Orzag (1971), who applied high-accuracy spectral method to this problem.

The tests demonstrate that our method allows to obtain 5-digit correspondence with Orzag (1971) on grids of 500-600 points, which can be considered an excellent result, since a comparison is made with a high-order spectral method.

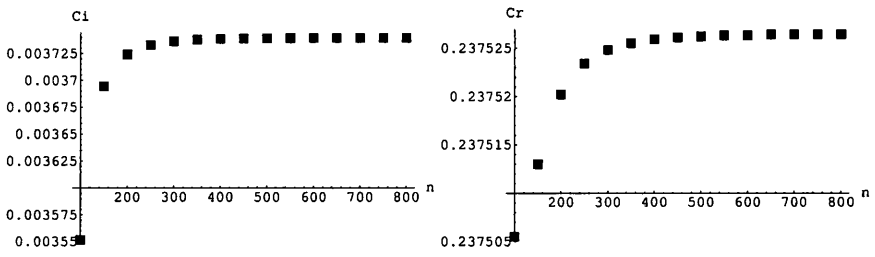


(a) Ci convergence (b) Cr convergence

Figure 4.2: Solution convergence for one-fluid plane Poiseuille flow

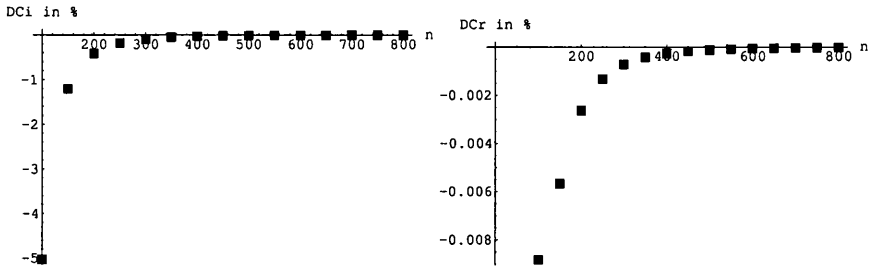


(a) Ci difference from Orzag solution

(b) Cr difference from Orzag solution

Figure 4.3: Solution convergence for one-fluid plane Poiseuille flow

Fig. 4.2-4.3 demonstrate grid convergence of the algorithm at a reference point from Orzag (1971) where $k = 1$, $Re = 10000$ and $c = 0.23752649 + 0.00373967i$, claimed to be valid to $10^{-8}$ in his work. The point $0.1 + 0.1i$ was used as an initial guess on all grids.

We see that the accuracy we can obtain on grids of about 150-200 points is about $1.0 - 0.5\%$ which is enough to calculate the shape of neutral curves and investigate modes behaviour. When a more accurate solution is desired (for example in critical Reynolds number computations) finer grids can be used.

**4.2.2.2 Two-fluids Poiseuille flow** Yantsios and Higgins (1988, 1989) performed rigorous numerical analysis of linear stability of two superposed fluids in plane Poiseuille flow. Their equations were written in coordinate system where $y \in [-n, 1]$ with the interface located at 0, and the velocity was normalised by the velocity at the interface. Comparison of our results with the cases studied in their paper shows that our solver can reproduce their results with good accuracy. All comparison data has been calculated on a grid with $(N_l = 250, N_a = 250)$.

In the short wave limit we compared the results for the complex wave speed from Table I of Yantsios and Higgins (1988). Here $n = 1$, $\mu_{la} = 5$, $k = 10$ and $\rho_{la} = 1$:

| | | Yiantsios & Higgins (1988) | | Our |
|---|---|---|---|---|
| $kR_{We}$ | $Re$ | Asymptotic | Numeric | Numeric |
| 1 | 1 | $0.99997 - i0.008122$ | $0.99998 - i0.008199$ | $0.99998 - i0.008199$ |
| 1 | 5 | $0.99930 - i0.040182$ | $0.99956 - i0.041184$ | $0.99956 - i0.041184$ |
| 2 | 1 | $0.99994 - i0.016460$ | $0.99996 - i0.016537$ | $0.99997 - i0.016538$ |
| 2 | 5 | $0.99861 - i0.083134$ | $0.99907 - i0.083491$ | $0.99907 - i0.083491$ |

Table 4.2: Comparison of our results for complex phase speed $c$ with Yantsios and Higgins (1988) results (short wave limit)

In the longwave limit we compared the results with Table II from Yantsios and Higgins (1988), showing the influence of gravity on the critical thickness ratio. Here $k = 0.001$, $Re = 1$ $\mu_{la} = 20$, $\rho_{la} = 1.5$ and $R_{We} = 0$:

| | | Yiantsios & Higgins (1988) | | Our |
|---|---|---|---|---|
| $R_{Fr}$ | $n$ | Asymptotic | Numeric | Numeric |
| 0.01 | 4.348 | $1.0181815 - i4.98 \cdot 10^{-10}$ | $1.0181815 - i4.99 \cdot 10^{-10}$ | $1.0181815 - i4.98 \cdot 10^{-10}$ |
| 0.1 | 3.633 | $1.1494009 - i4.76 \cdot 10^{-10}$ | $1.1494006 - i4.92 \cdot 10^{-10}$ | $1.1494006 - i4.92 \cdot 10^{-10}$ |
| 1 | 1.944 | $1.7437900 - i1.425 \cdot 10^{-8}$ | $1.7437885 - i1.439 \cdot 10^{-8}$ | $1.7437890 - i1.440 \cdot 10^{-10}$ |
| 10 | 0.620 | $1.8974670 + i8.493 \cdot 10^{-8}$ | $1.897466 + i8.494 \cdot 10^{-8}$ | $1.897467 + i8.494 \cdot 10^{-8}$ |

Table 4.3: Comparison of our results for complex phase speed $c$ with Yantsios and Higgins (1988) results (long wave limit)

It can be seen that the results are in excellent agreement.

## 4.3 Results

Interfacial instability gives rise to the broadband neutral curve. Our results for this neutral curve are in good agreement with the numerical and asymptotic results

presented in the paper by Blennerhassett (1980). However, as was mentioned before, the second neutral curve shown in Fig. 2 of this paper is, in fact, a closed loop which does not belong to a second, distinct, mode of instability in the flow. In order to understand the events leading to the formation of the neutral loop we consider real and imaginary parts of the complex phase speed $c_r(k)$ and $c_i(k)$ respectively, as functions of the wavenumber $k$ for a fixed Reynolds number. An example is shown below for $Re = 10000$ which corresponds to the middle part of the loop:

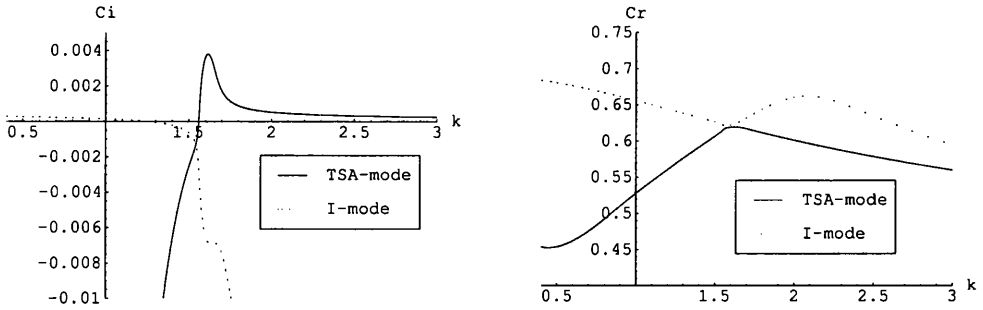


Figure 4.4: Mode structure at $Re = 10000$

As follows from the figure above, the loop is formed by two different modes, with the region inside the loop corresponding to stable disturbances. Later on we will show that the modes involved can be connected with the interfacial instability (I-mode) and Tollmien-Schlichting instability in air (TSA-mode), as labelled in the diagram. However one should bear in mind that the mode identification is a matter of some subtlety in this case because, in fact, the I-mode in the figure above is connected to the lower branch of the broadband neutral curve whereas the TSA-mode is obtained by continuation from the upper branch of the broadband neutral curve. In this case, in order to be able to trace mode behaviour in a consistent manner, we have chosen to identify I and TSA modes by their longwave

behaviour.

At lower Reynolds numbers the interfacial waves neutral curve is formed by one mode, therefore the mode structure observed at $Re = 10000$ has no direct continuation into lower Reynolds numbers:

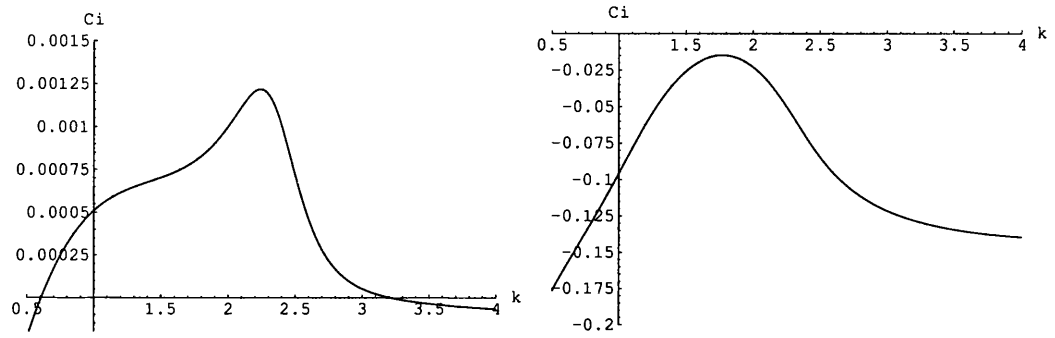


(a) I-mode (b) TSA-mode

Figure 4.5: Mode structure at $Re = 5000$

Let us consider the variation of the two modes with the Reynolds number in more detail. To this end, the values of the complex phase speed $c$ for the two modes are first calculated at a fixed point in the wavenumber-Reynolds number plane ($k = 1.4$, $Re = 10000$ in our computations) and then extended parametrically to other Reynolds numbers in as wide a range of wavenumbers as necessary. The results can be summarised as follows.

For sufficiently low Reynolds number, the I-mode forms the broadband neutral curve whereas the TSA-mode remains stable. As the Reynolds number increases, the distance between the mode curves in $(k, Re)$ parameter plane decreases. The imaginary part of the phase speed for the I-mode develops a local minimum which at $Re \simeq 8642$ gives rise to a narrow range of stable waves with $c_i < 0$ hence

indicating the beginning of the stable loop. At the same time the imaginary part of the phase speed for the TSA-mode develops a spike nearly touching the neutral level with $c_i = 0$:

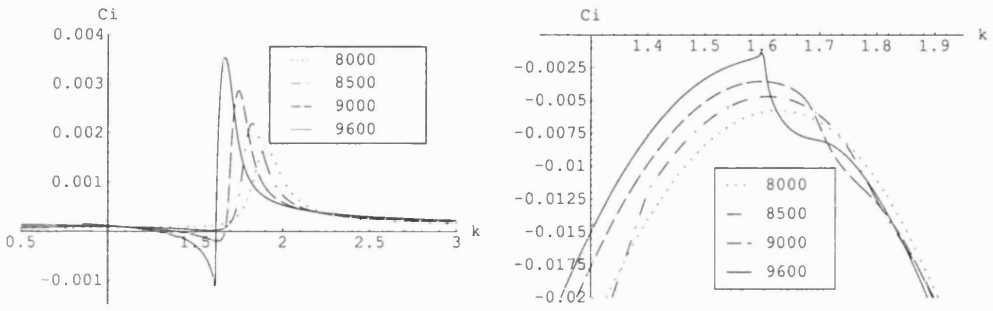


(a) I-mode (b) TSA-mode

Figure 4.6: Modes evolution before intersection, $Re = 8000 - 9600$

For the Reynolds numbers in this region the I-mode alone is responsible for the broadband interfacial instability (for both short and long waves) and for the neutral point of the loop and a range of stable waves inside the loop.

At the Reynolds number $Re = 9800$ approximately, the I-mode and TSA mode intersect and exchange branches. Now the loop is formed by two different modes with the mode identity essentially lost. A branch of the previously distinct TSA-mode is now connected with the interfacial I-mode for longer waves, the other branch of the TSA-mode is connected to the short-wave I-mode (Fig. 4.7).

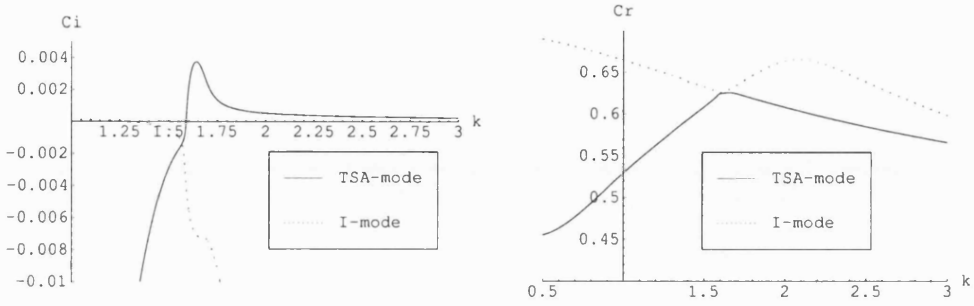


(a) Ci (b) Cr

Figure 4.7: First branch exchange

At still higher Reynolds numbers, the distance between the modes first increases but then it begins to decrease. The TSA-mode develops a local maximum in $c_i$ and the modes exchange branches once again between $Re = 12400$ and $Re = 12450$:

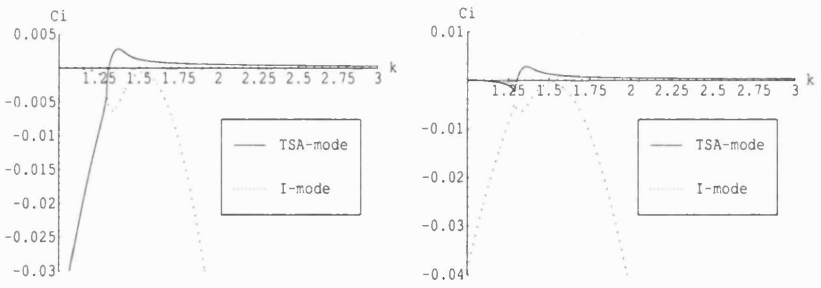


(a) Ci, Re=12400 (b) Ci, Re=12450

Figure 4.8: Second branch exchange

After the second mode crossing, the mode configuration returns to the arrangement typical for low Reynolds numbers, with both the loop and the broadband neutral curve formed by the I-mode alone. At still higher Reynolds numbers, the local

range of stable waves of the I-mode narrows down and eventually vanishes at $Re \sim 20553$. This point marks the closure of the loop.

The two intersections between the I-mode and TSA-modes described above take place at points representing stable waves. Before the first and immediately after the second mode crossing, i.e. at $Re < 9600$ and $Re \gtrsim 12450$, the TSA-mode is stable. However at somewhat higher Reynolds numbers, starting from $Re \sim 13767$, the TSA mode becomes unstable and forms its own neutral curve:

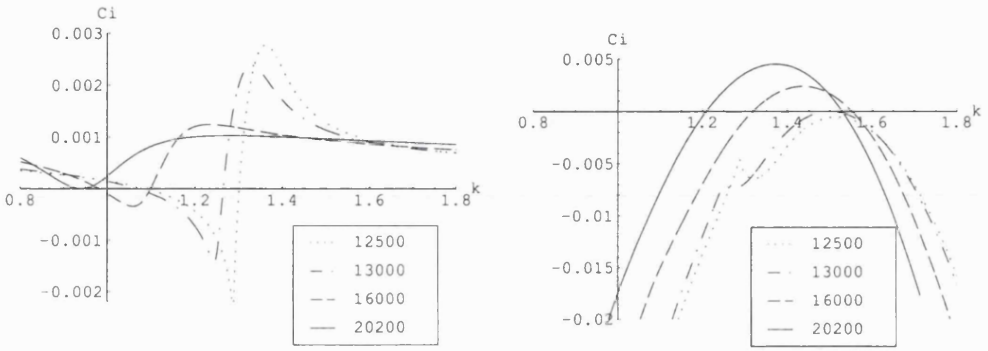


(a) I-mode (b) TSA-mode

Figure 4.9: Mode evolution, $Re = 12500 - 20200$

In our search for the starting points for the modes at $k = 1.6$ $Re = 10000$ we came across a root with $c = -0.1364402 - 0.0007882i$. At higher Reynolds numbers, this root leads to instability associated with a Tollmien-Schlichting mechanism acting in the liquid layer (water) or TSL-mode, for short. The overall pattern of the neutral curves for the three modes described above is shown on Fig. 4.10.

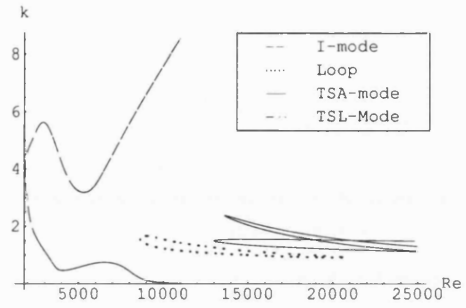


Figure 4.10: Neutral stability curves for all modes

The critical conditions for all three modes and the loop are summarised in the following table:

| Parameter | Surface waves | Loop starts | Loop ends | TSL-Mode | TSA-Mode |
|---|---|---|---|---|---|
| $Re$ | 3848.24 | 8641.96 | 20553.2 | 13767.3 | 12919.2 |
| $k$ | 1.02054 | 1.59378 | 0.936639 | 2.35807 | 1.50351 |
| $c_r$ | 0.395998 | 0.678935 | 0.448812 | 0.0288733 | 0.580395 |

Table 4.4: Critical conditions for mode coalescence study

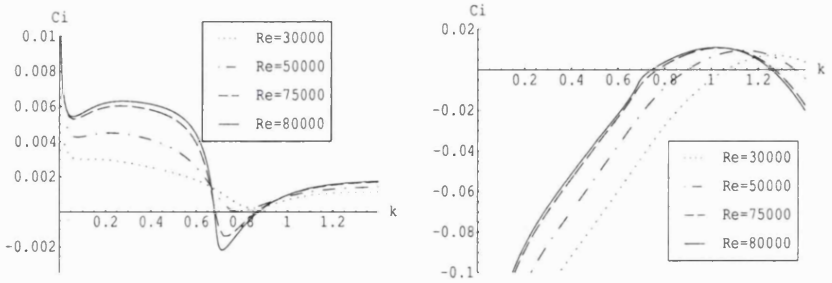


(a) I-mode (b) TSA-mode

Figure 4.11: Formation of the second stable region

At still higher Reynolds numbers, intersections between the I-mode and TSA-

mode reappear again, however accurate computations for these events become very demanding hence only a brief summary of our results will be presented here. Just before the next mode crossing, the $c_i\,(k)$ distribution for the I-mode again develops a local minimum that produces a stable region starting from $Re \sim 50450$, while the TSA-mode neutral curve is shifted towards lower wave numbers (Fig. 4.11).

The mode crossing itself occurs between $Re = 83000$ and $Re = 83400$. Afterwards the local minimum in the graph of $c_i\,(k)$ disappears and the modes become well separated:

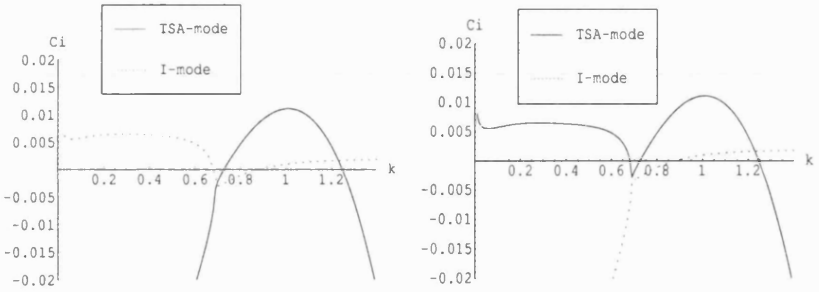


(a) Ci, Re=83000 (b) Ci, Re=83400

Figure 4.12: High Re branch exchange

In our description above, we assigned the TSA and TSL abbreviation to two distinct modes with reference to Tollmien-Schlichting instability mechanisms operational in air and in water separately. We see that in our case the Tollmien-Schlichting instability mechanism appears in distinct forms in the two media. This can probably be attributed to the large viscosity and density ratios for the two fluids involved. Nevertheless, a number of indirect observations and further parametric studies allow the modes to be linked with a particular physical mechanism.

Consider, for example, the phase speed of neutral TSA and TSL waves. In our computations above, the base flow speed at the interface is $u_{0a}(0) = 0.3076$. As follows from our computations, the phase speed for the unstable TSL-waves is lower than that at the interface and it tends to zero as $Re \to \infty$, whereas the phase speed for unstable I-waves and TSA-waves exceeds the flow speed at the interface which is in agreement with results reported Sangalli, McCready and Chang (1997).

An alternative argument helping to identify the two Tollmien-Schlichting modes can be based on the variation of the relative thickness of the liquid layer. Consider the case of decreasing water layer thickness. In the limit of a thin water film, the velocity distribution in the base channel flow approaches a parabolic Poiseuille flow profile in air and a Couette flow linear profile in water. In this limit the TSA mode should turn into the standard Tollmien-Schlichting instability in a channel filled with air. At the same time, since the Couette flow is stable to linear perturbations, one could expect some form of degeneration for the TSL-mode. In order to illustrate these considerations, we performed a set of computations for a fixed thickness of the air layer and a variable relative thickness of the liquid layer denoted as $n$ (in the computations above, $n = 1$). The base flow profile was altered accordingly. As expected, with the water layer thickness decreasing, the neutral curve for the TSA-mode approaches the neutral curve of the Tollmien-Schlichting mode in a single fluid case (Fig. 4.13-4.14).

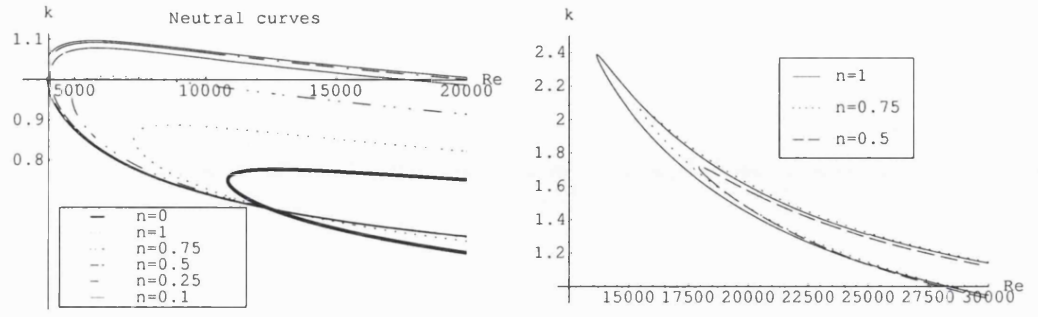


(a) TSA-mode (b) TSL-mode

Figure 4.13: TSA and TSL mode neutral curve behaviour for varying liquid layer thickness

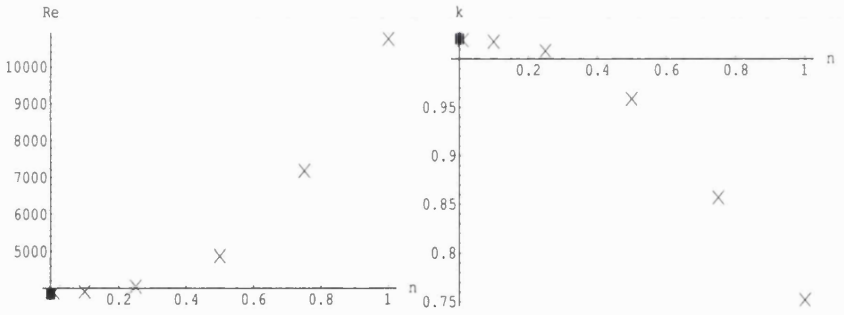


(a) Critical Reynolds (b) Critical wavenumber

Figure 4.14: TSA-mode critical parameters behaviour for varying liquid layer thickness (■ - Poiseuille flow of one fluid)

For these illustrations, the Reynolds number and wavenumber are renormalised to comply with the limit case of the Poiseuille air flow by taking the half-width of the channel as a characteristic length and the mean by profile as a characteristic velocity. The critical Reynolds number for the TSL-mode increases and tends to infinity for a film of vanishing thickness (here the characteristic length and velocity

have been renormalised to these of $n = 1$ case).

## 4.4 Conclusions

Based on the results obtained, we arrive at the following picture of the linear stability in this case. The TSL-mode was clearly identified as Tollmien-Schlichting mode by its asymptotic behaviour, since as $Re \to \infty$ the wave speed on the neutral curve tends to zero for this mode (checked to $Re \sim 10^6$). The wavespeed on the neutral curve also tends to zero and is always lower than the interface speed $O(10^{-2})$. I-Mode can be definitely attributed to the surface waves following the analysis of Blennerhassett (1980). Calculation made for the point of intersection between the lower branch of the neutral curve and the $Re$ axis were in good comparison with the results from the asymptotics of Blennerhassett (1980). The nature of the TSA-mode is clear from its asymptotic behaviour as water film thickness tends to zero. Therefore the TSA-mode can be clearly attributed to the shear mode in air and the TSL-mode - to the liquid shear mode.

The wavespeed of the neutrally stable solutions for Tollmien-Schlichting mode in air is faster than the velocity of the free boundary and this mode interacts with surface waves. The wavespeed of neutrally stable solutions for Tollmien-Schlichting mode in water is lower than the speed of the interface. That mode doesn't interact with two other modes and produces a neutral curve typical for Poiseuille-Couette flows (see, for example, Cowley and Smith (1985)) .

The interaction between the gas shear mode and interfacial mode occurs for the wavenumbers $k \in [1, 2]$ which corresponds to wavelengths of order of the channel height. The minimum initially developed by the $c_i(k)$ for the interfacial mode is located approximately at the same $k$ as the maxima of the stable gas shear mode.

Also the wave speeds of the interfacial mode and shear mode are close enough in the domain of interaction in $k$. It is possible that what we observe is in fact energy transfer from the interfacial waves to the gas shear mode, which takes place for the disturbances of $O(1)$ wavelengths. This leads to the excitation of the stable gas shear mode and stabilisation of the unstable interfacial mode. Apparently the conditions that allow for this energy transfer to take place can be periodical in $Re$ as the interaction and branch exchange is repeated at higher Reynolds numbers. Therefore it is possible that the stabilisation of the interfacial waves can be attributed to the interaction between interfacial and shear mechanisms of instability and energy transfer across the spectrum of the interfacial waves rather then the interaction between different parts of the interfacial instability spectrum alone (as suggested byKuru, Sangalli, Uphold and McCready (1993)).

Another example of the observed interaction between gas shear and interfacial modes can be found in the results obtained by Timoshin and Hooper (2000), which demonstrated that Tollmien-Schlichting mode and interfacial waves mode can have points of coalescence. The results presented in this chapter extend these observation to the case of channel flows. We can also note that the effect of interfacial waves stabilisation has been observed by different authors for a wide variety of problems, which suggests that it possesses certain structural stability.

# 5 Ice formation in Poiseuille channel flow

In this section we consider a linear stability problem for a 2D plane channel Poiseuille flow of air over water with ice layer located beneath the water layer. We are using the same coordinate system as in the previous chapter. The scheme of the flow configuration is shown below:

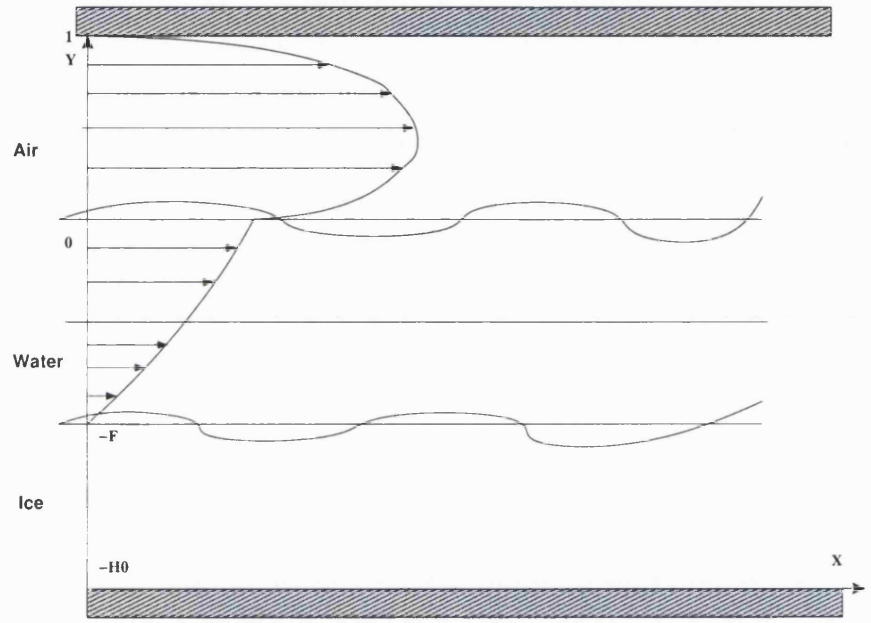


Figure 5.1: Channel flow scheme

Here $F$ denotes the initial thickness of the water film and $H_0 - F$ gives the initial thickness of the ice layer.

## 5.1 Formulation of the linear stability problem

In order to be able to compare results for instability calculations for the flow between fixed solid boundaries and the flow over an ice layer, the formulation

given by equations **(4.3)-(4.5)** of the previous chapter will be adapted to include the air flow in both the base state and the disturbances. As in Chapter 4, the air layer thickness is used as a reference length and integral mean velocity as characteristic velocity. Then, assuming a linear temperature profile in the base state, the linear stability formulation takes the following form:

At the upper wall ($y = 1$):

$$\begin{cases} T_a = 0 \\ v_a = 0 \\ \frac{dv_a}{dy} = 0 \end{cases} \tag{5.1}$$

In air:

$$\begin{cases} \frac{d^4 v_a}{dy^4} + (-2k^2 + ikRe(c - u_{0a}))\frac{d^2 v_a}{dy^2} + \\ \left(k^4 + ik^3 Re(u_{0a} - c) + ikRe\frac{d^2 u_{0a}}{dy^2}\right) v_a = 0 \\ \frac{d^2 T_a}{dy^2} + (-k^2 + ikRePr(c - u_{0a}))\, T_a - RePr\frac{dT_{0a}}{dy} v_a = 0 \end{cases} \tag{5.2}$$

At the air/water interface ($y = 0$):

$$\begin{cases} v_a = v_l \\ \frac{dv_a}{dy} - \frac{v_l}{u_{0a}-c}\frac{du_{0a}}{dy} = \frac{dv_l}{dy} - \frac{v_l}{u_{0a}-c}\frac{du_{0l}}{dy} \\ \frac{d^2 v_a}{dy^2} + k^2 v_a = \mu_{la}\left(\frac{d^2 v_l}{dy^2} + k^2 v_l\right) \\ \frac{d^3 v_a}{dy^3} - \mu_{la}\frac{d^3 v_l}{dy^3} - 3k^2\frac{dv_a}{dy} + 3\mu_{la}k^2\frac{dv_l}{dy} + ikRe(c - u_{0a})\frac{dv_a}{dy} - \\ ikRe\rho_{la}(c - u_{0a})\frac{dv_l}{dy} + ikRev_a\frac{du_{0a}}{dy} - ikRe\rho_{la}v_l\frac{du_{0l}}{dy} = \\ \frac{ikv_aRe}{(u_{0a}-c)}\left(\frac{1}{We}k^2\rho_{la} + Fr(\rho_{la} - 1)\right) \\ T_a - \frac{iv_a}{k(u_{0a}-c)}\frac{dT_{0a}}{dy} = T_l - \frac{iv_a}{k(u_{0a}-c)}\frac{dT_{0l}}{dy} \\ \frac{dT_a}{dy} = \lambda_{la}\frac{dT_l}{dy} \end{cases} \tag{5.3}$$

In water:

$$\begin{cases} \frac{d^4v_l}{dy^4} + (-2k^2 + ikRe\nu_{al}(c - u_{0l}))\frac{d^2v_l}{dy^2} + \\ \left(k^4 + ik^3Re\nu_{al}(u_{0l} - c) + ikRe\nu_{al}\frac{d^2u_{0l}}{dy^2}\right)v_l = 0 \\ \frac{d^2T_l}{dy^2} + (-k^2 + ikRePr\chi_{al}(c - u_{0a}))T_l - RePr\chi_{al}\frac{dT_{0a}}{dy}v_l = 0 \end{cases} \tag{5.4}$$

At the ice surface ($y = -F$):

$$\begin{cases} \frac{dv_l}{dy} + \frac{v_l}{\Theta_{il}c}\frac{du_{0l}}{dy} = 0 \\ T_l + \frac{iv_l}{\Theta_{il}kc}\frac{dT_{0l}}{dy} = 0 \\ \frac{dT_l}{dy} - \lambda_{il}\frac{dT_i}{dy} = -\frac{\chi_{al}PrRe}{St}v_l \end{cases} \tag{5.5}$$

Here as in the previous chapter, $v_a$ and $v_l$ represent the $y$-dependent amplitude function for the vertical disturbance velocity written as a travelling wave with the real wavenumber $k$ and the complex phase speed $c$. The formulation above consists of the no-slip and constant air temperature conditions at the upper channel wall **(5.1)**, Orr-Sommerfeld equations for the temperature and velocity disturbances in the air layer **(5.2)**, the velocity, temperature, stress and heat flux continuity at the air/water interface **(5.3)**, Orr-Sommerfeld equations for the temperature and velocity disturbances in the water layer **(5.4)** and tangential velocity, temperature and Stefan conditions at the ice boundary **(5.5)**. The perturbations of the ice surface and free-surface were eliminated from these equations using kinematic conditions on the corresponding boundaries.

The temperature disturbance in the ice layer is governed by the boundary-value problem **(5.6)**.

$$\begin{cases} \frac{d^2T_i}{dy^2} + \omega_i^2 T_i = 0 \\ T_i(-H_0) = 0 \\ T_i(-F) = -\frac{iv_l(-F)}{\Theta_{il}kc}\frac{dT_{0i}}{dy} \end{cases} \tag{5.6}$$

Where $\omega_i^2 = -k^2 + ikcRePr\chi_{ai}$. As in the boundary-value problem **(3.123)** in Chapter 3, the constant temperature conditions at the wall and ice surface are used. The solution to the boundary-value problem **(5.6)** can be written as:

$$T_i(y) = -\frac{iv_l(-F)}{\Theta_{il}kc}\frac{dT_{0i}}{dy}\frac{\sinh(i\omega_i(H_0+Y))}{\sinh(i\omega_i(H_0-F))} \tag{5.7}$$

Therefore, the heat flux at the ice/water boundary from the ice side (divided by $\lambda_i$) can be written as:

$$\begin{gathered} \lambda_{il}\frac{dT_i}{dy}(-F) = \lambda_{il}\frac{v_l(-F)\omega_i}{\Theta_{il}kc}\frac{dT_{0i}}{dy}\frac{\cosh(i\omega_i(H_0-F))}{\sinh(i\omega_i(H_0-F))} = \\ \lambda_{il}\frac{v_l(-F)\omega_i}{\Theta_{il}kc}\frac{dT_{0i}}{dy}\coth(i\omega_i(H_0-F)) \end{gathered} \tag{5.8}$$

This shows that the Stefan condition given by the last equation in **(5.5)** can be written as a relationship between the normal velocity disturbance and the gradient of temperature disturbances in the liquid phase, evaluated at the unperturbed ice surface $y = -F$:

$$\frac{dT_l}{dy}(-F) = v_l(-F)\left(\lambda_{il}\frac{\omega_i}{\Theta_{il}kc}\frac{dT_{0i}}{dy}\coth(i\omega_i(H_0-F)) - \frac{\chi_{al}PrRe}{St}\right) \tag{5.9}$$

The base-flow profile for velocities can be written in the following form:

$$\begin{aligned} u_{0a} &= (1 + b_a y + a_a y^2)\,\tfrac{1}{d}, \qquad 0 \le y \le 1 \\ u_{0l} &= (1 + b_l y + a_l y^2)\,\tfrac{1}{d}, \qquad -F \le y \le 0 \end{aligned} \tag{5.10}$$

for the flow in the air and liquid layers respectively. Here, the constant parameters are given by:

$$\begin{aligned} b_a &= \tfrac{\mu_{la}-F^2}{F(1+F)},\ a_a = -\tfrac{\mu_{la}+F}{F(1+F)}, \\ b_l &= \tfrac{1}{\mu_{la}}\tfrac{\mu_{la}-F^2}{F(1+F)},\ a_l = -\tfrac{1}{\mu_{la}}\tfrac{\mu_{la}+F}{F(1+F)}, \\ d &= \tfrac{F^4+4F^3\mu_{la}+6F^2\mu_{la}+4F\mu_{la}+\mu_{la}^2}{6F(1+F)^2\mu_{la}} \end{aligned} \tag{5.11}$$

in terms of the viscosity ratio $\mu_{la}$ and the relative thickness of the unperturbed water layer $F$. In the unperturbed state, the distributions of temperature in terms of the temperature at the air/water interface $T_{la}$ and initial coordinates of the water/ice boundary and lower wall are given by the following expressions:

$$\begin{aligned} T_{0a} &= (1 - T_{la})\,y + T_{la} \qquad 0 \le y \le 1 \\ T_{0l} &= \tfrac{T_{la}}{F}\,y + T_{la} \qquad -F \le y \le 0 \\ T_{0i} &= \tfrac{y+F}{F-H_0} Tw \qquad -H_0 \le y \le -F \end{aligned} \tag{5.12}$$

From the heat balance in the unperturbed state, on the air/water boundary, it follows that $T_{la} = \frac{F}{\lambda_{la}+F}$. Also from the heat balance in the unperturbed state on the water/ice boundary, it follows that $H_0 = F - \lambda_{il} Tw(\lambda_{la} + F)$. Recall, that $\lambda_{ia} = \frac{\lambda_i}{\lambda_a}$ and $\lambda_{la} = \frac{\lambda_l}{\lambda_a}$ represent the ice/air and water/air ratios of thermal conductivities.

## 5.2 Numerical approach for the Orr-Sommerfeld formulation

The numerical scheme that is used for the solution of the problem **(5.1)-(5.5)** is a straightforward extension of the method applied the problem without ice in the previous chapter (Chapter 4). The only difference from the previous chapter is the addition of temperature equations and boundary conditions which is done in the same manner as for the free-surface flows (Chapter 3), therefore we will not give a detailed account of the difference equations and solution method in the present section to avoid repeating the same information.

## 5.3 Longwave asymptotic solution

Consider longwave asymptotics for this problem in the same manner as we did for the free surface flows. The structure of disturbances with small wave number $k$ can be examined following the procedure outlined in Chapter 3 for the liquid-layer flow. The linear stability problem for the two-fluid flows has been investigated earlier by Yih (1967) (Couette-Poiseuille flows of the same density and thickness), by Blennerhassett (1980) (Poiseuille flow of water over air) and by Yantsios and Higgins (1988) ( flows with various values of viscosity ratio $\mu_{la}$ and density ratio $\rho_{la}$). For these problems it was generally necessary to consider both $O(k)$ and $O(1)$ approximations for the disturbance of the streamfunction as the $O(1)$ solution gave one neutrally-stable mode.

In our case, the coefficient in the Stefan condition **(5.9)** linking the perturbation of the ice surface to the temperature field disturbance is given by $\frac{\chi_{al} \cdot Pr \cdot Re}{St} k$. In order to keep the interaction between the disturbances of temperature and velocity

fields within the 1st order of longwave asymptotics, we will assume that $a = \frac{\chi_{al} \cdot Pr \cdot Re}{St} k \sim 1$. Let us analyse the domain where this assumption can be valid. The $O(1)$ longwave asymptotics requires that and $Rek \ll 1$. However, since the other part of coefficient $\frac{\chi_{al} \cdot Pr}{St}$ is relatively large ($\sim 1656$ for water/air/ice) we can assume that there is a domain where $k \ll 1$, $Rek \ll 1$ but $\frac{\chi_{al} \cdot Pr \cdot Re}{St} k \sim 1$ and the interaction of the ice layer with the flow is within $O(1)$ of longwave asymptotics.

It is convenient to rewrite the problem **(5.1)-(5.6)** in terms of the disturbance streamfunction $\psi$. Let us consider the following expansion as $k \to 0$ (here we use the superscript $\Sigma$ to denote the sums of the series):

$$\begin{cases} \psi_l^\Sigma \sim \psi_l + k\psi_l^1 + ... \\ T_l^\Sigma \sim T_l + kT_l^1 + ... \\ \psi_a^\Sigma \sim \psi_a + k\psi_a^1 + ... \\ T_a^\Sigma \sim T_a + kT_a^1 + ... \\ c^\Sigma \sim c + kc^1 + ... \end{cases} \tag{5.13}$$

Then, as $\psi = i\frac{v}{k}$, the equations and boundary conditions in terms of the disturbances of streamfunction and temperature become (at $O(1)$).

$$\begin{cases} \frac{d\psi_a}{dy} = 0 \\ \psi_a = 0 \quad (y = 1) \\ T_a = 0 \end{cases} \tag{5.14}$$

$$\begin{cases} \frac{d^4\psi_a}{dy^4} = 0 \\ \frac{d^2T_a}{dy^2} = 0 \end{cases} \quad (air) \tag{5.15}$$

$$\begin{cases} \psi_a = \psi_l \\ \frac{d\psi_a}{dy} - \frac{\psi_a}{u_{0a}-c}\frac{du_{0a}}{dy} = \frac{d\psi_l}{dy} - \frac{\psi_l}{u_{0a}-c}\frac{du_{0l}}{dy} \\ \frac{d^2\psi_a}{dy^2} = \mu_{la}\frac{d^2\psi_l}{dy^2} \\ \frac{d^3\psi_a}{dy^3} = \mu_{la}\frac{d^3\psi_l}{dy^3} \\ T_a - \frac{\psi_a}{(u_{0a}-c)}\frac{dT_{0a}}{dy} = T_l - \frac{\psi_a}{(u_{0a}-c)}\frac{dT_{0l}}{dy} \\ \frac{dT_a}{dy} = \lambda_{la}\frac{dT_l}{dy} \end{cases} \quad (y=0) \tag{5.16}$$

$$\begin{cases} \frac{d^4\psi_l}{dy^4} = 0 \\ \frac{d^2T_l}{dy^2} = 0 \end{cases} \quad (water) \tag{5.17}$$

$$\begin{cases} \frac{d\psi_l}{dy} + \frac{\psi_l}{\Theta_{il}c}\frac{du_{0l}}{dy} = 0 \\ T_l + \frac{\psi_l}{\Theta_{il}c}\frac{dT_{0l}}{dy} = 0 \\ \frac{dT_l}{dy} - \lambda_{il}\frac{dT_i}{dy} = ia\psi_l \end{cases} \quad (y=-F) \tag{5.18}$$

The boundary-value problem for the disturbance of the ice temperature $T_i$ in the longwave limit is given by:

$$\begin{cases} \frac{d^2T_i}{dy^2} = 0 \\ T_i(-H_0) = 0 \\ T_i(-F) = -\frac{\psi_l(-F)}{\Theta_{il}c}\frac{dT_{0i}}{dy} \end{cases} \tag{5.19}$$

The solution of the above problem can be written as:

$$T_i(y) = -\frac{\psi_l(-F)}{\Theta_{il}c}\frac{dT_{0i}}{dy}\frac{H_0+Y}{H_0-F} \tag{5.20}$$

From the expression for the unperturbed temperature in the ice layer **(5.12)**, it follows that, $\frac{dT_{0i}}{dy} = \frac{Tw}{F-H_0} = \frac{\lambda_{ai}}{(1+\lambda_{al}F)}$. Therefore, the Stefan condition for temper-

ature at the ice boundary ($y = -F$) can be written as:

$$\begin{array}{c} \frac{dT_l}{dy} = -\lambda_{il}\frac{\psi_l}{\Theta_{il}c}\frac{dT_{0i}}{dy}\frac{1}{H_0-F} + ia\psi_l = \\ \psi_l\left(-\frac{1}{\Theta_{il}c}\frac{\lambda_{al}}{(1+\lambda_{al}F)}\frac{1}{(H_0-F)} + ia\right) \end{array} \tag{5.21}$$

The general solution of the equations **(5.15)** and **(5.17)** is given by:

$$\begin{cases} \psi_{a,l} = C_{3a,l}y^3 + C_{2a,l}y^2 + C_{1a,l}y + C_{0a,l} \\ T_{a,l} = C_{5a,l}y + C_{4a,l} \end{cases} \tag{5.22}$$

Here $C_{ia,l}$ $(i = 0..5)$ are arbitrary constants that we have to determine from the boundary conditions. Boundary conditions on the upper boundary of the air layer **(5.14)** lead to the following system:

$$\begin{cases} C_{5a} + C_{4a} = 0 \\ C_{3a} + C_{2a} + C_{1a} + C_{0a} = 0 \\ 3C_{3a} + 2C_{2a} + C_{1a} = 0 \end{cases} \tag{5.23}$$

Conditions at the air/water interface **(5.16)** yield:

$$\begin{cases} C_{0a} - C_{0l} = 0 \\ C_{1a} - \frac{1}{u_{0a}-c}\frac{du_{0a}}{dy}C_{0a} - C_{1l} + \frac{1}{u_{0a}-c}\frac{du_{0l}}{dy}C_{0l} = 0 \\ C_{2a} - \mu_{la}C_{2l} = 0 \\ C_{3a} - \mu_{la}C_{3l} = 0 \\ C_{4a} - \frac{1}{(u_{0a}-c)}\frac{dT_{0a}}{dy}C_{0a} - C_{4l} + \frac{1}{(u_{0a}-c)}\frac{dT_{0l}}{dy}C_{0l} = 0 \\ C_{5a} - \lambda_{la}C_{5l} = 0 \end{cases} \tag{5.24}$$

Finally, from the conditions on the ice surface **(5.18)** we obtain the following system:

$$\begin{cases} 3C_{3l}F^2 - 2FC_{2l} + C_{1l} + \frac{1}{\Theta_{il}c}\frac{du_{0l}}{dy}\left(-C_{3l}F^3 + C_{2l}F^2 - FC_{1l} + C_{0l}\right) = 0 \\ -FC_{5l} + C_{4l} + \frac{1}{\Theta_{il}c}\frac{dT_{0l}}{dy}\left(-C_{3l}F^3 + C_{2l}F^2 - FC_{1l} + C_{0l}\right) = 0 \\ \frac{1}{\left(-\lambda_{il}\frac{1}{\Theta_{il}c}\frac{dT_{0i}}{dy}\frac{1}{H_0-F}+ia\right)}C_{5l} + C_{3l}F^3 - C_{2l}F^2 + FC_{1l} - C_{0l} = 0 \end{cases} \tag{5.25}$$

The temperature flux balance for the base-flow solution **(5.12)** leads to the following expressions for the temperature derivatives that we will need in order to solve the system **(5.23)-(5.25)**:

$$\frac{dT_{0a}}{dy}(0) = \frac{dT_{0l}}{dy}(0)\lambda_{la} = (1 - T_{la}) = \frac{\lambda_{la}}{\lambda_{la} + F} \tag{5.26}$$

$$\begin{gathered} \frac{dT_{0l}}{dy}(-F) = \lambda_{il}\frac{dT_{0i}}{dy}(-F) = \lambda_{il}\frac{Tw}{F-H_0} = \\ \lambda_{il}\lambda_{ai}\frac{1}{1+\lambda_{al}F} = \frac{\lambda_{al}}{1+\lambda_{al}F} = \frac{1}{\lambda_{la}+F} \end{gathered} \tag{5.27}$$

The system of equations **(5.23)-(5.25)** can be written in the matrix form $A \cdot X = 0$ where $X = (C_{ia,l})$ $i = 0..5$. Since the system is homogeneous, the solvability requirement can be expressed as $det(A) = f(c, F, H_0, a) = 0$, which results in the following quadratic equation for the complex phase speed of the disturbances:

$$A_2c^2 + A_1c + A_0 = 0 \tag{5.28}$$

Where the coefficients $A_{0-2}$ are given by the following expressions:

$$A_0 = 6iF(1+F)(1+H_0)(F+\lambda_{la})\mu_{la}(F(2+F)+\mu_{la})(F^2+\mu_{la}+2F\mu_{la}) \quad (5.29)$$

$$\begin{gathered}
A_1 = -i(H_0+\lambda_{la})(F^4+2F(3+2F)\mu_{la}+\mu_{la}^2)^2+ \\
(H_0-F)\mu_{la}(F^4(F(4i+3F(i+2a(1+F)^2(2+F)))+ \\
F(12a(1+F)^2(2+F)-i(4+3F))\lambda_{la}+6a(1+F)^2(2+F)\lambda_{la}^2)+ \\
F^2(F(36i+F(i(35+12F)+12a(1+F)^2(1+F(3+F))))-16i(\lambda_{la}-1)+ \\
F(24a(1+F^2)(1+F(3+F))-i(36+F(35+12F)))\lambda_{la}+ \\
12a(1+F)^2(1+F(3+F))\lambda_{la}^2)\mu_{la}+ \\
F(F(9i+2F(2i+3a(1+F)^2(1+2F)))-8i(\lambda_{la}-1)+ \\
F(12a(1+F)^2(1+2F)-i(9+4F))\lambda_{la}+ \\
6a(1+F^2)(1+2F)\lambda_{la}^2)\mu_{la}^2-i(\lambda_{la}-1)\mu_{la}^3)\Theta_{il}
\end{gathered} \quad (5.30)$$

$$A_2 = a\Theta_{il}(\lambda_{la}+F)^2(F-H_0)(F^4+2F(2+F(3+2F))\mu_{la}+\mu_{la}^2)^2 \quad (5.31)$$

The most compact form of the coefficients **(5.29)-(5.31)** was obtained with Mathematica symbolic engine. As in the free-surface problem, we will refer to longwave asymptotics roots as $c_+$ and $c_-$:

$$c_{+,-} = \frac{-A_1 \pm \sqrt{A_1^2 - 4A_0A_2}}{2A_2} \quad (5.32)$$

When $\lambda_{la} = 1$ and $a = 0$, the temperature field has no influence on the flow. And our expression for the complex phase speed can be compared against the expression obtained by Yantsios and Higgins (1988) for the complex phase speed in two-fluid flow without ice. If we use the same base flow normalisation as used by Yantsios and Higgins (1988), the expression **(5.32)** becomes:

$$c_+ = c_- = 1 + \frac{2(\mu_{la} - F^2)(\mu_{la} - 1)(F^3 + F^2)}{(F^2 + F)(F^4 + 4F^3\mu_{la} + 6F^2\mu_{la} + 4\mu_{la}F + \mu_{la}^2)} \tag{5.33}$$

which is the same expression as the $O(1)$ phase speed derived by Yantsios and Higgins (1988).

## 5.4 The behaviour of longwave asymptotic modes

In our analysis of the behaviour of the longwave asymptotic modes we will use fixed media properties given in the Table 2.1 of the Chapter 2. Also in order to reduce the number of free parameters in the problem we will consider water and air layers of equal thickness ($F = 1$), then $c_{+,-}$ depend only on $a$ and $H_0$. Analysing the expressions for the roots analytically proves to be a difficult task because of the complex algebraic form of the coefficients **(5.29)-(5.31)**. However, graphical analysis shows that in the domain of the validity of our asymptotic analysis ($a \sim 1$) one of the roots is unstable and another one is stable.

The dependence of longwave roots on $a$ for the air/water/ice media properties is illustrated on Fig. 5.2-5.3 for different values of $H_0$.

The dependence of longwave roots on $H_0$ for the air/water/ice media properties is illustrated on Fig. 5.4-5.5 for different values of $a$.

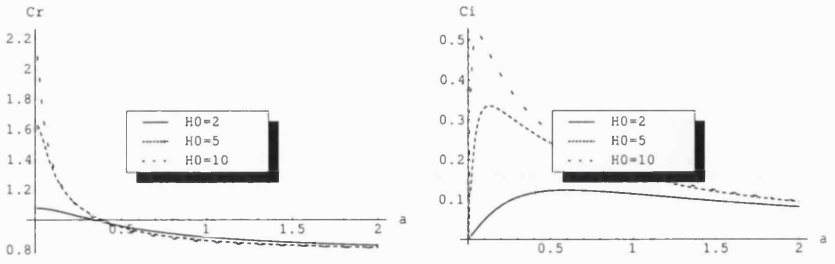


(a) Cr for mode C- (b) Ci for mode C-

Figure 5.2: Complex phase speed $c_-$ as a function of $a$

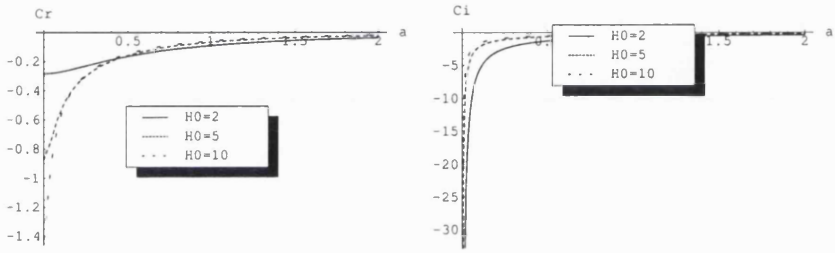


(a) Cr for mode C+ (b) Cr for mode C+

Figure 5.3: Complex phase speed $c_+$ as a function of $a$

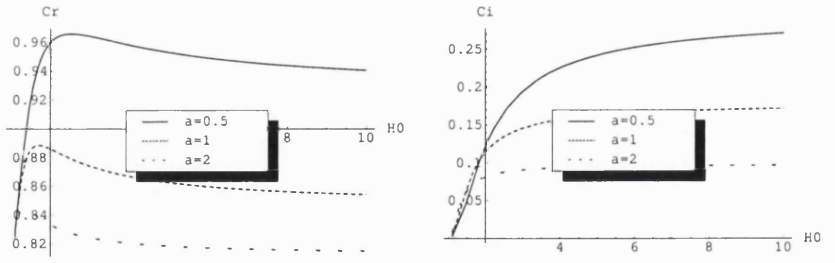


(a) Cr for mode C- (b) Ci for mode C-

Figure 5.4: Complex phase speed $c_-$ as a function of $H_0$

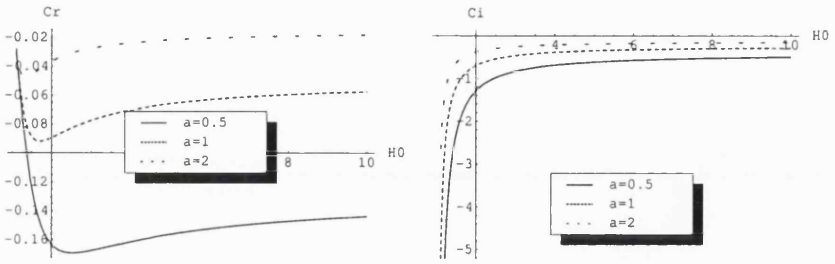


(a) Cr for mode C+ (b) Ci for mode C+

Figure 5.5: Complex phase speed $c_+$ as a function of $H_0$

Figures 5.2-5.5 show that the $c_-$ root of the longwave asymptotics appears to be unstable and the disturbances corresponding to this root propagate downstream while $c_+$ root appears to be stable and the disturbances corresponding to this root propagate upstream. The increase of the initial ice height (which corresponds to the increase of $H_0$) destabilises the unstable root. As in the case of free -surface flow, one of the longwave asymptotic roots, namely $c_-$, appears to correspond to the interfacial mode of the linear stability problem. The plots on Fig. 5.6 show the comparison between $c_-$ root of the longwave asymptotics and the interfacial mode (I-Mode) as a function of wavenumber $k$ for $Re = 10000$.

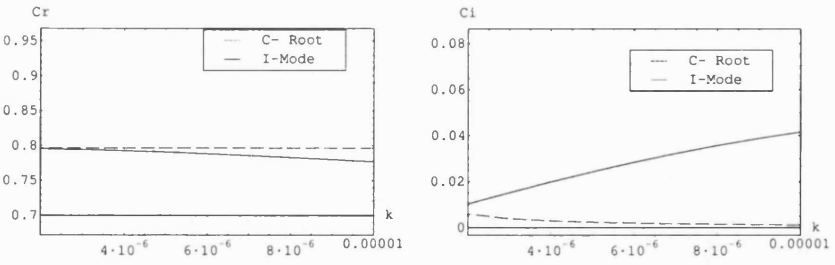


(a) Ci (b) Cr

Figure 5.6: Comparison between the interfacial mode and $c_-$ longwave mode

The $c_-$ longwave mode and the interfacial mode demonstrate similar behaviour, however the comparison between the longwave root and the surface mode is not as good as in the case of free-surface flow (see section "3.2.3 Longwave asymptotics for the linear stability problem").

Also our computations show that unlike in the free-surface case, there is no significant influence of the ice layer on the interfacial and shear mode for the channel flow and we have not found a domain where the new $c_+$ root becomes unstable.

## 5.5 Conclusions

In this chapter we have derived longwave asymptotics for the ice growth problem in the air/water/ice Poiseuille flow. The analytic expression for the longwave roots has been obtained. One root has been identified as the interfacial mode, and another root corresponds to the new mode which is introduced by the ice layer.

Also we have solved linear stability problem for this flow numerically. However, from our computations it follows that the ice layer does not affect interfacial instability significantly even in the longwave limit and the new mode does not become unstable. However the behaviour of the new mode should be a subject of further research.

# 6 Conclusions

In the end of this thesis, we would like summarise interesting results obtained in chapters 2-5.

In the second chapter, we obtained estimates for the Strouhal number of the problems of ice growth under water film, demonstrating analytically that the ice growth can be considered as quasi-steady with respect to the water flow in the experimental configurations of interest. We have also derived the existence criteria for steady $x$-independent solutions, solved $x$-independent unsteady problem numerically and in this simple model demonstrated the dependency of the time necessary to approach steady state on the Stefan number.

In the third chapter, we have developed new Froude number based double-deck theory for the boundary-layer scaled free-surface flows and used it to discover a new mode of upstream propagating instability arising because of the presence of the ice layer. We have obtained linear analytic 3D solution for $Pr = 1$, numeric solution in general linear stability problem and numeric solution of nonlinear problem. We have shown that the analytic solution we have obtained is applicable in case where $Pr \neq 1$, provided time is rescaled accordingly, thus we have demonstrated that in the linear problem the thermal boundary layer thickness affects the speed of disturbances propagation but has no significant impact on the shape of disturbances. For the linear stability equations, we have developed a novel $4^{th}$ order finite-differences scheme and for the nonlinear double-deck equations - a novel global-marching type scheme. We have discovered that the flow can become unstable to 3D perturbations before it becomes unstable to 2D perturbations for certain values of the initial ice thickness. Also we have analysed the effect of nonlinearity in this problem and provided an explanation of the physical mechanism

of upstream propagation observed. Also, in the third chapter of this thesis we considered the linear stability problem for a half-Poiseuille flow down an inclined plane covered with an ice layer when the film thickness is $O(1)$. We derived longwave asymptotics for the resulting Orr-Sommerfeld problem and demonstrated that instead of one mode given by longwave asymptotic solution for this problem without ice layer (Yih (1963)), two modes are obtained when an ice layer is present. Then, we solved the full Orr-Sommerfeld problem numerically, discovered the ice instability mode in this problem formulation using the double-deck solution as an initial guess, and investigated the behaviour of this new instability mode in a wide range of problem parameters. Also, in this chapter we matched the modes obtained from the longwave asymptotic analysis with the modes obtained from the numerical solution of the linear stability problem and identified the longwave modes $c_+$ and $c_-$ as ice and surface modes of the Orr-Sommerfeld problem respectively. Another important finding was the effect of longwave stabilisation of the surface mode in presence of an ice layer. We demonstrated that the presence of an ice layer can either increase or decrease the critical Reynolds number of the surface mode depending on the value of the angle of incline.

In the forth chapter, we have analysed the well-known problem of 2-fluid plane Poiseuille flow for air/water configuration and discovered the effect of intersection and branch exchange between the interfacial mode and the air shear mode. We have found that this effect is responsible for the stabilisation of disturbances with $O(1)$ wave numbers in a broad range of Reynolds numbers. We have also noted that the mode identity changes because of the intersection, suggested methods to establish mode identity in this case and built a clear picture of the behaviour of the three instability modes present in this problem.

Finally in the fifth chapter we have analysed the longwave stability of the ice layer under a water film in a 2-fluid plane Poiseuille flow of air over water. Unlike the case with no ice layer, where the $O(1)$ approximation yields one neutrally stable root, we have shown that in our case $O(1)$ approximation produces two roots. One of this roots is unstable and corresponds to the interfacial mode in the longwave limit, and the other root is stable and corresponds to a new mode. Unlike the free-surface case, this new mode appears to be stable in the range of parameters we have considered.

# 7 Appendix

## 7.1 Appendix A: Water/ice boundary conditions

**Kinematic condition** Assume the ice surface in some stationary Cartesian coordinate system is given by the following implicit function:

$$H(\overrightarrow{r} = (x, y, z), t) = 0$$

This form remains valid even if this surface cannot be represented as an analytic function of two coordinates in the chosen coordinate system. Let us assume that some set of characteristic values was used in order to obtain dimensionless variables.

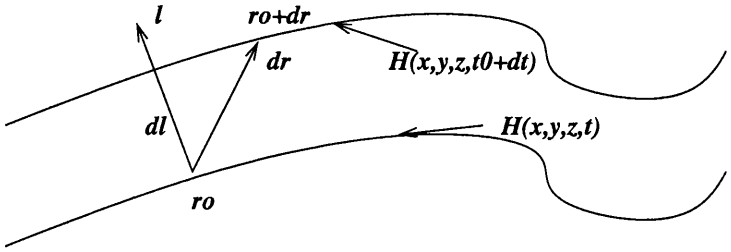


Figure 7.1: Surface evolution scheme

Consider a surface element $\overrightarrow{dS}$ at some point $\overrightarrow{r_0} = (x_0, y_0, z_0)$ at some moment of time $t_0$, and let $\overrightarrow{l} \| \nabla H$. Now the mass flux on that surface element at $t_0$ is: $\rho_l \cdot \overrightarrow{V_l} \cdot \overrightarrow{dS}$, where $\rho_l$ is density and $\overrightarrow{V_l}$ is the velocity of liquid phase at the interface. Thus the mass gained or lost through this surface element in time $dt$ is:

$$\rho_l \cdot \overrightarrow{V_l} \cdot \overrightarrow{dS} \cdot dt \tag{7.1}$$

This mass changes the shape of the surface. Let $dl$ be the distance between the surface position at $t_0$ and $t_0 + dt$ , measured along the normal to the ice surface at $(\vec{r_0}, t_0)$. The mass change due to the change of the surface shape is:

$$(\rho_l - \rho_i) \cdot dS \cdot dl \tag{7.2}$$

Therefore:

$$\rho_l \cdot \vec{V} \cdot \vec{dS} \cdot dt = (\rho_l - \rho_i) \cdot dS \cdot dl \tag{7.3}$$

or using the ice surface equation:

$$\rho_l \cdot \vec{V} \cdot \frac{\nabla H}{|\nabla H|} \cdot dS \cdot dt = (\rho_l - \rho_i) \cdot dS \cdot dl \tag{7.4}$$

When $\vec{dr} \to 0$ :

$$dl \to \vec{dr} \cdot \frac{\nabla H}{|\nabla H|} \tag{7.5}$$

Let $\vec{r_0} + \vec{dr}$ belong to the ice surface at $t_0 + dt$ , then:

$$H(\vec{r_0} + \vec{dr}, t_0 + dt) = H(\vec{r_0}, t_0) + \frac{\partial H}{\partial t} dt + \nabla H \cdot \vec{dr} + O(dr^2) + O(dt^2) \tag{7.6}$$

Hence as the point $(\vec{r_0}, t_0)$ belongs to the ice surface, in 1st order we obtain:

$$\nabla H \cdot \vec{dr} = -\frac{\partial H}{\partial t} dt \tag{7.7}$$

Substituting **(7.7)** into **(7.5)** and using the resulting expression for $dl$ in the mass balance equation **(7.4)**, we obtain the kinematic condition at the water/ice interface in the following form:

$$\vec{V_l} \cdot \nabla H = -\Theta_{il} \cdot \frac{\partial H}{\partial t} \tag{7.8}$$

Here $\Theta_{il} = 1 - \frac{\rho_i}{\rho_l} \sim 0.0797$ for ice/water near $0^oC$. Note that the kinematic condition expressed in this form will hold in all points of the ice surface, where $\nabla H$ exists.

**Stefan condition** The difference of the heat flux on the ice surface provides the energy for the phase change. In dimensional variables, the energy condition (Stefan condition) can be written as follows:

$$\lambda_i^* \frac{\partial T_i^*}{\partial \vec{n^*}} - \lambda_l^* \frac{\partial T_l^*}{\partial \vec{n^*}} = V_{ln}^* \cdot \rho_l^* \cdot H_{li} \tag{7.9}$$

Here $H_{li}$ is the latent heat. In general case, the Stefan condition cannot be applied in the form specified above to solidification/melting problems with density change. In these cases enthalpy conservation which yields the above expression does not correspond to the total energy conservation because of the volume change effect. However the ratio of the volume-change correction to the first order in the above expression (see for example Alexiades and Solomon (1993)) is in our case of order $\frac{V_{ln}^{*2}}{2H_{li}} \left(1 - \frac{\rho_i^*}{\rho_l^*}\right)^2 \sim 10^{-5} V_{ln}^{*2}$. Therefore it seems possible to neglect it bearing in mind that the correction term is negative and by dropping it we expect to underestimate the position of the ice/water interface (Alexiades and Drake (1992)).

Dividing the equation **(7.9)** by $\lambda_l^* \frac{DT}{L^*}$ we obtain:

$$\lambda_{il}\frac{\partial T_i}{\partial \vec{n}} - \frac{\partial T_l}{\partial \vec{n}} = \frac{U^* \cdot L^* \cdot H_{li} \cdot \rho_l^*}{\lambda_l^* \cdot DT}\frac{\overrightarrow{V_l} \cdot \nabla H}{|\nabla H|} = \tag{7.10}$$

$$\frac{H_{li}}{DT}\frac{1}{\lambda_l^*}\frac{\mu_a^* \cdot \rho_l^*}{\rho_a^*}\frac{\chi_a^*}{\chi_a^*}\frac{U^* \cdot L^* \cdot \rho_a^*}{\mu_a^*}\frac{\overrightarrow{V_l} \cdot \nabla H}{|\nabla H|} = \quad (\lambda = \rho C p \chi)$$

$$= \frac{\chi_{al} \cdot Pr \cdot Re}{St}\frac{\overrightarrow{V_l} \cdot \nabla H}{|\nabla H|}$$

Which gives us Stefan condition in the following form:

$$\lambda_{il}\frac{\partial T_i}{\partial \vec{n}} - \frac{\partial T_l}{\partial \vec{n}} = \frac{\chi_{al} \cdot Pr \cdot Re}{St}\frac{\overrightarrow{V_l} \cdot \nabla H}{|\nabla H|} \tag{7.11}$$

Here we used liquid specific heat based definition of the Stefan number in order to simplify the expression.

**Gibbs-Thomson effect** Temperature on the ice surface can be influenced by surface curvature (Gibbs-Thomson effect). Let $T_{fm}^*$ be the normal freezing temperature then, for the case when solid and liquid phases possess the same specific heats and densities, (see for example Alexiades and Solomon (1993) or Batchelor, Mofatt and Worster (2000)) the local freezing temperature can be written as $T_f^* = T_{fm}^* - \Gamma\kappa$, where $\kappa$ is the ice surface curvature and $\Gamma = \frac{T_{mf}^* \cdot \sigma_i^*}{\rho_i^* \cdot H_{li}}$.

Taking typical parameter values for ice - $T_{fm}^* = 273K$, $\sigma_i^* = 0.022\frac{N}{m}$, $H_{li} = 333\frac{KJ}{kg}$ yields $\Gamma \sim 2 \cdot 10^{-8} K \cdot m$. So in order for a freezing point to drop by 1 degree, the radius of curvature should be $\sim 4 \cdot 10^{-8} m$. Hence Gibbs-Thomson effect can usually be neglected in macro-scale problems.

In case of unequal specific heats and densities the Gibbs-Thomson relationship

becomes significantly more complicated. However the order of magnitude stays the same (Alexiades and Solomon (1993)).

## 7.2 Appendix B: Viscous dissipation and gravity influence on the energy equation

**Viscous dissipation** The influence of the viscous dissipation on the energy equation is determined by the Eckert number $Ek = \frac{U^{*2}}{Cp_a^* \cdot DT}$. The viscous dissipation term in the energy equation has the form of:

$$\frac{Ek}{2Re}\left(\frac{\partial V_i}{\partial x_j} + \frac{\partial V_j}{\partial x_i}\right)^2 \tag{7.12}$$

The Eckert number shows the relationship between the characteristic kinetic energy and internal energy change because of temperature variation. The relative order of the viscous dissipation term to diffusion term is given by: $\frac{Ek}{2}Pr$. In the equations for water the $Cp_{al}\nu_{la} \cong 0.018 \ll 1$ coefficient will be added to viscous dissipation. Taken into account that the coefficient added to the diffusion term $\chi_{la} \cong 36.7 > 1$, we see that if we can show that in the equations for the air layer in problems under consideration (channel flow and free-surface flow on a tilted plane) the viscous dissipation and gravitation terms are much smaller than the diffusion and convection terms, then we can neglect the corresponding terms and use the simplified energy equations both in air and water.

To estimate Eckert number let's assume that the characteristic temperature variation is $O(1)$ - $O(10)$ both for the tilted plane and channel flow case (Streitz, Ettema, Rothmayer and Tsao (1998), Gilpin (1979, 1981) and Seki, Fukusako and Younan (1984)) and for the wing surface/plate case (Vargas and Reshotko

(2000)). Also:

$$Cp = \begin{cases} air = 1004 \\ water = 4218 \end{cases} \frac{J}{kg \cdot K} \tag{7.13}$$

Then for the water channel/inclined plane flows Eckert number can be written as: $\alpha U^{*2}$, where $\alpha \sim 10^{-4:-5}$. Therefore we see that for $\frac{Ek}{2}Pr \sim 0.1 \Rightarrow U^* \sim 50\frac{m}{s}$. Maximum velocity on the air/water interface obtained in the experiments described in the introduction was $O(10\frac{m}{s})$ and viscous dissipation can be safely neglected. We do not have the experiments for the air/water/ice flows in a channel, however it is safe to assume that the characteristic velocities of the air/water interface will be less then the incoming flow velocity in the experimental investigations of the aircraft icing. In these experiments (for example, Vargas and Reshotko (2000)) the incoming flow velocity was $O(60)$.

Therefore it seems feasible to neglect viscous dissipation influence on the energy equation.

**Gravity** The gravity-related term in the energy equation has the following form:

$$\frac{Ek}{Fr}(\overrightarrow{Gm}, \vec{V}) \sim \frac{Ek}{Fr} \sin\phi \, |Gm| \, |V| \tag{7.14}$$

Here $\phi$ is the angle of the incline. The order of magnitude of the gravitational term to diffusion term ratio is given by $\frac{Ek}{Fr}RePrsin\phi$. For the flow on an inclined plane $\frac{Re}{Fr}\sin\phi \sim 1$.

Therefore the reasoning of the previous section applies and the term corresponding to the work of the gravitation forces can be safely neglected in the energy equation.

## 7.3 Appendix C: The order of approximation for the compact scheme for Orr-Sommerfeld-type equations

$$\begin{cases} \frac{v^{IV}_{n-1}+10v^{IV}_n+v^{IV}_{n+1}}{12} = \frac{v^{II}_{n-1}-2v^{II}_n+v^{II}_{n+1}}{\Delta y^2} \\ \frac{v^{II}_{n-1}+10v^{II}_n+v^{II}_{n+1}}{12} = \frac{v_{n-1}-2v_n+v_{n+1}}{\Delta y^2} \\ \frac{T^{II}_{n-1}+10T^{II}_n+T^{II}_{n+1}}{12} = \frac{T_{n-1}-2T_n+T_{n+1}}{\Delta y^2} \end{cases} \tag{7.15}$$

Since all of the above equations are similar, let us expand the second equation at $n \pm 1$ in Taylor series near $n$:

$$\frac{v_{n-1} - 2v_n + v_{n+1}}{\Delta y^2} = \frac{2}{\Delta y^2} \sum_{n=1}^{\infty} \frac{d^{2n}v}{dy^{2n}} \frac{\Delta y^{2n}}{(2n)!} \tag{7.16}$$

$$\frac{v^{II}_{n-1} + 10v^{II}_n + v^{II}_{n+1}}{12} = \frac{d^2v}{dy^2} + \frac{1}{6} \sum_{n=1}^{\infty} \frac{d^{2(n+1)}v}{dy^{2(n+1)}} \frac{\Delta y^{2n}}{(2n)!} \tag{7.17}$$

Therefore the second equation becomes:

$$\frac{2}{\Delta y^2} \sum_{n=1}^{\infty} \frac{d^{2n}v}{dy^{2n}} \frac{\Delta y^{2n}}{(2n)!} - \frac{d^2v}{dy^2} - \frac{1}{6} \sum_{n=1}^{\infty} \frac{d^{2(n+1)}v}{dy^{2(n+1)}} \frac{\Delta y^{2n}}{(2n)!} = (n+1=k) \tag{7.18}$$

$$= \frac{d^2v}{dy^2} + \frac{2}{\Delta y^2} \sum_{n=2}^{\infty} \frac{d^{2n}v}{dy^{2n}} \frac{\Delta y^{2n}}{(2n)!} - \frac{d^2v}{dy^2} - \frac{1}{6} \sum_{k=2}^{\infty} \frac{d^{2k}v}{dy^{2k}} \frac{\Delta y^{2(k-1)}}{(2(k-1))!} =$$

$$= \sum_{k=2}^{\infty} \frac{d^{2k}v}{dy^{2k}} \left( \frac{\Delta y^{2k}}{(2k)!} \frac{2}{\Delta y^2} - \frac{1}{6} \frac{\Delta y^{2(k-1)}}{(2(k-1))!} \right) =$$

$$= \sum_{k=2}^{\infty} \frac{d^{2k}v}{dy^{2k}} \frac{\Delta y^{2(k-1)}}{(2(k-1))!} \left( \frac{1}{k(2k-1)} - \frac{1}{6} \right)$$

But as for $k = 2$, we have $\frac{1}{k(2k-1)} - \frac{1}{6} = 0$, the second equation is equal to $(k - 3 = m)$:

$$\sum_{m=0}^{\infty} \frac{d^{2(m+3)}v}{dy^{2(m+3)}} \frac{\Delta y^{2(m+2)}}{(2(m+2))!} \left( \frac{1}{(m+3)(2m+5)} - \frac{1}{6} \right) = 0 + O(\Delta y^4) \qquad (7.19)$$

I.e. the formulated difference equalities are true to $O(\Delta y^4)$.

# References

Abramowitz M. and Stegun I.A. (ed), "Handbook of Mathematical Functions (with Formulas, Graphs, and Mathematical Tables)" , 1972

Alexiades V. and Drake J.B., "A weak formulation for phase change problems with bulk movement due to unequal densities", in "Free Boundary Problems: Theory and Applications" ed. by Chadam J. and Rasmussen H., Pitman Lecture Notes, Longman, New York, 1992

Alexiades V. and Solomon A.D., "Mathematical modeling of Melting and Freezing Processes", Hemisphere Publishing, 1993

Batchelor G.K., Mofatt H.K. and Worster M.G. (ed), "Perspectives in Fluid Dynamics: A Collective Introduction to Current Reasearch", Cambridge University Press, 2000

Benjamin T.B., "Wave formation in laminar flow down an inclined plane", J. Fluid Mech. vol. 2, p. 554, 1957

Bertschy J.R., Chin R.W and Abernathy F.H., "High-strain rate free-surface boundary layer flows", J. Fluid Mech., vol. 126, p. 443, 1983

Binnie A.M., "Experiments on the onset of wave formation on a film of water flowing down a vertical plane", J. Fluid Mech. , vol. 2, p. 551, 1957

Blennerhassett P. J., "On the Generation of waves by wind", Proc. R. Soc. Lond. A, vol. 298, p. 451, 1980

Bowles R.I., "Upstream influence and the form of standing hydraulic jumps in liquid-layer flows on favorable slopes", J. Fluid Mech, vol. 284, p. 63, 1995

Brattkus K. and Davis S.H. "Flow-induced morphological instabilities: stagnation-point flows", J. Cryst. Growth, vol. 89, p. 423, 1988

Briggs R.J. , "Electron-stream interaction with plasmas", Cambridge, MA: MIT Press, 1964

Cassel K.W., Ruban A.I. and Walker J.D.A., "An instability in supersonic boundary-layer flow over a compression ramp", J. Fluid Mech, vol. 300, p. 265, 1995

Chin R.W., Abernathy F.H and Bertschy J.R., "Gravity and shear wave stability of free surface flows. Part1: Numerical calculations", J.Fluid Mech., vol. 168, p. 501, 1986

Chung T.J., "Computational Fluid Dynamics", Cambridge University Press, 2002

Cohen E.R., Lide D.R. and Trigg G.L., "AIP Physics Desk Reference", 3rd ed., Springer-Verlag, 2003

Cowley S.J. and Smith F.T. "On the stability of Poiseuille-Couette flow: a bifurcation from infinity", J. Fluid Mech, vol. 156, p. 83, 1985

Davis S.H., "Hydrodynamic interactions in directional solidification", J. Fluid Mech., vol. 212, p. 241, 1990

De Bruin G.J., "Stability of a layer of liquid flowing down an inclined plane", J. Engng. Math., vol. 8, no 3, p. 259, July 1974

Drazin P.G. and Reid W.H., "Hydrodynamic stability", Cambridge University Press, 2003

Epstein M. and Cheung F.B., "Complex Freezing-Melting Interfaces in Fluid Flow", Ann. Rev. Fluid Mech., vol. 15, p. 293, 1983

Epstein M. and Cheung F.B., "Solidification and Melting in Fluid Flow, Advances in Transport Processes", vol. 3, p. 35, 1984

Floryan J.M., Davis S.H. and Kelly R.E., "Instabilities of a liquid film flowing down a slightly inclined plane", Phys. Fluids, vol. 30, issue 4, p. 983, 1987

Forth S.A. and Wheeler A.A., "Hydrodynamic and morphological stability of unidirectional solidification of a freezing binary alloy: a simple model.", J. Fluid. Mech., vol. 202, p. 339, 1989

Gilpin R.R. "Ice formation in a pipe containing flows in the transition and turbulent regimes", J. Heat Transf., vol. 103, p. 363, 1981

Gilpin R.R., "The Morphology of Ice Structure in a Pipe At or Near Transient Reynolds Numbers", Heat Transfer - San Diego, AIChE Symposium Series 189, vol. 75, p. 89, 1979

Glicksman M.E., Coriell S.R. and McFadden G.B., "Interaction of flows with the crystal-melt interface", Ann. Rev. Fluid Mech., vol. 18, p. 307, 1986

Gottlieb D. and Orszag S.A., "Numerical Analysis of Spectral Methods: Theory and application", 1983

Hesla T.I., Pranckh F.P., Preziosi L., "Squire's theorem for two stratified fluids", Phys. Fluids, vol. 29, issue 9, p. 2808, 1986

Hirata T., Gilpin R.R., Cheng K.C. and Gates E.M., "The Steady State ice layer profile on a Constant Temperature Plate in a forced Convection Flow – 1. Laminar regime", Int. J. Heat Mass Tran., vol. 22, p. 1425, 1979

Hirata T., Gilpin R.R. and Cheng K.C., "The Steady State ice layer profile on a Constant Temperature Plate in a forced Convection Flow – 2. The transition and turbulent regimes", Int. J. Heat Mass Transfer, vol. 22, p. 1435, 1979

Hirsh R.S., "High order accurate difference solutions of fluid mechanics problems using compact differencing technique", J. Comp. Phys., vol. 19, p. 90, 1975

Hobbs P.V., "Ice Physics", Clarendon Press, 1974

Hooper A.P. and Boyd W.G.C., "Shear-flow instability at the interface between two shearing fluids", J. Fluid Mech., vol. 128, p. 507, 1983

Hooper A.P. and Boyd W.G.C., "Shear-flow instability due to a wall and a viscosity discontinuity at the interface", J. Fluid Mech., vol. 179, p. 201, 1987

Hooper A.P., "The stability of two superposed viscous fluids in a channel", Phys. Fluids, vol.1, issue 7, p. 1133, 1989

Huebsch W.W., Rothmayer A.P., Unsteady Navier-Stokes Simulation Of flow Past Surface Ice geometries, AIAA Paper 2000-0232, 2000

Isaacson E. and Keller H.B., "Analysis of numerical methods", 1966

Joseph D.D. and Renardy Y.Y., "Fundamentals of two-fluid dynamics:, New York: Springer-Verlag , 1993.

Kuru W.C., Sangalli M., Uphold D.D. and McCready M.J., "Linear stability of stratified channel flow", Int. J. Multiphase Flow, vol. 21, n. 5, p. 733, 1995

Lee J.S., "Freezing Problems in Pipe Flows", PhD Thesis, Iowa State University, 1993

Li L., "Numerical study of nonlinear evolution equations, using compact difference", PhD Thesis, University of London, 1998

McCready M.J., Uphold D.D. and Gifford K.A. , "Interfacial wave-behaviour in oil-water channel flows: Prospects for a general Understanding", Proceedings of the Fifteenth Symposium on Energy Engineering Sciences, US Department of Energy, Basic Energy Sciences, 1997

Miesen R. and Boersma B.J., "Hydrodynamic stability of a sheared liquid film", J. Fluid Mech., vol. 301, p. 175, 1995

Orzag. S.A., "Accurate solution of the Orr-Sommerfeld stability equation", J. Fluid Mech, vol. 50-4, p. 689 , 1971

Ozgen S., Degrez G. and Sarma G.S.R., "Two-fluid boundary layer stability", Phys. Fluids, vol 10, issue 11, p. 2746, 1998

Poots G., "Ice and Snow accretion on Structures", Research Studies Press Ltd, 1996

Press W.H., Teukolsky S.A.,Vetterling W.T., Flannery B.P., "Numerical recipes in C", Cambridge University Press, 1992

Renardy Y., "Instability at the interface between two shearing fluids in a channel", Phys. Fluids, vol. 28, no. 12, p. 3441, 1985

Renardy Y., "Weakly nonlinear behaviour of periodic disturbances in two-layer Couette-Poiseuille flow", Phys. Fluids, vol. 1, issue 10, p. 1666, 1989

Rothmayer A.P. and Tsao J.C., "A Mechanism for Ice Roughness Formation on an Airfoil Leading Edge, Contributing to Glaze Ice Accretion", AIAA Paper 98-0485

Rothmayer A.P. and Tsao J.C., "Triple-Deck Simulation of Surface Glaze Ice Accretion", AIAA Paper 2000-0234

Rothmayer A.P. and Tsao J.C., "Water film runback on an Airfoil Surface", AIAA Paper 2000-0237, 2000

Rothmayer A.P. and Tsao J.C., "On the incipient Motion of Air Driven Water Beads", AIAA Paper 2001-0676, 2001

Ruban A.I., "Chisllenniy metod resheniyaa zadachi o svobodnom vzaimodeistvii", Uchenie Zapiski TsAGI, vol. 7, no. 2, p. 45, 1976 (in Russian)

Ruban A.I., "Chislennie metody v teorii vzaimodeistviya pogranichnogo sloya s nevyazkim potokom", Uchenie Zapiski TsAGI, vol. 21, no. 5, p. 3, 1990 (in Russian)

Sangalli M., McCready M.J. and Chang H.-C., "Stabilization mechanisms of short waves in stratified gas-liquid flow", Phys. Fluids, vol. 9, issue 4, p. 919, April 1997

Seki N., Fukusako S. and Younan G.W., "Ice-formation Phenomena for Water Flow Between Two Cooled Parallel Plates", J. Heat Trans., vol. 106, p. 498, 1984

Smyth N.F., "Dissipative effects on the resonant flow of a stratified fluid over topography", J. Fluid. Mech., vol. 192, p. 287, 1988

South M.J. and Hooper A.P., "Linear growth in two-fluids plane Poiseuille flow", J. Fluid Mech, vol. 381, p. 121, 1999

Squire H.B., "On the stability of three-dimensional distribution of viscous fluid between parallel walls", Proc. Roy. Soc. London Ser. A, vol. 142, p. 621, 1933

Stephan K., "Influence of heat transfer on melting and solidification in forced flow", Int. J. Heat and Mass Trans, vol. 12, p. 199, 1969

Streitz J.T, Ettema R., Rothmayer A. and Tsao P., "Initial Icing Formation on Planar Surfaces: Laboratory Experiments and Formulation", Iowa Space Grant Consortium Conference, 1998

Swinney H.L. and Gollub J.P., "Hydrodynamic instabilities and the transition to turbulence", Springer-Verlag, 1981

Sychev V. V., Ruban A. I., Sychev Vic. V. and Korolev G. L., "Asymptotic Theory of Separated Flows", Cambridge University Press, 1998

Thomas L.H., "The Stability of Plane Poiseuille Flow", Physical Review, vol. 91, n. 4, 1953

Timoshin S.N. and Hooper A.P., "Mode coalescence in a two-fluid boundary-layer stability problem", Phys. Fluids, vol. 12, n. 8, p. 1969, 2000

Vargas M. and Reshotko E., "Physical Mechanisms of Glaze Ice Scallop Formations on Swept Wings", AIAA-98-0491

Vargas M. and Reshotko E., "Parametric Experimental Study of the Formation of Glaze Ice Shapes on Swept Wings", AIAA-99-0094

Vargas M. and Reshotko E., "LWC and Temperature Effects on Ice Accretion Formation on Swept Wings at Glaze Ice Conditions", AIAA-2000-0483

Yao L.S., Prusa J., "Melting and Freezing", Advances in Heat Transfer, vol. 19, p. 1, 1989

Yiantsios S.G., Higgins B.G., "Linear stability of plane Poiseuille flow of two superposed fluids", Phys. Fluids, vol. 31, issue 11, p. 3225, 1988

Yiantsios S.G. and Higgins B.G., Erratum: "Linear stability of plane Poiseuille flow of two superimposed fluids", Phys. Fluids A, vol. 1, issue 5, 1989

Yih C.S., "Stability of two-dimensional parallel flows for three-dimensional disturbances", Q. Appl. Math., vol. 12, p. 434, 1955

Yih C-S, "Stability of Flow Down an Inclined Plane", Phys. Fluids, vol. 6, no. 3, p. 321, 1963

Yih C.-S. 1967, "Instability due to viscosity stratification," J. Fluid Mech. **27** , 337